Apoptotic B Cells: Their Interactions with Macrophages and Modulation by Rituximab

Felicity DeBari Herrington

BSc(Hons)

Submitted in fulfilment of the requirements for the degree of
Doctor of Philosophy

College of Medical, Veterinary and Life Sciences
Institute of Infection, Inflammation and Immunity
University of Glasgow

June 2014

Abstract

Apoptotic cells (AC) are able to modulate the immune system, dampening inflammation and triggering anti-inflammatory responses by various immune cells as a consequence of interaction and uptake. Rituximab (RTX) is an anti-CD20 monoclonal antibody used as a treatment in several autoimmune diseases, including rheumatoid arthritis (RA). Treatment results in B cell depletion, with B cell apoptosis known to contribute to RTX-mediated B cell death. However the simple removal of B cells from the system does not seem to account for all the beneficial effects of this biologic. We propose that RTX treatment in RA results in the re-establishment of temporary tolerance to the system, through an apoptotic B cell-dependent mechanism.

Initial *in vitro* and *in vivo* investigations were undertaken to explore the validity of this hypothesis. The present work sought to examine the immunomodulatory capacity of apoptotic B cells and to determine whether the potential anti-inflammatory effects of apoptotic B cells are modulated by RTX, with both *in vitro* methods and an *in vivo* model of autoimmunity utilized in these studies. The results presented in this thesis demonstrate that apoptotic B cells have comparable effects on bone marrow derived macrophage (BMDM) phenotype and function *in vitro* as previously described AC from other cellular sources. Surprisingly, in the *in vitro* assay system used, viable cells had the same immunomodulatory effects on BMDM as AC, for all criteria investigated. Preliminary studies indicate this may be a promising avenue of inquiry, however further work is needed before a conclusion can be reached as to the relative level of involvement of apoptotic B cell-mediated tolerance in the improvement seen on RTX treatment in RA.

Table of Contents

List of Tables

List of Figures

Acknowledgments

Firstly I would like to thank my supervisor, Dr Carl Goodyear. Your guidance and support throughout my PhD has been invaluable. I am extremely grateful for all the time and effort you have put into this thesis, and into my project as a whole - I couldn't have asked for a better supervisor. I would also like to thank my second supervisor, Professor Paul Garside, and my PhD programme coordinator, Professor Iain McInnes, for all their help and input along the way. Thanks also go to Dr Simon Milling for the use of his computer (and sound system), and saving me from a formatting nightmare!

A massive thank you goes to all the Goodyears, past and present – I couldn't have asked for a better group! You have all contributed to making my PhD experience what it was, and given me some unforgettable memories to take away with me. However, extra special thanks needs to be given to the 'old guard' - I miss our little family! Susan and Lindsay, you have both taught me so much throughout my time in the lab. Your patience ("I only use the centrifuge to spin things down"), help, and seemingly boundless knowledge have got me out of a jam on more than one occasion, and I will be eternally grateful to you both. Jamie, for the stream of fluffy animal pictures, terrible music, latex glove creations, and moral support; thank you. You have been a major part of my PhD and I'm glad to have had you as a partner in crime, no matter how many times I've threatened to hit you, or indeed, actually hit you. Jen, I am grateful for all the FACS knowledge, the coffees from K&J, dragging me to hot yoga and taking me on drunken nights out; it has all been appreciated, and more importantly, very much enjoyed. Pauline, you have always managed to be the calm in the chaos of the Goodyear lab. For all the bench-side chats and all the help (your amazing organizational skills have saved me on more than one occasion from growing old searching through fridges and freezers), thank you.

I also want to extend my thanks to the staff of the CRF, without whom a large part of this thesis would not have been possible, and to everyone in the GBRC who has helped me over the years. The advice, borrowed reagents, and general chat have all been appreciated. A particular mention has to be given to the GBM lab group, who took me on for my first year rotation project, and especially Bob and Agi. Without the two of you I would not have made it through those first few months of my PhD, and your mumbled conversations and wild mood swings in the microscopy room will be fondly remembered!

To all those friends who've kept me going along the way, thank you! Carolyn and Pamela, your continued friendship has been such a huge part of my time in Glasgow. Thank you for all the support, the long lunches and just generally, the good times, of

which there are far too many to count. Angie, thank you for being such a good desk neighbour, for the days out and the nights in, and for all the dancing. I promise, now I am finished I will make it down to visit you! Thanks also go to my late night thesis buddy, Trish. You made being in the office at all hours that little bit more bearable, and the endless stream of snapchats has provided continual amusement. Katie, for all the rum, roller-skating, and wilderness adventures; thank you. Here is my attempt at a thesis snow bear just for you :▸ . Peter, thank you for the nights at the union playing pool, pretending like we still belonged there, and for taking me on my first 'small-town' night out. In addition, I feel I should mention the unofficial office 'tea club' (you know who you are) – thank you for the random, and usually ridiculous, chat, the laughs, and the many, many cups of tea delivered to my desk.

I also need to say a massive thank you to my extended family, both biological and adopted (Diane, David and Auntie Christine). You have been a great source of encouragement and support throughout my time at university, and my life in general.

Tom, simply put, you have kept me sane - I don't know how I would have managed this without you. Thank you for always being there for me, for all the breakfasts, the trips to see the sea, and the hugs; for always knowing how to make me laugh, and for just being you. I love you.

And lastly, I want to thank my parents. Without you none of this would have been possible. I will never be able to repay you for the endless support, inspiration and love you have given me over the years. Thank you, thank you, thank you. This thesis is dedicated to you.

Author's Declaration

I declare that this thesis is the result of my own work. No part of this thesis has been submitted for any other degree at The University of Glasgow, or any other institution.

Felicity Herrington

Abbreviations

A

AC	apoptotic cells
ACAMP	apoptotic cell-associated molecular pattern
ACPA	anti-citrullinated protein/peptide antibodies
ADCC	antibody dependent cell-mediated cytotoxicity
ag	antigen
AnnV	Annexin V
APC	antigen presenting cell
ATP	adenosine triphosphate

B

B1	Tositumomab
BAC	bacterial artificial chromosome
BcR	B cell receptor
BM	bone marrow
BMDC	bone marrow-derived dendritic cell
BMDM	bone marrow-derived macrophages
Breg	regulatory B cell
BSA	bovine serum albumin

C

CII	collagen type II
CDC	complement dependent cytotoxicity
CFA	complete Freund's adjuvant
CFSE	carboxyfluorescein succinimidyl ester
CIA	collagen induced arthritis
CR3	complement receptor 3
CRT	calreticulin

D

DAMP	damage-associated molecular pattern
DAPI	4',6-diamidino-2-phenylindole
DC	dendritic cell
DMSO	dimethyl sulfoxide
DNA	deoxyribonucleic acid

E

EAE	experimental autoimmune encephalitis
EDTA	ethylendiaminetetraacitic acid
ELISA	enzyme-linked immunosorbent assay
ER	endoplasmic reticulum

F

FACS	fluorescence-activated cell sorter
FBS	foetal bovine serum
FcR	Fc receptor
Fcγ R	Fc gamma receptor
FDA	Food and Drug Administration
FITC	fluorescein isothiocyanate
FSC	forward scatter

G

GAD	glutamic acid decarboxylase
GAS-6	growth-arrest specific gene 6
GM-CSF	granulocyte-macrophage colony-stimulating factor

H

hCD20	human CD20
hCD20tg	human CD20 transgenic
HLA	human leukocyte antigen
HSP	heat shock protein

I

ICAM	intercellular adhesion molecule
i.d.	intradermal
IFNγ	interferon gamma
Ig	immunoglobulin
IL	interleukin
i.p.	intraperitoneal
i.v	intravenous

L

LNs	lymph nodes
LOX1	low-density lipoprotein-1
LPS	lipopolysaccharide

M

mAb	monoclonal antibody
MAC	mitochondrial apoptosis-induced channels
MARCO	macrophage receptor with collagenous structure
M-CSF	macrophage colony-stimulating factor
MFG-E8	milk-fat globule EGF factor 8
MFI	mean fluorescence intensity
MHC I	major histocompatibility complex class I

MHC II	major histocompatibility complex class II
mLN	mesenteric lymph node
mRNA	messenger ribonucleic acid
MZ	marginal zone

N

NFκB	nuclear factor kappa B
NK cell	natural killer cell
NHL	non-Hodgkin's lymphoma
NO	nitric oxide
NOD mice	non-obese diabetic mice
NOD-like	nucleotide-binding oligomerization domain-like
nt	no treatment

O

OA	osteoarthritis
OVA	ovalbumin
OVAp	OVA peptide
OVApro	OVA protein
ox-LDL	oxidised low-density lipoprotein

P

PAMP	pathogen-associated molecular pattern
PARP	poly ADP-ribose polymerase
PBMC	peripheral blood mononuclear cells
PBS	phosphate buffered saline
PC	phosphatidylcholine
PCD	programmed cell death
PCR	polymerase chain reaction
PE	phycoerythrin
PGE_2	prostaglandin E_2
PI	propidium iodide
PMA	phorbol-12-myristat-13-acetate
pLN	peripheral lymph nodes
PRR	patter recognition receptor
PS	phosphatidylserine
PSR	phosphatidylserine receptor

R

RA	rheumatoid arthritis
RANK	receptor activator of NFkB
RANKL	receptor activator of NFkB ligand

RBC	red blood cell
RF	rheumatoid factor
RNA	ribonucleic acid
RT	room temperature
RTX	Rituximab
RTX:OVA	Rituximab-ovalbumin peptide conjugate
RU	relative units

S

SA	streptavidin
s.c.	subcutaneous
SD	standard deviation
SE	shared epitope
SLE	systemic lupus erythematosus
SR-A	scavenger receptor A
SSC	side scatter

T

TcR	T cell receptor
tg	transgenic
TGF-β	transforming growth factor beta
Th cell	T helper cell
TLR	Toll-like receptor
TNFα	tumour necrosis factor alpha
TNFR1	tumour necrosis factor receptor 1
TNT	tunnelling nanotubes
TRAIL	TNF-related apoptosis-inducing ligand
Treg	regulatory T cell
TSP-1	thrombospondin 1

W

WT	wild type

#

7-AAD	7-amino-actinomycin D

Symbols

Δ	delta (change in)

Chapter 1: Introduction

1.1 The Immune System

The immune system has evolved to protect the body from invasion by pathogens, with the ability to recognize and mount an appropriate response to foreign antigens crucial for maintaining the health of an individual. In addition to this role in protection, the immune system is also responsible for the regulation of tolerance to harmless antigens, such as self-antigens. If a breakdown in tolerance occurs, unnecessary inflammatory responses are mounted that can result in chronic and detrimental inflammation, known as autoimmunity.

The immune system is comprised of two main branches, the innate immune system and the adaptive immune system, which work in close contact with one another. The innate immune system mounts the first line of defence, quickly responding to infection, while the adaptive immune system offers a slower, but more tailored response to specific pathogens, providing immunological memory and allowing an enhanced immune response on repeated encounters with a particular antigen.

1.2 Innate Immunity

The innate immune system has evolved to detect common, invariant molecular patterns expressed by pathogenic microorganisms, termed PAMPs (pathogen-associated molecular patterns), a concept originally proposed in the 1980s by Charles Janeway Jr [1]. Recognition of these molecular patterns results in the initiation of non-specific immune responses, and defects or deficiencies in innate effector mechanisms, such as the myeloid cell compartment [reviewed in [2] or complement proteins [reviewed in [3], results in recurrent microbial infections of varying severity.

The cellular component of the innate immune system is comprised of a number of distinct cell types: the myeloid cells (monocytes, macrophages and dendritic cells (DCs)), the granulocytes (neutrophils, eosinophils and basophils), and mast cells. Innate immune cells express a wide range of receptors known collectively as pattern recognition receptors (PRRs). PRRs recognise molecular patterns common to microbes, and can also recognise altered self-epitopes, such as those exposed during cell death. Toll-like receptors (TLRs) play a key

role in the recognition of microbial structures, initiating responses to a wide range of extracellular and endosomal microbes. TLR4 is expressed on the surface of innate effector cells, and as part of the TLR4:MD-2 complex is able to detect lipopolysaccharide (LPS) [4], a constituent of the cell membrane of Gram-negative

bacteria. TLR7 and TLR8 are localized to endosomes and bind to viral single-stranded RNA [5]. Scavenger receptors (SR) encompass a broad range of molecules expressed on the surface of macrophages and dendritic cells (DCs), as well as certain endothelial cells. SR-A binds to lipoteichoic acid [6], a major constituent of the cell wall of Gram-positive bacteria, while LOX-1 (lectin-like oxidised LDL-receptor 1) is able to bind both Gram-positive and Gram-negative bacterial products [7]. Detection of intracellular PAMPs is undertaken by cytosolic PRRs, including NOD-like receptors [8] and RIG-I-like receptors [9]. Recognition of pathogens via PRRs results in the initiation of multiple responses by innate cells. The production of chemokines recruits additional effector cells to sites of inflammation, the secretion of pro-inflammatory cytokines activates cells and helps to direct the immune response, and the up-regulation of co-stimulation molecules enables initiation of adaptive immune responses.

The complement cascade, along with collectins and ficolins [reviewed in [10], can be seen as the humoral arm of the innate immune response, contributing to the non-adaptive recognition of pathogens. Activation of the complement cascade results in the opsonization of target cells/microbes, mediating the removal of pathogens, through the recruitment and modulation of effector cells, the activation of pro-inflammatory mediators and direct killing by anti-microbial complexes.

Innate responses are immediate, but non-clonal. Activation of innate immunity initiates microbial clearance and containment, while alerting the adaptive immune response to the potential threat. The combination of innate and adaptive immunity generates a multifaceted response with the ability to recognize both invariant molecular patterns and specific antigens expressed by the pathogen, enabling its effective eradication from the system.

1.3 Macrophages

Macrophages are a heterogeneous immune cell population, which are present in almost all tissues of the body and are one of the main innate immune cells involved in the homeostatic clearance of dead and dying cells, a topic that will be discussed in depth later in this introduction. They are highly phagocytic cells, constitutively expressing a wide range of PRRs, including scavenger receptors, TLRs, phosphatidylserine receptors, integrins and complement receptors, enabling the recognition of specific phagocytic or endocytic ligands (see sections 1.2 and 1.8).

It was originally proposed that phagocytic mononuclear cells, including all macrophage populations, differentiated from circulating peripheral blood monocytes after migration

into the tissues, with this model known as the mononuclear phagocyte system (MPS) [11]. More recently, however, it has been demonstrated that this cell type can arise through several, distinct developmental pathways. During an immune response, circulating monocytes are recruited to sites of inflammation, differentiating into inflammatory macrophages, following a developmental pathway in keeping with the original model. Multiple tissue resident macrophage populations, however, have been shown to consist of both monocyte-derived cells, and cells with embryonic origins able to undergo self-renewal in the tissue [12]. Fate-mapping studies have shown that Langerhans cells [13], microglia [14], splenic red pulp macrophages, alveolar macrophages and certain peritoneal macrophages are established prenatally [15] and able to undergo self-renewal in the tissues. Within these populations developmental pathways can differ, deriving from both the embryonic yolk sac (i.e. microglia [14]) and from the fetal liver (i.e. Langerhans cells [13]). It has been demonstrated that peripherally derived macrophages are able to replace self-renewing tissue-resident macrophages after experimental ablation of these populations [16], with this tissue re-population postulated to take place under certain inflammatory settings, however it is not clear to what extent this occurs under physiological conditions *in vivo*.

Macrophages are highly plastic cells; the effector profile of a macrophage is dependant on the stimuli received on activation, resulting in a spectrum of different activated populations *in vivo* [17]. This spectrum of populations can be broadly split into two main subsets, based on functional and biochemical differences: the classically activated, M1-macrophages; and the alternately activated M2-macrophages, with monocyte-derived inflammatory macrophages classified as M1-like cells, while tissue resident macrophages are more M2-like in their phenotype. It is important to note however, that many populations of macrophages both *in vitro* and *in vivo*, do not fall fully into either of these subsets, with the M1/M2 descriptions offering a broad conceptual framework, rather than definitive populations. After differentiation into activated effector cells, macrophages retain a level of plasticity, and it has been postulated that the phenotype of a macrophage can change over time in response to environmental cues [18]. However, several cell surface markers are commonly used to help identify macrophages both *in vivo* and *in vitro*, including F4/80, CD11b, Ly6C and Ly6G [19] in the murine system. Cytokine production and the expression of additional cell-surface markers allow discrimination between different sub-populations, with the markers used for identification differing between human and murine cells.

1.3.1 M1 Macrophages

Classically activated M1-macrophages arise during cell-mediated immune responses, and are the pro-inflammatory macrophage subset. They are involved in resistance against microbial infection and tumours, with murine M1 macrophages activated by IFNγ alone, or IFNγ in combination with a TLR agonist (e.g. LPS) or other cytokines (TNFα/GM-CSF). IFNγ stimulates macrophage antimicrobial and tumoricidal properties; on recognition and phagocytosis of pathogens or infected cells, the target is taken up into endocytic vacuoles, which become acidified [20], creating an inhospitable environment, and facilitating destruction of the contents. If acidification is not sufficient, these vacuoles can bind with lysosomes containing microbicidal enzymes, such as hydrolases [21] and lysozyme [22]. These activated M1 macrophages can also undergo a respiratory burst, resulting in the increased production of nitric oxide (NO) and reactive oxygen species that are directly toxic to pathogens, enhancing their killing ability and further mediating the removal of microbes [23]. The uptake and destruction of pathogens by M1 macrophages results in the production of danger signals, such as the pro-inflammatory cytokines IL-1β, IL-6, IL-12, IL-23, TNFα and IFNγ, as well as chemokines and growth factors. The production of pro-inflammatory signals, combined with the expression of high-levels of surface MHC II (major histocompatibility complex class II) and co-stimulatory molecules characterizes murine M1 macrophages, and enables the effective presentation of pathogen-derived epitopes to T cells, augmenting the adaptive immune response.

1.3.2 M2 Macrophages

Alternately activated M2-macrophages are a heterogeneous group of non-inflammatory macrophages, which can be further sub-divided into distinct populations, with each of these populations having clear roles within the immune response.

In the murine system, regulatory M2 macrophages are activated in a two step process, generally by a combination of immune complexes and TLR ligands, however other factors can also induce their differentiation, including: prostaglandins, apoptotic cells, IL-10, TGF-β, glucocorticoids and FcγR (Fc gamma receptor) ligation, with different activatory stimuli generating slightly different regulatory populations. Activation by IL-10 results in the increased expression of FcγRI, II and III, and the scavenger receptor MARCO, and enhanced IL-10 production, while inhibiting antigen presentation via the down-regulation of MHC II and co-stimulatory molecules [24]. Alternately, regulatory macrophage activation by immune complexes and TLR4 ligands results in enhanced IL-10 production, but with high levels of co-stimulatory molecule expression and efficient

antigen presentation to Th2 cells [24]. Despite this, these diverse regulatory macrophage populations all have anti-inflammatory roles, involved in the dampening of active immune responses and the regulation of inflammation. Regulatory macrophages as a whole, are characterized by their enhanced production of the anti-inflammatory cytokine, IL-10, coupled with the decreased expression of the pro-inflammatory cytokine, IL-12 [17].

The second group of M2 macrophages are the wound-healing macrophages. This subset are activated by IL-4 and IL-13, which are released during tissue injury and by Th2 cells as part of type 2 mediated immune responses, such as allergy and parasitic infection. Murine M2 macrophages activated through IL-4 and IL-13 up-regulate expression of the mannose receptor (CD206) [25], scavenger receptors (SR-A and DC-SIGN) and the C-type lectin receptor Dectin-1 [26]. The up-regulation of the arginase gene (ARG1) is a prototypical marker for murine macrophage alternative activation, with the expression of ARG1 resulting in a shift toward arginase activity [27], directly contributing to the production of the extracellular matrix and playing significant roles in tissue repair and homeostasis. IL-4 activation of macrophages directly suppresses hallmarks of M1 macrophage activity, acting to inhibit both the respiratory burst [28] and the production of pro-inflammatory cytokines [29].

1.4 Adaptive Immunity

There is huge diversity within the adaptive immune system, enabling the recognition of vast numbers of unique epitopes expressed by microorganisms. Adaptive immunity is highly specific, allowing recognition of particular pathogens, with subsequent antigen-specific responses mounted. These responses result in long-standing immunological memory to the antigen in question. Effective adaptive immune responses involve antigen presentation by APCs, such as DCs and macrophages, and antigen recognition by lymphocytes expressing specific cell surface antigen receptors. There are two major populations of lymphocytes: the T cell and B cell populations. These cells express diverse repertoires of antigen-specific receptors, making this large pool of T and B cells highly effective against wide range pathogens.

T cells are only able to recognize cognate antigen in the context of self-MHC (major histocompatibility complex) expressed on the surface of APCs. There are two different classes of MHC molecules, MHC class I (MHC I) and MHC class II (MHC II), with presentation of a peptide in the context of MHC I resulting in peptide recognition by T cells expressing the CD8 co-receptor [30,31], while presentation in the context of MHC II results in recognition by T cells expressing the CD4 co-receptor [32]. The

different subclasses of T cell have diverse effector mechanisms and functions within the immune response. $CD8^+$ T cells are known as cytotoxic T cells, and are capable of direct killing of malignant or infected cells in response to activation. Cytotoxic T cells induce apoptosis in their target cell by engaging pro-apoptotic receptors on the target cell surface, or by the release of cytolytic proteins and enzymes that disrupt the target cell membrane and target intracellular apoptotic machinery. The $CD4^+$ T cells are a more heterogeneous population, comprised of multiple T helper (Th) cell subsets (Th1, Th2 and Th17) and the regulatory T cells (Tregs). Th cells exert their effector functions through the productions of cytokines, which are able to modulate immune responses, directing B cell antibody production and cell-mediated immunity. Each Th subset has a distinct role within the immune response, and can be characterized based on the production of signature cytokines [33,34]. Unlike the other $CD4^+$ T cell subsets, Tregs are anti-inflammatory cells, able to inhibit pro-inflammatory immune responses, both by direct cell-contact mechanisms, and the production of anti-inflammatory cytokines [35].

1.5 B cells

B cells have multiple immunological functions. They are able to mediate the adaptive humoral immune response, through their production of antibodies, and have additional roles as APCs. B cell can also secrete a range of cytokines, which are able to either suppress or enhance pro-inflammatory responses depending on the particular cytokines secreted. B cells are highly specific cells that recognize their cognate antigen through surface expressed immunoglobulins (Ig), termed B cell receptors (BcRs). Each B cells has a single specificity, expressing multiple copies of the same BcR.

Naïve B cells can be sub-divided into three distinct populations: B-1 B cells, B-2 B cells and MZ (marginal zone) B cells. B-1 B cells are the first B cells to appear during fetal development, with conventional follicular B cells (B-2 B cells) arising later [36]. B-1 B cells are a self-renewing B cell subset that comprise around 5% of the total B cell population, and are found primarily in the peritoneal and pleural cavities, with an important role in the defence of these sites. This B cell population can be further subdivided based on their surface expression of CD5, with $CD5^+$ B-1 B cells termed B-1a cells, while the $CD5^-$ subset are classed as B-1b cells [37], with these populations arising from different progenitors. All B-1 B cell populations express a restricted B cell receptor repertoire compared to the major B-2 B cell population. B-1 cells are involved in early, non-adaptive immune responses, directed mainly toward carbohydrate antigens, and are able to produce low-affinity ‘natural’ antibodies without the requirement of T cell help. However, B-1 cells are also able to rapidly produce specific T-independent antibodies

when stimulated, such as their secretion of mucosal IgA in response to commensal bacteria in the intestinal mucosa [38]. MZ B cells are also considered to be innate-like B cells, residing in the marginal sinus of the spleen, where they are well situated to respond to blood-borne pathogens. MZ B cells functionally resemble B-1 B cells, expressing a restricted BcR repertoire biased toward common environmental and self-antigens, and mediate mostly T cell-independent responses. It has been postulated that MZ cells may play a role in the presentation of antigen to T cells and NK cells [39].

B-2 B cells comprise the largest and most studied population of B cells, and it is the B-2 subset that will be focused on throughout this thesis.

1.5.1 Development

B cells, along with T cells and NK cells, are part of the lymphoid lineage, and originate from common lymphoid progenitors. Before birth, B cells can develop in specialized microenvironments in the yolk sac, fetal liver, and bone marrow; however, after birth B cell development is restricted to the bone marrow, with new B cells continually produced throughout life. After development in these specialized niches, B-2 B cells migrate to the periphery where they can become activated on recognition of their cognate antigen, differentiating into antibody-secreting plasma cells and memory B cells, and mounting an active immune response against invading pathogens.

In the bone marrow, stromal cell signals induce the differentiation of common lymphoid progenitors into B cell–specific progenitors, termed pro-B cells. These signals are delivered both through direct contact and secreted factors, with the early B-lineage growth factor, IL-7, the first environmental factor shown to be crucial for B cell development [40].

At the pro-B cell stage, the ordered rearrangement of immunoglobulin genes begins, with the heavy-chain locus rearranged first. Successful heavy-chain rearrangement results in the production of an intact μ heavy-chain, and the cessation of gene rearrangement. If a productive heavy-chain is not produced after rearrangement of both chromosomes, the pro-B cell is eliminated. The production of a functional μ heavy-chain enables the expression of the pre-BcR, and the subsequent development of the pro-B cell into a pre-B cell. In the pre-BcR complex the μ heavy-chain is paired with germline-encoded surrogate light chains, consisting of the λ5-like and Vpre-B proteins [41], and associates with Igα/Igβ heterodimers, enabling signal transduction through this complete pre-B cell receptor. The pre-BcR is expressed transiently [42], and it is unknown if pre-BcR signalling is ligand-dependent or the result of pre-BcR complex

aggregation, however, signalling through this receptor is essential for the progression of the cell along its developmental pathway. On expression of an effective pre-BcR and subsequent pre-BcR signalling, the cell undergoes multiple rounds of proliferation, giving rise to many resting small pre-B cells, and initiating the rearrangement of the light-chain locus [43]. The small resting pre-B cells arising from the same original pre-B cell undergo different light chain rearrangement, resulting in a distinct antigen specificity and increasing the overall diversity of the B cell repertoire. On rearrangement of both the heavy- and light-chain loci, allelic exclusion is employed, with rearrangement occurring one allele at a time and as such, only one specificity of BcR will be expressed on the cell surface.

Successful light-chain recombination enables the expression of intact BcR molecules on the surface of immature B cells. As the specificity of the expressed BcR is generated randomly, there is a possibility that the cell will be auto-reactive. In order to eliminate potentially self-reactive cells, the immature B cells undergo the process of central tolerance, in which they are exposed to self-antigen. Immature B cells are not fully functional, and antigen recognition does not result in activation, but in the removal of self-reactive clones, through either clonal deletion, induction of anergy, or receptor editing. Receptor editing is a process by which the BcR undergoes secondary light-chain rearrangement; if a non-autoreactive BcR is successfully produced the B cell will continue on its developmental pathway, if rearrangement results in another self-reactive BcR the B cell will be eliminated via clonal deletion. Immature B cells that do not undergo an interaction with self, or those that have undergone successful receptor editing, migrate out of the bone marrow and into the periphery where they recirculate throughout the body. Not all auto-antigens are expressed in central lymphoid organs however, and as such a number of autoreactive B cells will make it to the periphery where they undergo an additional round of tolerance induction in the attempt to rid the body of autoreactive cells [44].

These newly generated naïve B cells are non-dividing cells, with a very short life span, and in the absence of antigen recognition the majority will die by apoptosis within a few weeks. Once antigen has been encountered these B cells need to enter lymphoid follicles within secondary lymphoid organs, such as the spleen and lymph nodes, in order to survive and mature, with the follicles providing the necessary signals for B cell survival. However, there is limited space in available in the lymphoid follicles, and so newly generated B cells must compete with existing peripheral B cells for space. This competition favours existing B cells, which are already established in the stable peripheral B cell pool, with the expression of specific cell surface proteins, such as BLyS [45], contributing to their survival.

Naïve B cells continue to recirculate until they either succumb to cell death, or encounter cognate antigen, with BcR stimulation a critical signal for naïve B cell survival [46].

1.5.2 B cell Responses

B cell activation in response to the majority of antigens requires signals from cognate T cells, with these termed T-dependent antigens. To initiate B cell responses to T-dependant antigens, two stages of B cell activation must occur. The B cell must encounter antigen via its BcR, followed by interaction with cognate T cells in the lymphoid follicles. B cells are able to recognize antigen associated with DCs, however they are also able to interact with free soluble antigen, unlike T cells, which require the presentation of antigen in the context of self-MHC molecules. Following antigen recognition, the interaction of CD40 on B cells with CD40L expressed on T cells drives the B cell into the cell cycle, activating it and initiating antigen-dependent B cell development, with the cytokine milieu present at the time of activation influencing subsequent B cell differentiation. Activation leads to clonal expansion, generating high numbers of effector cells. These effector B cells are short-lived plasma cells, which remain in the periphery and are able to produce antibodies, secrete immunomodulatory cytokines and function as antigen-specific APCs. Antibody-secreting plasma cells are terminally differentiated cells, whose morphology and surface marker expression is distinct from that of naïve B cells. Plasma cells have an increased cytoplasmic to nuclear ratio, along with the presence of secretory vacuoles and additional rough endoplasmic reticulum [47], and down-regulate numerous B cell-specific surface molecules, including MHC II, B220 (CD45R), CD19, and CD20, amongst others [48]. These effector B cells may differentiate further in germinal centres, undergoing somatic hypermutation of their BcRs and subsequent affinity maturation, as well as antibody class switching, enhancing the humoral immune response and allowing different functions to be carried out by various antibody isotypes. Some of these activated germinal centre B cells alter their expression of chemokine receptors [49], obtaining the ability to migrate to the splenic red pulp, lymph node medullary cords and the bone marrow, where they survive as long-lived plasma cells, able to secrete antibody for many months [50]. The eventual formation of a pool of antigen-specific memory B cells ensures rapid and massive B cell proliferation on repeated antigen encounter, resulting in the generation of enhanced numbers of antigen specific plasma cells and a more effective secondary immune response.

Traditionally, the role of effector B cells has been seen to be the production of large amounts of antibodies. However, it is now recognized that along with antibody

production, B cells have multiple immunological functions, able to: secrete a broad range of cytokines; act as APCs, directly presenting antigen to T cells; and suppress pro-inflammatory responses both in *vitro* and *in vivo*.

1.5.2.1 Antibody Production

Although antibodies themselves do not directly remove pathogens, they have a broad range of biological activities, mediated through their binding to antigen and establishment of effector responses. Multiple antibody isotypes are able to activate the complement cascade, resulting in either complement-mediated lysis of the target cell, or its complement opsonization, leading to recognition and ingestion by phagocytes [51]. Antibodies can also directly opsonize antigens/cells, enhancing uptake by phagocytes through interaction of the antibody constant region with FcRs expressed on phagocytes. Antibody binding of target cells and subsequent FcR interaction can also result in antibody-dependant cell mediated cytotoxicity (ADCC), in which the activity of cytotoxic cells is directed toward specific target cells, resulting in uptake and destruction by macrophages and direct lysis by NK cells. Antibodies can also directly neutralize certain viruses and toxins, binding to the pathogen/pathogenic product, blocking their access to, and interaction with, their specific cell-surface receptors.

1.5.2.2 APC function

It has been known for many years that the presentation of cognate antigen by B cells to primed T cells initiates the direct T-B cell interactions required for these cells to become fully activated [52]. However, more recently, activated effector B cells have also been implicated as effective APCs, able to prime T cells and initiate their activation, with B cells particularly effective at presenting antigen in situations where its availability is limited [53]. The important of B cells as APCs has been confirmed *in vivo*, with antigen presentation by B cells shown to be crucial in the induction of several autoimmune disease models, including autoimmune arthritis [54], insulin-dependent diabetes mellitus [55] and murine lupus [56]. Presentation of antigen by B cells is also required for optimal development of memory $CD4^+$ T cells [57].

1.5.2.3 Cytokine secretion

B cells can also contribute to immune responses through the secretion of cytokines, with activated B cells able to produce an array of effector cytokines able to influence the outcome of the existing immune response. As with $CD4^+$ T helper cells, B cells can be classified into subsets according to the cytokine milieu they produce, with populations of both effector and regulatory B cell subsets described. Cytokine

production by B cells is dependant on both the combination of activatory signals received by the cell, and the cytokine milieu present at the time of activation.

Work by Lund and colleagues has identified two distinct populations of effector B cells based on their patterns of cytokine production [58], with these distinct subsets able to influence T cell responses. Co-culture of murine B cells with either Th1 or Th2 cells *in vitro* results in the polarization of the B cell population to either a Be1 or Be2 subset, respectively, with the Be1 subset producing high levels of the Th1 cytokines IFNγ and IL-2, and the Be2 subset producing enhanced IL-4. These subsets have also been identified *in vivo* in mice infected with pathogens known to skew the system to a Type 1 or Type 2 immune response [58].

B cells constitutively secrete particular cytokine profiles, however cytokine production by B cells can also be altered by stimulation, with signals such as TLR stimulation [59] and the activation state of the cell influencing the cytokine profile [60], demonstrating the context dependant nature of cytokine production by B cells.

Populations of regulatory B cells (Bregs) have also been described, with the immunomodulatory effect of these cells mediated largely through their production of the anti-inflammatory cytokine IL-10. IL-10 inhibits $CD4^+$ T cell polarization, along with pro-inflammatory cytokine production and antigen presentation by professional APCs. Bregs have been shown to suppress inflammatory responses in multiple disease models, including experimental autoimmune encephalitis (EAE) [61], collagen induced arthritis (CIA) [62] and colitis [63].

1.5.3 B cells in Autoimmunity

B cells play vital roles in helping to rid the body of invading pathogens, however if the delicate balance of the immune system is disrupted, and self-tolerance is broken, B cells can contribute to the pathology seen in autoimmunity. Auto-antibodies can be detected in patients with a variety of autoimmune diseases, including systemic lupus erythematosus (SLE) [64] and rheumatoid arthritis (RA) [65]. Auto-reactive B cells process and present self-antigens, driving autoimmune T cell responses [66]. Dysregulated patterns of cytokine production are seen by B cells from patients with autoimmunity, with enhanced production of pro-inflammatory cytokines and diminished anti-inflammatory cytokine secretion [67,68].

1.5.3.1 B cells in Rheumatoid Arthritis

The efficacy of Rituximab (RTX), a B cell depleting monoclonal antibody [69], in treating RA has definitively proven the involvement of B cells in the pathogenesis of disease. B cell involvement has also been shown to be crucial to several murine models of arthritis [54,70,71], and along with the clinical efficacy of RTX, this finding has renewed interest in B cells as a key player in RA pathogenesis. Although the involvement of B cells in RA pathogenesis is evident, the exact contribution of this population is unclear, with these cells are able to play several functional roles in the context of autoimmunity.

In RA, plasma cells produce autoantibodies including rheumatoid factor (RF) and anti-citrullinated peptides antibodies (ACPA). RA patients can be divided into subsets based on the presence or absence of autoantibodies, with 50-80% of RA patients having RF, ACPA, or both autoantibodies present in their sera [72]. RF is the classic autoantibody in RA and binds the constant region of Immunoglobulin G (IgG) molecules, however the presence of RF is not specific for RA [73], and a pathogenic role for RF in RA has yet to be identified. Infusion of RF from RA patients into healthy individuals is not able to cause even transient synovitis [74], indicating that these autoantibodies, at least by themselves, are not pathogenic. Although most ACPA positive patients are also positive for RF, ACPA are specific serological markers for RA and are increasingly being used for disease diagnosis [75]. ACPA occurrence can be seen several years before the onset of RA, and $ACPA^+$ patients differ from $ACPA^-$ patients in clinical disease phenotype, as well as their associations with environmental and genetic risk factors [76]. $ACPA^+$ disease is associated with increased joint damage, low remission rates, more severe disease course and a higher frequency of extra-articular disorders compared to $ACPA^-$ RA. The majority of genetic risk factors identified are associated with $ACPA^+$ disease, with confirmed $ACPA^+$ RA susceptibility genes including *PTPN22 and TRAF1/C5* [76]. These differences in genetic contributions to disease development underline the heterogeneity of RA, with $ACPA^+$ and $ACPA^-$ RA now considered distinct disease subgroups.

B cells also produce chemokines, including CXCL13 [77] and eotaxin-1 [78], and pro-inflammatory cytokines such as IFNγ, IL-4 and IL-6. These cytokines can provide non-specific help to bystander T cells, potentially adding to an environment already tipped toward autoimmunity. B cells also play a major role in the regulation of lymphoid tissue architecture through their ability to secrete lymphotoxin, a cytokine essential for the formation of lymphoid structures, including ectopic germinal centres, which can be seen in approximately 30% of RA patients.

B cells are also able to contribute to the T cell response in RA through the expression of co-stimulatory molecules crucial for T cell activation, such as CD80/86 and CD40, as well as their ability to act as APCs [reviewed in [79], supporting the activation of autoreactive T cells.

1.6 Rituximab

Rituximab, a genetically engineered chimeric monoclonal antibody (mAb) directed toward the B cell cell-surface antigen CD20, was approved by the Food and Drug Administration for treatment of refractory or relapsed non-Hodgkin's lymphoma in 1997. In 2001, an open label study was undertaken to assess the efficacy of Rituximab in the treatment of RA [80]. This study followed 5 patients with refractory RA for 12-17 months, with all RTX treated patients achieving the American College of Rheumatology 50% improvement criteria at 6 months post infusion. Following the success of this study several randomized, double-blind, placebo-controlled studies were undertaken

[81-83], all of which demonstrated the value of RTX as a treatment for RA. In 2006 RTX was approved for the treatment of adult patients with active RA who have had an inadequate response to anti-TNF therapy [84], and to date is the only selective B cell depleting agent approved for use in this autoimmune disease.

CD20 is a transmembrane phosphoprotein that belongs to the MS4A family of proteins [85] and is expressed on all cells of the B cell lineage except pro-B cells and plasma cells. CD20 is involved in many cellular signalling events including proliferation, activation, and differentiation, and on cross-linking results in apoptosis of the cell [86]. CD20 is an attractive target for B cell depletion as it is stable and highly expressed on B cells, is lineage specific, and does not circulate in the plasma as a free protein. As a result of this, the majority of new B cell depletion therapies under development are also targeted toward CD20, such as Tositumomab (B1), a murine IgG2a monoclonal antibody approved by the FDA in 2003 for the treatment of follicular non-Hodgkin lymphoma [87].

1.6.1 Mechanisms of B cell Depletion

Several mechanisms contribute to B cell depletion after RTX treatment: antibody-dependent cellular cytotoxicity (ADCC), complement-dependent cytotoxicity (CDC) and programmed cell death/apoptosis. Interactions between the Fc portion of the RTX and Fc receptors (FcRs) expressed on effector cells result in antibody-dependent cellular cytotoxicity (ADCC), a mechanism vital to the efficacy of RTX [88]. CDC has also been

shown to play a crucial role in RTX-mediated B cell depletion [89], however, the relative contribution of programmed cell death (PCD) following the binding of CD20 by RTX is disputed.

1.6.1.1 Antibody-Dependent Cellular Cytotoxicity

FcRs are expressed on a variety of effector cells including monocytes, macrophages, and NK cells. RTX is a chimeric antibody consisting of murine heavy and light chain variable regions and a human IgG1 constant region [reviewed in [90], and can be bound by members of the Fc-gamma receptor (FcγR) sub-family. When RTX interacts with CD20 on the surface of B cells the Fc region is able to associate with FcγRs on effector cells, with destruction of the opsonised B cell, either by phagocytosis or the release of toxic granules from the effector cell resulting [reviewed in [91].

Studies using tumour cell lines and human tumour models have demonstrated that anti-CD20 antibodies trigger ADCC both *in vitro* and *in vivo* [92]. However, a paper by Harjunpaa et al highlights the need for caution in extrapolating results gained in tumour cell lines to other cell lines, or indeed primary B cells. On *in vitro* co-culture of phorbol myristate acetate (PMA) activated peripheral blood leukocytes (PBL) and HF-1.3.4 lymphoma cells, enhanced lymphoma cell lysis is seen on addition of RTX [93]. However when Raji lymphoma cells were included in the cultures in place of the HF-1.3.4 cells, comparable levels of ADCC were seen to occur in the presence and absence of RTX [93].

Allelic polymorphisms of FcγRIIIa have been suggested as a determining factor for RTX efficacy [94]. It has been found that patients with the FcγRIIIa receptor 158V allotype, where valine (V) is encoded at the amino acid position 158 rather than phenylalanine, have a greater probability of experiencing a clinical response after RTX treatment for non-Hodgkin's lymphoma. This has led to the postulation that given the right polymorphism there is increased ADCC activity against lymphoma cells, suggesting that ADCC is an important mechanism of B cell depletion *in vivo*, at least in the setting of lymphoma. However the authors of the study point out that the association between the FcγR polymorphism and clinical response may be due to another genetic polymorphism in linkage disequilibrium with the *FCGR3A* gene.

1.6.1.2 Complement Dependent Cytotoxicity

The IgG constant region of RTX allows the antibody to be bound by complement proteins *in vivo*, making Rituximab highly effective at activating the classical pathway of complement [91]. This activation leads to the formation of membrane attack complexes

on the surface of RTX-opsonized B cells and subsequent cell lysis. The classical complement pathway also generates C3b proteins, which directly bind to, and opsonise B cells, resulting in phagocytosis and destruction of the cell.

The expression of complement-regulating proteins, such as CD59, has been associated with resistance to anti-CD20 therapy in some studies, with CD59 expressing cell lines shown to be resistant, either fully or partially, to RTX induced CDC *in vitro*, whereas $CD59^-$ cell lines are susceptible to CDC-mediated cell death [95]. Treatment of the CD59 expressing ARH-77 cell line with anti-CD59 neutralizing antibody significantly increases CDC *in vitro* [95], with similar results seen in a range of lymphoma cell lines [93]. Other studies however, have found that the expression of complement-regulatory proteins does not relate to the outcome of treatment with RTX. Weng and colleagues analyzed the expression of the complement inhibitors CD46, CD55 and CD59 on pre-treatment tumour cells in 29 patients who were then treated with Rituximab. No significant difference was seen in the levels of pre-treatment complement inhibitors expressed in any of the response groups (full, partial or non-response to treatment), demonstrating that complement inhibitor expression does not necessarily predict clinical outcome after RTX treatment [96], contradicting evidence that CDC is a major mechanism of RTX action. Furthermore, effective B cell depletion with anti-CD20 antibodies has also been observed in mice with genetic deficiencies in the complement proteins C3, C4 and C1q, [88] and anti-CD20 antibodies engineered with mutations in the Fc region to prevent C1q binding were no more or less effective at depleting B cells *in vivo* than their non-mutated counterparts [97].

However, a study by Meerten et al examining the relative contributions of ADCC and CDC in RTX-mediated depletion may explain these conflicting results. Peripheral blood monocytes were co-cultured with a human CD20 (hCD20) expressing T cell line, CEM-CD20, in which the expression levels of hCD20 can be altered, and RTX in the presence or absence of serum. Serum contains complement proteins, and therefore in the presence of serum both ADCC and CDC will take place, whereas in the absence of serum CDC will be inhibited. Using this experimental set up the authors were able to demonstrate that cell sensitivity to CDC correlates to the level of CD20 expression by a cell, with those cells not sensitive to CDC being cleared by ADCC and vice versa [98].

1.6.1.3 Programmed Cell Death (Apoptosis)

CD20 has been postulated to play a role in B cell survival [86], and it is thought that binding of anti-CD20 antibodies to CD20 molecules on the cell surface could initiate cell-signalling cascades, affecting several signalling pathways, and ultimately result in

B cell apoptosis. It has been suggested that CD20 molecules are indirectly associated with src-family kinases due to their constitutive association with lipid rafts in the cell membrane, and on cross-linking with anti-CD20 antibodies trans-activation of the src-kinases can occur initiating signalling cascades ultimately resulting in apoptosis [99] (Figure 1.1). However, the importance of programmed cell death as an *in vivo* mechanism of RTX-mediated B cell depletion is still disputed.

Studies have been undertaken utilising hCD20 x VavBcl-2 double transgenic (tg) mice, an "apoptosis resistant" mouse model with B cells that express human CD20, enabling the direct investigation of RTX rather than a mouse homologue. Beers and colleagues demonstrate that B cells from this mouse strain are no less susceptible to RTX-mediated B cell depletion than non-resistant hCD20tg targets [100], indicating that the induction of apoptosis is not a key effector mechanism of B cell depletion. However, other investigators have shown that the anti-apoptotic factor Bcl-2 is down-regulated in multiple tumour cell lines on treatment with Rituximab *in vitro* [101]. Although these results may be due to the use of tumour cell lines and therefore are not transferable to normal B cells *in vivo*, other studies also dispute the claim that apoptosis is not a mechanism of B cell depletion. RTX has been shown to up-regulate the expression of Raf-1 kinase inhibitor (RKIP), a negative regulator of two major cell survival pathways: the NFκB and ERK1/2 pathways, in Ramos and Daudi cells, leading to the down-regulation of the anti-apoptotic protein Bcl-xl [102,103], and the sensitization of these cells to apoptosis. In a study by Byrd et al reductions in the levels of certain anti-apoptotic factors were noted in patients with chronic lymphocytic leukaemia after treatment with RTX [104]. No changes in the levels of Bcl-2 or Bax were observed in this study, however the levels of two other anti-apoptotic proteins, Mcl-1 and XIAP, diminished notably after treatment [104]. These finding support the idea that apoptosis plays a role in B cell depletion by Rituximab, and could explain why Beers et al saw no change when modulating the expression of Bcl-2, as this particular anti-apoptotic factor may not be involved in the pathway of apoptosis initiated by anti-CD20 infusion. *In vivo* activation of caspase-9, caspase-3 and cleavage of poly(ADP-ribose) polymerase (PARP) have also been observed in chronic lymphocytic leukaemia patients treated with RTX, indicating activation of the mitochondrial pathway of apoptosis in RTX-induced B cell depletion.

1.6.2 Clinical Efficacy of Rituximab in Autoimmunity

Many of the suggested mechanisms for the efficacy of RTX as a treatment for autoimmune diseases centre on the depletion of pathogenic B cells, with the removal of

these inflammatory effectors directly helping to return immunological balance to a system otherwise tipped to autoimmunity.

It was initially hypothesised that the depletion of autoreactive B cells would lead to a reduction in the serum autoantibody titre of patients and an improvement of disease. However, it has since been seen in multiple studies there is little correlation between changes in titres of autoantibodies and disease activity, with this finding true of both RA [81] and SLE [105]. In RA, titres of RF, a well-recognized prognostic factor for aggressive disease [69], can decrease within the first few weeks after RTX treatment [81], however, as a pathogenic role for RF has yet to be elucidated, this reduction in serum levels cannot definitively be said to account for the clinical outcomes seen after RTX treatment. RTX treatment has also been shown to be effective in RA patients who are RF sero-negative [82], and so it may be hypothesised that the reduction of RF on treatment with Rituximab cannot be responsible for RTX efficacy in RA.

Studies in animal models however have highlighted a direct role for the removal of pathogenic B cells in the amelioration of symptoms in autoimmunity. B cell depletion has been shown to suppress disease in a mouse model of proteoglycan-induces arthritis by lessening the autoantibody response and reducing the numbers of autoreactive T cells present [71], underlining a role for pathogenic B cells as APCs during autoimmune responses. Work by Barr et al has demonstrated that the removal of IL-6 producing pathogenic B cells by B cell depletion therapy is responsible for the improvements seen after treatment in a multiple sclerosis model [68], highlighting the role of B cells as potent cytokine producing cells, with their production of pro-inflammatory cytokines able to contribute to disease pathology.

Several theories focusing on the indirect effects of RTX treatment on the immune system, rather than the removal of pathogenic B cells, have also been put forward. In the 'immune complex decoy hypothesis', Taylor and Lindorfer have suggested that the therapeutic efficacy of RTX treatment may be due to the recognition of RTX-opsonized B cells as immune complexes by FcγR-expressing effector cells *in vivo* [106]. The authors postulate that the formation of large numbers of these RTX-B cell immune complexes in the blood and lymphatic system would divert FcγR-expressing effector cells (i.e. monocytes, macrophages and neutrophils) away from interacting with inflammatory immune complexes deposited in inflamed tissues, resulting in the reduction of tissue damage.

Another theory, put forward by Silverman and Boyle in 2008, is the 'B cell roadblock hypothesis' [107]. This theory attributes the clinical efficacy of RTX to the blockade of

B cell trafficking. The authors propose that by ridding the system of pathogenic B cells, additional memory B cells are not able to enter the joint to promote the on-going inflammatory response, resulting in the gradual clinical improvement seen on RTX treatment. However, this hypothesis does not explain why the clinical effects of RTX treatment can in some cases be seen long after B cell repopulation, as following this line of thinking, pathogenesis should re-occur on B cell return. It has also been noted in multiple studies that not all joint B cells are necessarily depleted on RTX infusion [108,109], observations which also conflict with Silverman and Boyle's proposed theory.

Although several ideas have been presented as to the method by which RTX exerts its clinical efficacy, it is still not fully understood why the depletion of B cells with RTX alleviates RA disease symptoms.

1.7 Cell Death

Cell death is an essential biological process that is involved in a wide range of physiological processes, from embryogenesis and steady state tissue turnover, to lymphocyte clonal deletion and the resolution of immune responses. Many forms of cell death have been described [110], with apoptosis, necrosis, and autophagy comprising the most extensively studies forms of cell death. Cells are classified into these categories based on the morphological and biochemical features observed on cell death, and their subsequent interactions with phagocytes.

1.7.1 Necrosis

Necrosis occurs as a consequence of tissue damage or extreme cellular stress, and was originally thought to be an uncontrolled, passive form of cell death. However, more recent evidence has shown that under certain conditions programmed necrosis can take place, resulting in a form of regulated cell death devoid of the activation of caspases, a family of specialized proteases critical to apoptotic cell death [reviewed in [111].

Necrosis is morphologically characterized by a gain in cell volume and the swelling of cellular organelles, coupled with lysosomal leakage, and the loss of membrane integrity resulting in the release of intracellular contents. Clearance of necrotic cells is slower and less efficient than that of apoptotic cells, occurring after the release of intracellular material from the dying cell [112]. This release of intracellular material is often accompanied by the release of pro-inflammatory cytokines and endogenous danger signals, known as DAMPs (damage-associated molecular patterns), including heat shock proteins (HSP) [113], uric acid, nucleotides (RNA and DNA), and the chromatin

protein HMGB1 (high-mobility group box 1) [114]. The presence of DAMPs can initiate inflammation in the absence of infection, and as such, necrosis is generally classed an immunogenic form of cell death. However, this is not always the case. Work by Miles et al has shown that during both necrotic and apoptotic cell death human neutrophils release α-defensins, small anti-inflammatory peptides, with these peptides able to inhibit the secretion of pro-inflammatory cytokines from macrophages [115]. The anti-inflammatory properties of necrotic neutrophils *in vivo* has also been demonstrated, with administration of necrotic neutrophil supernatant able to protect mice from a model of peritonitis [115]. These findings reveal that the idea of necrosis as a purely inflammatory form of cell death is not necessarily accurate in all circumstances.

1.7.2 Apoptosis

Apoptosis is a controlled and highly regulated form of cell death. It is an active process, requiring energy in the form of ATP, and is characterized by specific morphological changes including cleavage of chromosomal DNA, nuclear condensation and fragmentation, and the formation of apoptotic bodies [reviewed in [116]. Although morphologically similar, apoptotic cell death describes a heterogeneous group of biochemical and functional forms of death, with activation initiated by two separate but overlapping pathways, the 'extrinsic' and the 'intrinsic' pathway.

The extrinsic pathway of apoptosis is initiated in response to external stimuli received by the cell (Figure 1.1). Extrinsic signals include the ligation of pro-apoptotic cell-surface receptors, such as Fas (CD95), TNFR1 (tumour necrosis factor receptor 1), or TRAIL (TNF-related apoptosis-inducing ligand). Ligation of these receptors initiates the activation of specialised proteases called caspases, with the cleavage of procaspase-8 into its active form initiating a cascade of proteolytic activity, resulting in the activation of the effector caspases 3, 6 and 7, along with a range of other degradative enzymes. These enzymes cause the breakdown of integral cell components, including but not limited to: nuclear lamins, which are fibrous proteins required for function of the nucleus; enzymes involved in DNA repair, such as PARP; and cytoskeletal proteins, leading to the breakdown of the cell and ultimately cell death.

The intrinsic pathway is initiated from within the cell itself in response to cellular stress, such as cellular starvation, growth factor depletion, increased cellular calcium concentration or DNA damage (e.g. from ionizing radiation or chemotherapeutic agents). This pathway of apoptosis involves the mitochondria of the cell, and is also referred to as the 'mitochondrial pathway' of apoptosis. Pro-apoptotic members of the Bcl-2 family of proteins migrate to the surface of the mitochondria forming

mitochondrial apoptosis-induced channels (MAC), releasing cytochrome *c* into the cytoplasm. Cytochrome *c* then binds to other cytoplasmic proteins to form the apoptosome and this protein complex goes on to activate caspase-9, an initiator caspase, which induces the same cascade of events as the extrinsic pathway of apoptosis, resulting in the death of the cell.

The formation of apoptotic bodies or blebs is a common feature of both pathways of apoptosis, preventing the release of intracellular matter into the surrounding environment. These apoptotic bodies, along with non-fragmented apoptotic cells, express specific 'find-me' and 'eat-me' signals (see section 1.8), recruiting phagocytes and resulting in their rapid clearance from the system, with uptake generally occurring in the absence of pro-inflammatory responses (see section 1.9).

1.7.3 Autophagy

Autophagy is the process by which a cell recycles its cellular components, and is considered to primarily be a survival mechanism up-regulated in response to stress conditions, however it is also postulated to be an alternative cell death pathway. Autophagy is a catabolic process, starting with the formation of a flat isolation membrane that surrounds a portion of the cytoplasmic material, forming an autophagosome. The autophagosomes then undergoes maturation, culminating in its fusion with lysosomal vesicles, where they deliver their contents, ready for degradation. The catabolites are then transported back into the cell's cytoplasm, ready for incorporation into new cellular components. Autophagy can be sub-dived into three forms, dependent on the mode of delivery of the autophagosome's contents to lysosomes: macroautophagy, microautophagy [reviewed in [117] and chaperone-mediated autophagy [reviewed in [118].

Autophagy is known to play important roles in embryonic development and tissue remodelling, however its role in cell death is disputed. Several studies have shown that autophagic cell death occurs under conditions in which apoptosis is inhibited [119,120], with *ex vivo* studies using cells from apoptotic-resistant $Bax^{-/-}Bak^{-/-}$ mice showing that the knockdown of essential autophagy gene products protects these cells from chemotherapeutic-induced death [120]. A more recent study by Petrovski et al has shown that the human breast cancer cell line, MCF-7, undergoes autophagic cell death in response to prolonged exposure to continued cell starvation with the clearance of autophagic cells resulting in distinct transcriptional responses in phagocytes [121], with these findings indicating autophagy is in fact a distinct form of cell death. However, other studies have shown that inhibition of autophagy, through various mechanisms,

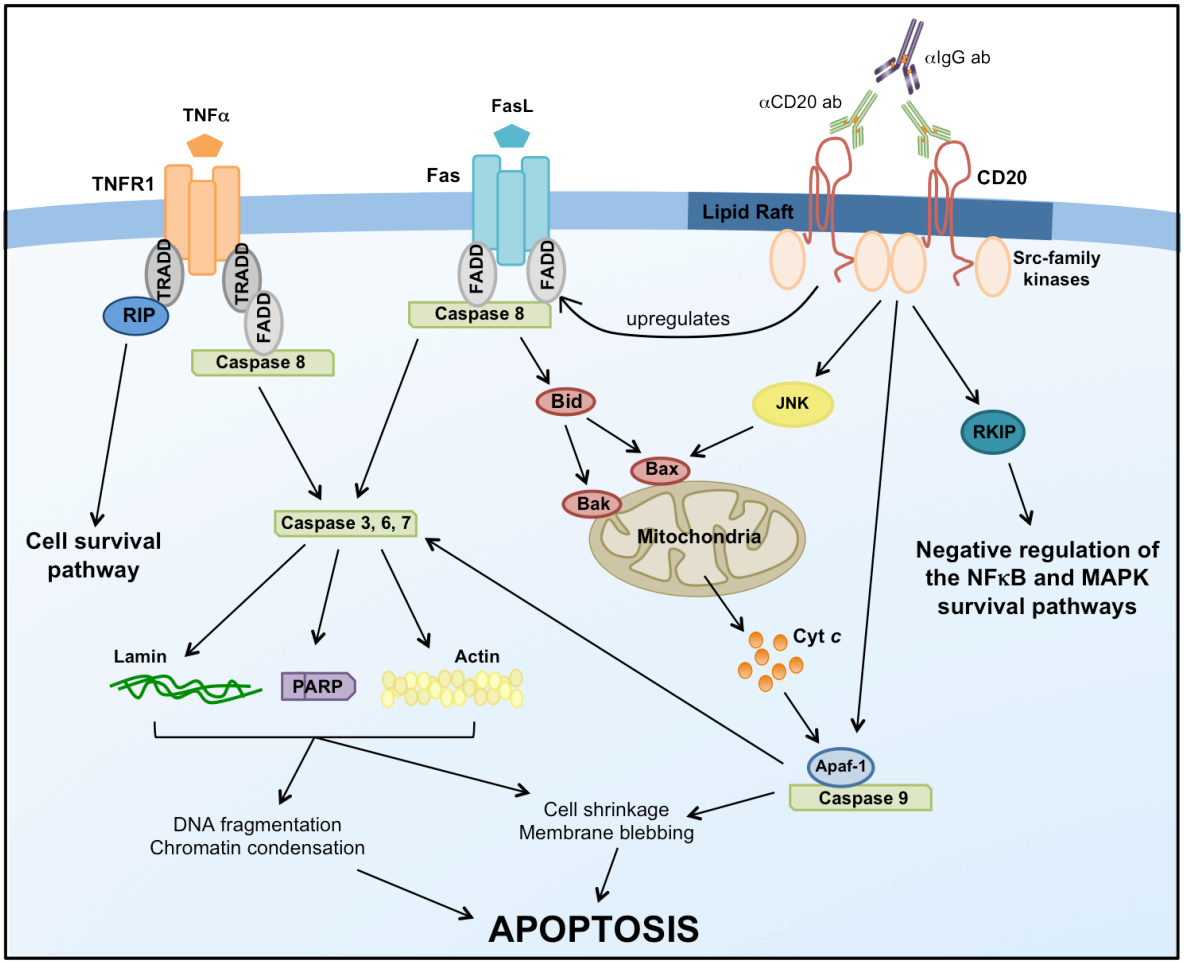

Figure 1.1 Schematic showing a selection of the apoptotic pathways in B cells.
Apoptosis can be triggered through a variety of mechanisms including ligation of cell surface receptors, such as Fas (CD95) and TNFR1, two prototypical apoptosis inducers. Ligation of these receptors initiates the activation of caspases. Cleavage of procaspase-8 into active caspase-8 initiates a cascade of events, resulting in the activation of the effector caspases 3, 6 and 7, along with a range of other degradative enzymes. These enzymes cause the breakdown of integral cell components (e.g. nuclear lamins, DNA repair enzymes such as PARP, and cytoskeletal proteins), resulting in the death of the cell. Caspase 8 can also activate pro-apoptotic proteins belonging to the Bcl-2 family, leading to cytochrome *c* release from the mitochondria and activation of caspase-9, and effector caspases, also ultimately resulting in cell death. It has been shown that CD20 molecules constitutively associate with lipid rafts in the cell membrane, and on cross-linking with anti-CD20 antibodies can initiate cell-signalling pathways ultimately leading to apoptosis of the B cell.

results in an increased rate of cell death [122,123], suggesting that autophagy may indeed be a pro-survival mechanism activated by dying cells in the attempt to cope with sub-optimal conditions, prior to cell death.

1.8 Recognition and Ingestion of Apoptotic Cells

Cells undergoing apoptosis are recognized by professional phagocytes (Figure 1.2), such as macrophages and immature DCs and rapidly engulfed, with the clearance of apoptotic cells (AC) without stimulation of the immune system crucial to the maintenance of peripheral self-tolerance.

Phagocytes are able to recognise AC via the expression of a range of PRRs, which along with the recognition of PAMPs, are able to detect changes in the composition of the plasma membrane of the AC. These changes are collectively termed 'ACAMPs' (apoptotic cell-associated molecular patterns) [reviewed in [124], or 'eat-me' signals. Coupled with the exposure of neo-epitopes by the AC, the down-regulation of a range of 'don't eat-me' signals normally expressed by healthy cells further encourages the rapid uptake of these dying cells by phagocytes. A number of soluble 'bridging molecules' are also involved in phagocyte binding of AC, adding a further layer of complexity to the process.

One of the most well characterized ACAMPs is the exposure of phosphatidylserine (PS) on the outer leaflet of the AC plasma membrane [125]. This change in membrane composition occurs very early in the apoptotic process and is an essential 'eat-me' signal involved in AC uptake [125], with multiple receptors and bridging molecules involved in its recognition. Fadok et al found that phagocytes could directly bind PS via specific phosphatidylserine receptors [126], however it is only more recently that the details of the receptors for PS have been elucidated, with multiple PR receptors now identified. The T cell/transmembrane, immunoglobulin, and mucin (TIM) proteins TIM-1, TIM-3 [127] and TIM-4 [128] have been shown to specifically bind PS exposed on the surface of AC in both humans and mice. These proteins differ in their expression patterns, with TIM-3 and TIM-4 expressed on phagocytic APCs and involved in AC uptake and cross-presentation of antigens [129]. Other PS receptors have also been identified, including CD300a in humans [130]; and RAGE (receptor for advanced glycation end-products) [131], Stabilin-2 [132], and brain-specific angiogenesis inhibitor 1 (BSAI1) [133] in mice. Work by Park et al has shown that BSAI1 binds directly to PS via thrombospondin type 1 repeats in its extracellular region, mediating AC engulfment by

macrophages both *in vitro* and *in vivo* [133]. Over-expression of BSAI1 in the J774 macrophage cell line results in the enhanced uptake of apoptotic thymocytes *in vitro,*

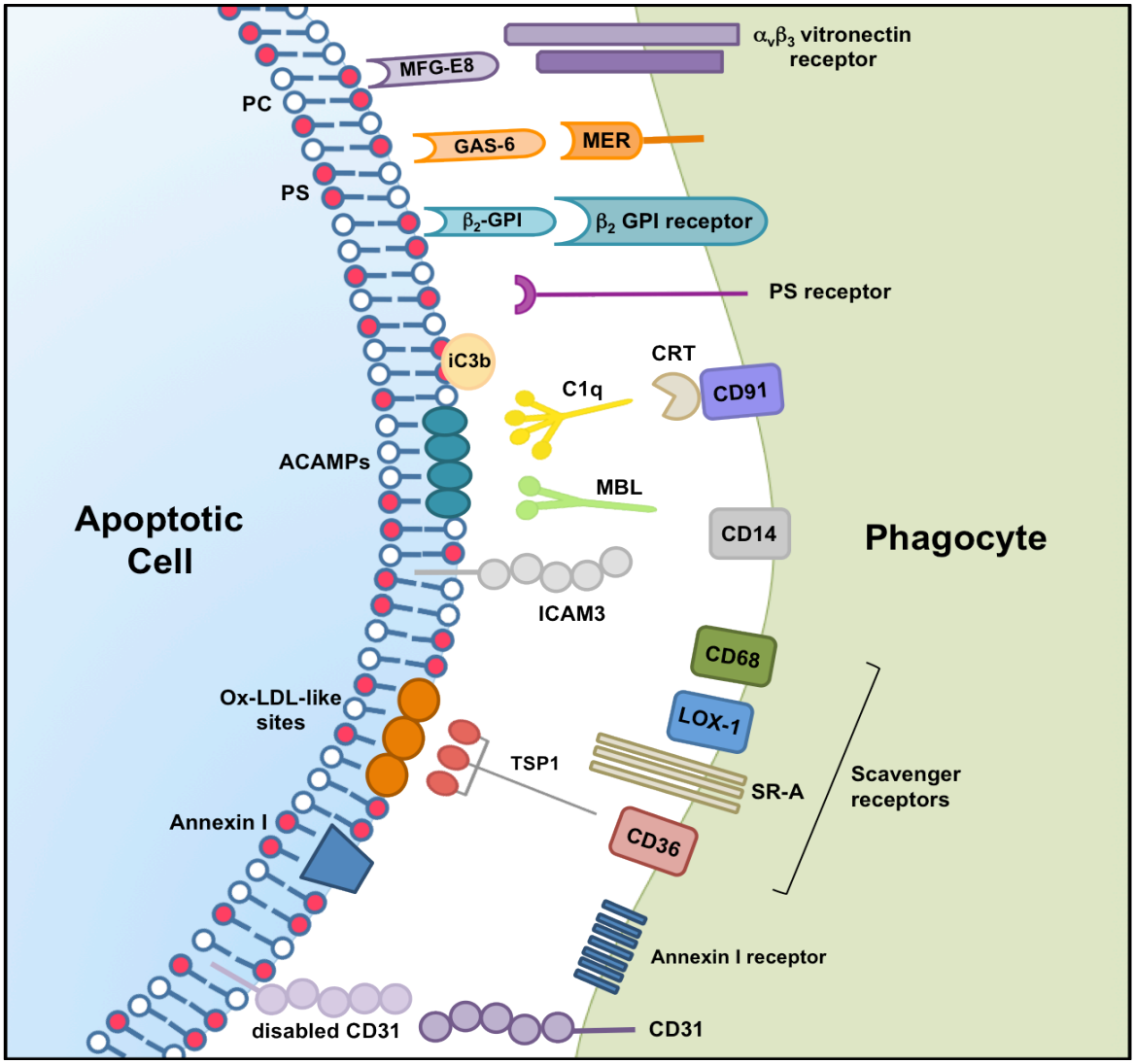

Figure 1.2 Schematic detailing the molecules involved in the binding and uptake of apoptotic cells by phagocytes.
Apoptotic cells expose PS (phosphatidylserine) on their outer surface, with the associated PC (phosphatidylcholine) internalization. PS is recognized by PS receptors directly, and the adapter molecules MFG-E8, GAS-6 and β2-GPI, with MFG-E8 then recognized by the αvβ3 integrin (vitronectin receptor), GAS-6 by MER family members and β2-GPI recognized by the β2-GPI receptor. In the presence of complement AC become opsonized with iC3b, which is subsequently bound by C1q. Binding of C1q by CD91 molecules on phagocytes is mediated by CRT (Calreticulin). It has been suggested that modification of surface antigens on AC results in the formation of conserved molecular patterns, termed 'ACAMPs' (apoptotic cell associated molecular patterns), leading to their recognition by phagocytes via collectins such as mannose-binding lectin (MBL). CD14 binds MBL, along with modified ICAM-3 (intercellular molecules adhesion molecule 3) expressed on the surface of AC. A variety of scavenger receptors are involved in AC adhesion and uptake, with newly formed Ox-LDL-like sites on the AC recognized either directly or through the use of adaptor proteins such as thrombospondin (TSP-1). On exposure of PS on the AC surface, Annexin I is also exposed, allowing recognition by Annexin I receptors expressed by phagocytes. Along with expression of apoptotic markers, the viable cell marker CD31 is de-activated, with disabled CD31 unable to induce cellular release by phagocytes on homotypic adhesion with active CD31.

while simultaneous i.p. injection of AC and BSAI1 blocking proteins into mice effectively inhibited AC phagocytosis by peritoneal macrophages [133].

Soluble bridging molecules allow additional, indirect recognition of PS by phagocytes. Milk-fat globule EGF factor 8 (MFG-E8) is a protein secreted by subsets of phagocytes, including activated macrophages [134]. It is able to bind PS via its C-terminal region and associates with the integrins $\alpha_v\beta_5$ and $\alpha_v\beta_3$ (the vitronectin receptor) on phagocytes [135], stimulating the engulfment of AC [134]. Growth-arrest specific 6 (GAS-6) is an abundant plasma protein that can bind to PS, with the closely related protein S also able to act as a bridging molecule during PS recognition [136]. Both Gas-6 and protein S are recognised by tyrosine-kinase receptors belonging to the TAM family, including Tyro3, Axl and Mer, with studies in mice that have a functional Mer knock-out have been shown to develop an SLE-like autoimmunity [137]. The serum protein, β2-glycoprotein I (β2GPI) has also been shown to bind to PS expressed on AC [138], however the specific β2GPI-receptor expressed by phagocytes is still not clear, with members of the LRP (lipoprotein receptor-related protein) receptor family indicated [139].

Although a key marker of apoptotic cells, several studies have suggested that PS exposure alone is not sufficient to induce AC uptake by phagocytes, and the recognition of other ACAMPs in conjunction with PS is needed to initiate AC uptake. Although this has not been conclusively shown, the modification of existing surface antigens does occur on AC, resulting in the generation of neo-epitopes, with these epitopes also detected by phagocytes during uptake.

Collectins, such as MBL (mannose-binding lectin), SP-A (surfactant protein A), SP-D (surfactant protein D) and the complement component C1q bind neo-epitopes expressed to the surface of late apoptotic cells, termed ‘collectin-binding sites’ [reviewed in [140]. Opsonization of AC by collectins promotes their uptake through subsequent interaction with the low-density lipoprotein (LDL)-receptor-related protein (LRP-1/CD91) and calreticulin (CRT) on the surface of phagocytes [141]. The binding of pentraxin-related C-reactive protein (CRP) to AC in parallel with C1q inhibits activation of the complement cascade by preventing the formation of the membrane-attack complex on the apoptotic cell surface [142], avoiding the initiation of pro-inflammatory responses toward AC antigens.

There is some evidence that that oxidation of the AC surface is an important component of their recognition by phagocytes [143], with the formation of oxidized low-density

lipoprotein (ox-LDL)-like sites on AC, detected as 'altered-self' by phagocytes. Recognition can be direct, through a variety of receptors including the scavenger receptors SR-A (scavenger receptor A) [144], CD68 [145], and LOX-1 (oxidized low-density lipoprotein-1) [146], or via the bridging molecule thrombospondin (TSP-1). The binding of TSP-1 enables indirect recognition by additional phagocytic scavenger receptors, such as the class-B scavenger receptor CD36 and the vitronectin receptor [147], with TSP-1 also able to bind to as-yet undefined neo-epitopes on the AC, termed 'TSP-1 binding sites' [reviewed in [140], further promoting the uptake of AC by phagocytes.

Functional alterations in adhesion molecules have also been noted on AC. ICAM-3 (intercellular adhesion molecule 3/CD50) is a cell adhesion molecule constitutively expressed on all leukocytes [reviewed in [148], and is involved in immune regulation via its interactions with LFA-1 (leukocyte functional antigen 1). The ICAM-3 expressed by AC has a functionally altered first Ig-like domain [149], leading to a switch in binding preference from the prototypic receptor LFA-1, to an alternative macrophage receptor, mediating interactions between apoptotic leukocytes and macrophages [150]. Another cell adhesion molecule, PECAM-1 (platelet endothelial cell adhesion molecule/CD31) is also involved in the binding of phagocytes to AC, with CD31 expressed by both viable and apoptotic cells. Binding of viable cells by macrophages through the homotypic adhesion of surface CD31 initiates CD31-mediated signalling, leading to the active detachment of the viable cell [151]. In AC, this CD31-mediated detachment from macrophages is disabled, promoting their binding and subsequent uptake by phagocytes [151].

Along with changes in the specific cell surface molecules expressed by AC helping to mediate tethering and uptake by phagocytes, the spatial distribution of these molecules is likely to be involved in the differentiation between cell states, as well as the down regulation\functional inactivation of 'don't eat-me' signals expressed by viable cells. Integrin-associated protein (IAP/CD47) is a cell surface glycoprotein expressed by all hematopoietic cells [152], and has been characterized as a marker of self on murine cells [153], acting as a 'don't eat-me' signal. CD47 is bound by SIRPα (signal regulatory protein alpha) expressed on macrophages, DCs and neutrophils, and sends a negative engulfment signal to the phagocyte [153], preventing clearance of the cell. On apoptosis, cells down-regulate CD47 expression and are no longer able to stimulate SIRPα and the downstream inhibitory signals necessary to avoid phagocytic uptake [154]. Complement opsonization of AC also plays a key role in their recognition and clearance by phagocytes, with viable cells expressing a range of complement regulators,

which inhibit the binding of complement and opsonization of healthy self-cells. CD46 (membrane cofactor protein) is one such regulator, ubiquitously expressed on all nucleated cells. Expression of CD46 is lost on apoptosis, leading to the binding of the classical complement components C3b and iC3b, and promoting phagocytosis of the AC [155].

If AC are not cleared in a timely fashion they undergo secondary necrosis, resulting in the release of intracellular material into the surrounding environment and initiating pro-inflammatory responses. In certain circumstances, this can lead to a break in tolerance to intracellular self-antigens, and chronic pathology, such as in SLE [156].

1.9 Immune Modulation by Apoptotic Cells

Due to its role in development and homeostasis, apoptosis has traditionally been thought to be intrinsically non-immunogenic, however in the 1990s multiple groups demonstrated that the uptake of AC can actively suppress inflammatory responses [157,158]. Based on these findings, an extensive body of work has arisen demonstrating that the binding and engulfment of AC actively induces a range of anti-inflammatory responses by phagocytes, playing a key role in the resolution of adaptive immune responses under normal circumstances, and potentially able to re-introduce tolerance to the immune system. However, the view that apoptosis results purely in anti-inflammatory, tolerogenic responses, while necrosis results in pro-inflammatory responses, has been shown to be an oversimplification. Recent tumour vaccination studies have established that cells can either undergo immunogenic or non-immunogenic apoptosis depending on the apoptotic stimulus, with immunogenic AC able to stimulate an active antigen-specific immune response [159].

1.9.1 Immunogenic Apoptosis

The immunogenicity of apoptotic cells has been shown to be dependant on the early exposure of CRT on the AC surface [160]. CRT is a Ca^{2+}-binding chaperone that is usually located in the lumen of the endoplasmic reticulum (ER) [reviewed in [161]. Surface exposure of CRT defines immunogenic AC and acts as an immunogenic 'eat-me' signal for phagocytes [160]. Several cell death stimuli can induce the exposure of CRT and subsequent immunogenic apoptosis, including anthracyclins, UVC exposure and ionizing radiation. Immunogenic apoptosis has been most widely studied within the setting of cancer therapy, with the efficacy of many chemotherapeutics depending on the generation of antigen specific T cell responses.

A study by Albert et al looking into the cross-presentation of exogenous antigen by DC was one of the first to provide evidence that antigen-specific T cell responses can be generated after the acquisition of antigens from apoptotic cells [162]. Human DC cultured *in vitro* with apoptotic influenza-infected monocytes were able to acquire viral antigens from the AC and generate influenza-specific cytotoxic T cells that could effectively target infected DC [162]. Interestingly, in this system influenza-infected necrotic cells were unable to provide sufficient antigen to DC in order to prime influenza-specific cytotoxic T cell responses.

Further work has supported the idea of immunogenic apoptosis. Kotera et al have shown that the immunization of mice with DC pulsed with either apoptotic or necrotic B16-BL6 melanoma cells, resulted in the inhibition of melanoma growth [163]. CT26 colon cancer cells treated with anthracyclins are rapidly cleared by DC on injection into immunocompetent mice, resulting in the priming of anticancer T cell responses that are able to prevent the growth of live CT26 cells *in vivo* [164]. Injection of apoptotic RMA cells, a T cell lymphoma cell line, into C57BL/6 mice results in the induction of tumour-specific cytotoxic T cell responses [165]. Conversely, injection of necrotic RMA cells was unable to elicit tumour-specific responses [165], indicating that in this model apoptotic cells were more able to elicit inflammatory responses than necrotic cells.

These findings demonstrate that the dogma of apoptosis being a tolerogenic, anti-inflammatory process, unable to stimulate pro-inflammatory responses, is an oversimplification. However, in many situations this is seen to be the case.

1.9.2 Non-immunogenic Apoptosis

Billions of cells undergo apoptosis everyday in an individual without inciting inflammatory responses, demonstrating the non-immunogenic nature of physiologically occurring apoptosis. Investigation of the immunomodulatory capacity of AC has demonstrated that not only does non-immunogenic apoptosis occur without the stimulation of pro-inflammatory responses, but that the interactions of AC with phagocytes can actively exert anti-inflammatory effects on the system, affecting a wide variety of immune responses including cell maturation, antigen presentation and local cytokine production.

Maturation of DC is inhibited upon AC ingestion, preventing their development into competent antigen presenting cells. To become fully activated, T cells must recognize their cognate antigen in the context of MHC followed by a ‘signal 2’, delivered in the form of co-stimulation by the APC or the production of specific cytokines. Immature

murine DC are unable to upregulate the co-stimulatory molecule CD86 [166], after phagocytosis of AC, and show a diminished ability to produce pro-inflammatory cytokines such as IL-12 [166], resulting in a reduced capacity to stimulate T cell activation and subsequent adaptive immune responses.

Many studies have documented that the uptake of AC by phagocytes has potent anti-inflammatory effects on innate effector cells. *In vitro* co-culture of human monocyte-derived macrophages with AC results in the decreased production of pro-inflammatory cytokines, including IL-8, TNFα, and IL-1β, coupled with the increased production of the anti-inflammatory cytokine TGF-β [157]. Work by Chong et al has shown that human NK cell interaction with apoptotic Jurkat, PLB-985 or $CD4^+$ T cells results in increased TGF-β secretion *in vitro*, and that this TGF-β production is able to suppress the generation of IFNγ by stimulated NK cells [167]. AC can also have direct effects on the production of inflammatory mediators, with the binding and phagocytosis of AC able to inhibit pro-inflammatory cytokine gene transcription by macrophages, independent of subsequent AC engulfment [168]. This negative feedback response to AC helps to regulate unwanted inflammation and may contribute to immune contraction and the termination of immune responses.

Interaction with AC also effects the production of other immune mediators by macrophages. On co-culture with AC, macrophages increase production of the anti-inflammatory prostaglandin PGE_2 [157], with concomitant inhibition of pro-inflammatory eicosanoids and LPS-induced NO generation also seen [169].

The anti-inflammatory effects of AC have also been demonstrated *in vivo*. In a murine model of pneumonia, mice with genetic defects in macrophage apoptosis were shown to have enhanced recruitment of neutrophils to sites of lung inflammation and increased production of inflammatory cytokines, resulting in a greater degree of pulmonary inflammation [170]. In this model, intratracheal administration of apoptotic macrophages into the lungs was able to decrease the amount of local inflammation to levels comparable with wild-type animals [170]. Injection of AC into the peritonea or lungs of mice after induction of inflammation at these sites, has also been shown to reduce inflammatory infiltrates, as well as stimulate local TGF-β production, enhancing the resolution of inflammation [171]. Furthermore, in a murine model of arthritis, i.v. injection of apoptotic thymocytes protects mice from arthritis through the generation of IL-10-producing regulatory B cells [172], indicating the beneficial effects of AC administration in the context of autoimmunity.

Interestingly, in a large proportion of the studies looking into the immunosuppressive effects of AC, the apoptotic stimuli used should induce immunogenic apoptosis according to the reports into CRT exposure [134,160,164]. However, investigators have repeatedly demonstrated anti-inflammatory effects of the resultant AC populations. These findings indicate that exposure of CRT alone cannot fully account for the immunogenicity of AC, with other factors evidently involved in the generation of pro- or anti-inflammatory responses to AC. The activation state of the AC at time of death [173], the number of AC [165], the phagocyte involved in AC uptake [174], the presence of innate immune stimulation at the time of AC uptake [175], the release of soluble mediators by AC [176] and the cytokine milieu present at AC uptake [165], have all been implicated in the nature of the response to AC. However, in the majority of work looking into immunomodulation by AC, the concept of immunogenic vs. non-immunogenic apoptosis is not discussed, and these disparate finding are not addressed. Despite this, a considerable body of evidence supports the idea that AC are able to induce anti-inflammatory responses on binding/engulfment by phagocytes both *in vitro* and *in vivo*, and may have the potential to re-introduce tolerance to the immune system. The response of the immune system to AC is highly complex, and further work is needed to enable a better understanding of these processes and their regulation *in vivo*.

1.10 Hypothesis and Aims

We hypothesise that RTX treatment in autoimmunity, specifically focusing on RA, may re-introduce temporary tolerance to the immune system (Figure 1.3). If on treatment with RTX apoptosis of B cells is caused, the B cells will be phagocytosed by APC in a non-inflammatory context. The phagocytosed B cell, and any antigens it has internalized, will therefore be degraded and presented by the APC in a tolerogenic environment. If the B cell had previously taken up self-antigen, specifically the putative self-antigen the RA response is directed toward, presentation of this arthritogenic antigen in a non-inflammatory, tolerizing environment may result in the re-introduction of temporary tolerance to the RA system.

Li et al have explored the concept of using the *in vivo* production of AC to re-introduce tolerance to self-antigens in the context of autoimmunity, with a murine model of type 1 diabetes utilized [177,178]. In these studies, non-obese diabetic (NOD) mice were administered plasmid DNA vaccinations encoding a beta cell auto-antigen, glutamic acid decarboxylase (GAD), and the pro-apoptotic protein BAX. The vaccination induced the synthesis of GAD in target cells, followed by apoptosis of these newly self-antigen containing cells. The GAD-BAX vaccinated mice showed a significant reduction in diabetes onset compared to both untreated mice, and those treated with a vaccine

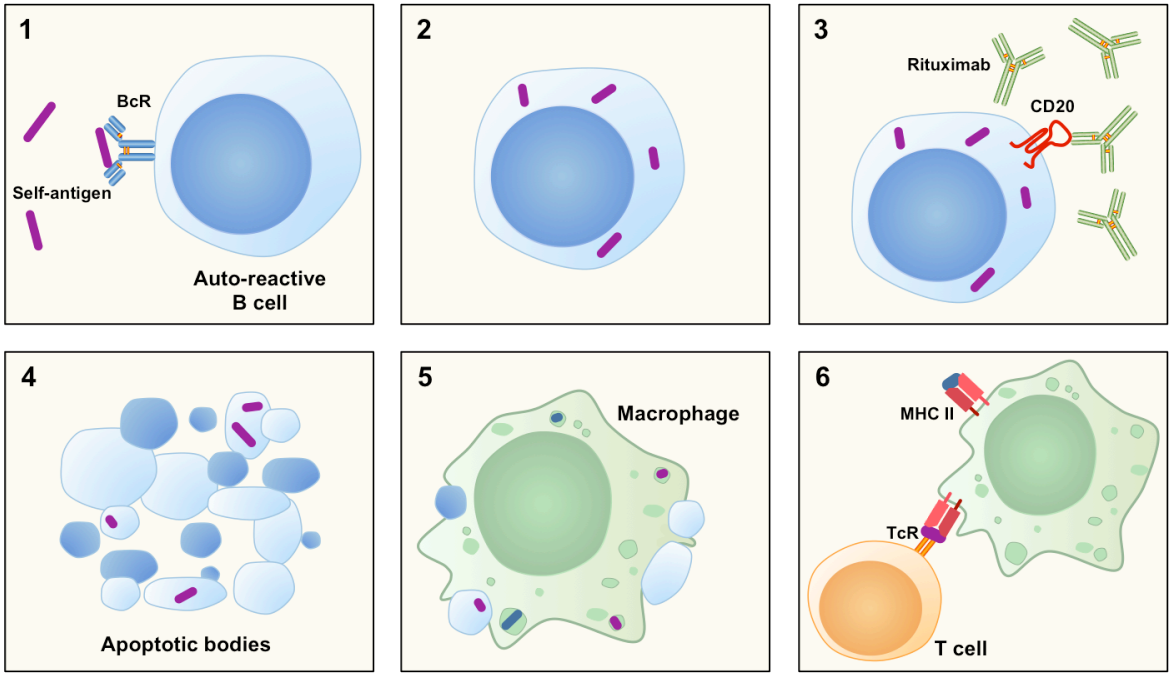

Figure 1.3 Schematic detailing our hypothesis: Rituximab-mediated B cell apoptosis helps to re-introduce tolerance to self-antigens in autoimmunity.
1-2. Autoreactive B cells encounter self-antigen and internalize it via their BcR. **3.** RTX binds to CD20 on B cells and induces cell death through apoptosis. **4.** The AC resulting from these autoreactive B cells contain fragments of previously internalized self-antigen. **5.** These AC cleared by macrophages, ingesting the apoptotic bodies and the self-antigen they contain. Phagocytosis of AC will polarize the macrophage to a regulatory/anti-inflammatory phenotype. **6.** The self-antigen taken will be processed and presented to T cells by the macrophage via MHC II. The presentation of self-antigen in an anti-inflammatory environment will result in T cell tolerization to the self–antigen, dampening down the inflammatory response seen in RA and introducing a temporary tolerance to the system.

containing GAD alone. The investigators showed that the GAD containing apoptotic cells were phagocytosed by DCs, and hypothesize that the uptake of auto-antigen containing AC by dendritic cells was able to re-introduce peripheral tolerance to the autoimmune system [177]. Further studies demonstrated that not only can this vaccine construct prevent disease onset, it is also able to ameliorate established diabetes in this mouse model, with 50% of NOD mice treated with the GAD-BAX vaccine subsequent to disease onset showing improvement of symptoms [178]. These studies, although undertaken in a diabetes model, prove that the uptake of apoptotic cells containing self-antigen is able to modulate the progression of autoimmune disease. As the self-antigen that the pathogenic response is directed toward in RA is still unknown, a vaccination approach could not be undertaken in this disease setting. However, the RTX-mediated induction of apoptosis in auto-antigen containing B cells, may have comparable effects on the immune system in RA, helping to re-establish tolerance in a system skewed toward inflammation.

The aim of the current study was to begin to unravel the possibility of this hypothesis. The role of apoptotic B cells and their immunomodulatory capacity was focused on, with the following questions specifically addressed:

1. Do apoptotic B cells have the same immunomodulatory capacity as other apoptotic lymphocytes?

2. Does Rituximab binding to B cells affect the way in which they interact with other cells of the immune system, both prior to cell death and after B cell apoptosis?

3. Are macrophages able to present antigen they themselves have not directly encountered, but that they have acquired as the result of the phagocytosis of apoptotic B cells?

4. Are apoptotic B cells (induced by either irradiation or RTX treatment) able to modulate inflammatory responses *in vivo*?

Chapter 2: Materials and Methods

2.1 Animals

2.1.1 Mouse strains

Human CD20 transgenic (hCD20tg) C57BL/6 mice and hCD20tg DBA mice were both bred in-house (Central Research Facilities, University of Glasgow, Glasgow, U.K.). Expression of the human CD20 gene was detected using polymerase chain reaction (PCR) (see 2.1.2), and wild-type (WT) littermates were used as controls. WT DBA1/J mice were purchased from Charles River. Homozygous C57BL/6 OT-II mice, which express T cell receptors (TcR) that recognise the ovalbumin (OVA) peptide 323-339 in the context of I-A^b, were used as T cell donors for *in vitro* assays (section 2.3.4). Age matched mice were used for all experiments. All animals were maintained under standard animal house conditions in accordance with local and home office regulations.

2.1.2 Genotyping of hCD20tg mice

Mice expressing the human CD20 gene were identified by genotyping of tail DNA using PCR. Mice were genotyped using two different primer pairs designed in-house, one specific for human CD20 *Exon* 2 (Forward: 5'-CACAAGGTAAGACTGCCAAAAATC-3', Reverse: 5'-ATATACAAGCCCCAAAACCAAAAG-3') and one for the *5' Bac* region (Forward: 5'-ATTGTTTGAGTGCTCAGCATG-3', Reverse: 5'-GGGAAAAACAATATTGCCTCC-3') (purchased from Integrated DNA Technologies). In detail, mouse tail-tips were lysed using Alkaline Lysis Buffer (see appendix) for 60 minutes at 95^oC. The DNA containing solution was then neutralized using an equal volume of Neutralization Buffer (see appendix). 10µl of this DNA solution was then readied for PCR by addition of Green Loading Buffer (Promega), the forward and reverse primers for the gene section being investigated, dNTP mix and Taq polymerase (both from Promega), following the manufacturer's instructions. The samples were then loaded onto a 2% Agarose gel, consisting of 2g Agarose dissolved in 100ml 1x TAE (see appendix), and run at 100 volts for 45-80min. A band of 100kbp for *5'Bac*, and 400kbp for *Exon 2*, indicated the presence of the hCD20 transgene.

2.1.3 Phenotyping of hCD20tg mice

The presence and expression pattern of the hCD20 protein was verified in mice identified as having the human CD20 transgene via PCR genotyping. Blood, spleen and LN single cell suspensions (see 2.2.1 and 2.2.2) were analysed via flow cytometry (see 2.5.1).

Cells were stained using readily available anti-human CD20 FACS antibodies, or with fluorescently labelled Rituximab (Genetech) (see Tables 2.2 and 2.3). Rituximab (RTX) was conjugated to the fluorochrome AlexaFluor-488, using an AlexaFluor-488 Protein Labeling Kit from Invitrogen, according to the manufacturers instructions. To label the protein, 2mg/ml RTX was diluted in a 1M bicarbonate solution (Invitrogen). The RTX mixture was then added to a vial of the AlexaFluor-488 (AF-488) reactive dye, and stirred for 1hr at room temperature (RT). The AF-488 labelled RTX (RTX-488) was then purified using the purification column provided, separating the RTX-488 conjugate from unincorporated dye. Once the fraction containing the RTX-488 conjugate had been collected, the absorbance of the conjugate solution was measured using a Nanodrop (Thermo Scientific), and the degree of labelling calculated following the manufacturer's instructions. The labelling resulted in a final ratio of 6.9M of dye per mole of antibody, falling within the optimal range of 4-9 moles of AF-488 per mole of IgG used.

2.2 Harvesting, preparation and culturing of cells

2.2.1 Preparation of single cell suspensions from secondary lymphoid organs

Mice were euthanized using an increasing concentration of carbon dioxide gas (CO_2), and the spleen, thymus and/or various lymph nodes harvested and placed in complete RPMI (cRPMI) medium (see appendix). Single cell suspensions were prepared by passing the organs through a 40µm cell strainer (VWR) into cRPMI using the plunger of a sterile 5ml syringe. The cell suspensions were made up to 5ml with complete RPMI, and centrifuged at 450g for 5min. Supernatants were poured off, and the cell pellet resuspended. LN cells were then resuspended in 2ml-10ml complete RPMI, without a red blood cell (RBC) lysis step being undertaken. To the splenocyte and thymocyte suspensions, 1ml of ACK lysis buffer (Gibco, Life Technologies) was added to the resuspended pellet to remove RBC contamination. The cells were left to incubate at RT for 1min, after which 10ml of cRPMI was added to stop the reaction, and the cells again centrifuged at 450g for 5min. The splenocytes and thymocytes were then resuspended in 10ml of cRPMI ready for counting. Cells were counted using a haemocytometer, with Trypan Blue (Fluka Analytical) staining used to identify viable cells. Cells were then resuspended at the desired concentration in the appropriate media ready for further use.

2.2.2 Preparation of single cell suspensions from blood

Blood samples were taken both from live mice, and directly after euthanization. For live animal blood samples, mice were bled from the tail vein, with up to 100µl of blood

collected in heparinised capillary tubes. For blood collection post-mortem, mice were euthanized using an increasing concentration of CO_2 and blood extracted directly from the vena cava into a syringe flushed with 0.25M EDTA. Blood samples were then processed in the same manner. An ammonium chloride solution (StemCell) was added at 10x the volume of the sample and incubated for 10min on ice to remove RBC contamination. cRPMI was then added to stop the reaction, the cells centrifuged at 450g for 5min, and resuspended in fresh cRPMI ready for counting. Cells were counted using a haemocytometer, with Trypan Blue (Fluka Analytical) staining used to identify viable cells. Cells were then resuspended at the desired concentration in the appropriate media ready for further use.

2.2.3 Preparation of bone marrow derived macrophages (BMDM)

Macrophages were prepared from the bone marrow of either WT littermate DBA mice or WT littermate C57BL/6 mice. Mice were euthanized and the hind legs removed for bone marrow (BM) harvesting. Under sterile conditions, the BM was flushed from both femurs and tibias using a 5ml syringe filled with cRPMI. To break up any clumps of BM the cell suspension was repeatedly taken up and pushed out of the syringe. The cell suspension was then passed through a 40µm cell strainer (VWR), washed in cRPMI, centrifuged and counted as described in 2.2.1. For the generation of L929 BMDM the BM cells were plated at a concentration of $6x10^6$ – $8x10^6$ cells per 9cm petri dish, in cRPMI supplemented with 20% L929 cell supernatant (see 2.2.5.), which was 2x sterile filtered before addition to *in vitro* BM cell cultures. For the generation of GM-CSF BMDM, $10x10^6$ BM cells were plated at a concentration of $1x10^6$ cells/ml in cRPMI supplemented with 5ng/ml recombinant murine GM-CSF and 5ng/ml murine IL-3 (both from Peprotech). On day 3 the BMDM were given 5ml additional supplemented media. All BMDM were used 6-7 days after isolation. To remove the adherent BMDM from the petri dishes, all media was removed, non-adherent cells washed off, and ice cold PBS added to the plates. This was left for 1min and the cells then scraped off using a cell scraper. The resultant cell suspension was collected, washed, and resuspended in cRPMI ready for counting and subsequent use.

2.2.4 Isolation of peritoneal macrophages

Primary macrophages were isolated from the peritoneal cavity of WT littermate C57BL/6 mice. Mice were euthanized, and 7ml of PBS + 2mM EDTA was injected into the peritoneal cavity through the peritoneal membrane. The abdomen of the mouse was then massaged to encourage the detachment of peritoneal macrophages from the internal surface of the membrane, and the solution taken up into a clean syringe. The

cells were washed with cRPMI, centrifuged at 450g for 5min, resuspended in 5ml cRPMI and counted ready for use.

2.2.5 Culture of the L929 cell line

The L929 cell line is a murine fibrosarcoma cell line that secretes M-CSF into its cell culture supernatant [179]. This supernatant can then be used to supplement cell culture media to induce the growth and development of murine bone marrow derived macrophages (see 2.2.3).

To generate the L929 supernatant, L929 cells were cultured in 100ml cRPMI in T150 flasks (Corning) until they reached confluence, and then for a further 4 days to allow a build up of M-CSF in the supernatant. The M-CSF-enriched media was then removed, and centrifuged at 450g for 5min to remove any cell debris. The supernatant could then be aliquoted and stored at -20^{o}C for future use.

2.2.6 $CD19^{+}$ B cell isolation

hCD20tg mice were euthanized by increasing concentration of CO_2, and peripheral LNs (cervical, inguinal, popliteal, axillary, brachial and aortic LNs) and spleen were extracted, placed in cRPMI, single cell suspensions prepared (see 2.2.1) and the suspensions combined. $CD19^{+}$ B cells could then be isolated using the EasySep Mouse B cell Enrichment Cocktail kit (StemCell Technologies) according to the manufacturer's instructions, under sterile conditions. In detail, single cell suspensions were resuspended in PBS + 2% FBS, and 5% normal rat serum, at a concentration of $1x10^{8}$ cells/ml, and transferred into a sterile 5ml capped FACS tube. The B cell Enrichment Cocktail was added to the cell suspension at 50µl/ml and incubated at 4^{o}C for 15min. After the incubation period, Biotin Selection Cocktail was added at 100µl/ml, and the mix incubated for a further 15min at 4^{o}C. The Magnetic Particles were then added at a concentration of 100µl/ml and the cell suspension incubated at 4^{o}C for another 5min. The cell suspension was then made up to 2.5ml with PBS + 2% FBS, and placed in an EasySep purple magnet for 5min at RT. With the tube still in the magnet, the suspension was poured into a fresh tube. This transferred the B cells to the fresh tube, while the unwanted cell fraction was retained in the original tube by the magnet. The $CD19^{+}$ B cell suspension was then centrifuged, and the pellet resuspended in 10ml complete RPMI, and counted as in 2.2.1, ready for use.

2.2.7 $CD4^+$ T cell isolation

C57BL/6 WT littermates, or C57BL/6 OT-II, mice were euthanized and the spleens extracted, placed in cRPMI, and single cell suspensions prepared as described in 2.2.1. $CD4^+$ T cells were isolated from the spleens and LNs using the EasySep Mouse $CD4^+$ T cell Enrichment kit (StemCell Technologies) according to the manufacturer's instructions, under sterile conditions. In detail, single cell suspensions were centrifuged and resuspended in PBS + 2% FBS, with 1mM EDTA, at a concentration of $1x10^8$ cells/ml, and transferred in to a sterile 5ml capped FACS tube. Normal rat serum was added to the cell suspension at 50µl/ml cells. The $CD4^+$ T cell Enrichment Cocktail was then added to the cell suspension at 50µl/ml and incubated at 4°C for 15min. After the incubation period, the Biotin Selection Cocktail was added at 100µl/ml, and the mix further incubated for 15min at 4°C. The Magnetic Particles were then added at a concentration of 100µl/ml and the cell suspension incubated at 4°C for another 5min. The cell suspension was then made up to 2.5ml with PBS + 2% FBS, and placed in an EasySep purple magnet, without the cap, for 5 minutes at RT. With the tube still in the magnet, the cell mix was poured in to a fresh tube. The T cells were transferred to this fresh tube, while the unwanted cell fraction was retained in the original tube by the magnet. The $CD4^+$ T cell suspension was then centrifuged, and the pellet resuspended in 10ml cRPMI, and counted ready for use (see 2.2.1).

2.2.8 CFSE staining of cells

Primary B cells, T cells and thymocytes, were stained with CFSE (Carboxyfluorescein Diacetate Succinimidyl Ester) (Invitrogen) to allow tracking of the cells by flow cytometry. Purified B cells, T cells and/or thymocytes (2.2.6, 2.2.7 and 2.2.1, respectively) were washed twice in 20ml PBS and centrifuged at 450g for 5min. The cells were resuspended in fresh PBS at a concentration of $1x10^7$ cells/ml. A stock solution of 5mM CFSE in DMSO was then added, to give a final concentration of 2.5µM CFSE and incubated for 5min at RT, in the dark with shaking. To stop the staining reaction and quench any unbound dye, the cells were washed twice in 20ml cRPMI and resuspended in fresh media ready for use.

2.2.9 CellTrace violet staining of cells

BMDM, prepared as previously described in 2.2.3, were stained with CellTrace Violet Cell Proliferation Kit (Invitrogen) according to the manufacturers instructions. In brief, cells were resuspended at $1x10^6$ cells/ml in PBS and CellTrace Violet added to the suspension at a final working concentration of 5µM. Cells were incubated for 20min at

37°C, protected from light. To stop the staining reaction, 5 times the original staining volume of cRPMI was added to the cells and incubated for a further 5min. Cells were then washed in cRPMI, and resuspended in fresh media ready for use.

2.2.10 Induction of apoptosis by irradiation

Peripheral LNs, spleens and thymuses were harvested from mice as previously described in 2.2.1. $CD19^+$ B cells were isolated using the EasySep Mouse B cell Enrichment Cocktail kit and $CD4^+$ T cells isolated using the EasySep Mouse T cell Enrichment Cocktail kit as described in 2.2.6 and 2.2.7, respectively. Cells were then resuspended at $1x10^6$cells/ml in cRPMI and irradiated using an XRAD225 x-ray irradiation system (Precision X-ray Inc.). Cells were given a dose of 30Gy, and subsequently incubated for 4hr at 37°C, 5% CO_2, to ensure the majority of cells had undergone apoptosis before use, as confirmed by flow cytometry (section 2.5.1.2)

2.2.11 Induction of apoptosis by Etoposide treatment

Peripheral LNs, spleens and thymuses were harvested from mice as previously described in 2.2.1. $CD19^+$ B cells were isolated using the EasySep Mouse B cell Enrichment Cocktail kit and $CD4^+$ T cells isolated using the EasySep Mouse T cell Enrichment Cocktail kit as described in 2.2.6 and 2.2.7, respectively. Cells were then resuspended in 10μM Etoposide (Sigma) at a concentration of $2x10^6$ cells/ml and incubated overnight at 37°C, 5% CO_2. Cells were washed 3 times in cRPMI prior to subsequent use. Flow cytometry was used to confirm majority of cells had undergone apoptosis before use, as described in section 2.5.1.2.

2.3 *In vitro* assays

2.3.1 Kinetics of Rituximab internalization

Fluorescently labelled Rituximab (RTX-488) (see 2.1.3) was used in conjunction with an AF-488 quenching antibody (Invitrogen) to investigate the kinetics of RTX internalization by hCD20tg B cells *in vitro*.

B cells were isolated from hCD20tg C57BL/6 mice (see 2.2.6), resuspended at $1x10^6$ cells/ml in cRPMI, and 1ml of the cell suspension transferred into 5ml FACS tubes. The B cells were then incubated with either 2μg/ml RTX-488 or no stimulation, for 0min, 15min, 30min, 60min, 3hr, 6hr or 24hr, at 37°C, 5% CO_2. To inhibit any further RTX internalization after incubation, cells were fixed with either: a 4% Formalin solution

for 5min at RT, for flow cytometric analysis; or the Cytofix/Cytoperm kit (BD Bioscience) for 30min at RT, for use in fluorescent microscopy.

For flow cytometric analysis of internalization, half of the cells from each time-point were incubated with an anti AF-488 antibody (see 0), which effectively quenches the signal from any surface-bound AF-488 [180]. Cells were then run on a FACSCalibur. For each time-point, comparison of the MFI of AF-488 between B cells that had had their surface AF-488 quenched, and those that had not, allowed the relative level of RTX internalization to be determined.

For fluorescent microscopy, B cells from early time-points were stained with rhodamine-conjugated phalloidin (section 2.5.2.1), cytospun onto slides (section 2.5.2.2) and visualized using an ApoTome Microscope (Zeiss) (section 2.5.2.3).

2.3.2 BMDM interactions with apoptotic cells

To allow comparison of the effects of differing apoptotic cells on macrophages, *in vitro* assays were performed in which BMDM were co-cultured with apoptotic cells derived from either B cells, T cells or thymocytes.

L929 BMDM and/or GM-CSF BMDM were prepared from the bone marrow of C57BL/6 WT littermates on day 0, and fed on day 3 (see 2.2.3).

On day 6, the BMDM were plated out at $3x10^5$ cells/ml in cRPMI into 5ml FACS tubes, with 1ml of the cell suspension per tube, for later FACS analysis. BMDM were also plated out into 96 well, flat bottom plates at $1x10^6$ cells/ml in cRPMI, for later collection of supernatants. In some assays 100U IFNγ was added to each BMDM containing tube/well. All BMDM were then incubated overnight at 37^{o}C, 5% CO_2. Etoposide treated B cells, T cells, and thymocytes were also set up on day 6, as described in 2.2.11, and incubated overnight to induce apoptosis. Where the Etoposide treated cells were to be used for the evaluation of BMDM – AC interaction levels via flow cytometry, the lymphocytes were CFSE stained prior to Etoposide treatment (section 2.2.8), to allow later identification. Apoptotic lymphocytes to be co-cultured with BMDM to be used for BMDM phenotypic analysis were not CFSE stained.

On day 7, further single cell suspensions of thymocytes, B cells, and T cells were prepared (see 2.2.1, 2.2.6 and 2.2.7, respectively), and CFSE stained (see 2.2.8) if appropriate to the assay being undertaken. The cells were then resuspended at $1x10^6$ cells/ml in cRPMI, and half of each newly isolated cell population irradiated to

induce apoptosis, as detailed in 2.2.10. After the incubation period, the irradiated and non-irradiated lymphocyte preparations were washed and resuspended at $5x10^6$ cells/ml in fresh cRPMI. At this stage Etoposide-treated cells were washed extensively to remove all Etoposide from the cell suspensions, before also being resuspended at $5x10^6$ cells/ml in fresh cRPMI. The FACS tubes containing BMDM were centrifuged at 450g for 5min, the media poured off and the cells resuspended in the remaining cRPMI. 300µl of the irradiated, non-irradiated or Etoposide-treated cell suspensions were added to the appropriate tubes, and 100µl to the desired wells, to give a final ratio of 5:1, AC to BMDM. In certain adaptations of the assay, E.coli LPS (Sigma) was added to tubes/wells at a concentration of 100ng/ml or 1ng/ml. Co-cultures to be analysed by flow cytometry for BMDM – AC interaction levels were incubated for 0, 15, 30 or 60min at 37°C, 5% CO_2. At the end of the desired length of co-culture, these cells were washed in 3ml ice cold PBS + 5mM sodium azide to inhibit any further cell-cell interactions. Cells were then FACS stained, fixed, and run on a FACSCalibur (see 2.5.1). The co-cultures set up in 96 well plates were incubated for 24hr at 37°C, 5% CO_2 before having the cell culture supernatants removed and frozen down at -20°C, ready for later use in cytokine ELISAs (see 2.5.4). Co-cultures to be analysed by flow cytometry in order to determine changes in BMDM phenotype were incubated for 6 or 24hr at 37°C, 5% CO_2. At the end of the desired length co-culture, these cells were washed in 3ml ice cold PBS + 5mM sodium azide, before being FACS stained and run on a MACSQuant (see 2.5.1).

2.3.3 BMDM interactions with pre-treated B cells

The *in vitro* assay used to examine the interactions of BMDM with apoptotic cells (see 2.3.2) was modified to allow investigation of whether RTX binding to B cells has an effect on the way B cells, or apoptotic cells originating from these B cells, interact with different populations of BMDM under inflammatory and non-inflammatory conditions.

In detail, BMDM were prepared from the bone marrow of C57BL/6 WT littermates on day 0, and supplemented with either L929 supernatant or GM-CSF and IL-3, as required. BMDM were fed on day 3 (see 2.2.3).

On day 6, the BMDM were plated out at $3x10^5$ cells/ml in cRPMI into 5ml FACS tubes, with 1ml of the cell suspension per tube, for later FACS analysis. BMDM were also plated out into 96 well, flat bottom plates at $1x10^6$ cells/ml in cRPMI, for later collection of supernatants. All BMDM were then incubated overnight at 37°C, 5% CO_2. Also on day 6, B cells were isolated from hCD20tg C57BL/6 mice (see 2.2.6), CFSE stained (see 2.2.8), resuspended in cRPMI at $1x10^6$ cells/ml, and incubated with either 100µg/ml RTX, 100µg/ml human polyclonal IgG or no stimulation for 30min at 37°C, 5% CO_2. These cells

were then washed 2x in cRPMI, Etoposide treated (see 2.2.11) and incubated overnight to induce apoptosis.

On day 7, a further single cell suspension of primary B cells was prepared (see 2.2.6), CFSE stained (see 2.2.8), and incubated with RTX or controls, as previously stated. The cells were then washed 2x in cRPMI and resuspended at $1x10^6$ cells/ml. Half of each pre-treated group was irradiated to induce apoptosis, as detailed in 2.2.10. After the incubation period, the B cells were washed and resuspended at $5x10^6$ cells/ml in fresh cRPMI. At this stage the Etoposide treated B cells were washed a minimum of 3x, and resuspended at $5x10^6$ cells/ml in fresh cRPMI. The FACS tubes containing BMDM were centrifuged at 450g for 5min, the supernatant poured off and the cells resuspended in the remaining media. 300µl of the irradiated, non-irradiated or Etoposide pre-treated B cell suspensions were added to the appropriate tubes, and 100µl to the desired wells, to give a final ratio of 1:1, 3:1 or 5:1 (B cells:BMDM), as stated. In certain adaptations of the assay, E.coli LPS (Sigma) was added to tubes/wells at a concentration of 100ng/ml or 1ng/ml. Co-cultures to be analysed by flow cytometry for BMDM – B cell interaction levels were incubated for 15min – 3hr at 37°C, 5% CO_2. At the end of the desired length of co-culture, the cell-cell interactions were stopped by washing with 3ml ice cold PBS + 5mM sodium azide. Cells were then FACS stained for the macrophage marker F4/80, fixed, and run on a FACSCalibur (see 2.5.1). The co-cultures set up in 96 well plates were incubated for 24hr at 37°C, 5% CO_2 before having the cell culture supernatants removed and frozen down at -20°C, ready for later use in cytokine ELISAs (see 2.5.4).

2.3.4 Secondary presentation of antigen by BMDM

In vitro assays were developed in the lab to allow investigation of the ability of macrophages to present antigen previously internalized by apoptotic cells to T cells, a process we have termed 'secondary presentation'. For this system OVA was used as the model antigen, with the activation of OVA-specific T cells isolated from OTII T cell receptor (TcR) transgenic mice used as a read out of successful antigen presentation by the BMDM. Figure 2.1 gives an overview of the experimental design.

L929 BMDM were prepared from the bone marrow of C57BL/6 WT littermates on day 0, and fed on day 3 (see 2.2.3).

On day 6, the spleens and peripheral LNs were harvested from hCD20tg C57BL/6 mice and the B cells isolated (see 2.2.6). The B cells were then incubated overnight at 37°C,

5% CO_2 with either a RTX-OVA peptide conjugate protein (RTX:OVA) or control antigens at 100µg/ml, 30µg/ml or 15µg/ml.

The RTX:OVA conjugate was prepared using Sulpho-MBS (Thermo Scientific Peirce), an amine-to-sulfhydryl cross-linker, with RTX conjugated to an $OVA_{323-339}$ peptide that has an added cysteine residue at the N-terminus, to allow chemical conjugation. In detail, the Sulpho-MBS cross-linker was added to 0.1mM RTX, at a final concentration of 1mM and the mixture incubated for 30min at RT. Excess cross-linker was then removed using a Zeba Spin Desalting Column (ThermoScientific). $OVA_{323-339}$ peptide was then added to the RTX containing fraction in a 4:1 peptide:protein-NH_2 molar ratio, and incubated for a further 30min at RT. The RTX:OVA conjugate was run through an Amicon Ultra 100K concentrating column (Millipore) to remove any unbound OVA peptide. A Nanodrop 1000 (ThermoScientific) was used to measure the concentration of the conjugate protein, which was stored at 4°C until use. 100µg of RTX:OVA was estimated to contain 50µg of RTX and 50µg of OVA peptide.

Also on day 6, the BMDM were plated out into either 24 well tissue culture plates, or 96 well plates, at a concentration of $1x10^6$ cells/ml in cRPMI, and 100units of IFNγ added to each BMDM containing well and incubated overnight at 37°C, 5% CO_2.

The following day (day 7), the antigen-treated B cells were washed extensively and resuspended at $1x10^6$ cells/ml in fresh cRPMI. These cells were then co-cultured with the BMDM, at a ratio of 1:1 (BMDM:B cells), with 100ng/ml E.coli LPS (Sigma), for 3hr at 37°C, 5% CO_2. As a control, wells containing B cells alone were also set up, and processed in the same way as the BMDM wells for the remainder of the assay. After co-culture, all media was removed from the wells and the BMDM washed extensively to remove any un-phagocytosed B cells. 1ml fresh cRPMI was then added to the wells ready for overnight BMDM - OTII T cell co-culture. OTII T cells were isolated, as detailed in 2.2.7, and resuspended at $1x10^6$ cells/ml in cRPMI. $1x10^6$ OTII T cells were added to appropriate wells, with a final volume of 2ml per well, and incubated overnight at 37°C, 5% CO_2.

On day 8, cells from the 24 well plates were stained for flow cytometric analysis to allow investigation of the expression levels of CD69, an early activation marker of T cells (see 2.5.1).

On day 10, supernatants were collected from the 96 well plates for use in IL-2 cytokine ELISAs (see 2.5.4), and the cells used for *in vitro* proliferation assays (see 2.5.3).

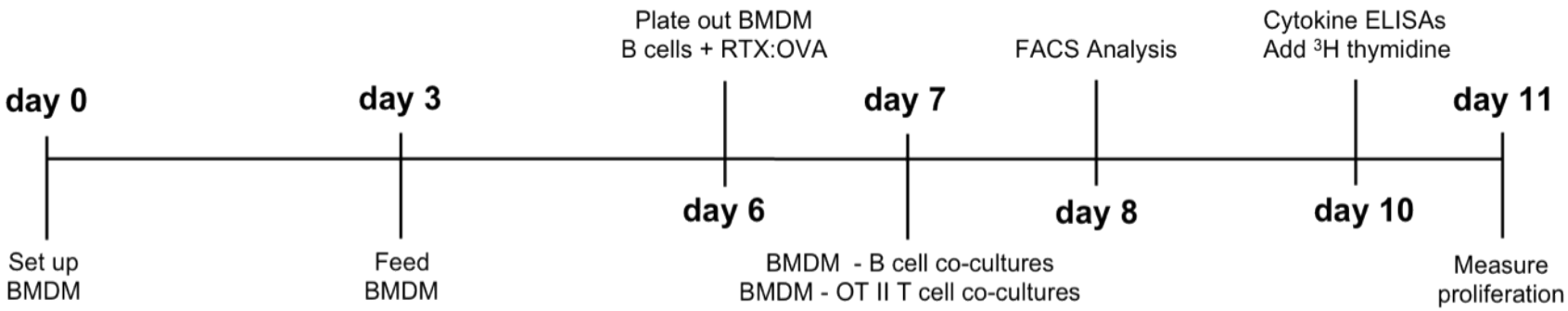

Figure 2.1 Secondary Presentation Assay Protocol
Overview of the protocol for an *in vitro* assay to assess whether bone marrow derived macrophage (BMDM) phagocytosis of B cells that have previously encountered antigen can result in the successful presentation of this antigen to T cells. BMDM were generated and co-cultured for 3hr with primary, RTX:OVA pre-treated B cells. The BMDM were then extensively washed before subsequent co-culture with OTII T cells. Antigen presentation to the OTII T cells was assessed by flow cytometry, IL-2 cytokine ELISA and measurement of T cell proliferative responses.

2.4 Animal models

2.4.1 Rituximab treatment of mice

A single dose of Rituximab (RTX) (Genetech) was administered intravenously (i.v.) at 100µg/mouse. In the case of RTX treatment of collagen-induced arthritis (CIA), the monoclonal antibody was administered either on day -4 or 0, with day 0 being the day of CIA induction. In the case of RTX treatment of healthy hCD20tg C57/B6 mice, RTX was administered on day 0, with mice euthanized on day 7, and the extent of B cell depletion analysed by FACS analysis (see 2.5.1). ChromPure whole human IgG (Jackson Laboratories) was used as a control.

2.4.2 Adoptive cell transfers

Spleen and LN cells were harvested from either hCD20tg DBA mice or WT littermates (as detailed in 2.2.1) and the B cells isolated (see 2.2.6). Purified viable B cells were then transferred into WT DBA mice, with $5x10^6$ cells transferred via i.v. injection in to the tail vein. In the case of apoptotic cell adoptive transfers, B cells were irradiated to induce apoptosis (as described in 2.2.10), and either $5x10^6$ or $0.5x10^6$ apoptotic cells transferred per mouse, via i.v. injection into the tail vein.

2.4.3 Collagen induced arthritis

Collagen induced arthritis (CIA) [181] was induced by intra-dermal (i.d.) injection of an emulsion of 100µg of either chicken collagen type II (chicken CII) (Chondrex), or bovine collagen type II (CII) (Chondrex, MD Bioscience or Sigma, as stated) with 200µg Complete Freund's Adjuvant (CFA) on day 0. CFA was prepared by resuspending 100mg of *Mycobacterium tuberculosis H37 Ra* (Difco Laboratories) in 25ml of Incomplete Freund's Adjuvant (Sigma) to give a 4mg/ml CFA solution. Mice were boosted on day 21 by i.p. injection of 100µg CII in PBS. In certain CIA runs RTX treatment was given (see 2.4.1), and/or adoptive transfers of B cells or apoptotic cells performed (as detailed in 2.4.2).

Disease was monitored by the measurement of paw/ankle swelling using calipers, and both a 16-point and 24-point scale clinical scoring system. The 16-point scale monitors general inflammation of the paw as shown in Table 2.1. The 24-point score monitors joint inflammation, with each inflamed joint being assigned a score of 1, and the maximum score per paw being 6 (5 digits plus wrist/ankle).

Table 2.1 ***16-Point Clinical Scoring System for CIA***

Score	Description
0	Normal
1	Redness
2	Swelling of one joint (wrist/ankle or digit)
3	Swelling of two or more joints
4	Severe swelling (all joints)

B cell responses were assessed by serum ELISA (as detailed in 2.5.5) on day 40-45, and T cell responses measured by *in vitro* proliferation assays (as described in 2.5.3).

2.4.3.1 Analysis of radiographic pathology in CIA

For some CIA runs, post-mortem x-rays were taken of the hind paw to determine the level of radiographic pathology incurred during the model. Paws were flattened in histology cassettes, fixed with formalin for 7-14 days and x-rays taken using the Kodak Fx-Pro. Images were captured using an exposure time of 2.5min at 35KVP, with the f-stop set to 4, and illumination correction was applied. The images were then scored for radiological bone damage, with a maximal score of 27 possible. The scoring system employed was based on a method developed by collaborators at Cardiff University and Prince Charles Hospital, Cardiff. In detail, the 5 metacarpophalangeal (MCP) joints, along with the base of the 1st metatarsal bone were scored for erosions, osteopenia and evidence of periostial reactions, while the 2nd distal tarsal was scored for joint space loss with adjacent bone and osteopenia. The joint space between the 4th and 5th distal tarsal and fibulare, as well as that between the intermedium and centrale, were also scored for loss of definition and osteopenia. A score of 1 was assigned for evidence of each parameter, and a score of 0 in the absence of evidence. An overview of the joints scored and representative images of a healthy and an arthritic paw are given in Chapter 7, Figure 7.12.

2.4.4 Delayed type hypersensitivity responses

Mice were immunized subcutaneously (s.c.) with an emulsion of 100µg of ovalbumin (OVA) (Sigma) with Complete Freunds Adjuvant (CFA) on day 0. On day 14 mice were re-challenged with 100µg of heat aggregated ovalbumin (HAO) s.c. in the footpad [182,183]. Control mice received PBS instead of either OVA/CFA or HAO, or were left naive.

To make the HAO, OVA was resuspended at 20mg/ml in PBS and heat-inactivated in a water bath for 2hr at 80^{o}C. The suspension was then centrifuged at 450g for 5min, and

the supernatant discarded. The pellet was then washed in cold PBS, resuspended at a final concentration of 20mg/ml, aliquoted and stored at -20°C. Prior to use the HAO was thawed, and a syringe used to disperse any visible clumps.

To assess the model, mice were monitored for inflammation, with paw thickness measured at 24 and 48hr post HAO challenge. T cell responses were measured by *in vitro* proliferation assays (as described in 2.5.3) as well as IL-2 cytokine ELISAs (see section 2.5.4).

2.5 Analysis of responses

2.5.1 Flow cytometric analysis

Peripheral LNs, mesenteric LNs, peyers patches and spleen were analysed by flow cytometry, as well as peritoneal lavage and blood samples. Cells from *in vitro* assays were also analysed.

2.5.1.1 Basic extracellular staining

For cell surface staining, $3x10^5$ – $1x10^6$ cells were transferred to 5ml FACS tubes, washed with 1ml FACS buffer (see appendix) and centrifuged at 450g for 5min. The cell pellet was resuspended, 100µl of a 1:100 dilution of Fc Block (BD Bioscience) added and the cells incubated for 5-15min at 4°C. Antibodies for extracellular staining were diluted in FACS buffer and 50µl of this mix added to each tube and incubated for 20min at 4°C in the dark. An overview of the FACS antibodies and dilutions used are given in Tables 2.2 and 2.3. Cells were then washed with 1ml of FACS buffer and centrifuged at 450g for 5min. Where a biotin-conjugated primary antibody was used for cell surface staining, a further staining step involving a fluorochrome-labelled streptavidin was required. The streptavidin was diluted in FACS buffer and 50µl of this mix added to each tube and incubated for 20min at 4°C in the dark. After the final staining step, cells were washed with 1ml of FACS buffer, centrifuged at 450g for 5min, and resuspended in 300µl FACS buffer ready to be run on either a FACSCalibur (BD Bioscience) or a MACSQuant (Miltenyi) as stated. Samples that were not run immediately were fixed for later analysis. Cells to be fixed were resuspended in 250µl Cytofix/Cytoperm (BD Bioscience) and incubated for 20min at 4°C in the dark. Cells were then washed twice with 1ml 1x perm wash solution (BD Bioscience), once with 1ml FACS buffer, and resuspended in 300µl FACS buffer ready to be run. All FACS data were analyzed using FlowJo software (TreeStar).

2.5.1.2 Detection of apoptosis via FACS

AnnexinV-FITC, 7-AAD and Cell Via-Probe (all BD Bioscience) staining was used to detect the kinetics of apoptosis of B cells in response to various *in vitro* treatments. B cells were isolated from either C57BL/6 hCD20tg mice or WT littermates (as detailed in 2.2.6), and resuspended in cRPMI. Cells were then either incubated with 100µg/ml RTX, irradiated (see 2.2.10), or Etoposide-treated (see 2.2.11) depending on the conditions being investigated. At various time-points after the initial treatment, $1x10^6$ cells were transferred into 5ml FACS tubes ready for staining. Cells were then washed once with 1ml FACS buffer (see appendix), and twice more with 1ml 1x AnnexinV buffer (eBioscience). The cells were then resuspended in 100µl of 1x AnnexinV buffer, and 5µl of AnnexinV-FITC added per tube, before incubation at 4°C for 30min. Cells were washed with 1ml of AnnexinV buffer, centrifuged at 450g for 5min, and resuspended in 300µl AnnexinV buffer ready to be run on either a FACSCalibur (BD Bioscience) or a MACSQuant (Miltenyi) as stated. 10min prior to the cells being run, 10µl of 7-AAD or Cell Via-Probe solution was added to each tube. This solution was not removed before the running of samples.

2.5.1.3 Acid stripping of surface staining

Acid stripping was employed to remove bound fluorochromes from the surface of cells previously stained for flow cytometric analysis. Single cell suspensions were prepared as stated in 2.2.1, and stained with either cell surface lineage markers or RTX-488 (see 2.5.1.1). After staining cells were washed in 1ml FACS buffer, the supernatant poured off and the cells resuspended in the remaining buffer. 500µl-1ml 0.5M sodium chloride + 0.2M acetic acid was added to relevant tubes and incubated at 4°C for either 4min or 10min depending on the protocol in use. Cells incubated for 4min were then washed twice with 2ml TBS (see appendix), once with 1ml FACS buffer and then resuspended in 300µl FACS Buffer. Cells that were incubated for 10min were then washed twice with 2ml TBS, followed by two more acid incubations with TBS washes in between each, for a total of 3 or 4 acid incubations, as stated. After the final acid incubation step, cells were washed twice more with 2ml TBS, once with 1ml FACS buffer and then resuspended in 300µl FACS Buffer. All acid stripped cells were analyzed on a FACSCalibur.

2.5.1.4 Quenching of surface staining using Trypan Blue

Trypan Blue was utilized to quench the signal from surface-bound fluorochromes on cells previously stained for flow cytometric analysis. Single cell suspensions were prepared at stated in 2.2.1, and stained with cell surface lineage markers (see 2.5.1.1).

Table 2.2 ***Anti-human antibodies***

Target	Fluorochrome	Clone	Dilution/ Concentration	Supplier
CD20	v450	L27	1:40	BD Biosciences
CD20	FITC	2H7	1:40	BD Biosciences
CD20	PE	2H7	1:40	BD Biosciences
CD20	PECy5	2H7	1:40	BD Biosciences
CD20	APC	2H7	1:40	BD Biosciences
CD20	AF-488	Rituximab	1-2µg/test	Conjugated in Lab

Table 2.3 ***Anti-mouse antibodies***

Target	Fluorochrome	Clone	Dilution	Supplier
CD3e	FITC	145-2C11	1:200	BD Pharmingen
CD3e	PE	145-2C11	1:200	BD Pharmingen
CD3e	APC	145-2C11	1:200	BD Pharmingen
CD4	FITC	H129.19	1:200	BD Pharmingen
CD5	PE	53-7.3	1:200	eBioscience
CD11b	v450	M1/70	1:200	BD Horizon
CD11b	APC-Cy7	M1/70	1:200	BD Pharmingen
CD11c	PE-Cy7	HL3	1:200	BD Pharmingen
CD19	PerCP-Cy5.5	1D3	1:200	BD Pharmingen
CD19	APC	1D3	1:200	BD Pharmingen
CD19	PE-Cy7	1D3	1:200	BD Pharmingen
CD21	FITC	7G6	1:200	BD Pharmingen
CD23	PE	B3B4	1:200	BD Pharmingen
CD24	PE	M1/69	1:200	BD Pharmingen
CD40	PE	3/23	1:200	BD Pharmingen
CD45	APC	30-F11	1:200	eBioscience
CD69	PE	H1.2F3	1:200	eBioscience
CD69	PE-Cy5	H1.2F3	1:200	eBioscience
CD86	FITC	GL1	1:200	BD Pharmingen
CD206	AF647	C068C2	1:200	BioLegend
B220	PEcy7	RA3-6B2	1:200	eBioscience
Biotin	PE	Streptavidin	1:1000	eBioscience
DO11.10 TcR	APC	KJ1.26	1:200	BD Pharmingen
F4/80	PE	BM8	1:400	BioLegend
F4/80	APC	BM8	1:200	eBioscience
GR1 (Ly6C/Ly6G)	APC	RB6-8C5	1:100	BD Pharmingen
IgD	FITC	11.26c.2a	1:200	BD Pharmingen
IgD	APC	11-26	1:200	eBioscience
IgM	PE	R6-60.2	1:200	BD Pharmingen
Ly6C	PerCP	Al-21	1:100	BD Pharmingen
MHC I-A^b	PE-Cy7	AF6-120.1	1:200	BioLegend
MHC I-A^q	Biotin	KH116	1:200	BD Pharmingen

After staining cells were washed in 1ml FACS buffer, the supernatant poured off and the cells resuspended in the remaining buffer. 500µl/1ml 0.4% Trypan Blue (Sigma) was then added to relevant tubes, and incubated for either 1min or 2min, as stated. Cells were washed 2 times in 3ml cRPMI, once with 1ml FACS Buffer, and resuspended in 300µl FACS buffer before running on a FACSCalibur.

2.5.1.5 Quenching of surface AlexaFluor-488 staining

An anti-AF-488 quenching antibody (Invitrogen) was used after B cell incubation with RTX-488 to quench the signal emitted from surface bound RTX-488. B cells were incubated with RTX-488 for various time-points and then fixed (see 2.3.1). After this fixation step, 1ml FACS buffer was added to the tubes and centrifuged at 450g for 5min. Cells were then washed in 1ml FACS buffer, followed by 1ml of sodium phosphate buffer (see appendix), and resuspended in 100µl sodium phosphate buffer. 5µl anti-AF-488 antibody was added to each tube, and incubated at 4°C for 20min. After incubation, cells were washed in 1ml of sodium phosphate buffer and resuspended in 300µl of sodium phosphate buffer ready to be run on a FACSCalibur.

2.5.2 Fluorescent Microscopy

2.5.2.1 Phalloidin staining

A proportion of the B cells used to investigate the kinetics of RTX internalization (see 2.3.1) were stained with rhodamine-conjugated phalloidin (Sigma), a high-affinity F-actin probe, to enable detection of the cell membrane by fluorescence microscopy.

To do this, $3x10^5$ Cytofix/Cytoperm fixed B cells were washed twice with 1ml 1x perm wash solution (BD Bioscience), and resuspended in 200µl perm wash. The B cells were then stained with 50µg/ml rhodamine-phalloidin and incubated for 30min at RT. Cells were washed 3 times with 1ml 1x perm wash solution and resuspended at $5x10^4$ cells/75µl FACS buffer, ready to be cytospun onto slides (see section 2.5.2.2) and visualized (see 2.5.2.3).

2.5.2.2 Cytospins

Samples for analysis by fluorescent microscopy were cytospun onto slides. Single cell suspensions were resuspended in FACS buffer at $5x10^4$ cells/75µl, with 75µl transferred onto a Superfrost Plus microscope slide (VWR) using a cytospin (450g for 5mins). Slides were left to dry, before the mounting using Vectashield mounting media containing DAPI

(Vector). Cover slips were sealed using clear nail varnish, and slides were stored at -20°C in the dark until visualisation on an ApoTome Microscope (Zeiss).

2.5.2.3 Visualization of cells

All slides were visualized using an ApoTome Microscope (Zeiss).

2.5.3 Proliferation assays

To measure the relative ability of lymphocytes to proliferate in response to a particular antigen, the incorporation of radioactive tritiated-thymidine (^{3}H-thymidine) into newly synthesized cells was determined. Mice were euthanized and single cell suspensions prepared, as described in 2.2.1. Cells were added to a 96 well plate at a concentration of $3x10^5$ – $5x10^5$ cells/well. Cells were incubated with cRPMI alone or media supplemented with OVA or CII, depending on the antigen used initially. OVA was added at concentrations of 1mg/ml and 500µg/ml, while CII was added at either 30µg/ml or 60µg/ml. Plates were incubated for 72-96hr at 37°C, 5% CO_2 before pulsing with 12.5µl ^{3}H-thymidine per well, for an additional 16hr. PMA and Ionomycin stimulation of cells (at 5ng/ml and 350ng/ml, respectively) was used as a positive control, and plates were incubated for 24hr at 37°C, 5% CO_2 before pulsing with 12.5µl ^{3}H-thymidine for a further 16hr. The cells were then harvested onto filter mats (Perkin Elmer) using a Harvester 96 - Mach III cell harvester (Tomtec). Once the filter mats had dried, they were placed in MicroBeta sample bags (Perkin Elmer), scintillation fluid added (Wallac), and analysed using a Betaplate scintillation counter (Wallac).

2.5.4 Cytokine ELISAs

2.5.4.1 Sandwich ELISAs

Cytokine expression was tested in *in vitro* culture supernatants. ELISAs were carried out according to the manufacturer's protocols (Table 2.4). In general, 96-well half volume high-binding plates (Fisher Scientific) were coated with capture antibody in recommended coating buffer (see appendix) and incubated overnight at 4°C. Plates were then washed 3-5 times with phosphate-buffered saline + 5% Tween (PBST) (see appendix), and blocked with blocking buffer (see appendix) for 1hr to inhibit non-specific antibody binding. Plates were washed a following 3-5 times with PBST. The standards and samples were then added in triplicate and the plates incubated for 2hr at RT. For TGF-β ELISAs all samples were acid activated prior to addition to the ELISA plate in order to activate any latent TGF-β1 present. To do this, 20µl 1N HCl was added to 100µl of sample and incubated at RT for 10min. The samples were then neutralized with

20µl of 1N NaOH. Depending of the cytokine being investigated certain samples were diluted in assay diluent (see appendix) before addition to the plate. After the sample incubation plates were washed 5x with PBST. Depending on the kit in use, at this stage either a working detector solution, made up of the detection antibody and streptavidin-HRP, was added, or the detection antibody alone. Both of these were left for an hour at RT. For the plates where only the detection antibody was added, after another wash step, streptavidin-HRP was added for 30min at RT. Once the plates had been incubated with both the detection antibody and streptavidin-HRP, either together or alone, plates were washed a further 7 times and TMB substrate added to wells in order to develop the plates. This was left for between 2-30min depending on the cytokine in question. The reaction was then stopped using 4N sulphuric acid, and plates read at 450nm.

Table 2.4 ***Cytokine ELISAs***

Cytokine	Company	Detection Range
Mouse IL-1β	BD Bioscience	31.25 – 2000 pg/ml
Mouse IL-6	BD Bioscience	15.62 – 1000 pg/ml
Mouse IL-10	BD Bioscience	31.25 – 2000 pg/ml
Mouse IL-12	eBiosciences	4.69 – 300 pg/ml
Mouse TNFα	BD Bioscience	15.62 – 1000 pg/ml
Mouse TGF-β	eBiosciences	15.62 – 1000 pg/ml

2.5.4.2 Competitive binding ELISAs

Prostaglandin E_2 expression was tested in *in vitro* culture supernatants by competitive binding ELISAs (Cayman Chemicals), which were carried out according to the manufacturer's instructions, with all kit reagents reconstituted/diluted in Ultra Pure water (Cayman Chemicals). Samples, either neat or diluted in cell culture medium (cRPMI), and standards diluted in cRPMI were added to pre-coated plates, with 50µl each of Prostaglandin E_2 AChE Tracer and Prostaglandin E_2 monoclonal antibody (both supplied with the kit) directly added to the sample containing wells. Relevant control wells were also set up at this time according to the manufacturers protocol, the plates covered, and incubated for 18hr at 4°C. Plates were then washed 5 times with 1x wash buffer, and 200µl of the developer, Ellman's Reagent, added to each well (both supplied with the kit). The plates were then covered with plastic film and developed at RT, in the dark, with shaking for 60-90min. Ellman's Reagent cannot over-develop, and so no stop solution was added to these ELISAs before the plates were read at 405nm.

2.5.5 Serum ELISAs

Levels of type II collagen (CII) specific IgG1 and IgG2a, as well as total IgG and total IgG1, were tested in the serum of mice used in collagen-induced arthritis (CIA) models (as detailed in 2.4.3). Serum ELISAs were developed in house. As with cytokine ELISAs, 96-well half volume high-binding plates (Fisher Scientific) were used. For total IgG and IgG1 ELISAs plates were coated with goat anti-mouse IgG (Southern Biotech) at 5ug/ml in PBS and incubated at 4^{o}C overnight. For CII-specific IgG1 and IgG2a plates were coated with either ELISA grade chicken collagen, or ELISA grade bovine collagen, at 5ug/ml in 1x collagen diluent (all from Chondrex), and incubated overnight at 4^{o}C. Plates were then washed 4 times with PBST (see appendix), and blocked with PBS + 3% BSA for 1hr at RT. Plates were washed a following 4 times with PBST, and serum samples and standards added, and the plates incubated for 2hr at RT.

Table 2.5 gives an overview of the standards and their dilutions, as used for each serum ELISA. For CII-specific serum ELISAs commercially available standards are not available, and so a dilution range of pooled sera from CIA animals was used to create standard curve values, with a scale of 'relative units' (RU) used for analysis. Multiple dilutions of each serum sample were included in the assay to ensure a final result that fell within the standard curve.

Table 2.5 ***Serum ELISA standards***

ELISA	Standard	Range/Dilution
Total IgG	Polyclonal IgG	1.56 - 100ng/ml
Total IgG1	Polyclonal IgG1	0.62 - 40ng/ml
CII IgG1	Pooled sera	1:3000 - 1:2187000
CII IgG2a	Pooled sera	1:3000 - 1:2187000

After the sample incubation, plates were washed 4x with PBST. The appropriate secondary antibody, diluted 1:3000 in PBS + 1% BSA, was then added to the plate and incubated for 1hr at RT. Anti-IgG HRP (Southern Biotech), was used as the secondary antibody for total IgG ELISAs. Anti-IgG1 HRP (Bethyl) was used as the secondary antibody for both the total IgG1, and CII-specific IgG1 ELISAs, while anti-IgG2a HRP (BD Bioscience) was used for the CII-specific IgG2a ELISAs. Plates were washed a further 4 times in PBST, and TMB substrate added to every well in order to develop the plates. This was left for between 1-10min, until the standard curve could be visualized. The reaction was then stopped using 4N sulphuric acid, and plates read at 450nm.

2.6 Statistical analyses

The GraphPad Prism computer program was used to perform all statistical analyses, with different analyses utilised depending on the data being investigated. When comparing two sets of data, either a T-test or a Mann-Whitney test was used, depending on the distribution of the data. A One-way ANOVA (or non-parametric equivalent) was used for the comparison of three or more data groups in experiments with only one variable factor. A post-test was employed if overall significance was detected, with Bonferroni's test used. A two-way ANOVA was used for the comparison of three or more data groups in experiments with two variable factors (i.e. the CIA model). Figure legends state the statistical test used for each set of data. *p* values of 0.05 or less were considered to be statistically significant, with * = $p<0.05$, ** = $p<0.01$, *** = $p<0.001$. Data in graphs are shown as means ± SD.

Chapter 3: Macrophage Interactions with Apoptotic Cells

3.1 Introduction

Cell death is a crucial biological process that is pivotal in regulating steady state tissue turnover and homeostasis, as well as playing a major role in the resolution of immune responses, with three main forms of cell-death existing: apoptosis, necrosis, and autophagy. Cells can be placed into each of these categories depending on the morphological and biochemical features observed on cell death, and their subsequent interactions with phagocytes.

Apoptosis is a controlled and highly regulated form of cell death, characterized by cleavage of chromosomal DNA, nuclear condensation and fragmentation, and the formation of apoptotic bodies that prevent the release of intracellular matter into the surrounding environment. AC are rapidly cleared from the system by phagocytes, in the absence of pro-inflammatory responses. Apoptosis can be activated by two pathways: the 'intrinsic' pathway, which is initiated from within the cell itself in response to severe cell stress, DNA damage, or the loss of cell survival factors; and the 'extrinsic' pathway, which is initiated in response to external stimuli received by the cell in the form of the ligation of pro-apoptotic receptors expressed on the cell's surface, such as Fas and TRAIL. Both pathways of apoptosis are active processes requiring energy in the form of ATP, and result in the activation of specialised proteases called caspases, leading to the breakdown of integral cell components and cell death.

Necrosis occurs as a consequence of tissue damage or extreme cellular stress, and is characterized by swelling of cellular organelles, coupled with lysosomal leakage, and the loss of membrane integrity. Originally thought to be an uncontrolled, passive form of cell death, evidence had shown that certain forms of programmed necrosis take place, resulting in regulated caspase-independent mechanisms of cell death. Clearance of necrotic cells is slower and less efficient than that of apoptotic cells, occurring after the release of intracellular material from the dying cell [112], inducing inflammatory responses in the surrounding environment.

Autophagy is a catabolic process that can be involved cell survival, as well as cell death, through the recycling of cellular components in response to cell starvation, with important roles in embryonic development and tissue remodelling. Autophagic cell death results from prolonged exposure to continued cell starvation, and is associated with extensive vacuolization of the cytoplasm [121], with specific proteins involved in the formation of large autophagic vesicles. The clearance of autophagic cells results in distinct transcriptional responses in phagocytes [121], leading to pro-inflammatory outcomes.

Millions of cells undergo apoptosis every day, and so the rapid clearance of AC without stimulation of the immune system is crucial to maintaining peripheral tolerance to self. If not cleared in a timely fashion, apoptotic cells will undergo secondary necrosis, leading to the release of intracellular material into the surrounding environment, which in certain circumstances can lead to in a break in tolerance to intracellular self-antigens, and chronic pathology, such as in SLE [156].

The non-inflammatory clearance of AC is dependent on the interaction of AC with phagocytes during cell tethering and uptake, with changes in the surface membrane composition of the AC detected, as well as functional alterations in adhesion molecules (i.e. ICAM-3 [149]) and inhibitory molecules (i.e. CD31 [151]), collectively termed 'ACAMPs' [reviewed in [124]. One of the most well characterized changes undergone by AC is the exposure of PS on the cell surface [184], with this change in membrane composition being a key "eat-me" signal involved in AC uptake [125]. Phagocytes are able to recognise PS directly via specific PS receptors on their surface, or via soluble adaptor proteins that allow additional, indirect recognition of PS by phagocytes. MFG-E8 [134], β2-glycoprotein I [138] and GAS-6 [136], are all able to bind exposed PS on the AC surface, with each adaptor molecule then recognized by its specific receptor on the phagocyte. Alongside alterations in membrane composition, modification of existing surface antigens occurs on AC, resulting in the generation of neo-epitopes, however, the specifics of these processes are not yet fully understood. Collectins, such as MBL and the complement component C1q bind to the surface of late apoptotic cells, promoting uptake through subsequent interaction with CD91 and CRT on the surface of phagocytes [141], with ACAMPs thought to be the target for this interaction. Oxidization of the AC surface results in the formation of ox-LDL-like neo-epitopes on the AC surface, which can be recognized directly by scavenger receptor A (SR-A) [144] and LOX1 [146], and also act as TSP-1 binding sites, allowing indirect recognition by additional phagocytic scavenger receptors. Changes in the specific cell surface molecules expressed by AC help to mediate tethering and uptake by phagocytes, however certain molecules considered to be markers of AC, are also exposed on viable cells (i.e. PS), and as such the spatial distribution of these molecules is likely to be involved in the differentiation between cell states.

Clearance of apoptotic cells was originally thought to occur simply in the absence of pro-inflammatory signals, however in the late 1990s, work by Voll et al showed that the uptake of AC can actively suppress inflammatory responses [158], with apoptotic peripheral blood lymphocytes shown to induce increased production of the anti-inflammatory cytokine IL-10 and decreased production of the pro-inflammatory

cytokines TNFα, IL-1β and IL-12 by human monocytes on stimulation with LPS. Over the past two decades, a huge body of work has arisen that supports this finding that AC are able to modulate the immune system, actively promoting anti-inflammatory responses in a range of phagocytes. Ingestion of AC by immature DC results in a diminished ability to produce pro-inflammatory cytokines such as IL-12, and inhibition of DC maturation [166], with immature murine DC that ingest apoptotic neutrophils unable to upregulate the co-stimulatory molecule CD86, resulting in a reduced capacity to stimulate T cell proliferation [166]. Cytokine production by NK cells is also affected by interaction with AC. *In vitro* co-culture of human NK cells and apoptotic Jurkat, PLB-985 or $CD4^+$ T cells results in significant increases in TGF-β production by the NK cells, with this TGF-β production able to suppress further IFNγ secretion by the NK cells in response to stimulation [167]. Along with modulating cytokine production by innate immune cells, uptake of AC by phagocytes has also been shown to alter secretion of other immune mediators, and angiogenic growth factors [185]. Co-culture of apoptotic Jurkat T cells with murine peritoneal macrophages results in increased production of anti-inflammatory prostaglandins such as PGE_2, with concomitant inhibition of pro-inflammatory eicosanoids and LPS-induced NO generation [169]. The immunomodulatory effects of AC have also been confirmed *in vivo*. In a murine model of CIA, intravenous injection of apoptotic thymocytes, up to one month before arthritis induction, was able to protect mice from disease and led to increased secretion of IL-10 by $CD4^+$ T cells on *in vitro* re-stimulation [172], indicating the ability of AC to alter adaptive cell function as well as innate cell function.

This body of evidence supports the idea that AC are able to induce anti-inflammatory responses on binding/engulfment by phagocytes both *in vitro* and *in vivo*, and may have the potential to re-introduce tolerance to the immune system. We hypothesize that treatment with Rituximab in the context of RA may re-introduce a temporary tolerance to the immune system, caused, at least in part, by the generation of large numbers of apoptotic B cells (Figure 1.3). If on treatment with RTX, apoptosis of B cells is caused, the B cells will be cleared by APCs, with the binding and engulfment of AC inducing a range of anti-inflammatory responses in the APC. As that uptake of apoptotic B cells by phagocytes will be in a non-inflammatory context, peptides resulting from B cell degradation will be presented by the APC in a 'tolerogenic' context. If the ingested B cell has previously taken up self-antigen, specifically the putative self-antigen the RA response is directed toward, presentation of this antigen in a non-inflammatory, tolerizing environment, may result in the re-introduction of temporary tolerance to the RA system. Although the effects of uptake of a variety of different AC have been investigated, apoptotic B cells have not been used as the model AC for any of these

studies. For that reason, as an initial step to understanding the potential validity of our hypothesis, the immunosuppressive effects of apoptotic B cells were examined, and specifically whether apoptotic B cells have the same immunomodulatory capacities as other, more commonly studied AC. To do this, *in vitro* assays were set up in which bone marrow derived macrophages (BMDM) were co-cultured with a variety of apoptotic cells, allowing direct comparison of the outcomes of co-culture. Primary murine B cells, T cells and thymocytes were utilized, with apoptosis inducted either by x-irradiation or Etoposide-treatment of cells.

Chapter objectives:

- To investigate whether BMDM and apoptotic B cells undergo similar levels of interaction as BMDM and other AC
- To explore whether the interaction of BMDM and apoptotic B cells alters BMDM phenotype, specifically their antigen presenting potential and activation
- To determine whether the interaction of BMDM and apoptotic B cells results in changes in the BMDM function

3.2 Results

3.2.1 Induction of apoptosis by irradiation

Apoptosis is a naturally occurring form of programmed cell death, however it can be also induced by various external stimuli. To assess whether AC originating from different populations of lymphocytes interact differently with macrophages, primary B cells, T cells and thymocytes isolated from C57BL/6 mice were used as model AC, with apoptosis induced *ex vivo* by ionizing radiation. Ionizing-radiation comprises several different type of radiation, with gamma-irradiation [186-188] and x-irradiation [189-191] both repeatedly used in the literature to induce apoptosis. Throughout this thesis x-irradiation was utilized to induce apoptosis, due to access to an XRAD225 x-ray irradiation system.

Lymphocytes are known to be particularly radiosensitive compared to other cell types, however on irradiation cell death in lymphocytes does not occur immediately, but after a latent period [192], with the length varying depending on both the radiation dose and culture conditions. If left for prolonged periods of time apoptotic cells will undergo secondary necrosis. For use in co-culture with BMDM, a population of apoptotic, but not necrotic, irradiated lymphocytes was desired, along with a population of still viable non-irradiated lymphocytes, and so the optimal length of lymphocyte incubation post treatment was determined.

To do this, spleens were harvested from mice, single cell suspensions prepared and the B cells isolated. The B cells were then divided into two groups, resuspended at $1x10^6$ cells/ml in cRPMI, and one group irradiated. Both groups were then incubated for varying lengths of time, as stated. The time points begin after B cell separation *ex vivo*, and indicate the length of incubation after irradiation, starting at 0hr. Cell were then stained with AnnexinV and 7-AAD, and analysed by flow cytometry to allow detection of live, apoptotic and dead cells (see Table 3.1). AnnexinV is a calcium-dependent phospholipid-binding protein that specifically binds to phosphatidylserine (PS), while 7-AAD is a fluorescent intercalator that emits a signal on binding to DNA. Viable cells, which have intact cell membranes, will exclude 7-AAD and do not express sufficient levels of PS on their surface to result in a detectable AnnexinV signal, resulting in a double negative population of cells. During apoptosis, the cell membrane remains intact, however PS becomes exposed on its outer surface. As such, apoptotic cells stain positive for AnnexinV, but are $7\text{-}AAD^-$. In dead cells and necrotic cells (including those undergoing secondary necrosis), membrane integrity is lost, allowing 7-AAD to enter the cell and bind to DNA, resulting in a $7\text{-}AAD^+$ population. Due to the loss of membrane integrity necrotic and dead cells will also be $AnnexinV^+$ as the protein will be able to enter these cells, and bind to PS constitutively expressed on the inner leaflet of cell membranes.

Table 3.1 ***Detection of cell viability by FACS***

	FACS Stains	
	Annexin V	**7-AAD**
Viable Cells	-	-
Apoptotic Cells	+	-
Necrotic Cells	+	+

At the 0hr time-point comparable levels of live, apoptotic and dead B cells were seen in both the irradiated and non-irradiated groups, with the proportion of dead cells remaining comparable at all time-points investigated (Figure 3.1a-d). However, by the 3hr time-point substantially less viable cells were present in the irradiated cell population (36.1±12.6%) compared to the non-irradiated cells (66.8±4.2%) (Figure 3.1b), with this reduction in viable cells in the irradiated cell population coupled with an increased proportion of apoptotic cells (irr: 50.5±9.3% vs. non-irr: 23.7±4.3%) (Figure 3.1c). At the 6hr and 8hr time point this pattern continued, with considerably more apoptosis observed in the irradiated cell population when compared to the non-irradiated cells (6hr – irr: 71.7±1.4% vs. non-irr: 40.7±4.1%, 8hr – irr: 82.3±2.7% vs. non-irr: 58.1±7%). Although markedly more apoptosis was seen in the irradiated cell

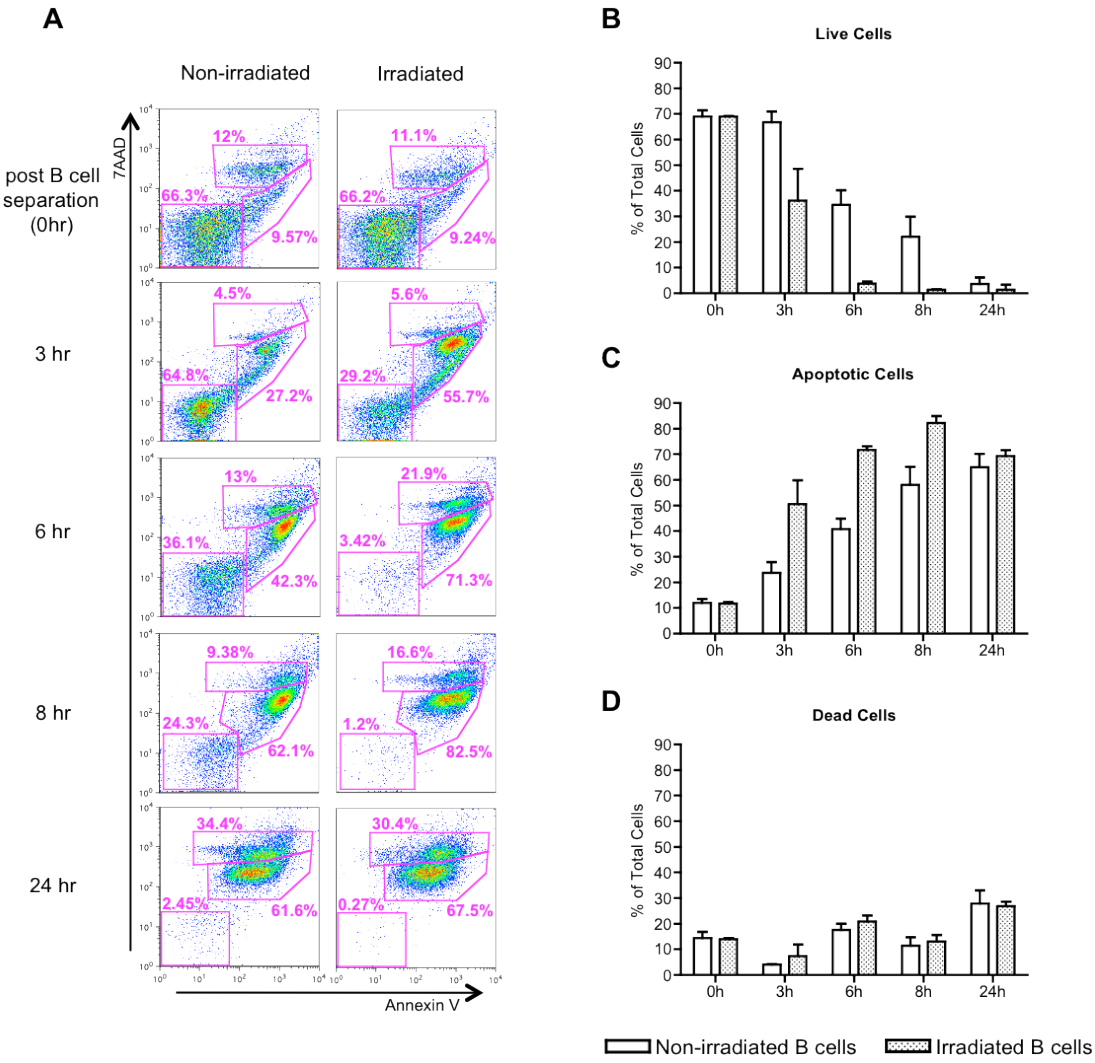

Figure 3.1 Induction of B cell apoptosis by irradiation
Single cell suspensions wells were prepared from the combined spleen and LNs of WT C57BL/6 mice, and either irradiated or left non-irradiated. Cells were then incubated for varying time-points and stained with 7-AAD and Annexin V, and analysed by flow cytometry to allow detection of live, dead and apoptotic cells. (**A**) Representative FACS plots showing the gating used to differentiate live, dead and apoptotic cells at each of the time points and for each treatment group, with viable cells 7-AAD$^-$AnnexinV$^-$, apoptotic cells 7-AAD$^-$AnnexinV$^+$ and dead cells staining double positive for 7-AAD and AnnexinV. (**B**) Graph of pooled data showing the percentages of live non-irradiated or irradiated B cells over a 24hr period of in vitro culture. (**C**) Graph of pooled data showing the percentages apoptotic non-irradiated or irradiated B cells over a 24hr period of in vitro culture. (**D**) Graph of pooled data showing the percentages late apoptotic/dead non-irradiated or irradiated B cells over a 24hr period of in vitro culture. (n=1, 3 replicates)

populations at the 6 and 8hr time-points, after 6hr of culture a substantial proportion of apoptotic cells were also observed in the non-irradiated cell population, with only 34.5±5.7% of B cells viable at 6 hours, 22±7.8% at 8hr and 3.5±2.6% at 24hr (Figure 3.1b). At the 24hr time-point, the proportions of live and dead cells were again comparable between the two groups.

These findings demonstrate that x-irradiation of murine B cells induces substantial levels of apoptosis, with a significant increase in the proportion of apoptotic cells observed between 3-8hr after irradiation, compared to non-irradiated cells. However, after 6hr, the non-irradiated cells also began to undergo high levels of apoptosis. As such, to ensure a large apoptotic population in the irradiated group while maintaining a mostly viable cell population in the non-irradiated cells, it was decided that both irradiated and non-irradiated cells would be used in BMDM co-cultures after 3-4hr of incubation.

3.2.2 Interactions of L929 BMDM with irradiated apoptotic cells

In vitro assays were performed to investigate whether AC originating from different populations of lymphocytes interact differently with macrophages. Murine BMDM were grown for 6 days in media supplemented with M-CSF-containing L929 supernatant (L929 BMDM), and half the cells stimulated overnight with 100U IFNγ. Thymocytes were isolated from C57BL/6 mice, with B cells purified from the spleens, and T cells from peripheral LNS. All lymphocytes were CFSE-stained, and half of the cells from each lymphocyte population were irradiated to induce apoptosis, with viable cells used for comparison, and all cells incubated for 4hr. The L929 BMDM incubated overnight with IFNγ were further stimulated with 10ng/ml LPS (activated L929 BMDM). All BMDM were mixed with CFSE-stained viable or irradiated B cells, T cells or thymocytes, at a ratio of 5:1 (lymphocytes:BMDM) and co-cultured for 15min. The co-cultures were then stained for the macrophage lineage marker F4/80 and the resultant levels of cell-cell or cell-AC interaction were analyzed by flow cytometry.

In the samples tested, viable cells were gated on using forward scatter (FSC) and side scatter (SSC), and within this population the $F4/80^+$ cells were defined as BMDM. $F4/80^+CFSE^+$ cells were deemed to be BMDM undergoing interactions with CFSE-stained lymphocytes/AC, with the $F4/80^+CFSE^{hi}$ populations also investigated independently (Figure 3.2a).

When L929 BMDM were co-cultured with either viable or irradiated cells, the vast majority of the BMDM population became $CFSE^+$ for all conditions investigated (Figure

3.2b-d). Within the $CFSE^{+}$ population of BMDM, two distinct sub-populations were detected, a $CFSE^{hi}$ and $CFSE^{lo}$ population. When the $CFSE^{hi}$ population of L929 BMDM was investigated, differences between the co-culture conditions became apparent. On co-culture of BMDM with irradiated lymphocytes in the absence of stimulation, a significantly higher percentage of $CFSE^{hi}$ BMDM were present in the BMDM + irradiated thymocyte condition (20.9±3.6%) compared to the BMDM co-cultures with irradiated B cells, or irradiated T cells (7.4±1.4% and 7.7±2.9%, respectively) (Figure 3.2d). When activated BMDM were utilized in the co-cultures, significantly more $CFSE^{hi}$ BMDM were detected after co-culture with irradiated B cells (29.3±2.4%), compared to the un-stimulated BMDM co-cultured with irradiated B cells (7.4±1.4%). Viable cells were used in BMDM co-cultures for comparison, with lower levels of interaction between BMDM and viable lymphocytes expected, compared to irradiated lymphocytes. Comparable levels of $CFSE^{hi}$ BMDM were seen on co-culture of viable or irradiated T cells with either un-stimulated BMDM (8.6±2.3% and 9.1±0.7%, respectively) or activated BMDM (7.7±2.9% and 9.3±0.3%, respectively). When viable or irradiated thymocytes co-cultures were compared, similar levels of $CFSE^{hi}$ BMDM were also observed when both un-stimulated and activated BMDM were utilized for the co-cultures. However, co-culture of L929 BMDM with viable B cells resulted in unexpectedly high proportions of $CFSE^{hi}$ BMDM. Co-culture of un-stimulated BMDM with viable B cells resulted in a substantially greater percentage of $CFSE^{hi}$ BMDM compared to those co-cultured with irradiated B cells (42.1±8.9% vs. 7.4±1.7%), and also when compared to either viable T cells or thymocytes (42.1±8.9% vs. 8.6±2.3% and 25.3±12.5%, respectively). The levels of interaction seen with viable B cells was also markedly increased when activated BMDM were utilized in the co-culture conditions (66.5±1.2% $CFSE^{hi}$), compared to un-stimulated BMDM.

To begin to understand whether BMDM co-culture with AC in this sytem resulted in any immunomodulatory effects on the BMDM, the production of IL-10 and TNFα by activated L929 BMDM was quantified after co-culture with AC. Co-culture with irradiated B cells, T cells or thymocytes had no effect on IL-10 production, compared to BMDM cultured alone (3813±521pg/ml) (Figure 3.3a), with viable cells also having no effect on IL-10 levels. Co-culture of activated L929 BMDM with irradiated T cells or thymocytes resulted in a slight decrease in TNFα production (2654±222pg/ml and 2389±234pg/ml, respectively), compared to activated BMDM (3919±584pg/ml). The data also indicate a decrease in TNFα secretion after co-culture with irradiated B cells (3059±987pg/ml) (Figure 3.3b). Unexpectedly, co-culture with viable B cells, T cells and thymocytes also seemedly decreased production of TNFα (1978±238pg/ml, 2389±234pg/ml, and 2798±234pg/ml, respectively).

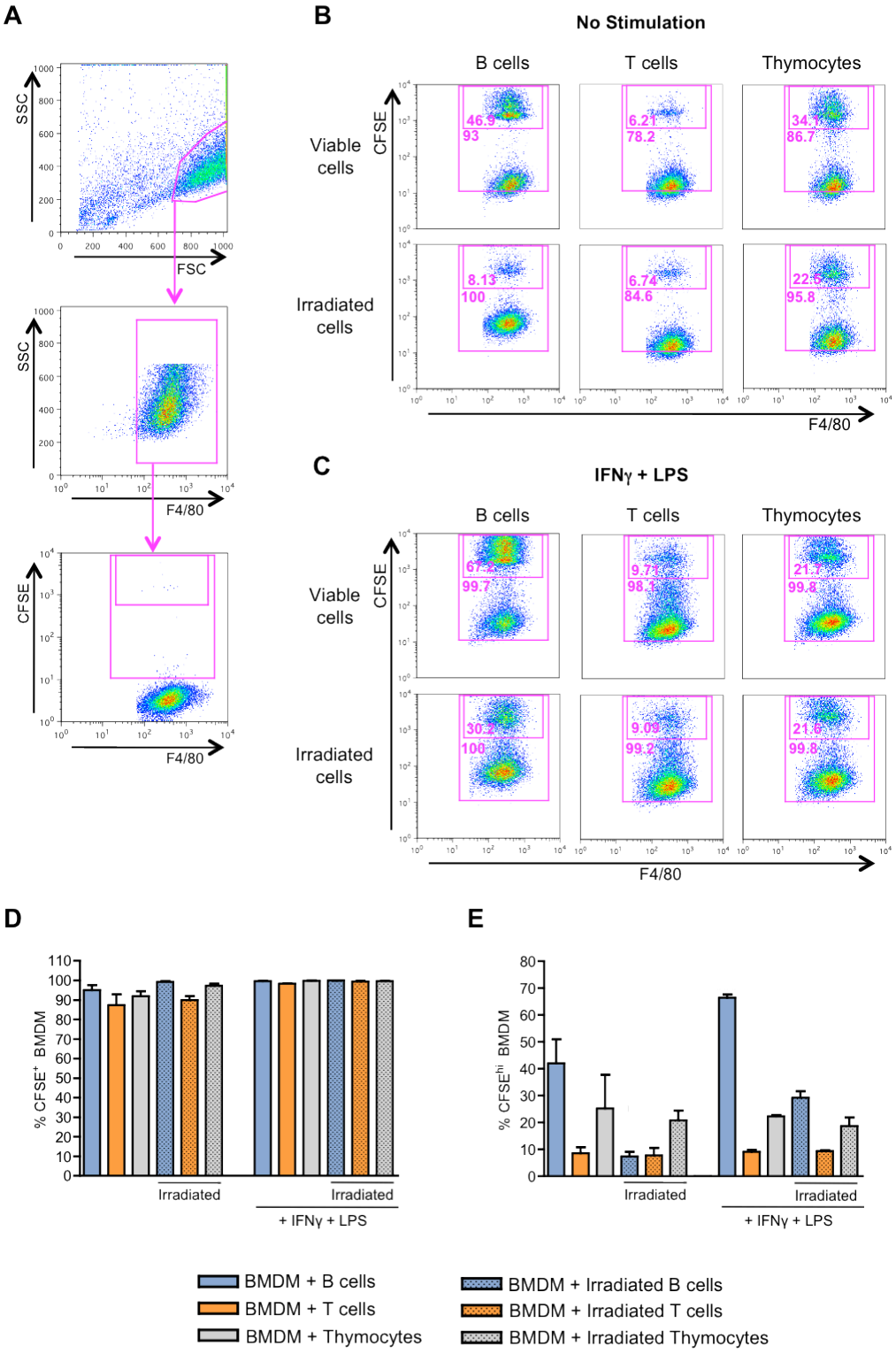

Figure 3.2 Interaction of L929 BMDM with irradiated apoptotic cells
Murine BMDM were grown in cRPMI supplemented with M-CSF containing L929 supernatant. BMDM were co-cultured with CFSE stained viable or irradiated primary B cells, T cells or thymocytes for 15min in the presence or absence of 100U IFNγ and 10ng/ml LPS, and analyzed by flow cytometry. (**A**) Gating strategy used to define $CFSE^{+}$ and $CFSE^{hi}$ BMDM. First panel: SSC vs. FSC. Second panel: SSC vs. F4/80. Third panel: CFSE vs. F4/80. (**B**) Representative FACS plots showing the levels of interaction seen between un-stimulated L929 BMDM and viable and irradiated lymphocytes. Panels: CFSE vs. F4/80. (**C**) Representative FACS plots showing the levels of interaction seen between IFNγ + LPS stimulated L929 BMDM and viable and irradiated lymphocytes. (**D**) Graph of pooled data showing the percentage of $CFSE^{+}$ BMDM. (**E**) Graph of pooled data showing the percentage of $CFSE^{hi}$ BMDM. (No stim: n=2 from 2 independent experiments, LPS+IFNγ: n=1)

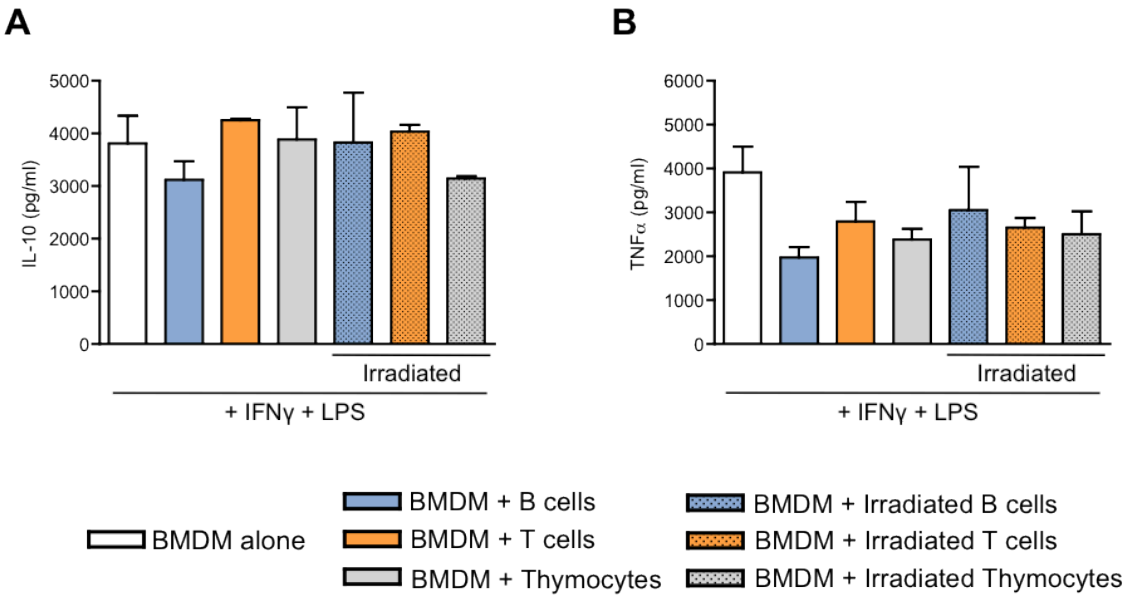

Figure 3.3 Cytokine production by activated L929 BMDM after co-culture with apoptotic cells
Murine BMDM were grown in cRPMI supplemented with L929 cell supernatant. BMDM were stimulated with 100U IFNγ overnight, and on d7 adherent cells were co-cultured overnight with viable or irradiated primary B cells or thymocytes, in the presence of 10ng/ml LPS. Cytokine production by L929 BMDM was quantified using ELISAs. (**A**) Graph showing IL-10 production (pg/ml). (**B**) Graph showing TNFα production (pg/ml). (n=1, 3 replicates)

These findings demonstrate that, the proportion of L929 BMDM undergoing elevated cell-cell interactions after co-culture with irradiated apoptotic cells varied between the different conditions, with the pattern of interaction altered by the BMDM activation state. The co-culture of L929 BMDM with viable cells resulted in unexpectedly high proportions of elevated cell-cell interactions, regardless of the activation state of the BMDM, with significantly more $CFSE^{hi}$ BMDM detected in the co-cultures containing viable B cells compared to the other viable cell conditions. On quantification of cytokine production by BMDM after co-culture, TNFα production decreased, while no change in IL-10 concentration was detected, for all AC investigated. Surprisingly, in this assay system co-culture of BMDM with viable cells had the same modulatory effects on BMDM cytokine production as co-culture with AC, for all cell types investigated.

3.2.3 Investigation of the $CFSE^{hi}$ and $CFSE^{lo}$ populations of L929 BMDM after co-culture

As shown, culture of L929 BMDM with CFSE-stained lymphocytes resulted in two distinct $CFSE^{+}$ BMDM populations, a $CFSE^{hi}$ population and a $CFSE^{lo}$ population. It was theorized that the CFSE signal in the $CFSE^{lo}$ BMDM group could potentially be due to the uptake of free CFSE that had leached into the cell culture media from CFSE-stained lymphocytes by BMDM. To determine whether this was the case, L929 BMDM were co-cultured with either CFSE-stained thymocytes or CFSE-stained thymocyte conditioned media. The CFSE-stained thymocyte conditioned media was produced by culturing viable or irradiated CFSE-stained thymocytes in cRPMI for 4hr, with the supernatant from these cultures collected and used for BMDM co-culture. The CFSE signal of the BMDM was then analyzed by flow cytometry.

In the samples tested, viable cells were gated on using FSC and SSC, and within this population the $F4/80^{+}$ cells were defined as BMDM. Within this $F4/80^{+}$ population, the proportion of $CFSE^{+}$ cells was investigated, with BMDM cultured in cRPMI alone used to set the $CFSE^{-}/CFSE^{+}$ gate (Figure 3.2a). L929 BMDM that were co-cultured with either viable or irradiated thymocytes showed a large increase in CFSE signal, with over 95% of BMDM detected as $CFSE^{+}$ after co-culture (Figure 3.4b, c). However L929 BMDM co-cultured with the CFSE-stained thymocyte conditioned media showed no increase of CFSE signal above background.

Once it was confirmed that both the $CFSE^{hi}$ and $CFSE^{lo}$ BMDM populations were in some way interacting with CFSE-stained AC/lymphocytes, rather than free CFSE, additional analysis of the flow cytometry data was undertaken in an attempt to further understand the interactions taking place. To do this, the $CFSE^{hi}$ and $CFSE^{lo}$ populations of BMDM

were gated on individually (Figure 3.5a) and the FSC vs. SSC profiles of these subsets compared. When an overlay was produced comparing the $CFSE^{hi}$ BMDM and $CFSE^{lo}$ BMDM populations resulting from co-culture of un-stimulated L929 BMDM with either irradiated or viable lymphocytes (Figure 3.5b), it can be seen that the $CFSE^{hi}$ BMDM generally have a higher FSC than the $CFSE^{lo}$ BMDM, with these results replicated in the conditions containing stimulated BMDM. This reveals that the $CFSE^{hi}$ BMDM are larger in size than the $CFSE^{lo}$ BMDM, indicating these cells are potentially undergoing interactions with whole cells or complete AC. The $CFSE^{lo}$ population, on the other hand, may in some way be taking up small amounts of CFSE from the stained cells, or undergoing interactions with small apoptotic blebs or cell debris, or rather than whole cells, however without further work this cannot be conclusively stated.

3.2.4 Induction of apoptosis by Etoposide treatment

In the literature, many different methods of inducing apoptosis *in vitro* are utilized, including irradiation [157], chemotherapeutic treatment [168,193], and the culture of cells in the absence of survival factors [194]. There is a growing body of work demonstrating that different methods of apoptosis induction give rise to AC with varying characteristics, resulting in altered responses to these AC by other cells of the immune system [reviewed in [195]. As uptake of viable cells had the same effects on BMDM function as uptake of AC in this system, it was decided to investigate the interactions of BMDM with another form of AC in an attempt to obtain results more closely resembling those in the published literature. Etoposide is a topo-isomerase inhibitor, with *in vitro* treatment of cells resulting in damage to cellular DNA and subsequent apoptosis [196]. Etoposide-treated lymphocytes were added to the co-culture assay system to allow comparison of the interaction of BMDM with these AC to the interactions of BMDM with irradiated AC. Before the use of Etoposide-treated AC in the co-culture system, the kinetics of cell death after Etoposide-treatment was determined.

To do this, spleens and LNs were harvested from C57BL/6 mice, combined, and the B cells isolated. The B cells were then resuspended in 10μM Etoposide and incubated for up to 24hr. The time points begin after B cell separation *ex vivo*, and indicate the length of Etoposide-treatment, starting at 0hr. An aliquot of cells was removed at each time-point and stained with 7-AAD and Annexin V, before analysis by flow cytometry to allow detection of live, apoptotic and necrotic/dead cells at each time-point.

At the 0hr time-point the majority of B cells were still viable (76.1±0.9%), with a moderate level of apoptotic cells (15.4±0.1%) and negligible levels of dead cells detected (4±0.1%) (Figure 3.6a and b). Similar proportions of viable, apoptotic and dead

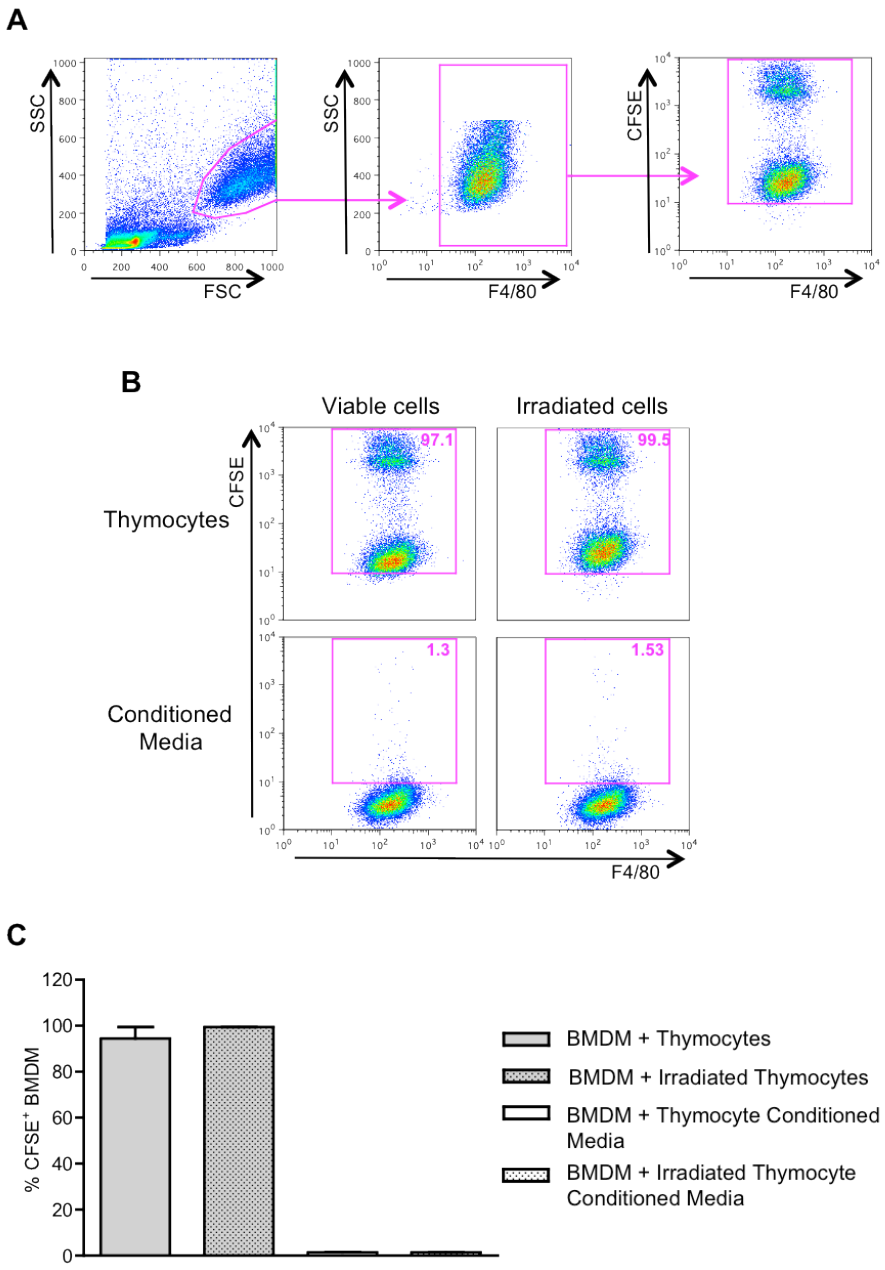

Figure 3.4 Co-culture of BMDM with CFSE$^+$ thymocyte conditioned media does not result in an increased CFSE signal within the BMDM population
Murine L929 BMDM were co-cultured with CFSE-stained viable or irradiated thymocytes, or CFSE-stained thymocyte conditioned media, for 15min and analyzed via flow cytometry. (**A**) The gating strategy used to identify L929 BMDM in samples. First panel: SSC vs, FSC. Second panel: SSC vs. F4/80. Third panel: CFSE vs. F4/80. (**B**) Representative FACS plots showing CFSE staining of BMDM after co-culture with either viable or irradiated thymocytes, or CFSE-stained thymocyte conditioned media. Panels: CFSE vs. F4/80. (**C**) Graph of pooled data showing the percentage of CFSE$^+$ BMDM. (n=1, 3 replicates)

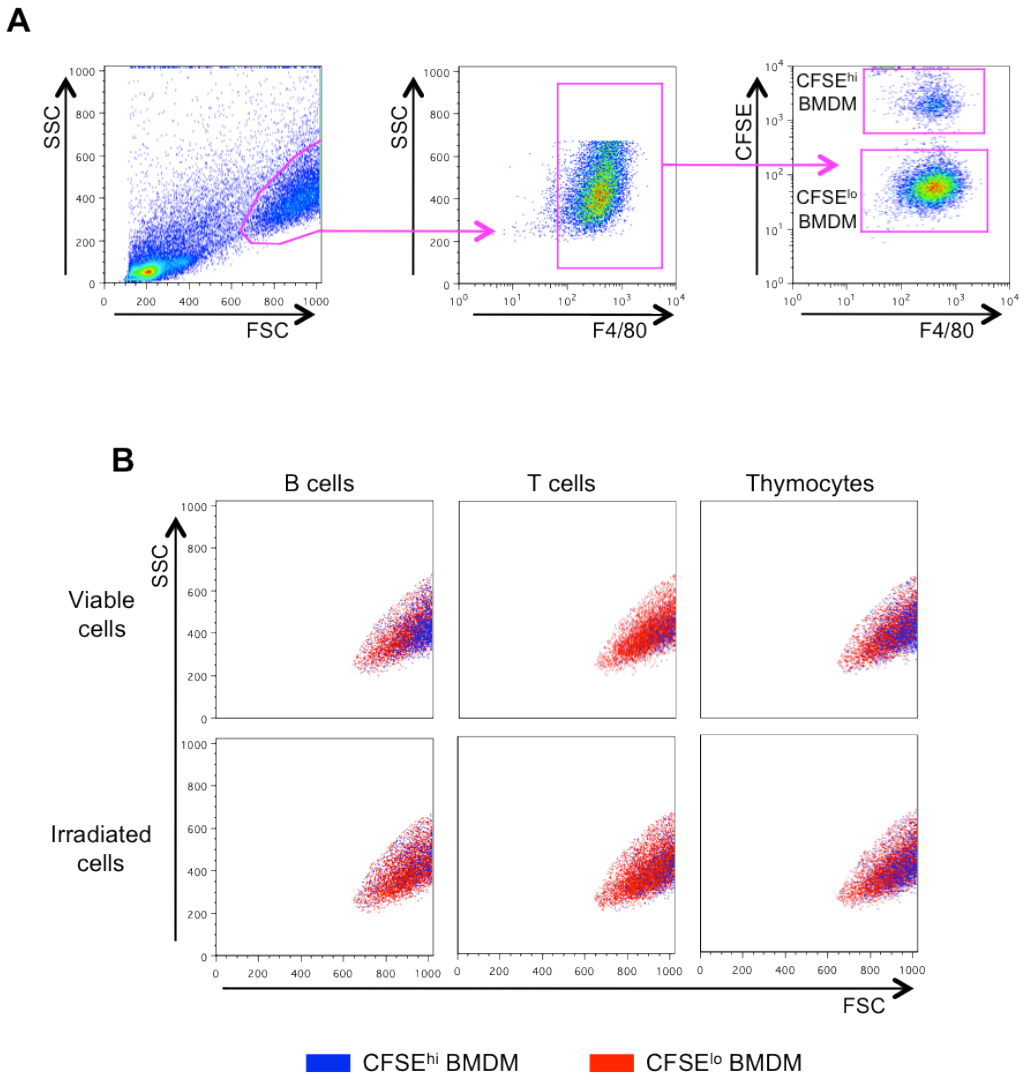

Figure 3.5 The CFSE^{hi} population of BMDM have a greater forward scatter profile than CFSE^{lo} BMDM after co-culture

Murine BMDM were grown in cRPMI supplemented with M-CSF containing L929 supernatant. On d7 adherent cells were co-cultured with CFSE stained viable or irradiated primary B cells, T cells or thymocytes for 15min and analyzed by flow cytometry. (**A**) Gating strategy to identify CFSE^{hi} and CFSE^{lo} BMDM. First panel: SSC vs, FSC. Second panel: SSC vs. F4/80. Third panel: CFSE vs. F4/80. (**B**) Representative images showing overlays of the forward scatter and side scatter properties of the CFSE^{hi} and CFSE^{lo} BMDM subsets. Panels: SSC vs. FSC. (n=1, 3 replicates)

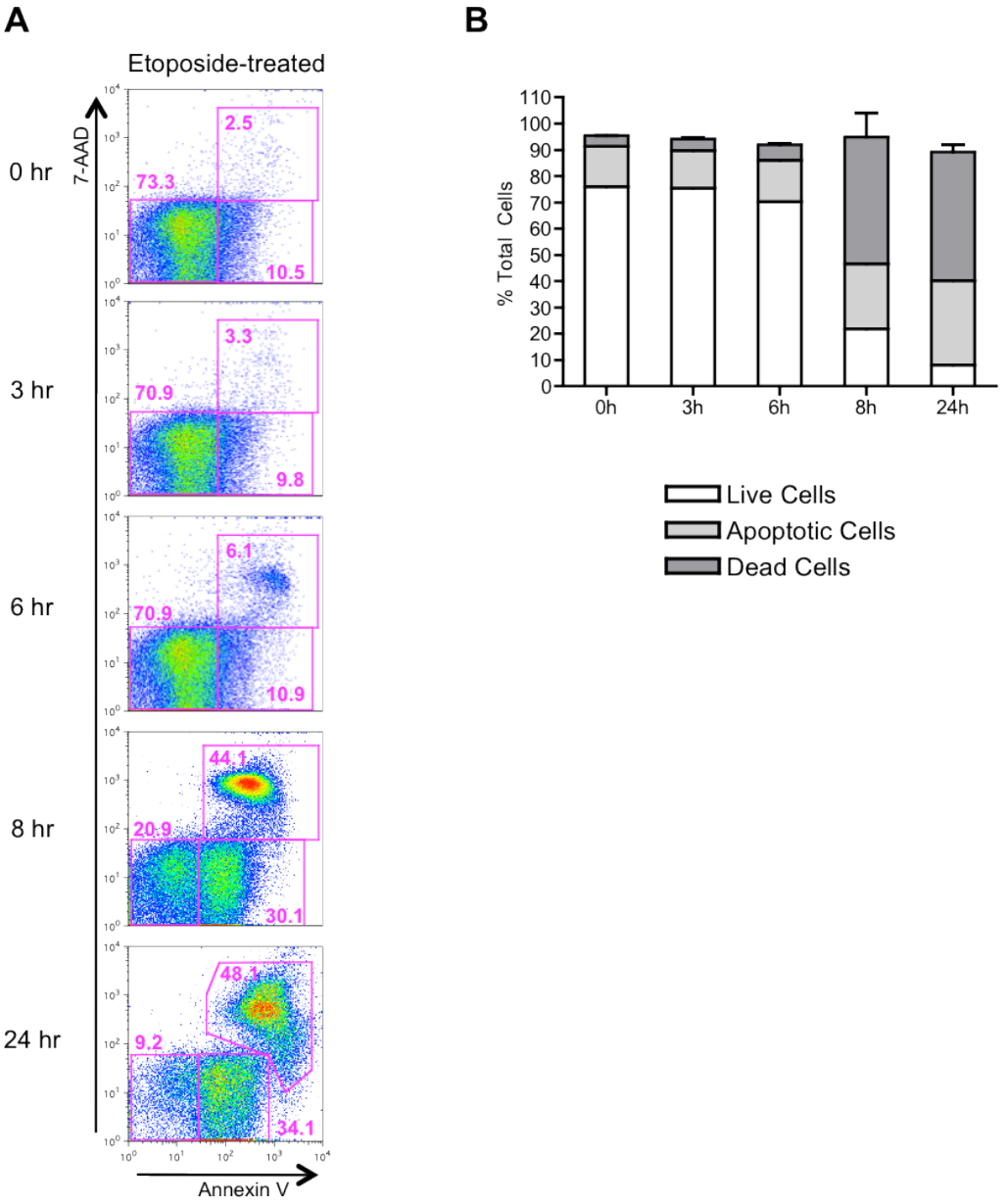

Figure 3.6 Induction of B cell apoptosis by Etoposide treatment
B cells were isolated from the combined spleen and LNs of WT C57BL/6 mice and cultured in 10μM Etoposide. Cells were then incubated for 0, 3, 6, 8 or 24hr, stained with 7-AAD and Annexin V and cell viability analysed by flow cytometry. (**A**) Representative FACS plots showing the gating used to differentiate live, dead and apoptotic cells at each of the time points. Panels: 7-AAD vs. Annexin V, with viable cells 7-AAD$^-$AnnexinV$^-$, apoptotic cells 7-AAD$^-$AnnexinV$^+$ and dead cells 7-AAD$^+$ and AnnexinV$^-$. (**B**) Graph of pooled data showing the percentages of live, apoptotic and dead cells over a 24hr period of *in vitro* culture. (n=1, 3 replicates)

cells were seen at the 3 and 6hr time-points. After 8hr of Etoposide treatment a large increase in the number of double positive cells was seen, with 43.9±8.1% of the B cells 7-AAD$^+$Annexin$^+$, with a concomitant decrease in viable cells (21.9±2%) and a similar percentage of apoptotic cells (24.9±6.9%). At the 24hr time-point, very few cells were still viable (8.2±1.2%) with a slight increase in apoptotic cells indicated (33.9±3%), and a high proportion of dead cells (49±2.9%).

In accordance with the available protocols on Etoposide-treatment of cells and these findings, cells were incubated overnight in 10μM Etoposide to allow sufficient proportions of cells to undergo apoptosis, prior to use in co-culture assays.

3.2.5 Interactions of L929 BMDM with irradiated or Etoposide-treated apoptotic cells

In vitro assays were performed to investigate whether the agent used to induce apoptosis affects the interactions between AC and L929 BMDM, and whether this effect is consistent when using AC originating from different lymphocyte populations. To do this, murine BMDM were grown for 7 days in media supplemented with M-CSF-containing L929 supernatant. The day before co-culture, B cells, T cells and thymocytes were isolated from C57BL/6 mice, CFSE-stained and incubated overnight with 10μM Etoposide to induce non-immunogenic apoptosis. On the day of co-culture, additional B cells, T cells and thymocytes were isolated from C57BL/6 mice, CFSE-stained, and half of the cells from each newly isolated lymphocyte population were irradiated to induce immunogenic apoptosis, and the irradiated and non-irradiated cells incubated for 4hr. The L929 BMDM were mixed with either viable, irradiated or Etoposide-treated B cells, T cell or thymocytes, at a ratio of 1 BMDM:5 lymphocytes, and co-cultured for 15min. The co-cultures were then stained for the macrophage lineage marker F4/80, and levels of cell-cell or cell-AC interaction analyzed by flow cytometry.

CFSE$^+$ and CFSE^{hi} BMDM were gated on as described in Figure 3.2a. No difference was seen in the proportion of CFSE$^+$ BMDM on co-culture with either irradiated or viable lymphocytes, or Etoposide-treated thymocytes (Figure 3.7). However, co-culture of BMDM with Etoposide-treated B cells or T cell resulted in a decrease in the proportion of CFSE$^+$ BMDM (73.7±1.5% and 66.7±8.7%, respectively), compared to all other conditions.

No difference in the proportion of CFSE^{hi} BMDM was seen when BMDM were co-cultured with either irradiated (5.6±1.1%), Etoposide-treated T cells (2.2±0.1%,), or viable T cells (8.8±0.7%). However, Etoposide-treatment of thymocytes resulted in a slightly reduced proportion of CFSE^{hi} BMDM after co-culture (13±1.3%), compared to co-culture with

irradiated thymocytes (23±3%) or viable thymocyte (24.8±2.2% $CFSE^{hi}$ BMDM). Although the Etoposide-treated thymocytes showed reduced levels of interaction with the L929 BMDM compared to the other thymocyte treatments investigated, this condition still resulted in a notably greater proportion of $CFSE^{hi}$ BMDM compared to the other Etoposide-treated lymphocytes (BMDM+Etop. B cells: 5.2±0.1%, BMDM+Etop. T cells: 2.2±0.1%). This pattern of increased interaction of thymocytes compared to the other lymphocyte populations investigated was also reflect in the irradiated conditions, with a greater proportion of $CFSE^{hi}$ BMDM resulting from co-culture with irradiated thymocytes than with either irradiated B cell or irradiated T cells (23±3% vs. 11.2±1.2% and 5.6±1.1%, respectively). When the $CFSE^{hi}$ BMDM population was examined after co-culture of L929 BMDM with viable lymphocytes, as seen in the previous assay, either similar or enhanced levels of interaction were seen within each lymphocyte group, compared to its apoptotic counterparts, although this increase was far subtler in the T cell and thymocyte populations. On co-culture of viable B cells with BMDM, 40.6±2.3% of BMDM were $CFSE^{hi}$, significantly more than either of the apoptotic B cell conditions (BMDM+irr B: 11.2±1.2% and BMDM+Etop. B: 5.2±0.1%), or indeed, the viable T cell or thymocytes co-cultures (8.4±0.7% and 24.8±2.2%, respectively).

These findings show that under the experimental conditions used, apoptotic thymocytes undergo increased interactions with L929 BMDM compared to apoptotic B cells or T cells, regardless of the method of apoptosis induction. In both the B cell and thymocyte populations, Etoposide-treatment resulted in a reduced levels of interaction with BMDM, compared to their irradiated counterparts, with no difference in BMDM-T cell interaction observed between the apoptotic stimuli. Surprisingly, BMDM co-culture with viable B cells resulted in a significantly higher proportion of cell-cell interaction than any of the other conditions investigated.

3.2.6 Changes in L929 BMDM phenotype after co-culture with irradiated or Etoposide-treated apoptotic cells

To determine whether cell-cell interactions between L929 BMDM and different populations of AC can alter BMDM phenotype, the expression levels of a range of surface markers was investigated. L929 BMDM-AC co-cultures were set up as before, in the presence or absence of 1ng/ml LPS stimulation. The co-cultures were incubated for either 6 or 24hr before being analysed by flow cytometry.

The effect of 1ng/ml LPS stimulation on the antigen-presenting potential and activation of the L929 BMDM was investigated; with the expression of MHC II, CD86, CD40, CD69 and CD206 examined. Expression levels were normalized, with expression of the marker

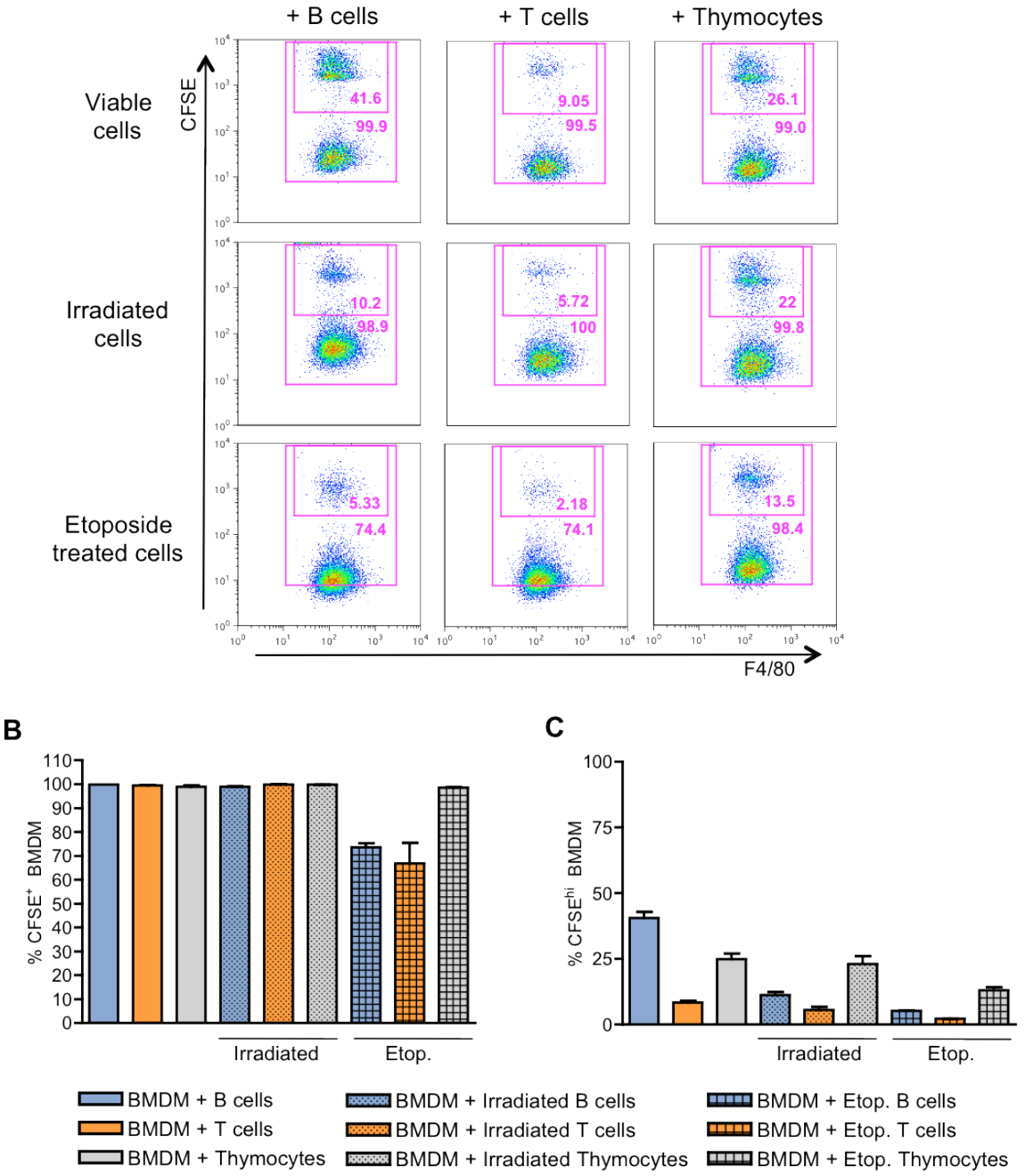

Figure 3.7 L929 BMDM show enhanced cell-cell interactions with viable B cells
Murine BMDM were grown in cRPMI supplemented with M-CSF containing L929 supernatant. On d7 adherent cells were co-cultured with CFSE stained viable, irradiated, or etoposide treated primary B cells, T cells or thymocytes for 15min and analyzed by flow cytometry. (**A**) Representative FACS plots showing the levels of interaction seen between L929 BMDM and apoptotic lymphocytes. Panels: CFSE vs. F4/80. (**B**) Graph of pooled data showing the percentage of $CFSE^{+}$ BMDM. (**C**) Graph of pooled data showing the percentage of $CFSE^{hi}$ BMDM. (n=1, 3 replicates)

by BMDM at 6hr without LPS stimulation used as the control population. MHC II is used by professional APCs, such as macrophages, to present antigen, with ligation of the co-stimulatory molecules CD86 and CD40 involved in defining the outcome of antigen recognition. On stimulation with 1ng/ml LPS MHC II expression by the BMDM was decreased at 6hr (75±16% of that on control BMDM) compared to un-stimulated BMDM, however by 24hr more MHC II was expressed by the BMDM + LPS (41±4% vs. 57±18%) (Figure 3.8a). At 6hr CD86 expression was increased on low-level LPS stimulation (96±13% vs. 137±24%), however by 24hr no difference could be detected between the stimulated and un-stimulated BMDM (Figure 3.8b). CD40 expression was unchanged by LPS stimulation at 6hr, however a dramatic increase was observed at the 24hr time-point after stimulation, with expression increasing to 774±108% of that on control BMDM (Figure 3.8c).

The expression of two macrophage activation markers was also explored. CD69 is an early activation marker, with its up-regulation indicating cell activation [197]. CD206, also commonly know as the mannose receptor, is a C-type lectin receptor that is mainly expressed on the surface of regulatory subsets of macrophages. Expression of both CD69 and CD206 was enhanced by stimulation with LPS at both the 6 and 24hr time-points (Figure 3.8d, e). At 6hr CD69 expression on BMDM+LPS was 2498±961% of control expression, and at 24hr was 3059±1074% compared to 240±210% on the un-stimulated BMDM. CD206 expression was 193±16% of the control on BMDM+LPS at 6hr, while at 24hr it was 86±4% of the control compared to 48±3% on the un-stimulated BMDM.

The effect of BMDM-AC co-culture on the antigen-presenting potential of the BMDM was investigated; with the expression of MHC II, CD86 and CD40 examined. At the 6hr time-point, co-culture of L29 BMDM with Etoposide-treated B cells or thymocytes, in the absence of LPS, had no effect on the expression of MHC II, CD86 or CD40, compared to L929 BMDM cultured under the same conditions alone (Figure 3.9a-c, left panels), however co-culture with irradiated B cells induced significant up-regulation of all three markers. MHC II expression increased to 176±38% of that on control BMDM, CD86 to 148±39% and CD40 to 156±11%. Co-culture of L929 BMDM with irradiated thymocytes resulted in the up-regulation of the co-stimulatory molecules CD86 (148±39% of control) and CD40 (169±41% of control), however no change in MHC II expression was seen. Interestingly, viable B cells also induced enhanced expression of these molecules, with CD86 increased to 138±9% and CD40 146±27% of control levels. Viable thymocyte co-culture however, had no effect on the expression of these molecules. In the presence of low-level LPS, no change in CD86 or CD40 expression was seen in any co-culture condition, however co-culture with Etoposide-treated thymocytes or viable B cells increased the expression of MHC II by L929 BMDM (136±18% of control and 156±30% of

control, respectively). At the 24hr time-point MHC II expression was significantly up-regulated on L929 BMDM co-cultured with any of the apoptotic cells investigated in the absence of LPS (BMDM+irr B: 146±7%, BMDM+irr thy: 153±25%, BMDM+Etop. B: 137±7%, BMDM+Etop. thy: 147±23% of control expression) (Figure 3.9a, right panel).

Interestingly, co-culture with viable B cell or thymocytes also induced up-regulation of MHC II, with levels increasing to 134±14% of the control on co-culture with viable B cells, and to 136±21% on co-culture with viable thymocytes. In the presence of low-level LPS, no change in MHC II expression was observed at the 24hr time-point, with levels of CD86 also staying equivalent to controls, both in the presence and absence of LPS (Figure 3.9b, right panel). CD40 expression was enhanced after 24hr of L929 BMDM co-culture with irradiated B cells in the absence of low-level LPS, with expression increasing to 128±6% of that of control cells, however no change was seen in the other apoptotic cell co-cultures (Figure 3.9c, right panel). Enhanced expression of CD40 was also induced after co-culture of L929 BMDM with viable B cells, with surface levels increasing to 129±10% of controls.

The expression of activatory and regulatory markers was explored in order to help determine whether the co-culture of BMDM with different AC has an effect on macrophage polarization. At 6hr, co-culture with all AC investigated, except the irradiated B cells, had no effect on CD69 expression in the absence of low-level LPS (Figure 3.10a – left panel) Co-culture with irradiated B cells resulted in the up-regulation of CD69 to 222±115% of control expression. In the presence of LPS, L929 BMDM co-culture with Etoposide-treated thymocytes resulted in the down-regulation of CD69 expression, with levels decreasing to 58±5% of baseline. No other BMDM-AC co-culture resulted in the modulation of CD69 at 6hr in the presence of LPS. Co-culture with viable B cell or thymocytes also resulted in no change in CD69 expression at 6hr, in the presence or absence of low-level LPS. At this time-point, in the absence of LPS, CD206 expression by BMDM was comparable for co-culture conditions investigated, however the data indicates a decrease in expression on co-culture with irradiated or viable B cells, however this was not significant (Figure 3.10 – left panel). Addition of low-level LPS to the irradiated B cells or thymocytes, or Etoposide-treated B cells co-cultures had no effect on CD206 expression by BMDM, however on co-culture with Etoposide-treated thymocytes, expression decreased to 63±5% of baseline. At the 24hr time-point a decrease from baseline in the expression of both CD69 and CD206 was seen in all co-culture conditions (apoptotic and viable cells) in the presence of low-level LPS (Figure 3.10a and b – right panels). In the absence of LPS, co-culture of L929 BMDM with irradiated B cells resulted in the increased expression of CD69 to 202±89% of baseline, however irradiated thymocytes, Etoposide-treated cells nor viable cells had any effect

on CD69 expression. Co-culture with both irradiated B cells and Etoposide-treated thymocytes induced a decrease in CD206 expression at 24hr in the absence of LPS, with BMDM co-cultures with irradiated B cells expressing 72±6% of baseline CD206 and those co-cultured with Etoposide-treated thymocytes expressing 78±7%. The other apoptotic cells had no effect on CD206 expression, however co-culture with viable B cells was also able to down-regulate its expression, with 72±4% of baseline expression at 24hr. Viable thymocytes did not have the same effect as viable B cells, and no change in CD206 expression was observed in this co-culture condition.

These data indicate that different AC populations can have differing effects on L929 BMDM phenotype under certain *in vitro* culture conditions, with these differences seeming to be greater after short-term culture. However, in the presence of low-level LPS, the differences in the effects of the four populations of AC on BMDM phenotype were greatly reduced at the 6hr time-point, and totally eliminated at 24hr.

3.2.7 Changes in L929 BMDM function after co-culture with irradiated or Etoposide-treated apoptotic cells

To determine whether the interaction of L929 BMDM with AC had functional effects on the BMDM, the production of soluble immune mediators by BMDM was investigated after overnight co-culture with AC. Sandwich ELISAs were utilized to quantify the levels of pro-inflammatory (IL-12, TNFα, and IL-6) and anti-inflammatory (IL-10 and TGF-β) cytokines present in the cell culture supernatants, while a competitive binding ELISA was used to quantify production of the prostaglandin PGE_2, a physiologically abundant eicosanoid known have immunomodulatory properties.

When co-cultured alone, un-stimulated L929 BMDM produced minimal levels of IL-12 (20±5pg/ml), TNFα (32±4pg/ml) and IL-6 (20±6pg/ml) (Figure 3.11a-c – left panels). On co-culture with AC, no effect was seen on the production of IL-12 (Figure 3.11a – left panel), however levels of TNFα and IL-6 were decreased, resulting in levels of secretion below the minimum detection limit of the assays used (15.6pg/ml for both assays) (Figure 3.11b and c – right panels). Viable cells had the same effects on pro-inflammatory cytokine production as AC for all cytokines investigated. On the addition of 1ng/ml LPS to the culture system, L929 BMDM produced increased levels of IL-12 (133±18g/ml), TNFα (134±14pm/ml) and IL-6 (2182±97pg/ml) (Figure 3.11a-c – right panels) compared to those cultured in the absence of LPS. Co-culture with AC had no effect on the production of IL-12 or TNFα production by LPS treated BMDM, compared to the L929 BMDM cultured alone in the same conditions. Surprisingly, the data indicate a reduction in TNFα secretion by L929 BMDM after co-culture with either viable B cells

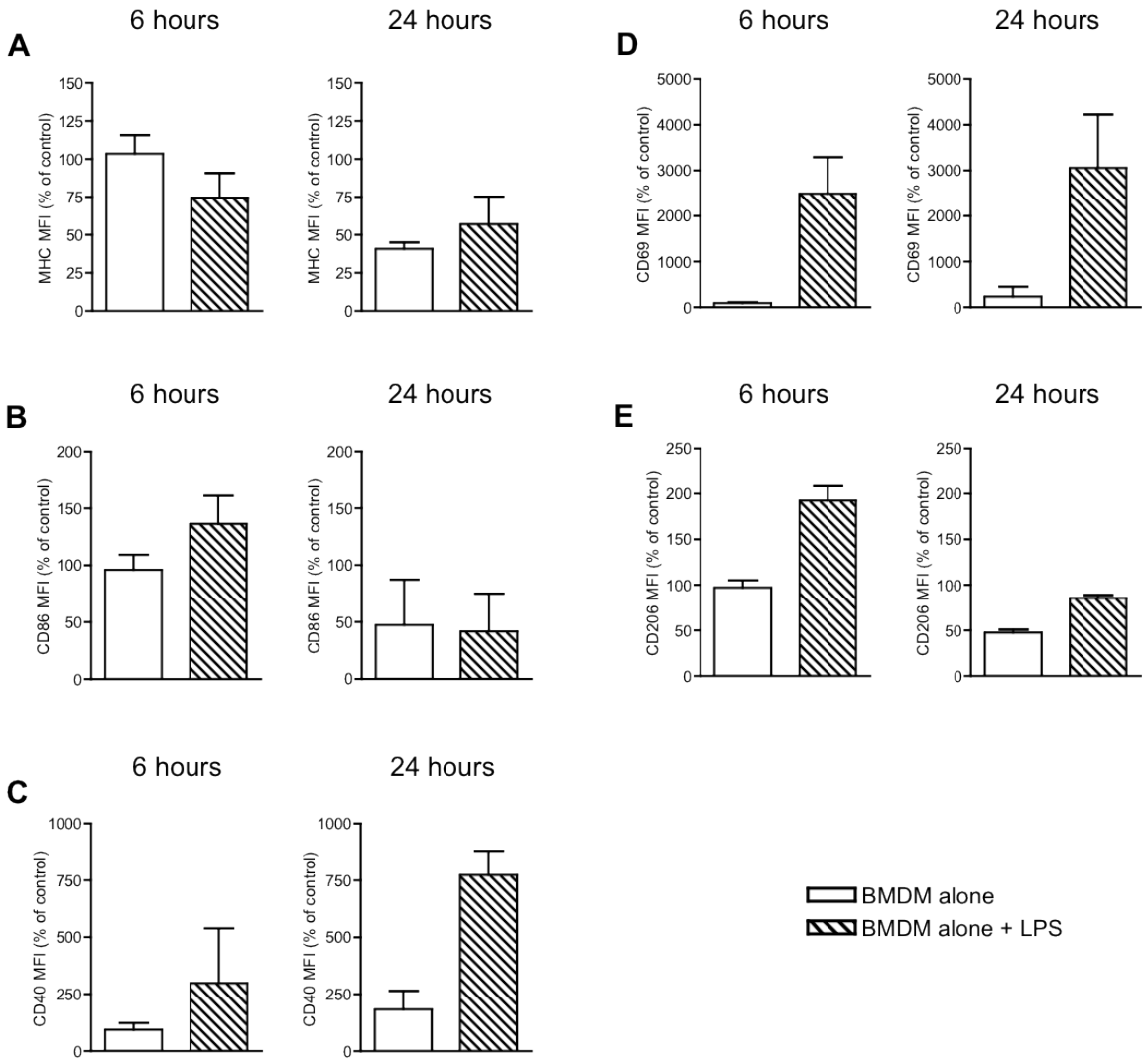

Figure 3.8 Stimulation of L929 BMDM with LPS alters their phenotype
Murine BMDM were grown in cRPMI supplemented with M-CSF containing L929 supernatant. On d7 adherent cells were stimulated with 1ng/ml LPS. After 6hr and 24hr incubations cells were stained for expression of molecules involved in antigen presentation and cell activation and analyzed by flow cytometry. Expression levels of cell surface markers were normalized, with expression of the marker by BMDM at 6hr without LPS stimulation used as the control population. Graphs showing the normalized MFIs for (**A**) MHC II (**B**) CD86, (**C**) CD40, (**D**) CD69, and (**E**) CD206. White bars = BMDM alone, striped bars = BMDM alone + 1ng/ml LPS. (n=2, data from 2 independent experiments with 3 replicates each)

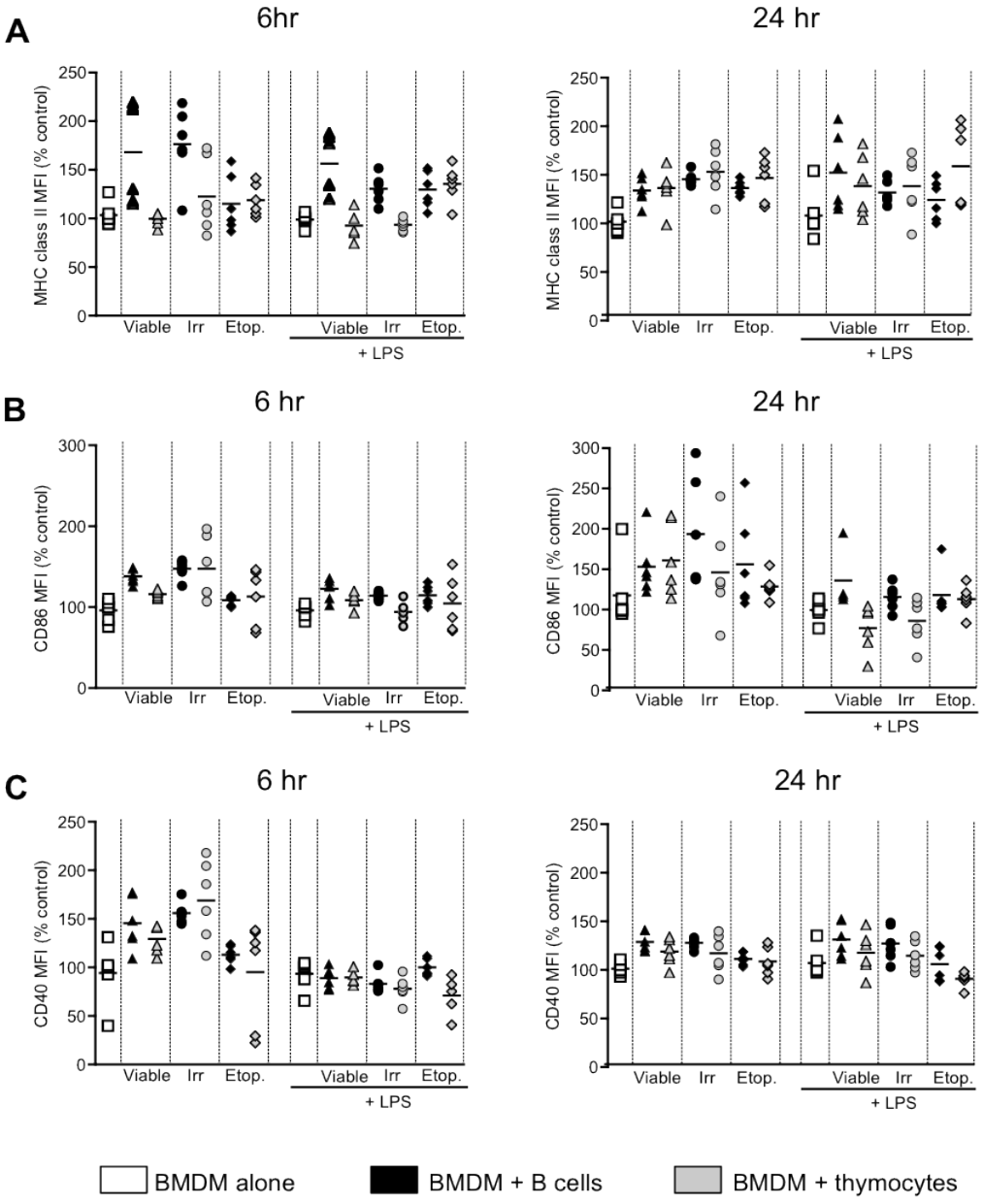

Figure 3.9 Co-culture with viable or apoptotic cells alters the antigen-presenting potential of L929 BMDM

Murine BMDM were grown in cRPMI supplemented with M-CSF containing L929 supernatant. On d7 adherent cells were co-cultured with viable, irradiated, or Etoposide-treated primary B cells or thymocytes, in the presence or absence of 1ng/ml LPS. After 6hr and 24hr of co-cultures cells were stained for expression of molecules involved in antigen presentation and analyzed by flow cytometry. Expression levels of cell surface markers were normalized, with expression of the marker by BMDM alone without used as the control population. Graphs showing the normalized MFIs of (**A**) MHC II, (**B**) CD86, and (**C**) CD40. White symbols = BMDM alone, black symbols = BMDM + B cells, grey symbols = BMDM + thymocytes. (n=2, data from 2 independent experiments)

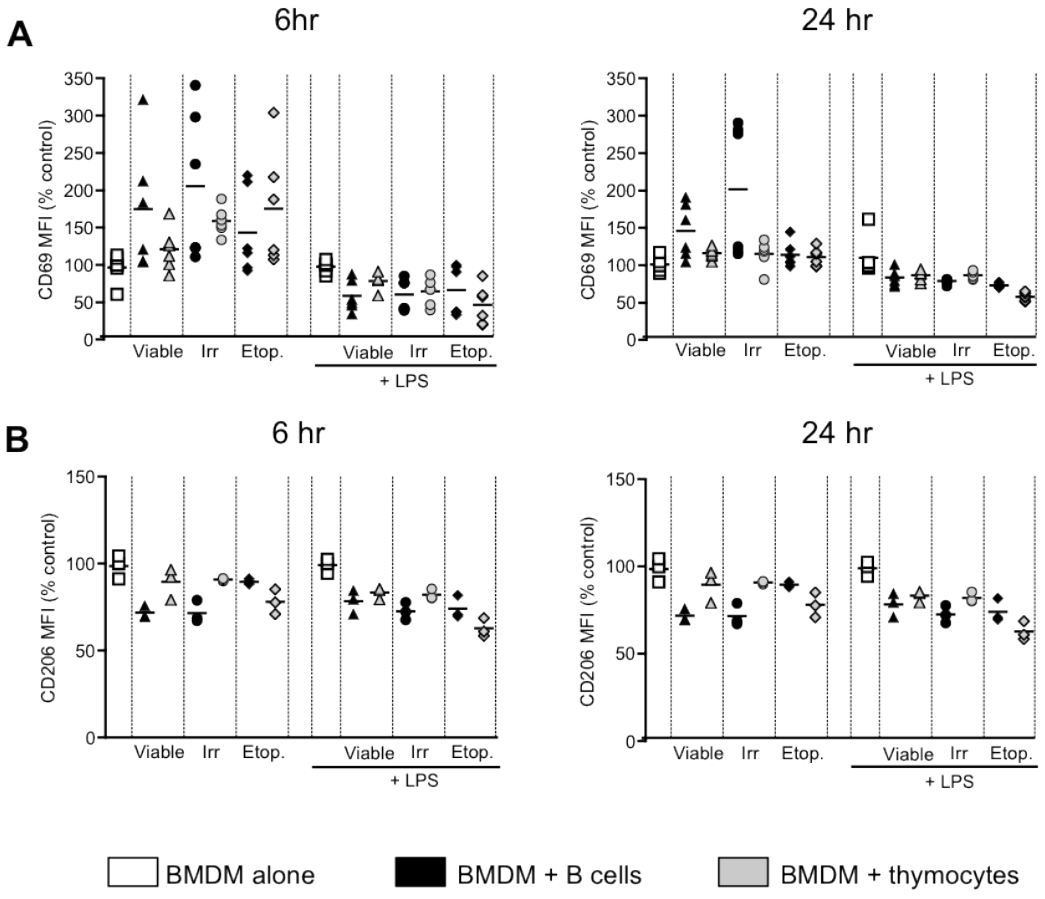

Figure 3.10 Co-culture with viable or apoptotic cells alters L929 BMDM activation
Murine BMDM were grown in cRPMI supplemented with M-CSF containing L929 supernatant. On d7 adherent cells were co-cultured with viable, irradiated, or Etoposide-treated primary B cells or thymocytes, in the presence or absence of 1ng/ml LPS. After 6hr and 24hr of co-cultures cells were stained for expression of molecules involved in cell activation and analyzed by flow cytometry. Expression levels of cell surface markers were normalized, with expression of the marker by BMDM alone without used as the control population. Graphs showing the normalized MFIs for (**A**) CD69 and (**B**) CD206. White symbols = BMDM alone, black symbols = BMDM + B cells, grey symbols = BMDM + thymocytes. (CD69 n=2, with data from 2 independent experiments, CD206 n=1, data from a single experiment)

(62±19pg/ml) or thymocytes (103±25pg/ml). Co-culture of L929 BMDM with viable, irradiated or Etoposide-treated cells in the presence of 1ng/ml LPS resulted in an increase in IL-6 production (5313±858pg/ml), compared to BMDM cultured alone, however with the number of repeats undertaken, signifiance was not reached in any condition.

IL-10 secretion by L929 BMDM was not affected by co-culture with AC in the presence or absence of LPS, as compared to secretion by BMDM alone (no LPS: 104±90pg/ml, LPS: 1888±987pg/ml), with viable cells also having no effect (Figure 3.12a). No change in the production of TGF-β by L929 BMDM after co-culture with AC was detected, in either the presence or absence of LPS (Figure 3.12b). However the results gained from the TGF-β ELISAs were extremely variable, and therefore a subtle change in levels could have been obscured.

Production of PGE_2 by L929 BMDM in response to co-culture with AC was also investigated. PGE_2 can be secreted by macrophages in response to a range of stimuli [157,198,199], and the addition of exogenous PGE_2 has been shown to be able to regulate cytokine production by macrophage populations [157,200,201]. A competitive binding ELISA was used to quantify PGE_2 levels, and as such, all concentrations were normalized to the media only control and expressed as a change in PGE_2 concentration above this background (Δ PGE_2).

Co-culture of the L929 BMDM with all AC populations resulted in a marked increase in PGE_2, compared to BMDM cultured alone (47±4 pg/mlΔ PGE_2) (Figure 3.12c). Although this increase was seen on co-culture of L929 BMDM with all AC, more PGE_2 was secreted by the BMDM on co-culture with irradiated cells, compared to those co-cultured with AC from the same origin which had undergone Etoposide-treatment (L929+irr B: 362±25pg/ml vs. L929+Etop. B: 271±27pg/ml Δ PGE_2, and L929+irr thy: 376±22pg/ml vs. L929+Etop. thy: 101±17pg/ml Δ PGE_2). Co-culture with viable B cells and thymocytes also resulted in increased PGE_2 secretion, with 304±6pg/ml and 280±23pg/ml Δ PGE_2, respectively.

These data confirm that AC are able to modulate cytokine production by L929 BMDM, with both pro-and anti-inflammatory cytokine production altered on overnight co-culture with AC, regardless of the activation state of the BMDM. Secretion of PGE_2 by L929 BMDM was significantly increased after co-culture with all AC populations. All AC investigated induced similar effects on the BMDM, with the AC origin and route of apoptosis induction seemingly immaterial to the outcome of co-culture. Interestingly,

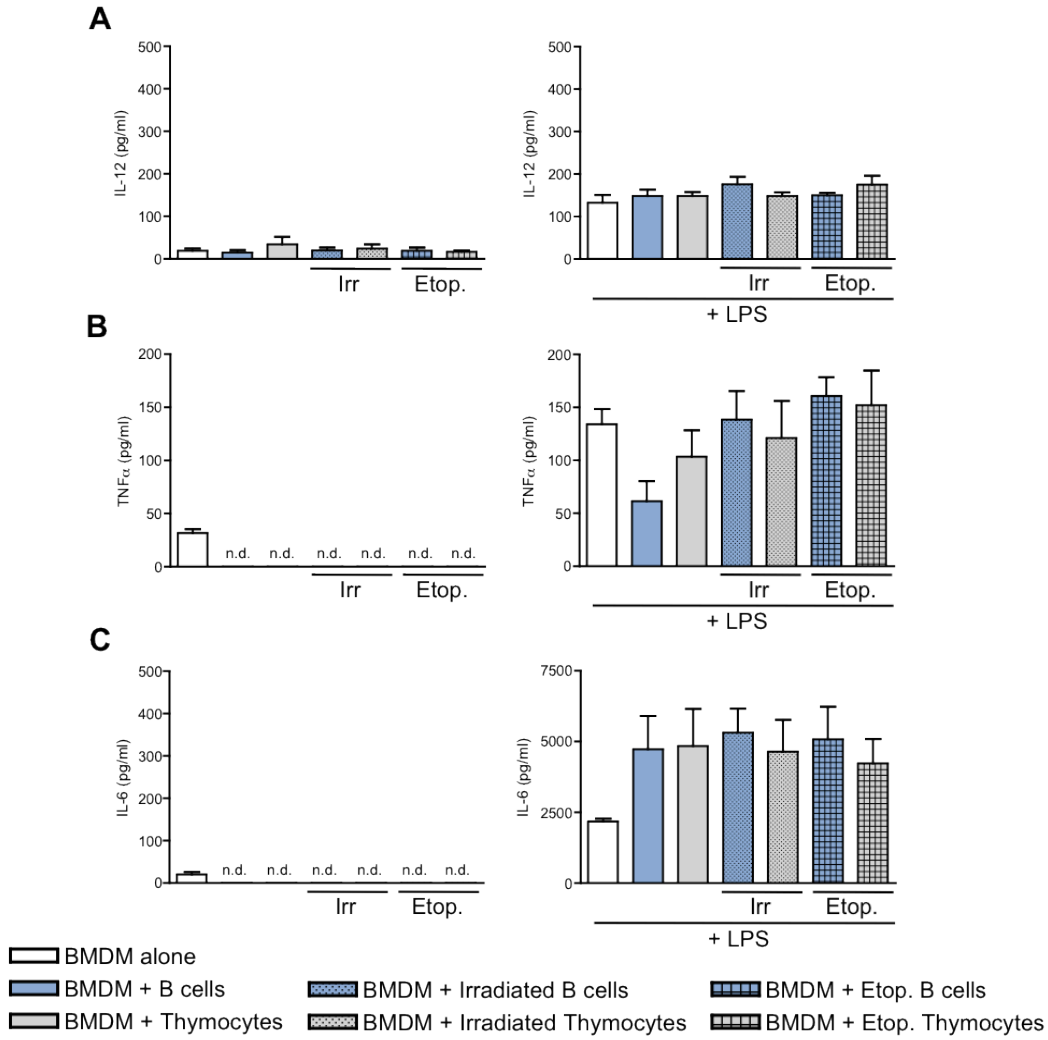

Figure 3.11 Pro-inflammatory cytokine production by L929 BMDM after co-culture
Murine BMDM were grown in cRPMI supplemented with L929 cell supernatant. On d7 adherent cells were co-cultured overnight with viable, irradiated, or etoposide treated primary B cells or Thymocytes, in the presence or absence of 1ng/ml LPS. Cytokine production by L929 BMDM was quantified using ELISAs. (**A**) Graph of IL-12 produced (pg/ml). Left column: no LPS, Right column: + LPS. (**B**) Graph of TNFα produced (pg/ml). Left column: no LPS, Right column: + LPS. (**C**) Graph of IL-6 production (pg/ml). Left column: no LPS, Right column: + LPS. (n=1, 3 replicates)

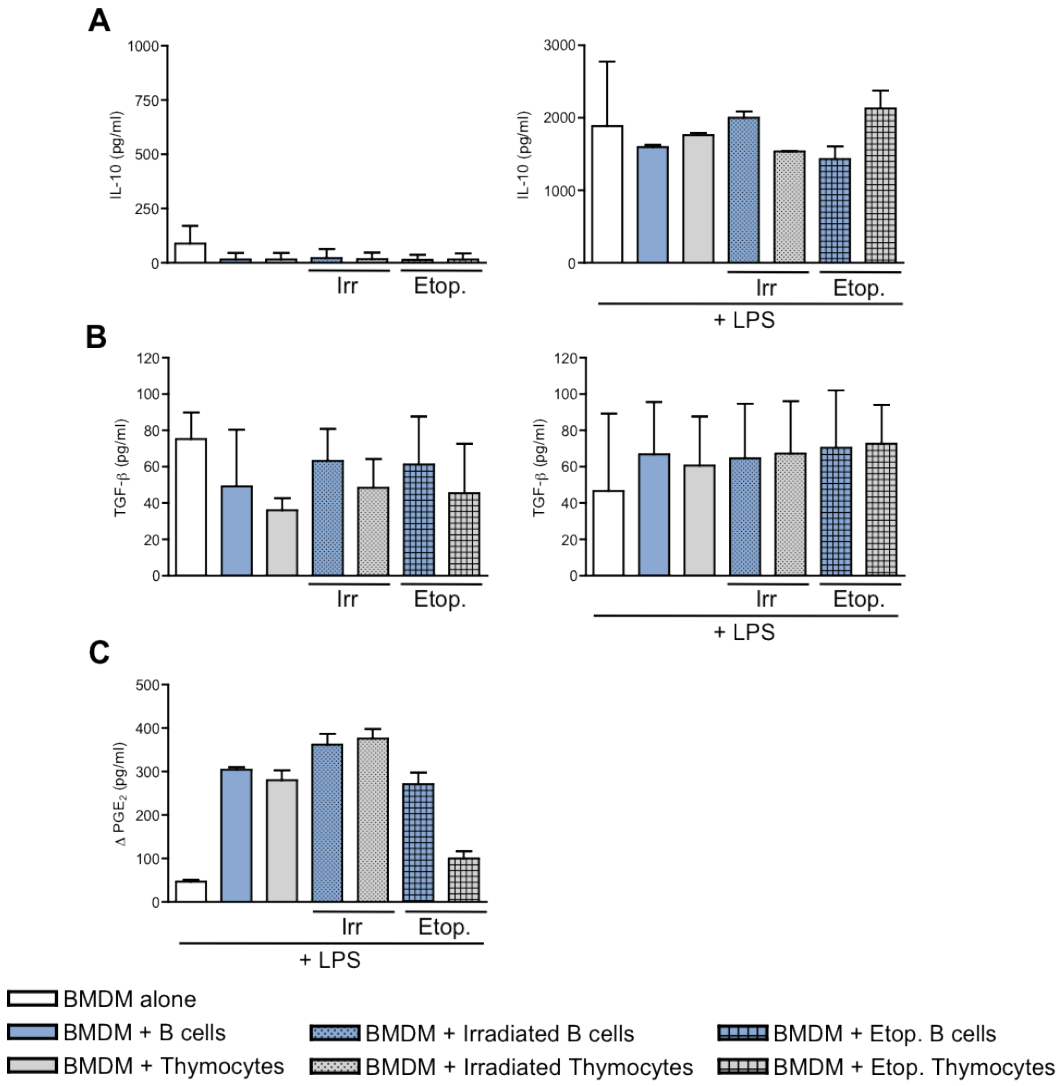

Figure 3.12 Anti-inflammatory cytokine and PGE_2 production by L929 BMDM after co-culture
Murine BMDM were grown in cRPMI supplemented with L929 cell supernatant. On d7 adherent cells were co-cultured overnight with viable, irradiated, or etoposide treated primary B cells or thymocytes, in the presence or absence of 1ng/ml LPS. Cytokine and PGE_2 production by L929 BMDM were quantified using ELISAs. (**A**) Graph of IL-10 produced (pg/ml). Left column: no LPS, Right column: + LPS. (**B**) Graph of TGF-β produced (pg/ml). Left column: no LPS, Right column: + LPS. (**C**) Graph of PGE_2 produced (pg/ml) in the presence of LPS. (IL-10 and TGF-β n=2, from 2 independent experiments, PGE_2 n=1)

under the experimental conditions used, viable cells showed the same immunomodulatory properties as apoptotic cells, with affects on both cytokine and PGE_2 production.

3.2.8 Comparison of interactions of L929 BMDM and GM-CSF BMDM with apoptotic cells

There are multiple methods of *in vitro* maturation that can be used to generate macrophage populations from bone marrow cells, and depending on the method chosen considerable variability is seen in the resultant macrophage phenotype. Macrophages are highly plastic cells, with a spectrum of activated phenotypes, however these can be broadly split into two main subsets – the classically activated, M1-macrophages, and the regulatory/wound-healing M2-macrophages [17]. BMDM generated using M-CSF-containing L929 cell supernatant are considered to be 'M2-like' macrophages [202], resembling non-inflammatory, regulatory macrophages found *in vivo,* while those generated using GM-CSF are considered to be more like an M1 macrophage.

After observing the interactions of L929 BMDM with apoptotic cells, we wanted to investigate whether similar patterns of interaction would result from co-culture of AC with a more inflammatory population of macrophages. To do this, BMDM were generated in media supplemented with GM-CSF and IL-3 (GM-CSF BMDM), giving rise to a population of M1-like macrophages [202], and the previous co-culture experiments repeated using this BMDM population: mature, adherent GM-CSF BMDM were co-cultured with CFSE-stained viable, irradiated or Etoposide-treated B cell or thymocytes for 15min, at a ratio of 5 lymphocytes/AC:1 BMDM. The decision was made to no longer include T cell co-culture conditions in this assay, due to technical issues with the method of T cell purification. 1ng/ml LPS stimulation was added to certain conditions during the co-cultures, and L929 BMDM included for comparison. As before, interaction levels were analyzed by flow cytometry (Figure 3.13a).

No difference was seen in the proportion of $CFSE^+$ GM-CSF BMDM observed after co-culture with either irradiated B cells or thymocytes (Figure 3.13b – left panel). A reduction in $CFSE^+$ BMDM was observed when GM-CSF BMDM were co-cultured with Etoposide-treated B cells or thymocytes in the absence of LPS, compared to the co-cultures with irradiated lymphocytes (GM-CSF+Etop. B: 58.2±14.8%% and GM-CSF+Etop. thy: 60.7±13% vs. GM-CSF+irr B: 98.1±2.1% and GM-CSF+irr thy: 95.7±3%). When GM-CSF BMDM were co-cultured with Etoposide-treated B cells in the presence of LPS, a decrease in the proportion of $CFSE^+$ BMDM was also seen compared to all other conditions. Viable B cells and thymocytes were included as a control, with the resultant

levels of $CFSE^{+}$ BMDM comparable to those seen after co-culture with irradiated cells, both in the presence and absence of LPS. The levels of $CFSE^{+}$ L929 BMDM were more consistent than that of the $CFSE^{+}$ GM-CSF BMDM. A decrease in the proportion of $CFSE^{+}$ L929 BMDM was observed on co-culture with Etoposide-treated B cells in the absence of LPS (73.3±21.1%) (Figure 3.13b – right panel).

On investigation of the population of GM-CSF BMDM undergoing elevated AC interactions ($CFSE^{hi}$ BMDM), it could be seen that regardless of the origin of the AC, or the mode of apoptosis induction, a similar proportion of $CFSE^{hi}$ GM-CSF BMDM were observed after co-culture in the absence of LPS (GM-CSF+irr B: 3.6±2.3%, GM-CSF+irr thy: 5±0.7%, GM-CSF+Etop. B: 2.5±0.6%, GM-CSF+Etop. thy: 3.8±0.4%) (Figure 3.13c – left panel). Similar levels of $CFSE^{hi}$ GM-CSF BMDM were also detected after co-culture with viable B cells and thymocytes, in the absence of LPS. On addition of LPS into the BMDM-AC co-culture system, no differences were seen in the proportion of $CFSE^{hi}$ GM-CSF BMDM after co-culture with any of the AC investigated, or with viable thymocytes. However, co-culture of GM-CSF BMDM with viable B cells in the presence of LPS resulted in a slight increase in $CFSE^{hi}$ BMDM (12.8±0.5% $CFSE^{hi}$), compared to all other co-culture conditions. Although an increase in the percentage of $CFSE^{hi}$ BMDM was observed after co-culture with viable B cells, the levels of $CFSE^{hi}$ BMDM were still relatively low. As with the GM-CSF BMDM, co-culture of L929 BMDM with all AC resulted in comparable percentages of $CFSE^{hi}$ BMDM, however co-culture with viable B cells resulted in a significantly increased proportion of $CFSE^{hi}$ L929 BMDM compared to all other conditions (no LPS: 50.8±21.8%, + LPS: 52.3±20% $CFSE^{hi}$) (Figure 3.13c – right panel). The percentages of $CFSE^{hi}$ L929 BMDM after co-culture were consistently higher than those observed in the GM-CSF BMDM co-cultures, regardless of the culture conditions.

Together these findings show that in this experimental set up GM-CSF BMDM undergo lower levels of interaction with AC than L929 BMDM, however, the pattern of interaction within the two BMDM populations is similar. The method used to induce apoptosis affected the overall interaction levels seen, with Etoposide-treated cells tending to undergo less interaction with BMDM. Within each BMDM population, similar levels of enhanced interaction were observed in all co-cultures incorporating apoptotic B cells and thymocytes, in the presence and absence of LPS, with viable thymocyte also showing similar levels of interaction with BMDM. Surprisingly, the co-culture of GM-CSF BMDM or L929 BMDM with viable B cells resulted in a significant increase in the proportion of $CFSE^{hi}$ BMDM, compared to the AC-containing co-cultures.

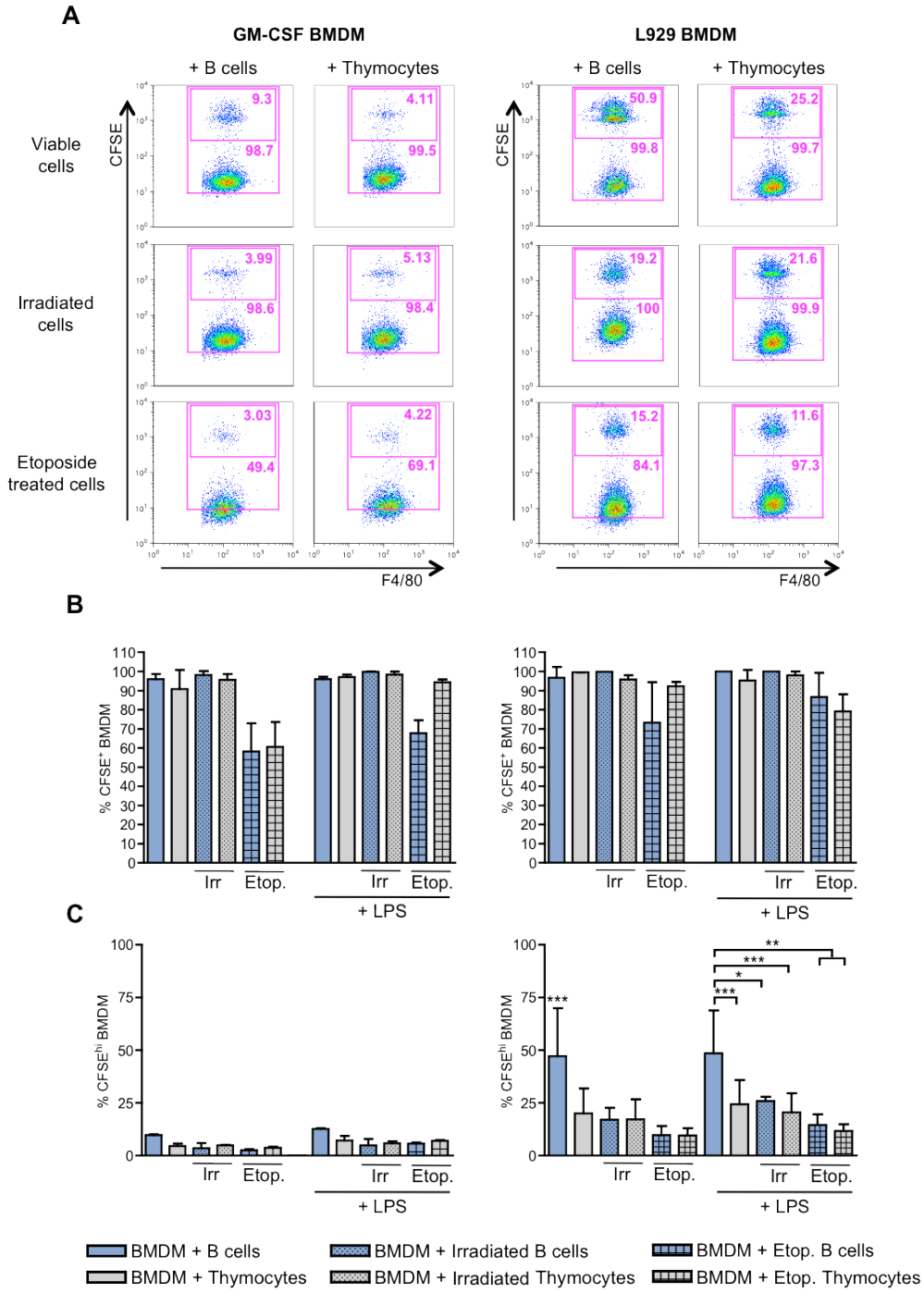

Figure 3.13 L929 BMDM show enhanced cell-cell interactions compared to GM-CSF BMDM
Murine BMDM were grown in cRPMI supplemented with either M-CSF containing L929 supernatant or recombinant murine GM-CSF + IL-3. On d7 adherent cells were co-cultured with CFSE stained viable, irradiated, or Etoposide-treated primary B cells or thymocytes for 15 minutes, in the presence or absence of 1ng/ml LPS and analyzed by flow cytometry. (**A**) Representative FACS plots showing the levels of interaction seen between the GM-CSF BMDM or L929 BMDM and the apoptotic lymphocytes. Panels: CFSE vs. F4/80. (**B**) Graph of pooled data showing the percentage of $CFSE^{+}$ GM-CSF BMDM (left) and L929 BMDM (right). (**C**) Graph of pooled data showing the percentage of $CFSE^{hi}$ GM-CSF BMDM (left) and L929 BMDM (right). (L929 BMDM n=3, from 3 independent experiments, GM-CSF BMDM n=2, from 2 independent experiments). Statistics used: One Way ANOVA followed by Bonferroni's post test, with * = $p<0.05$, ** = $p<0.01$ and *** = $p<0.001$.

3.2.9 Changes in GM-CSF BMDM function after co-culture with apoptotic cells

To determine whether the interaction of GM-CSF BMDM with AC had any functional effect on the BMDM, the production of soluble mediators by GM-CSF BMDM after overnight culture with AC was investigated. The levels of the cytokines IL-12, TNFα, IL-6, IL-10, and TGF-β present in the cell culture supernatants were quantified by ELISA, with a competitive binding ELISA used to quantify production of PGE_2.

Unlike the L929 BMDM, in the absence of LPS stimulation, no TNFα, IL-6 or IL-10 could be detected in any condition containing GM-CSF BMDM (data not shown). The L929 BMDM secreted detectable levels of all three of these cytokines when cultured alone (Figures 3.11 and 3.12). In the absence of LPS, a decrease in IL-12 production was observed on co-culture of GM-CSF BMDM with either irradiated (GM-CSF+irr B: 12±5pg/ml, GM-CSF+irr thy: 16±8pg/ml) or Etoposide-treated cells (GM-CSF+Etop. B: 8±4pg/ml, GM-CSF+Etop. thy: 11.8±6.7pg/ml), compared to the BMDM cultured alone (99±30pg/ml) (Figure 3.14a – left panel). This finding differed from that seen on co-culture of L929 BMDM with AC in the absence of LPS, in which no change in IL-12 was seen compared to BMDM cultured alone (Figure 3.11). Interestingly, co-culture with viable cells also resulted in a reduction of IL-12 secretion (GM-CSF+B: 9±4pg/ml, GM-CSF+thy: 12±5pg/ml). In the presence of LPS, co-culture of GM-CSF BMDM with AC had no effect on the levels of IL-12 (Figure 3.14a – right panel), IL-6 (Figure 3.14c) or IL-10 secretion (Figure 3.15a), compared to BMDM cultured alone, with viable cells also having no effect on the production of these cytokines. Co-culture of L929 BMDM with AC in the presence of LPS also had no effect on IL-12 or IL-10 secretion (Figure 3.12), however co-culture with AC increased IL-6 production by these BMDM (Figure 3.11). A marked decrease in TNFα was detected on co-culture, with GM-CSF BMDM cultured alone producing 42±7pg/ml TNFα, while TNFα sectretion by BMDM co-cultured with either AC or viable cells dropped below the 15.6pg/ml detection limit of this assay (Figure 3.14b). As with L929 BMDM (Figure 3.12), no change in the production of TGF-β was detected on co-culture of GM-CSF BMDM with AC, in either the presence or absence of LPS (Figure 3.15b), however the results gained from this ELISA were extremely variable and therefore a subtle change in levels could have been obscured.

Production of PGE_2 by GM-CSF BMDM in response to co-culture with AC was also investigated. When GM-CSF BMDM were cultured in the absence of LPS, no PGE_2 was detectable above background in any condition (data not shown), mirroring the results seen with L929 BMDM. In the presence of LPS, co-culture of GM-CSF BMDM with irradiated B cells or thymocytes resulted in an increase in PGE_2 (98±35pg/ml and

117±20 pg/ml Δ PGE_2, respectively), compared to the GM-CSF BMDM cultured alone (17±5pg/ml Δ PGE_2) (Figure 3.14c). GM-CSF BMDM co-culture with Etoposide-treated cells did not affect the levels of PGE_2 (21±8pg/ml Δ PGE_2). Co-culture of GM-CSF BMDM with viable B cells and thymocytes also induced an increase in PGE_2 production compared to BMDM alone, with a 66±16pg/ml Δ PGE_2 and 95±22pg/ml Δ PGE_2 seen, respectively. This pattern of PGE_2 production differed from that of the L929 BMDM. GM-CSF BMDM cultured alone in the presence of LPS produced markedly less PGE_2 than L929 BMDM cultured in the same conditions (17±5pg/ml Δ PGE_2 vs. 47±4 pg/ml Δ PGE_2), with co-culture of L929 BMDM with either AC or viable cells resulting in a substantial increase in PGE_2 (Figure 3.12c).

These data confirm that AC are able to modulate immune-mediator production by M1-like GM-CSF BMDM, with both pro-inflammatory cytokine and PGE_2 production altered on overnight co-culture with AC. All AC investigated induced similar effects on cytokine production by GM-CSF BMDM, with the AC origin and route of apoptosis induction seemingly immaterial to the outcome of co-culture, however GM-CSF BMDM production of PGE_2 was only increased by co-culture with AC induced by irradiation, not Etoposide-treatment. Interestingly, under the experimental conditions used, co-culture with viable cells had the same immunomodulatory effects on cytokine secretion by GM-CSF BMDM as apoptotic cells, however viable cell co-culture had varying effects on PGE_2 production by the BMDM.

3.3 Discussion

- As an initial step to understanding the potential validity of our hypothesis, we used an *in vitro* assay to examine the immunosuppressive effects of apoptotic B cells, with a focus on whether apoptotic B cells have the same immunomodulatory capacities as other more commonly studies AC.
- Apoptotic B cells underwent similar levels of interaction with macrophages as the other apoptotic cells examined, and had comparable ability to alter macrophage phenotype and function. These findings show that apoptotic B cells have the same capacity to modulate the immune response as other more commonly studied AC.
- Unexpectedly, BMDM underwent increased levels of interaction with viable B cells, compared to other viable lymphocyte populations and all AC investigated. All the viable cell populations investigated were able to recapitulate the AC-driven modulation of macrophage phenotype and function, with further work needed to fully understand this result.

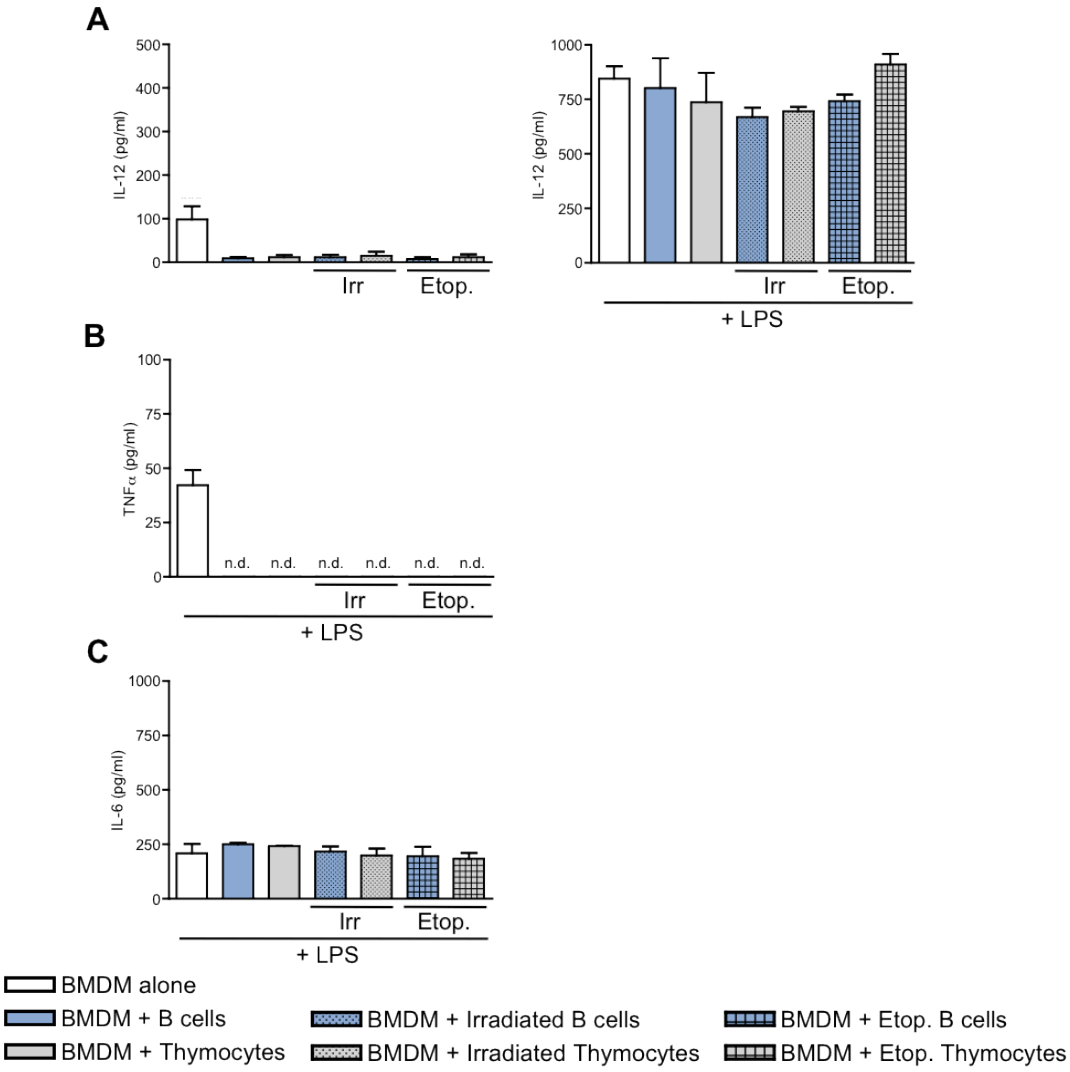

Figure 3.14 Pro-inflammatory cytokine production by GM-CSF BMDM after co-culture
Murine BMDM were grown in cRPMI supplemented with recombinant murine GM-CSF and IL-3. On d7 adherent cells were co-cultured overnight with viable, irradiated, or Etoposide-treated primary B cells or thymocytes, in the presence or absence of 1ng/ml LPS. Cytokine production by GM-CSF BMDM was quantified using ELISAs. (**A**) Graph of IL-12 produced (pg/ml). Left column: no LPS, Right column: + 1ng/ml LPS. (**B**) Graph of TNFα produced (pg/ml) in the presence of LPS. (**C**) Graph of IL-6 production (pg/ml) in the presence of LPS. (n=1, 3 replicates)

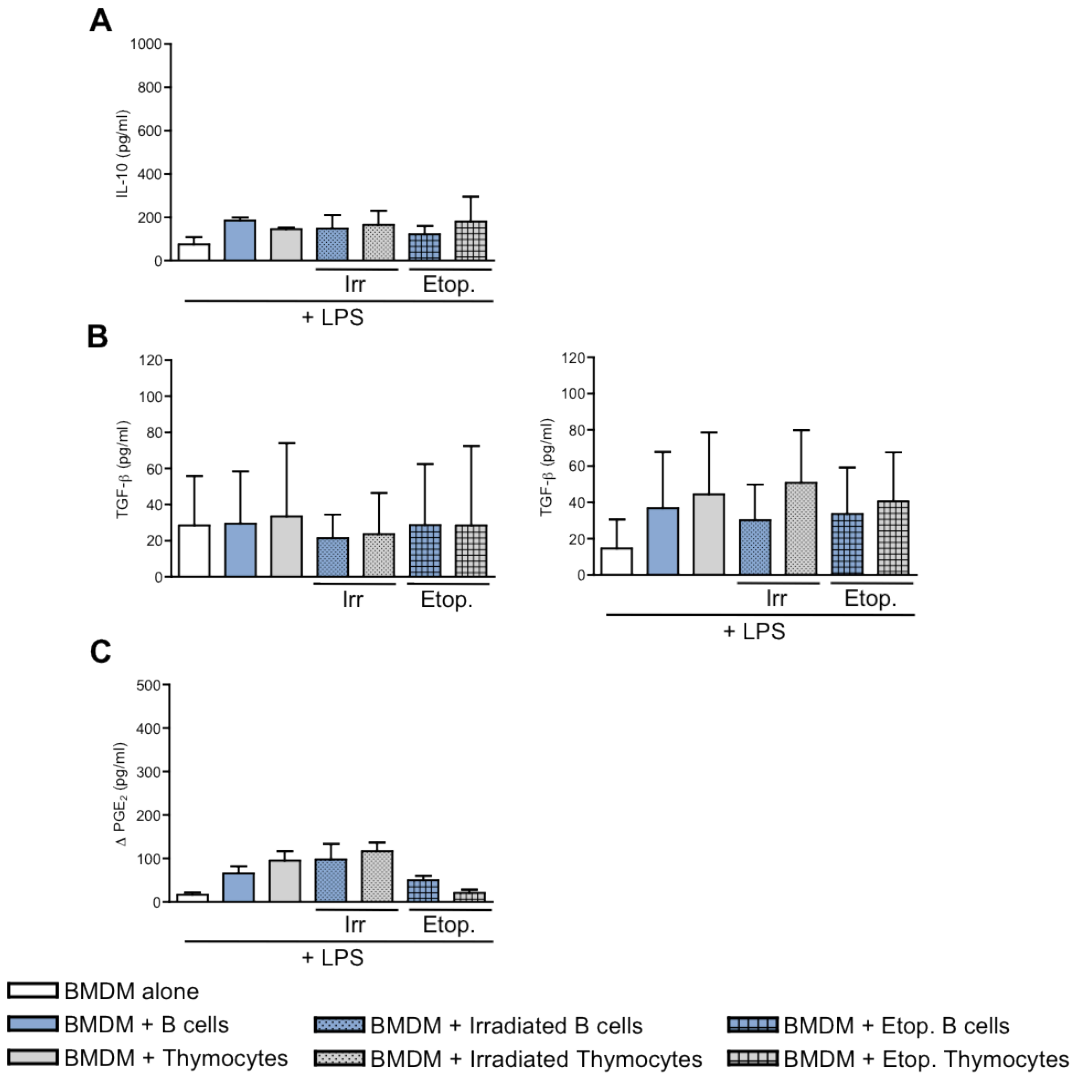

Figure 3.15 Anti-inflammatory cytokine and PGE_2 production by GM-CSF BMDM after co-culture

Murine BMDM were grown in cRPMI supplemented with recombinant murine GM-CSF and IL-3. On d7 adherent cells were co-cultured overnight with viable, irradiated, or etoposide treated primary B cells or Thymocytes, in the presence or absence of 1ng/ml LPS. Cytokine and PGE_2 production by GM-CSF BMDM were quantified using ELISAs. (**A**) Graph of IL-10 produced (pg/ml) in the presence of LPS. (**B**) Graph of TGF-β produced (pg/ml). Left column: no LPS, Right column: + 1ng/ml LPS. (**C**) Graph of PGE_2 produced (pg/ml) in the presence of LPS. (IL-10 and TGF-β n=2, from 2 independent experiments, PGE_2 n=1)

- These preliminary results support our hypothesis, and indicate that the RTX-mediated generation of large numbers of apoptotic B cells *in vivo* would be able to dampen down inflammation, and potentially help halt the progression of autoimmunity.

On co-culture of BMDM with either irradiated or viable CFSE-stained lymphocytes, the vast majority of BMDM became $CFSE^{+}$, with two distinct $CFSE^{+}$ BMDM populations detected: a $CFSE^{hi}$ population and a $CFSE^{lo}$ population. It had been expected that co-culture would result in a single $CFSE^{+}$ BMDM population (BMDM interacting with lymphocytes) and a $CFSE^{-}$ BMDM population (BMDM not interacting with lymphocytes). As this was not the case, the cause of the two $CFSE^{+}$ populations was sought.

It was initially speculated that uptake of free CFSE in the media by the BMDM could account for the $CFSE^{lo}$ BMDM population. However both the $CFSE^{hi}$ and $CFSE^{lo}$ BMDM populations were shown to be interacting directly with lymphocytes rather than free CFSE, as co-culture of BMDM with CFSE-stained thymocyte conditioned media alone did not result in a detectable CFSE signal in the BMDM population. In co-cultures resulting in large proportions of $CFSE^{hi}$ BMDM, a step-wise increase in CFSE staining is seen within this population, while the $CFSE^{lo}$ population shows a more homogenous pattern of CFSE staining and no clear separation from the unstained BMDM, indicating an overall population shift. This staining pattern suggests that the $CFSE^{hi}$ BMDM may be undergoing specific, high-level interactions with/uptake of whole cells or AC, as interaction with each additional CFSE-stained cell would result in a clear increase in CFSE signal. In contrast, the staining seen within the $CFSE^{lo}$ BMDM population could be the result of interaction with/uptake of small apoptotic blebs or cell debris, resulting in a more homogenous spread of CFSE staining. When the relative sizes of the $CFSE^{hi}$ and $CFSE^{lo}$ BMDM were compared it could be seen that the $CFSE^{hi}$ population of BMDM have high forward scatter properties compared to the $CFSE^{lo}$ BMDM population signifying that they are larger cells, and indicating that these BMDM have either already ingested or are in the process of taking up CFSE-stained AC, resulting in this size increase. The $CFSE^{hi}$ BMDM also had moderate-to-high side scatter properties compared to the $CFSE^{lo}$ BMDM population, indicating increased cell granularity, which may be a result of the formation of intracellular vesicles due to AC uptake. These finding support the idea that the $CFSE^{hi}$ BMDM are undergoing specific interactions with whole cells/AC.

On further investigation of the results, it is, however, unlikely the $CFSE^{lo}$ population are interacting with small apoptotic blebs. In preparation of the CFSE-stained thymocyte conditioned medium used to prove the necessity of CFSE-stained cells in co-culture to get a $CFSE^{lo}$ BMDM population, thymocyte samples were centrifuged at 450g to pellet

the cells, and the supernatants removed to use as conditioned media. Although this speed is sufficient to pellet cells, it is not fast enough to pellet small apoptotic blebs and high-speed ultra-centrifugation of the samples would be required. Therefore, if the $CFSE^{lo}$ BMDM population resulted from the interaction of BMDM with $CFSE^{+}$ apoptotic blebs, the $CFSE^{lo}$ BMDM population would also have been present after incubation in conditioned media, however this was not the case. These findings led to the supposition that the staining seen in this $CFSE^{lo}$ BMDM population was due to a type of low-level CFSE uptake directly from the stained cells. Without further investigation into this BMDM population, a definite conclusion as to the cause of this BMDM subset could not be made, and such work was too much of a digression from the aims of this thesis to pursue, however several routes of thinking were explored in an attempt to offer a potential explanation.

Trogocytosis is the process by which immune cells are able to extract surface molecules from other immune cells, incorporating them into their own cell membrane, and can occur within minutes of cell-cell interactions [reviewed in [203]. Trogocytosis entails the transfer of complete membrane fragments, rather than the transfer of individual molecules, resulting in the simultaneous transfer of target and non-target molecules [204]. It was hypothesized that transfer of small volumes of CFSE-stained cytosol from the lymphocytes to the BMDM may have occurred via trogocytosis of molecules from the lymphocyte cell surface, resulting in a $CFSE^{lo}$ BMDM population. However, on closer inspection of the literature, it was ascertained that this process could not explain the findings in the present co-culture assays. Trogocytosis by phagocytes, also termed 'shaving' or 'antigenic modulation', has been shown to be dependent on Fc-receptor interactions with antibody opsonized target cells [205]. Antibodies bound to the surface of opsonized target cells create antibody-antigen complexes that can be recognized by FcR expressed on phagocytes, such as monocytes/macrophages, leading to the removal of complete antibody-antigen complexes and associated membrane fragment. The shaving of RTX-CD20 complexes from the surface of B cells by monocytes is a well documented examples of this process [206]. Non antibody-dependent mechanisms of trogocytosis also exist, however these are dependent either on specific ligand recognition by NK cells [207], or cognate antigen interaction by B cells [208] and T cells [204], with no antibody-independent mechanisms documented for phagocytes. As such, this potential explanation of CFSE transfer was found to be invalid.

Another potential theory put forward to explain the $CFSE^{lo}$ BMDM population was the transfer of small amounts of CFSE to the BMDM via inter-cellular membrane nanotubes. These nanotubes, also called tunneling nanotubes (TNT), occur commonly between immune cells *in vitro* allowing the exchange of intracellular proteins and lipids between

cells, and are postulated to have *in vivo* roles in immune defense and developmental processes, as well as the spread of pathogens and cancer progression [reviewed in [209]. TNT can form within a few minutes of culture [210], with increased cell proximity resulting in greater numbers of nanotubes present between cells [211]. TNT connect a wide variety of cells including macrophages [212], B cells [213], T cells [214] and dendritic cells (DCs) [211], with characterization of these nanotubes revealing variations in formations, structure and functional properties between cells types, and even within single cell populations [212]. The diffusion of fluorescent marker proteins between the cytoplasm of cells via TNT has previously been observed. On co-injection of Lucifer Yellow and Texas red dextran into individual THP-1 cells the fluorescent markers transferred to TNT-connected cells within 60 seconds of injection, with Lucifer Yellow consistently detectable in several connected cells, while Texas dextran red was intermittently detectable in adjacent cells [211]. These findings support the theory that small amounts of CFSE may have been transferred to the BMDM from TNT-connected lymphocytes in the co-culture assays presented in this chapter, with the length of time of co-culture used sufficient to allow TNT formation and CFSE transfer. However, in disagreement with this theory, the permeability to small cytoplasmic molecules does not seem to apply to all TNT. Studies in the rat pheochromocytoma cell line, PC12, demonstrate that neither the small molecule calcein, nor cytoplasmically expressed green fluorescent protein, were transferred in detectable amounts between TNT-connected cells [210]. None of the literature in this area of research specifically investigates either the potential of CFSE to transfer between TNT-connected cells, or nanotubes formation between the mixture of cells included in our co-culture conditions, and as such it cannot be conclusively stated one way or the other whether TNT are responsible for the $CFSE^{lo}$ BMFM population, however they do offer a promising potential explanation.

The proportion of $CFSE^{hi}$ BMDM observed after co-culture varied between the different AC conditions, although these differences were minor, and as such may not be biologically relevant. It is interesting to note however, that in all BMDM co-cultures containing apoptotic T cells, consistently low proportions of $CFSE^{hi}$ BMDM were observed compared to the other co-culture conditions investigated, regardless of the BMDM activation state. This result was also seen when viable T cells were included in the assays, and may indicate that the BMDM are less able to interact with T cells in the absence of antigen, compared to other cell populations. However further work would need to be undertaken to explore this suggestion before a firm conclusion could be made, with a much larger range of cell types investigated in the co-culture conditions.

Unexpectedly, the co-culture of BMDM with viable B cells consistently resulted in the highest proportions of $CFSE^{hi}$ BMDM. One potential explanation for the results of BMDM-viable cell co-culture in the present assays could be the presence of apoptotic material in the so-called 'viable cell' conditions. Although apoptosis was not intentionally induced in these conditions, cells cultured *in vitro* in the absence of specific growth factors have a finite life span, and some level of spontaneous apoptosis will have occurred. This idea is supported by the observation that the BMDM, especially the L929 BMDM, undergo increased high-level interactions with the 'viable' B cells, compared to either the 'viable' T cells or thymocytes, as it is known that B cells are particularly prone to spontaneous cell death in culture [215]. Consequently, it would be expected that a larger proportion of the cells in the viable B cell condition would be apoptotic, or expressing very early apoptotic markers (ACAMPs) compared to the other 'viable' conditions, resulting in increased interactions with the BMDM. Although a proportion of cells in these non-irradiated conditions will be apoptotic, in order to discriminate from the other treatment groups and maintain consistency with the rest of the chapter, this un-treated group will still be referred to as the viable group. It has been shown that the irradiated conditions contain a greater proportion of apoptotic cells compared to the viable cell conditions (Figure 3.1), however the increased interaction may be a result of the type of apoptosis undergone by the cells, rather than the overall amount. There is a growing body of evidence detailing differences in the forms of apoptosis resulting from various induction stimuli, with the interactions of these AC with cells of the immune system resulting in distinct responses [reviewed in [216]. Therefore, the form of cell death resulting from a lack of survival factors in the viable conditions could differ from that induced by x-irradiation, leading to the expression of diverse ACAMPs, which would be recognized by different receptors on the BMDM leading to altered levels of interaction with these distinct forms of AC. Indeed, consistently lower interaction levels were observed with Etoposide-treated AC compared to irradiated AC, and although minor, this difference in interaction levels could also indicate an altered ability of these BMDM to interact with AC induced via different cell death stimuli. If this is the case, it could explain why the non-irradiated viable cell conditions show high levels of interaction with the BMDM, and are able to modulate BMDM function in the same ways as the irradiated cultures. However, differences in the kinetics of the BMDM-viable cell/BMDM-AC interactions may also go some way to explain this finding. In the assays utilized in this chapter, BMDM were co-cultured with either viable or irradiated B cells for 15min resulting in a higher level of BMDM-viable B cell interaction observed. In chapter 4 of this thesis (Figures 4.6 and 4.9) BMDM were co-cultured either viable or irradiated B cells for 3hr, and it can be seen that comparable proportions of $CFSE^{hi}$ BMDM resulted from these co-cultures, indicating that the increased levels of

interaction seen with viable B cells after 15min may be due to the time-point investigated, rather than an intrinsic characteristic of BMDM-viable B cell interactions.

In the literature an assortment of different macrophages populations have been used to investigate the immunomodulatory effects of AC uptake [157,217-219]. As such, it was examined whether BMDM-AC interaction in these co-culture assays differed, depending on the type of macrophage used, and if utilizing a different population would give rise to results more in keeping with those predicted, based on the published literature. To do this, the interaction of AC with GM-CSF BMDM was explored. There is substantial variability in macrophage phenotypes associated with the various methods of BMDM generation, with a large body of work looking into the phenotype and function of these different subsets. Generation of BMDM using recombinant GM-CSF produces an M1-like population of macrophages, which resemble the classically activated, inflammatory population of cells found *in vivo,* with M1 macrophages characterized by their ability to secret pro-inflammatory cytokines and their expression of MHC II and CD86. Recombinant GM-CSF can also be used to generate bone marrow-derived dendritic cells [220], with cells generated using these similar protocols commonly categorized as immature DCs, and as such there is some disagreement in the literature as to whether GM-CSF induced cells are indeed macrophages, or dendritic cells. However, work by Lari and colleagues has demonstrated the ability of GM-CSF generated BMDM to differentiate into osteoclasts, the bone resorbing cells of the body [221]. Osteoclasts arise *in vivo* from the fusion of monocytes and/or macrophages, resulting in the formation of large multinucleated cells, capable of producing lytic enzymes and acids that degrade bone [reviewed in [222]. The ability to generate osteoclasts from GM-CSF BMDM indicates that these cells have not committed to the DC lineage, and this ability, along with the expression of common macrophage surface markers such as CD11b, the M-CSF receptor and F4/80 by these cells [202] can be taken as conformation that this cell population are in fact a macrophage subset. As a side note, there is currently some debate as to whether macrophages and DCs are separate cell populations at all, or if instead, DCs are a specialized macrophage subset adapted for antigen presentation [223-225], in which case the GM-CSF generated cells could theoretically be both DCs and macrophages, however this possibility will not be explored here.

M-CSF-containing L929 supernatant produces a more regulatory, M2-like phenotype of macrophages. M2 macrophages can be distinguished by their expression of the IL-4 receptor, high level expression of scavenger receptors, CD206 (the mannose receptor) [25], and C-type lectins (CLECs) [reviewed in [226], with this enhanced expression of PRRs facilitating the binding of both pathogens and apoptotic cells by this macrophage population.

In the *in vitro* assays undertaken, lower levels of interaction were seen between AC/viable cells and GM-CSF BMDM compared to L929 BMDM, regardless of the cell type or the method used to induce apoptosis. M2-like L929 BMDM have been shown to be highly phagocytic, in comparison to GM-CSF BMDM [227], and so the reduced interaction of GM-CSF BMDM with AC during co-culture can be attributed to intrinsic cell characteristics, rather than a consequence of the assay. Differences in expression of PRRs, as well as cell adhesion molecules, will influence the relative ability of these BMDM populations to interact with other cells. Studies looking at human monocyte-derived macrophages have shown differences in the morphology, expression of cell surface markers and suppressive activity of macrophages differentiated using M-CSF compared to those differentiated using GM-CSF. M-CSF macrophages are elongated, spindle-like cells expressing all 3 FcγRs (CD16, CD32 and CD64), as well as the $\alpha_v\beta_5$ integrin and high levels of CD14, and show enhanced IL-10 production. GM-CSF macrophages however, show weak IL-10 production, indicating limited suppressive function, and have a round, fried egg-like morphology. These M1 macrophages express only 2 types of FcγR (CD32 and CD64), express $\alpha_v\beta_3$ rather than $\alpha_v\beta_5$, and express minimal CD14 [228]. Although focused on human macrophages, these results highlight the differences in the expression of surface molecules involved in cell-cell interactions by M-CSF and GM-CSF differentiated macrophages. The effects of these colony stimulating factors on murine macrophage phenotype and function have also been shown, with culture of peritoneal macrophages in the presence of recombinant M-CSF resulting in the marked increase in the synthesis and stable surface expression of the macrophage scavenger receptor (MSR) [229], as well as an increase in surface expression of the complement receptor, CR3. In this study, M-CSF also enhanced specific peritoneal macrophage functions, as demonstrated by the enhanced uptake of fluorescently labeled lipoprotein, an MSR ligand, and increased cation-independent adhesion to serum-treated tissue culture plastic [229].

In an attempt to understand the outcomes of the BMDM-AC interactions observed, the effect of co-culture on L929 BMDM antigen presenting potential and activation was investigated. To do this, the relative expression levels of a range of cell surface markers were compared using flow cytometry. Very few differences were detected in the L929 BMDM on co-culture with AC of different origins, but from the same apoptotic treatment group. The only notable phenotypic difference after co-culture was the expression of CD69, with L929 BMDM co-cultured with irradiated B cells in the absence of LPS expressing substantially more of this early activation marker than those co-cultured with irradiated thymocytes, however this finding was variable. This increased expression was unexpected, as although not demonstrated in macrophages, it has

previously been shown that AC are able to inhibit the expression of CD69 on activated T cells *in vitro* [230].

When the overall ability of AC to modulate L929 BMDM phenotype was compared to BMDM cultured alone, it could be seen that levels of co-stimulatory molecules expressed by the BMDM incubated with AC were unchanged, with MHC II expression increased in the absence of LPS in all conditions containing AC. Previous work by Barker et al has shown that co-culture of L929 BMDM with apoptotic neutrophils does not alter expression levels of the co-stimulatory molecules CD40, CD80 or CD86 by BMDM [219], although in this study MHC II expression also showed no change on co-culture [219]. Alternately, work looking at murine red pulp macrophages has demonstrated an up-regulation of both MHC II and CD86 after interaction with apoptotic thymocytes [231], indicating that different populations of macrophages respond differently to AC in terms of their expression of MHC II and co-stimulatory molecules. As such, the expression pattern of these markers by L929 BMDM on AC co-culture is likely due to the macrophage population used. The BMDM used in both the present study and that by Barker et al [219], were generated using L929 supernatant, however bone marrow was harvested from BALB/c mice in the work of Barker et al, and from C57BL/6 mice in the present work, which could account for the differences seen.

The expression of CD69 and CD206 on L929 BMDM was also investigated. When expression levels by BMDM co-cultured with AC were compared to BMDM cultured alone, a small decrease in the expression of CD69 was observed in the presence of 1ng/ml LPS, regardless of the cell type or apoptotic stimuli, with the same reduction in expression seen in CD206. As the decrease was minor it is hard to know whether this level of variation would be biologically relevant, but if so, these results indicate that in the present assay system co-culture of BMDM with AC is able to down-regulate LPS-induced BMDM activation, but does not skew the population to a more M2-like population, as would be indicated by increased CD206 expression.

The ability of AC to modulate the secretion of soluble immune-mediators by macrophages has been extensively documented, and ELISAs were undertaken to determine whether the BMDM-AC interactions observed were having functional effects on the BMDM in terms of the production of soluble immune mediators. All AC investigated had the same effects on cytokine production by L929 BMDM, with the levels of IL-12, TNFα, IL-6, IL-10 and TGF-β investigated. Unexpectedly, in our co-culture assays, viable cells had the same effects on cytokine secretion by L929 BMDM as AC for all cell types tested. Decreased production of both TNFα and IL-6 could be detected after AC/viable cell co-culture, however no change in the production of IL-12, IL-10 or

TGF-β was observed in any condition. These finding do not fully fit with the concept of AC suppression of macrophage inflammatory responses, however within the published body of work there is a level of variability. On co-culture with apoptotic neutrophils, human monocyte-derived macrophages down-regulate their production of the pro-inflammatory cytokines IL-8, TNFα, and IL-1β, and increase production of the anti-inflammatory cytokine TGF-β, however no detectable difference in IL-10 secretion is seen [157,232]. An increase in TGF-β production, with concomitant inhibition of TNFα, nitric oxide and iNOS (inducible nitric oxide synthase) production is seen in both classically activated murine peritoneal macrophages and the RAW 264 macrophage cell line on co-culture with apoptotic Jurkat T cells [169]. AC uptake by the murine macrophage cell line J774 markedly decreases their ability to secrete TNFα, as well as the chemokines MIP-1α, MIP-2, and CXCL1 (previously called KC) on LPS-stimulation, with TGF-β production also increased [218]. Interestingly, in this study, along with the production of chemokines and pro-inflammatory cytokines, the production of the anti-inflammatory cytokine IL-10 was also mildly suppressed [218].

When cytokine production by GM-CSF BMDM after AC co-culture was investigated, a different pattern of modulation was observed than that seen in the L929 BMDM population. Unlike the L929 BMDM, a decrease in IL-12 production was seen, however no change in the production of IL-6 was detected after co-culture of GM-CSF BMDM. As with the L929 BMDM, co-culture with viable cells had the same effects on cytokine secretion by GM-CSF BMDM as co-culture with AC. The GM-CSF and L929 BMDM used in these assays have arisen from the same precursors, but differentiated in response to different growth factors, reflecting the ability of macrophages *in vivo* to develop into different populations depending on their environment. The disparity in the functional outcome of co-culture between the two BMDM populations demonstrates the intrinsic differences between these different macrophage subsets, reflecting their varied roles during an immune response.

PGE_2 production by the BMDM was also examined. The addition of exogenous PGE_2 to human monocyte-derived macrophages in culture has been shown to suppress inflammatory cytokine production [157], with the production of PGE_2 by macrophages after uptake of AC thought to help regulate the inhibition of pro-inflammatory cytokine production in an autocrine manner. In the current co-culture system, an increase in PGE_2 production was seen on co-culture of both L929 and GM-CSF BMDM with AC, however the expected concomitant decrease in inflammatory cytokines was not observed. This finding indicates that only under certain conditions is PGE_2 sufficient to inhibit the release of pro-inflammatory cytokines by macrophages after interaction with

AC. Viable cells had the same ability as AC to modulate PGE_2 production by the L929 BMDM, however their effect on GM-CSF BMFM was more variable, as was the effect of the AC investigated.

Within each treatment group the different AC had comparable effects on cytokine secretion and PGE_2 production by the BMDM. Inducers of apoptosis stimulate cell death through particular biochemical pathways, with different pathways involved depending on the initial stimulus, and so it is not surprising that AC induced through the same mechanism, in the same environment, have similar effects on phagocytes. Although this result was seen repeatedly in these co-culture assays, there is evidence indicating that *in vivo* this would not always be the case, with other factors able to override the influence of apoptosis induction. For example, the activation state of AC is able to influence the responses of DC *in vitro* [173]. Ingestion of apoptotic resting peripheral blood mononuclear cells (PBMCs) does not provide maturation signals to human monocyte-derived DC, however uptake of apoptotic activated PBMCs is able to induce the expression of the maturation markers CD80, CD83 and CD86 by the DC, as well as production of pro-inflammatory cytokines [173]. In this study gamma-irradiation was used to induce apoptosis in both the resting and activated PBMC groups, demonstrating that although the mechanisms of apoptosis induction plays a key role in the response of the immune system to AC, other factors are also at play. Murine macrophages that phagocytose AC in the presence of Toll-like receptor (TLR) ligands have been shown to have a different cytokine profile than those that encounter either stimulus alone, demonstrating that the environment in which AC are encountered can influence the subsequent response by phagocytes [175].

Viable cells were originally included in the assay a control; as no antigen is present in the current assay system, considerable viable cell-BMDM interaction was not expected. However, throughout the work undertaken in this chapter viable cells were found to have the same immunomodulatory capacity as AC, with viable B cells showing higher levels of interactions with both L929 and GM-CSF BMDM than any of the AC populations investigated. This was an unexpected finding. *In vivo* secretion of TGF-β in inflamed peritonea of ICR mice is enhanced by clearance of apoptotic Jurkat cells, but not viable Jurkat cells, administered intraperitoneally [171]. In this model, peritoneal and lung macrophages also showed a significant increase in the uptake of apoptotic cells compared to viable cells on investigation of peritoneal or bronchoalveolar lavage fluid cytospins [171]. As such, the results seen in the present work do not fit with the available literature. As discussed previously, the interaction of BMDM with the viable cells, and their effects on BMDM function may be due to AC contamination within this condition. However, another theory could also be proposed. Unlike BMDM, which are

generated *in vitro*, macrophages *in vivo* do not exist in isolation; they are part of a system in which both apoptotic and viable cells are continually present. If non-specific cell-cell interactions take place *in vivo* as a part of normal cell encounters, such as through the interaction of cell adhesion molecules, any potential effects interaction with viable cells may have on macrophages would have already occurred. Therefore, the administration of exogenous viable cells, such as in the study mentioned above, would not be expected to have additional influence on the macrophage phenotype or activity, and as such no change would be detected. Within this interaction model, the administration of additional AC could still impact macrophage responses. Under steady state conditions, AC are rapidly cleared from the system and as a result, macrophages would not be expected to encounter large numbers of AC simultaneously. The introduction of a large number of AC at the same time could tip the balance from immunologically silent AC clearance by phagocytes, to an actively anti-inflammatory form of clearance, skewing macrophage phenotype and subsequent function. Based on this theory, it could therefore be suggested that the present *in vitro* findings regarding the action of viable cells on BMDM are an artefact of the assay system utilized, as the BMDM included in the co-culture conditions had never previously encountered any cells other than BMDM, and so interaction with viable cells had demonstrable effects. Whereas *in vivo,* macrophages will have already undergone interactions with viable cells prior to any baseline measurement taken. If this theory were correct, it would be expected that similar results would be gained from other *in vitro* assays comparing viable cell and AC co-culture conditions.

Although the majority of work looking into the effects of AC uptake by phagocytes does not include viable cell controls, a small number do. Fadok et al have shown that the *in vitro* co-culture of murine macrophages and apoptotic thymocytes results in a higher phagocytic index, compared to that when viable thymocytes were included in co-culture conditions, with this score taking into account both the percentage of macrophages that had phagocytosed cells and the average number of cells per macrophage, [125]. Co-culture of RAW macrophages with apoptotic Jurkat cells induces increased TGF-β secretion and an accompanied inhibition of TNFα production, however co-culture with viable Jurkat cells has no effect on cytokine production by RAW cells [169], however in these studies viable cells do not influence macrophage. Although these studies do not initially support the hypothesis proposed, it is interesting to note that neither utilizes BMDM. In the first, thioglycollate elicited peritoneal macrophages were examined, a population of macrophages that have developed *in vivo*, while the second used the macrophage RAW cell line rather than primary cells. As a result, the results gained in these studies are not directly comparable to those in the present body of work.

However, further work is needed to understand the interactions observed between BMDM and viable cells in the present co-culture assays, and to explore whether viable cells are able to modulate macrophage phenotype and function under conditions not explored with the current assay system.

Together these findings indicate that under the experimental conditions used, AC of different origins have similar levels of interaction with BMDM and do not greatly differ in their ability to alter macrophage phenotype or function. However, in all conditions investigated, viable cells show the same ability as AC to modulate macrophage phenotype and function, adding a layer of complexity to the previous literature, and warranting further investigation.

Chapter 4: The Effects of Rituximab on B cell – Macrophage Interactions

4.1 Introduction

Many cell populations are known to be involved in the pathogenesis of RA, with a role for B cells being highlighted by the success of the biologic RTX, a monoclonal antibody (mAb) that depletes B cells [69]. Although the involvement of B cells in RA pathogenesis is now evident, the exact contribution of B cells is still unclear, as these cells are able to perform multiple roles in the context of autoimmunity, including the production of autoantibodies [54], the secretion of pro-inflammatory cytokines, the expression of co-stimulatory molecules crucial for T cell activation [233], as well as being able to act as APCs [54]. To help enable a better understanding of the part B cells play in RA disease pathogenesis, the mode of action of effective agents targeted at this cell population needs to be elucidated.

RTX was originally developed and approved for use in the treatment of B cell lymphoma [91], but is now commonly used to treat RA patients after failure of anti-TNF therapies. Rituximab targets CD20, a transmembrane phosphoprotein that belongs to the MS4A family of proteins [234], which is expressed on the cells of the B cell lineage; with the exception of pro-B cells and plasma cells. Treatment with anti-CD20 mAb results in rapid and prolonged B cell depletion [reviewed in [106] and improvement of disease symptoms, with the effects of treatment on occasion lasting long after B cell repopulation had occurred.

Three mechanisms contribute to RTX-mediated B cell depletion: antibody-dependent cellular cytotoxicity (ADCC), complement-dependent cytotoxicity (CDC) and apoptosis. It is widely accepted that interactions between the Fc portion of the anti-CD20 mAb and FcRs expressed on effector cells resulting in ADCC are vital to the efficacy of RTX [88]. CDC has also been shown to play a central role in B cell depletion after RTX treatment [93], acting in synergy with ADCC. Cell sensitivity to CDC correlates to the level of CD20 expression by B cells [98], with those cells not sensitive to CDC being cleared by ADCC and vice versa. The role of RTX-mediated apoptosis in B cell depletion has been shown by multiple groups [235-237], however there is some disagreement as to its contribution *in vivo* [238], with many B cells lines refractory to RTX-mediated apoptosis [239,240].

Although there is clear consensus that RTX treatment ameliorates RA activity, the mechanisms by which it exerts its beneficial effect remains unclear. We hypothesize that one of these mechanisms of action may be the re-introduction of a temporary tolerance to the immune system, both through the generation of large numbers of apoptotic cells and the indirect effects of RTX-mediated B cell depletion on other cells of the immune system. On infusion with RTX, B cells present in the peripheral blood are

quickly depleted [241], however clearance of B cells from secondary lymphoid organs is a slower process [242], with residual B cell populations often left in secondary and tertiary lymphoid organs after infusion [243,244]. This means that B cells, potentially with surface-bound or internalized RTX, can be present in the system for considerable lengths of time before being cleared, and during this time these cells are able to interact with other cells of the immune system.

It has recently been shown by Kamburova and colleagues that *in vitro* culture of human T cells with RTX-treated B cells results in a skewing of the T cell population to a Th2-like phenotype, as demonstrated by an increase in expression of the Th2-associated markers CCR4 and GATA3, and enhanced IL-4 production [245]. Further *in vivo* studies have shown that a single dose of RTX is able to alter the phenotype and function of non-depleted B cells present in secondary lymphoid organs after treatment [244]. LN were collected during renal transplant surgery from patients that had previously undergone RTX treatment, and the LN mononuclear cells isolated using density gradient centrifugation. On stimulation with αCD40 and IL-21 *ex vivo*, the B cells from RTX-treated patients showed decreased levels of IgM production, compared to those from non-RTX-treated controls, coupled with increased expression of mRNA for activation-induced cytidine deaminase, an enzyme involved in class switch recombination, indicating that RTX treatment can have a direct effect on B cell signaling cascades and subsequently, B cell function. In this study the authors also demonstrated that *in vitro* stimulation of T cells with the LN B cells from RTX-treated patients resulted in a weaker Th17 response, compared to stimulation with non-RTX-treated B cell controls, as measured by intracellular cytokine production [244]. These findings demonstrate that RTX stimulation of B cells can directly affect B cell function, as well as the interactions of these cells with other immune effector cells, prior to their clearance from the system.

The focus of the work in this chapter is to explore whether RTX binding to B cells can affect the way B cells interact with APCs. To do this, *in vitro* assays were performed utilizing primary hCD20tg B cells and murine BMDM, grown in media supplemented with either M-CSF-containing L929 supernatant, or GM-CSF and IL-3. The B cells were labelled with CFSE and incubated with RTX, before extensive washing to remove free antibody. In certain versions of the assay, B cells from each pre-treatment were irradiated, allowing comparison of the effects of viable and apoptotic RTX pre-treated B cells. BMDM were mixed with the CFSE-stained viable or irradiated pre-treated B cells and co-cultured, with flow cytometry used to determine the resultant levels of cell-cell interaction, and ELISAs undertaken to look at alterations in cytokine production.

Chapter objectives:

- To investigate whether BMDM undergo altered levels of interaction with RTX pre-treated B cells, compared to untreated or IgG pre-treated B cells
- To visualize the type of interactions BMDM and RTX pre-treated B cells undergo, and examine whether these differ from those between BMDM and untreated or IgG pre-treated B cells
- To explore whether the interaction of BMDM with RTX pre-treated B cells has an effect on BMDM function and phenotype

4.2 Results

4.2.1 Optimisation of Rituximab internalisation protocol

Before the effects of RTX on B cell – macrophage interactions were explored, a better understanding of the kinetics of RTX internalisation by hCD20tg B cells *in vitro* was sought. To do this, RTX conjugated to AlexaFluor488 (RTX-488) was used, allowing analysis of RTX uptake by flow cytometry. In order to differentiate between total bound RTX-488 and internalized RTX-488, a method of removing cell surface staining was sought. This would enable the levels of internalized RTX to be determined, as well as calculation of the relative levels of surface bound RTX.

Cells were stained with either anti CD3-FITC, anti CD3-PE anti CD19-PerCPCy5.5 or anti-CD19-APC and two different methods to remove cell surface fluorescence examined; incubation with trypan blue to quench any surface signal [246-248], and acid stripping of the surface bound antibody [249,250]. To quench the fluorescent signal, stained cell samples were incubated with 0.4% trypan blue for 2min at either 4^{o}C or RT. When incubated at either 4^{o}C or RT, no decrease in signal was seen for any of the four fluorochromes tested, as determined by the MFI values for each fluorochrome (Figure 4.1a).

A range of acid stripping protocols are documented in the literature, and two different methods were were explored. In the first, cells were incubated with 1ml 0.5M NaCl + 0.2M acetic acid for 4min at 4^{o}C, prior to washing and FACS analysis (acid strip 1), whereas in the second they were incubated with 0.5M NaCl + 0.2M acetic acid for 10min, washed, and again incubated with acid and washed two further times, before being analysed by flow cytometry (acid strip 2). For the second protocol either 0.5ml or 1ml of acid was used, with certain samples incubated at 4^{o}C and others at RT. A substantial decrease in surface fluorescence was observed for all fluorochromes tested with the first acid strip protocol used, with 54±2% of the original FITC, 1±0% of the PE,

24±0% of the PerCPCy5.5 and 35±3% of the APC signal present after treatment compared to stained, un-stripped samples (Figure 4.1a). A substantial reduction in surface fluorescence was also observed for all fluorochromes tested when the second acid strip protocol was used, regardless of the volume of acid or incubation temperature (Figure 4.1a). For both the PE and APC signal, the method of acid stripping did not alter the final level of surface fluorescence seen, with the majority of PE and APC staining removed by all acid strip protocols tested. However, for FITC the acid strip 2 protocol with 1ml of acid at RT was markedly less able to reduce surface fluorescence than the other three variations of the acid strip 2 protocol, with 73±11% of the original signal remaining compared to 37±2% after the acid strip 2 protocol with 1ml acid at 4°C, 34±0.4% after the acid strip 2 protocol with 0.5ml of acid at 4°C, and 44±1% after using the acid strip 2 protocol with 0.5ml of acid at RT. The acid strip 1 protocol was considerably more effective at reducing the PerCPCy5.5 signal than the acid strip 2 protocol with 0.5ml of acid at 4°C, with only 24±0% of the original signal remaining after treatment, compared to 48±0.7%.

The effect of both trypan quenching and acid stripping on cell viability was also investigated. The trypan quenching protocol used, along with the acid strip 1 protocol, had no adverse effects on cell viability compared to the un-treated stained cells, as determined by flow cytometry. Examination of the cells FSC and SSC was used to detect viable cells (Figure 1b), with trypan quenching at 4°C resulting in 67±0.7% of the total cell population viable, trypan quenching at RT resulting in 64±0.1% and the acid strip 1 protocol resulting in 68±3% (Figure 4.1c). However, when the acid strip 2 protocol, which employed multiple rounds of acid incubations, considerable decreases in the proportion of viable cells was seen, ranging from 23±6% of the total cells remaining viable cells down to only 4±0% (Figure 4.1b, c).

The acid strip 1 protocol showed potential as a method of removal of surface bound RTX-488, however it was decided to investigate a further method to inhibit cell surface fluorescence. This decision was made for two reasons: firstly, a high level of surface FITC remained after treatment, which could obscure true internalization values; and secondly, acid stripping affects antibodies of all fluorochromes, and therefore the use of this protocol would mean that no other antibodies could be used alongside the RTX-488. Incubation of pre-stained cells with an anti-AlexaFluor488 (anti-488) antibody allows specific quenching of any AF488 surface signal [180]. Primary hCD20tg B cells were incubated with RTX-488 for 20min before being incubated with the anti-488 antibody for a further 20min, and analyzed by flow cytometry. In order to determine the optimal volume of anti-488 antibody needed to quench the RTX-488 signal an antibody titration was undertaken.

In the samples tested, viable B cells were gated on using FSC and SSC, and within this population, those that had interacted with RTX were defined as $FSC^{int}RTX\text{-}488^{+}$ cells, as shown in Figure 4.2a. Incubation with the anti-488 antibody did not alter the overall proportion of RTX^{+} B cells (Figure 4.2b), however a considerable decrease in the intensity of the AF488 staining could be seen (Figure 4.2c). B cells incubated with RTX-488 alone had an MFI of 254±0, whereas, when the cells were incubated with RTX-488 followed by 5µl anti-488 their MFI was 35±0.5, with RTX-488 followed by 10µl anti-488 it was 31±0.4, with RTX-488 followed by 15µl it was 33±0.1 and with RTX-488 followed by 20µl anti-488 it was 30±0.6 (Figure 4.2d). Cell viability was not affected by anti-488 incubation (data not shown).

As an outcome of these investigations, it was decided to utilize the anti-488 quenching antibody in the studies of RTX internalization by hCD20tg B cells, rather than trypan quenching or acid stripping.

4.2.2 RTX internalisation by hCD20tg B cells and cell survival

To investigate the kinetics of RTX internalization by hCD20tg B cells, primary B cells were isolated from the combined spleen and LNs of an hCD20tg C57BL/6 mouse and incubated with RTX-488 for 0min, 15min, 30min, 1hr, 3hr, 6hr and 24hr. Half of the cells from each time-point were then incubated with anti-488 antibody, to quench the surface RTX-488 signal, with the difference in MFIs between the anti-488 treated and untreated groups used to calculate relative RTX internalization over time.

In the samples tested, viable B cells were gated on using FSC and SSC, and within this population those that had interacted with RTX were defined as $FSC^{int}RTX\text{-}488^{+}$ cells, as shown in Figure 4.3a. At the early time-points, incubation with the anti-488 antibody resulted in a decrease in the percentage of $RTX\text{-}488^{+}$ B cells (0min: 6.3±2.1% vs. 1.9±0.5%, 15min: 94.5±0.3% vs. 47.2±3.9%, 30min: 95.5±0.2% vs. 83.2±2.3%), however from 1hr onwards, incubation with anti-488 antibody did not alter the overall proportion of $RTX\text{-}488^{+}$ B cells (Figure 4.3b and c). After 30min of incubation, maximal binding of RTX-488 to B cells in this system was achieved, as evidenced by the increasing total MFIs seen at the 0min (86±11) and 15min (192±4) time-points, compared to the consistent total MFIs of the later time-points (30min: 283±4, 1hr: 300±2, 3hr: 290±3, 6hr: 292±5, and 24hr: 236±11) (Figure 4.3d). The amount of internalized RTX-488 remained at baseline levels for the first 30min, with MFIs comparable to the 0min time point (0min: 51±7, 15min: 41±0.6, 30min: 53±1). After 3hr of culture the majority of bound RTX had been taken up by the B cells (external MFI: 76±3.1 vs. internal MFI: 215±2.5) and

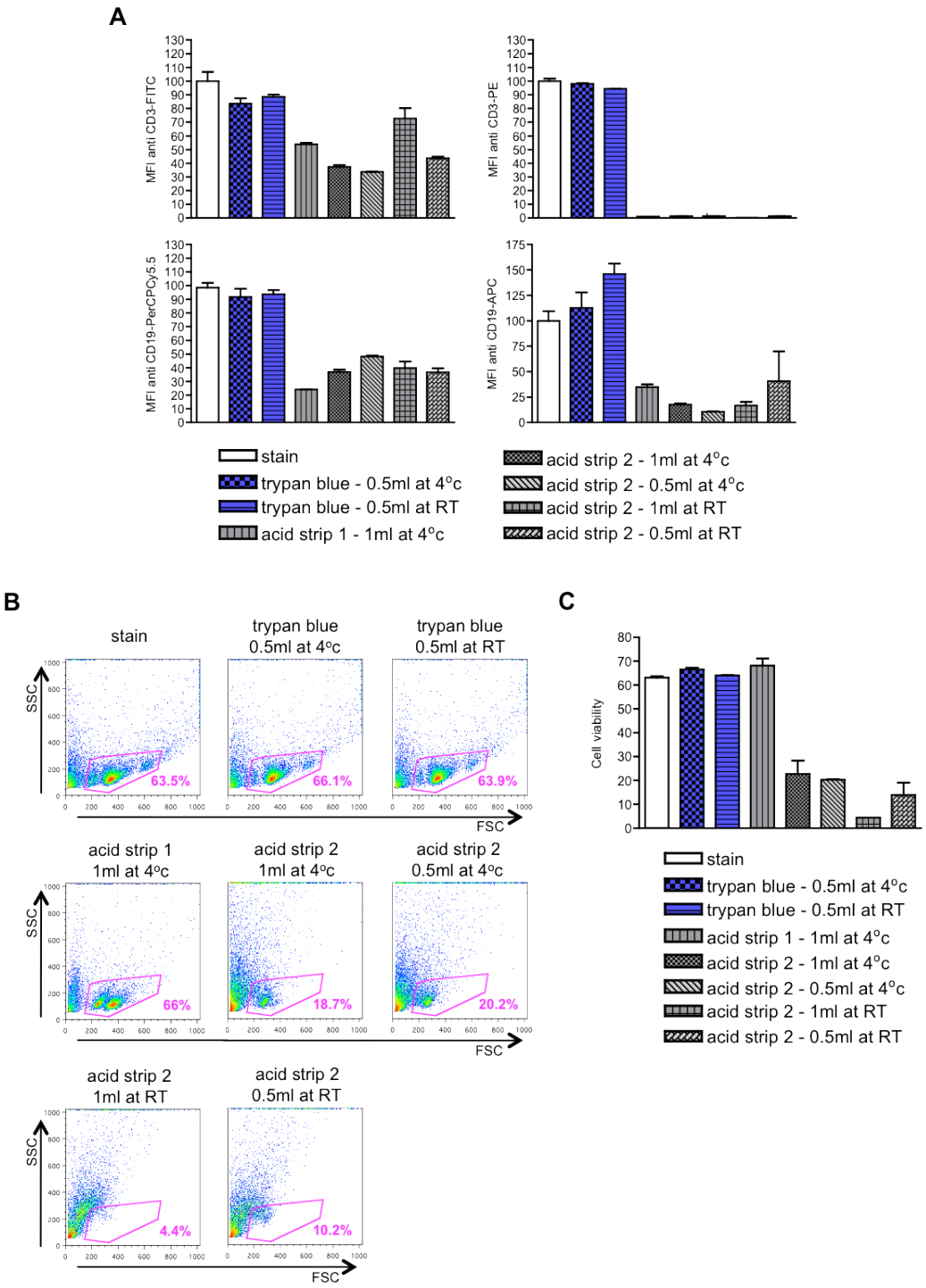

Figure 4.1 Acid stripping of cells removes surface fluorescence but has adverse effects on cell viability

Spleens and LN were isolated from WT DBA mice, combined, and FACS stained with either anti CD3-FITC, anti CD3-PE, anti CD19-PerCPCy5.5 or anti CD19-APC. The signal of the surface staining was then either quenched by incubation with trypan blue for 2min, or was stripped using one of two acid stripping protocols: acid strip 1 cells - incubated with 1ml 0.5M NaCl + 0.2M acetic acid for 4min at 4°C; and acid strip 2 cells - incubated with 0.5M NaCl + 0.2M acetic acid for 3x 10min. Volumes and temperatures are indicated in the figure. Cell samples were then analyzed by flow cytometry. (**A**) Graphs showing the levels of surface staining for each fluorochrome tested after removal protocols undertaken, normalised to the MFI of stained cells. (**B**) Representative FACS plots showing cell viability after staining removal protocols undertaken. Panels: SSC vs. FSC. (**C**) Graph of pooled data showing the percentage of viable cells after the various trypan quenching and acid stripping protocols. (n=2, data from 2 independent experiments)

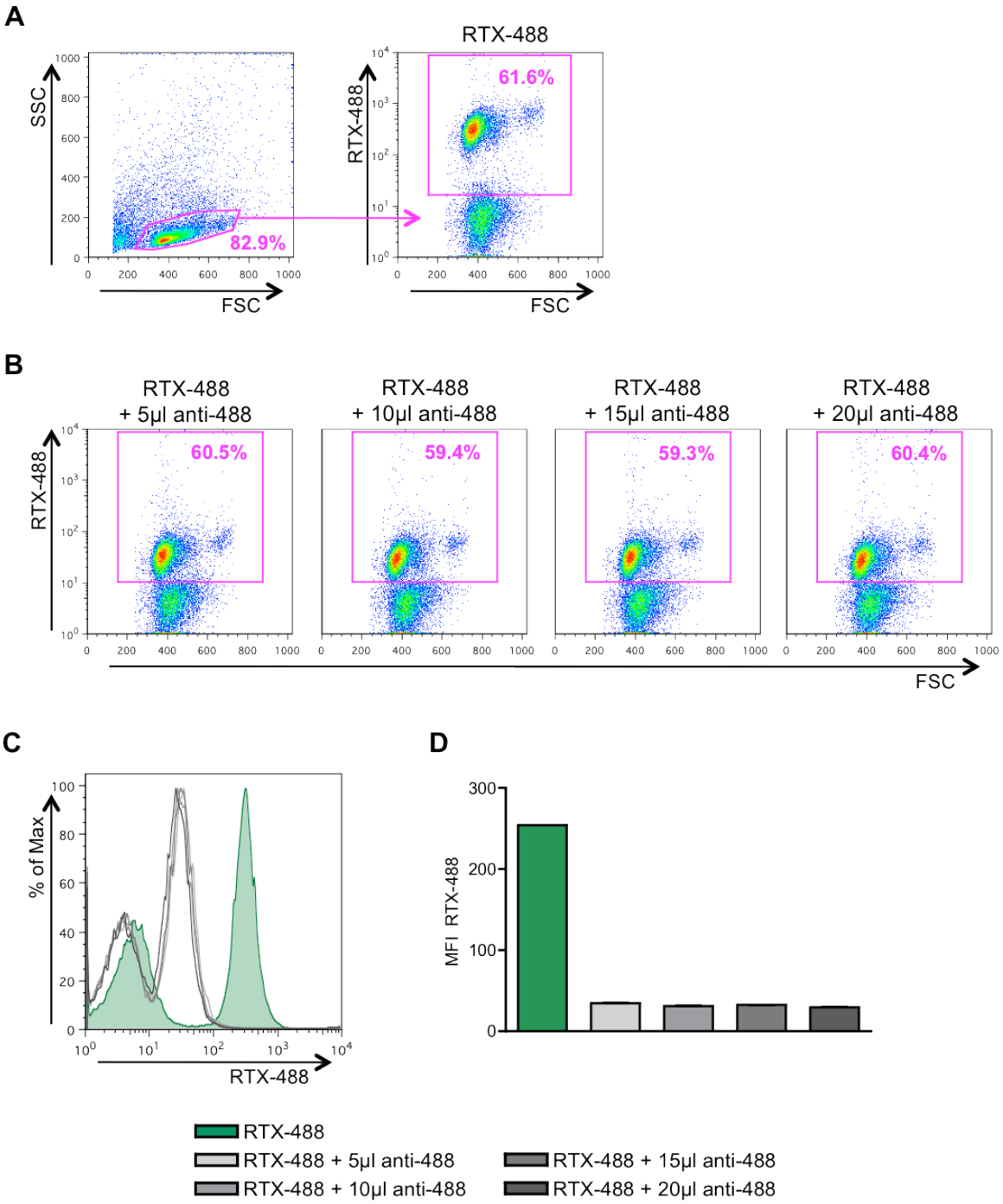

Figure 4.2 Titration of anti-448 antibody
Spleens and LN were isolated from an hCD20tg C57BL/6 mouse, combined, and incubated with RTX-488 for 20min. Cells were then incubated with the anti-488 antibody for 20min before being analyzed by flow cytometry. (**A**) FACS plots demonstrating the gating strategy used to define RTX^+ B cells. First panel: SSC vs. FSC. Second panel: RTX-488 vs. FSC. (**B**) Representative dot plots showing the percentage of RTX^+ B cells after treatment with 5µl, 10µl, 15µl or 20µl of anti-488 antibody. Panels: RTX-488 vs. FSC. (**C**) Representative histograms showing the levels of RTX-488 staining after treatment with varying amounts of anti-488 antibody. (**D**) Graph of pooled data showing the reduction in the levels of RTX staining (MFI) after treatment with anti-488 antibody compared to un-treated cells. RTX-488 = RTX-AlexaFluor488 conjugate, anti-488 = anti-AlexaFluor488 antibody. (n=2)

remained so for the length of the study (6hr - external MFI: 49±6 vs. internal MFI: 243±2, 24hr - external MFI: 38±12 vs. internal MFI: 198±7).

To visualize the internalization of RTX by hCD20tg B cells, primary B cells were isolated from the spleen and LNs of an hCD20tg C57BL/6 mouse and incubated with RTX-488 for either 0, 15 or 30min. Cells were then stained with rhodamine-conjugated phalloidin, a fluorescent F-actin probe, to allow visualization of the cell cytoskeleton, and slides prepared with DAPI added to label the nuclei of the cells. The slides were then analyzed using a Zeiss ApoTome, at x63 magnification. At the initial 0min time-point no RTX-488 staining can be seen on the B cell (Figure 4.4). By the 15min time-point RTX-488 has bound the B cell, as indicated by its co-localization with phalloidin at the cell surface, seen in the composite image. This co-localization continues after 30min of culture, with a more distinct area of RTX-488 binding visible. Unfortunately, due to the small amount of cytoplasm found in B cells it was not possible to differentiate between surface-bound and internalized RTX using this method, as all bound RTX appeared at the surface co-localized with phalloidin, and a distinct internal or external signal could not be detected. As such, investigation was not continued to the later time-points.

It has previously been shown that addition of RTX to *in vitro* cultures of human B cells, does not increase the occurrence of cell death, either through apoptosis or necrosis [245]. We wanted to confirm this finding with hCD20tg B cells, and so the effect of RTX on hCD20tg B cell survival *in vitro* was investigated. To do this, primary B cells were isolated from the spleen and LNs of hCD20tg C57BL/6 mice and incubated with either RTX or IgG, or left un-treated, up to 24hr. The B cells were then stained with ViaProbe (7-AAD solution) and Annexin V to assess the levels of cell death at each time-point, and analysed by flow cytometry (Figure 4.5).

The proportions of live, dead and apoptotic cells were comparable for RTX-treated hCD20tg B cells and control cells at all time-points investigated, with viable B cells defined as ViaProbe$^-$AnnexinV$^-$ double negative cells, apoptotic cells as ViaProbe$^-$ AnnexinV$^+$, and dead/necrotic cells a double positive for ViaProbe and AnnexinV (Figure 4.5a). At the 8hr time-point the majority of B cells were viable regardless of treatment (nt: 66.5±1.3%, RTX: 71.1±0.4%, IgG: 68.8±1%), however by 24hr in culture only a small proportion of B cells were still viable (nt: 6±0.6%, RTX: 12.8±0.6%, IgG: 8.3±1.7%), with the majority of cells staining ViaProbe$^-$Annexin V$^+$ (nt: 77.2±8.1%, RTX: 73.4±1.6%, IgG: 76.4±4.4%), indicating they were undergoing apoptosis (Figure 4.5b-d).

These findings demonstrate that over time, RTX is removed from the surface of hCD20tg B cells via its internalization, with the majority of bound RTX located within the cell

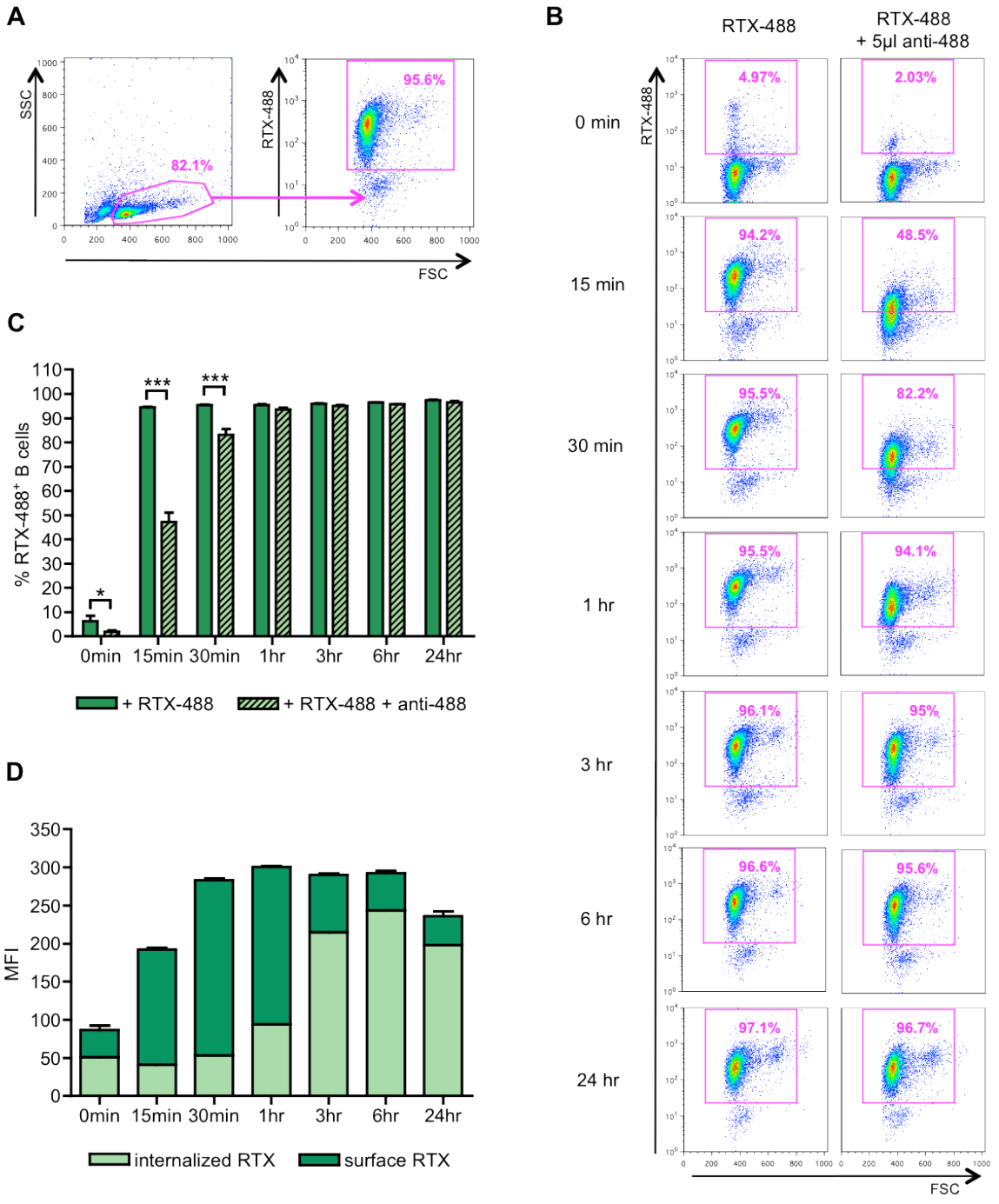

Figure 4.3 RTX is internalized by hCD20tg B cells
The spleen and LNs of an hCD20tg C57BL/6 mouse were combined, and B cells isolated and incubated with RTX-488 for 0min, 15min, 30min, 1hr, 3hr, 6hr or 24hr as shown. Half of the cells from each time-point were then incubated with anti-488 antibody to remove the surface RTX-488 signal and the difference in MFIs between the anti-488 treated and untreated groups used to assess RTX internalization. (**A**) FACS plots demonstrating the gating strategy used to define RTX^+ B cells. First panel: SSC vs. FSC. Second panel: RTX-488 vs. FSC. (**B**) Representative dot plots showing the percentage of RTX^+ B cells in untreated samples and samples treated with anti-488 antibody, at each time point. Panels: RTX-488 vs. FSC. (**C**) Graph of pooled data showing the percentage of RTX-488^+ B cells in the treated and untreated group at each time point. (**D**) Graph showing the relative levels of internalized and surface RTX at each time-point over a 24hr period. (n=1, 3 replicates) Statistics used: One-way ANOVA performed on complete data set in (C), followed by Bonferroni's post test, with * = $p<0.05$ and *** = $p<0.001$.

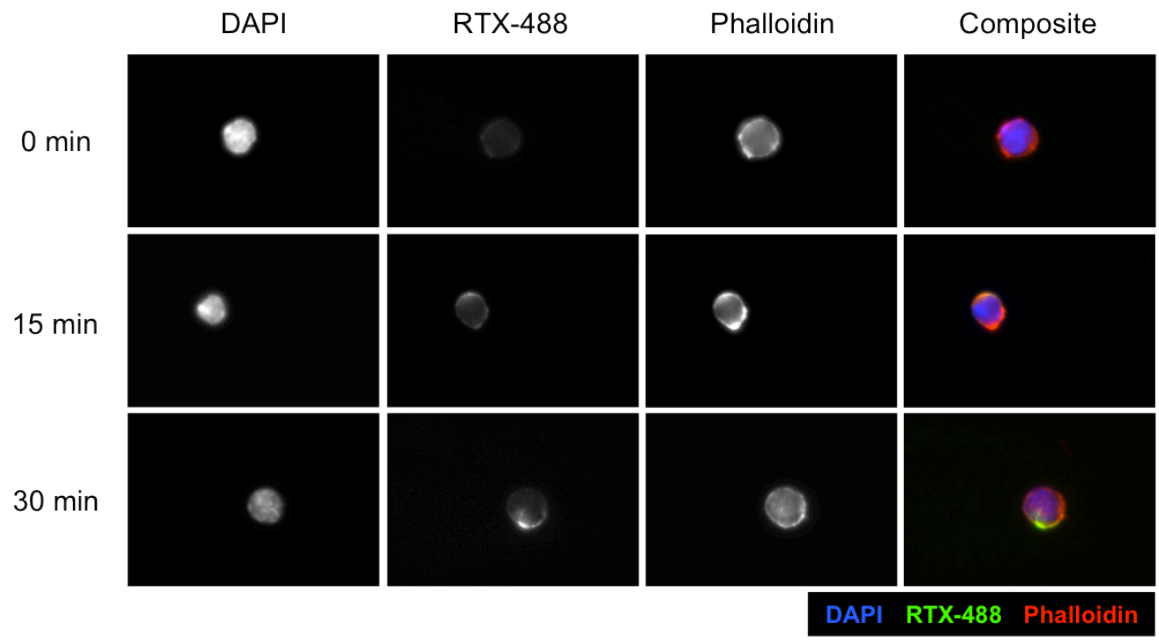

Figure 4.4 Visualization of Rituximab binding to hCD20tg B cells
B cells were isolated from the spleen and LNs of an hCD20tg C57BL/6 mouse and incubated with RTX-488 for 0min, 15min or 30min, as shown. Cells were then stained with DAPI and phalloidin, cytospun on to slides and visualised using a Zeiss ApoTome (magnification: x63). Column 1: DAPI staining. Column 2: RTX-488 staining. Column 3: phalloidin staining. Column 4: Composite image, with DAPI in blue, RTX-488 in green and phalloidin in red.

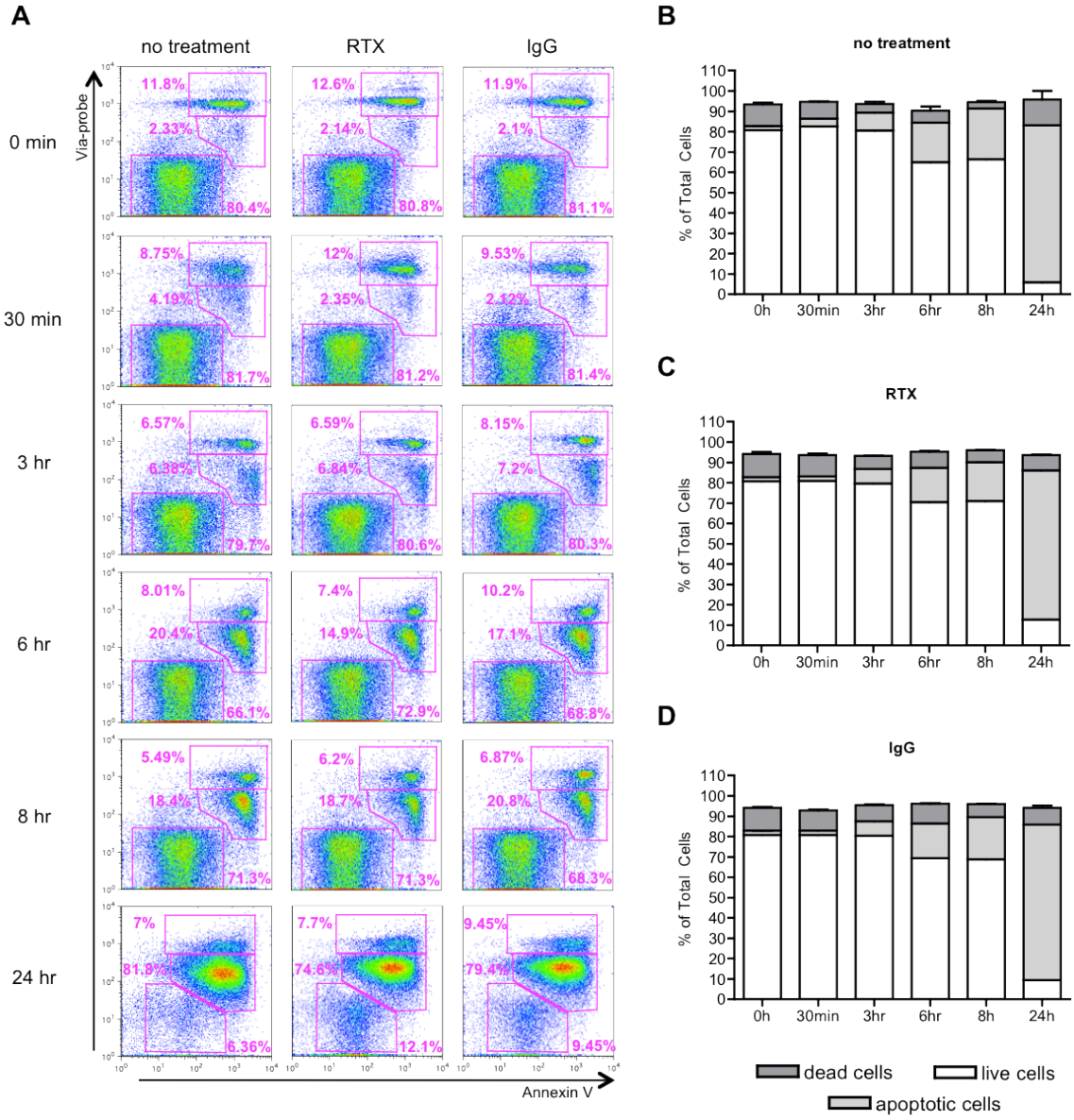

Figure 4.5 Incubation with RTX does not alter B cell survival *in vitro*
B cells were isolated from the combined spleen and LNs of hCD20tg C57BL/6 mice and incubated with RTX or controls for 0min, 30min, 3hr, 6hr, 8hr or 24hr, as shown. Cells were then stained with ViaProbe (7-AAD solution) and Annexin V, and analysed by flow cytometry to allow detection of live, dead and apoptotic cells. (**A**) Representative FACS plots showing the gating used to differentiate live, dead and apoptotic cells at each of the time points and for each treatment group. Panels: ViaProbe vs. Annexin V, with viable cells ViaProbe$^-$AnnexinV$^-$, apoptotic cells ViaProbe$^-$ AnnexinV$^+$ and dead cells ViaProbe$^+$ and AnnexinV$^+$. (**B**) Graph showing the percentages of live, dead and apoptotic un-treated B cells over a 24hr period of *in vitro* culture. (**C**) Graph showing the percentages of live, dead and apoptotic RTX-treated B cells over a 24hr period of *in vitro* culture. (**D**) Graph showing the percentages of live, dead and apoptotic IgG-treated B cells over a 24hr period of *in vitro* culture. (n=1, 3 replicates)

after 3hr. These results also reveal that RTX treatment of hCD20tg B cells *in vitro* does not effect cell survival as compared to un-treated hCD20tg B cells.

4.2.3 B cell ingestion by L929 BMDM

In vitro assays were then performed to investigate whether RTX binding to B cells has an effect on the way B cells, or apoptotic cells originating from these B cells, interact with L929 BMDM *in vitro*. Murine BMDM were grown for 7 days in media supplemented with M-CSF-containing L929 supernatant, before being stimulated overnight with IFNγ. Primary

B cells were purified from the combined spleens and LNs of hCD20tg C57BL/6 mice, and incubated with either RTX or controls for 30min, before extensive washing to remove free antibody. Half of the cells from each pre-treatment were irradiated to induce apoptosis, and all B cells incubated for 4hr. Adherent L929 BMDM were mixed with CFSE-stained viable or irradiated RTX pre-treated B cells, in the presence of LPS, at a ratio of 1 BMDM:1 B cell, and co-cultured for 3hr. In previous *in vitro* assays undertaken to investigate the interaction of L929 BMDM with AC (Chapter 3) cells were co-cultured for 15min, however the length of co-culture was increased for this adaptation of the assay to allow time for the BMDM to phagocytose the pre-treated B cells, therefore enabling the investigation of the later effects of these interactions. The levels of cell-cell interaction were analyzed by flow cytometry.

In the samples tested, viable cells were gated on using FSC and SSC, and within this population the $F4/80^+$ cells were defined as BMDM. Within this $F4/80^+$ population, $CFSE^+$ cells were deemed to be BMDM undergoing interactions with CFSE-stained B cells, as shown in Figure 4.6a. When co-cultured with viable B cells, L929 BMDM showed significantly higher levels of interaction with RTX pre-treated hCD20tg B cells compared to IgG pre-treated B cells (28.4±1.6% $CFSE^+$ BMDM vs. 16.5±7.8%). The results also indicated a higher level of interaction with RTX pre-treated viable B cells compared to un-treated viable B cells, however this finding was not significant (Figure 4.6b and c). When co-cultured with irradiated pre-treated B cells, significantly higher cell-cell interactions occurred between the L929 BMDM and the RTX pre-treated cells, compared to both the untreated and IgG-treated cells, with 38.8±1.9% $CFSE^+$ L929 BMDM in the RTX pre-treated co-cultures compared to 31.4±3.9% $CFSE^+$ L929 BMDM in the un-treated co-cultures, and 25.2±3.3% $CFSE^+$ L929 BMDM in the IgG pre-treated co-cultures (Figure 4.6b and c).

To determine whether the enhanced cell-cell interaction between L929 BMDM and RTX pre-treated B cells had any functional effect on the BMDM, the levels of IL-10 and TGF-β

in the cell culture supernatants were investigated. IL-10 and TGF-β are both anti-inflammatory cytokines, with an increase in production of these mediators indicating a skewing of the macrophage population to a more regulatory phenotype. No change in IL-10 production was seen on co-culture of L929 BMDM with RTX pre-treated viable (495±77pg/ml IL-10) or irradiated B cells (535±118pg/ml) compared to the BMDM alone (327±113pg/ml) (Figure 4.7a). However, a significant increase in IL-10 production was seen on co-culture of L929 BMDM with viable IgG pre-treated (673±7pg/ml IL-10) and irradiated IgG pre-treated B cells (554±30pg/ml IL-10) compared to BMDM cultured alone. No change in TGF-β production was seen on co-culture of L929 BMDM with any of the pre-treated B cells compared to the BMDM cultured alone (Figure 4.7b).

These findings indicate that RTX binding to B cells does have an effect on the way B cells directly interact with L929 BMDM, and this effect continues even once the B cell has undergone apoptosis. These data also show that under the conditions studied, this increase in L929 BMDM interaction with RTX pre-treated B cells does not influence output of anti-inflammatory cytokines by the BMDM.

4.2.4 Comparison of interaction of pre-treated B cells with BMDM and peritoneal macrophages

To assess whether the activation status of the BMDM would influence their interaction with pre-treated B cells, the previous assay was repeated with a range of activated BMDM. L929 BMDM were generated as described previously and then divided into four separate groups: one stimulated with both IFNγ and LPS (BMDM+IFNγ+LPS), one with IFNγ alone (BMDM+IFNγ), one with LPS alone (BMDM+LPS), and one group left un-stimulated (BMDM). Primary peritoneal macrophages were isolated from WT C57BL/6 mice and included for further comparison. The BMDM and peritoneal macrophages were co-cultured at a 1:1 ratio with pre-treated B cells for 3 hr, as before, and cell-cell interactions analyzed by flow cytometry.

In the samples tested, BMDM undergoing interactions with pre-treated B cells were gated on, as shown previously (Figure 4.6a). A similar series of gating was used to identify $CFSE^+$ peritoneal macrophages, with viable cells gated on using FSC and SSC, and macrophages defined as the live $F4/80^+$ cells. $CFSE^+F4/80^+$ cells were considered to be peritoneal macrophages undergoing cell-cell interactions with pre-treated B cells (Figure 4.8).

The activation state of the L929 BMDM did not affect their ability to interact with pre-treated viable or irradiated B cells, with similar levels of $CFSE^+$ BMDM seen in all culture

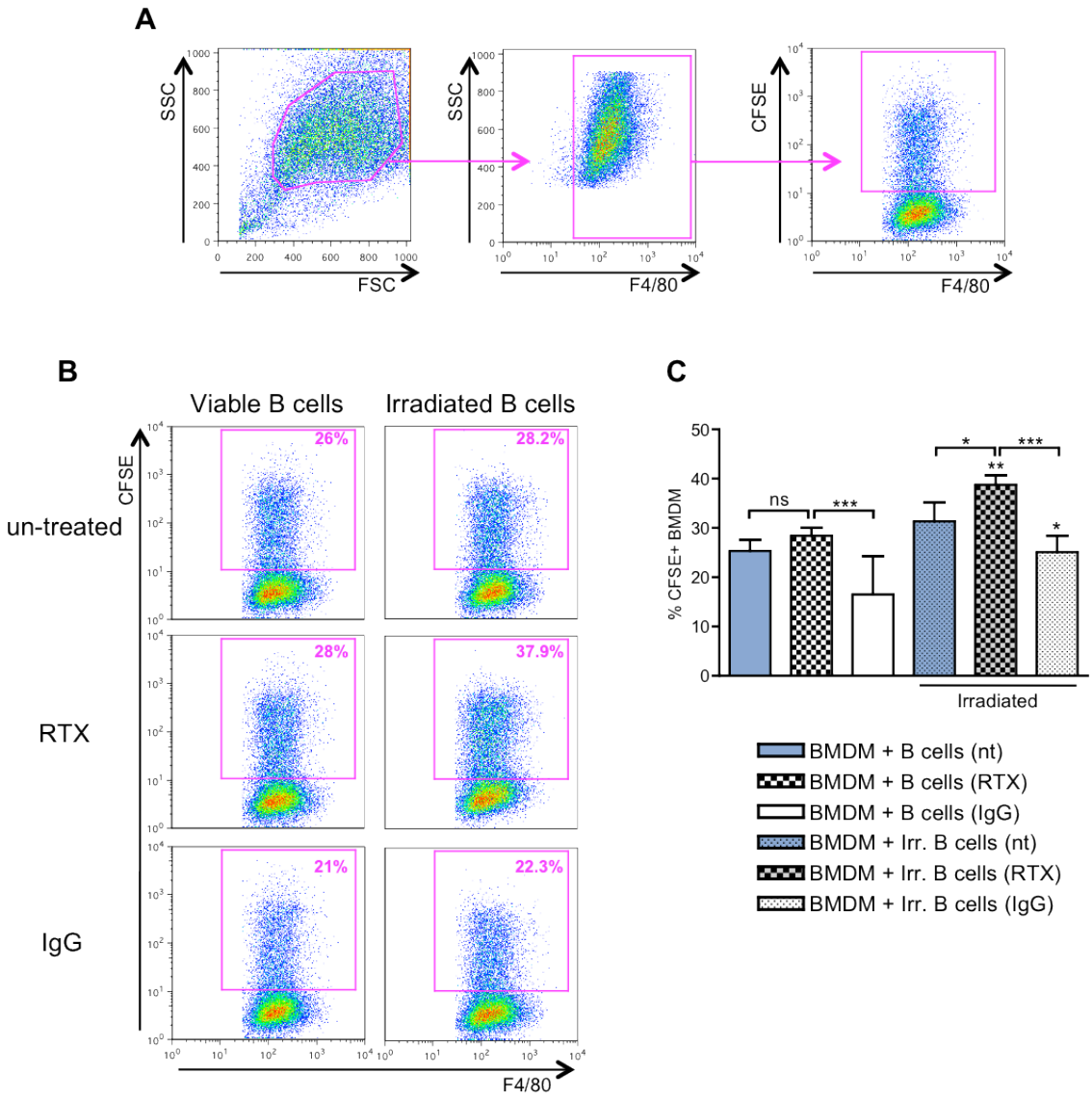

Figure 4.6 L929 BMDM show higher levels of cell-cell interaction with RTX pre-treated B cells compared to un-treated B cells

Murine BMDM were grown for 7 days in cRPMI supplemented with M-CSF containing L929 supernatant. Adherent cells were stimulated with 100U IFNγ and 100ng/ml LPS, before co-culture with CFSE stained viable or irradiated pre-treated B cells, at a ratio of 1:1 for 3hr, and interaction levels analyzed by flow cytometry. (**A**) FACS plots showing the gating strategy used to identify $CFSE^+$ BMDM. First panel: SSC vs. FSC. Second panel: SSC vs. F4/80. Third panel: CFSE vs. F4/80. (**B**) Representative FACS plots showing levels of BMDM interaction with pre-treated viable and irradiated B cells. Panels: CFSE vs. F4/80. (**C**) Graph of pooled data showing the percentage of $CFSE^+$ BMDM after co-culture with pre-treated viable and irradiated B cells. nt: no pretreatment, RTX: Rituximab. (n=2, data representative of 2 separate experiments) Statistics used: One-way ANOVA performed on full data set in (C), followed by Bonferroni's post test, with * = $p<0.05$, ** = $p<0.01$, and *** = $p<0.001$

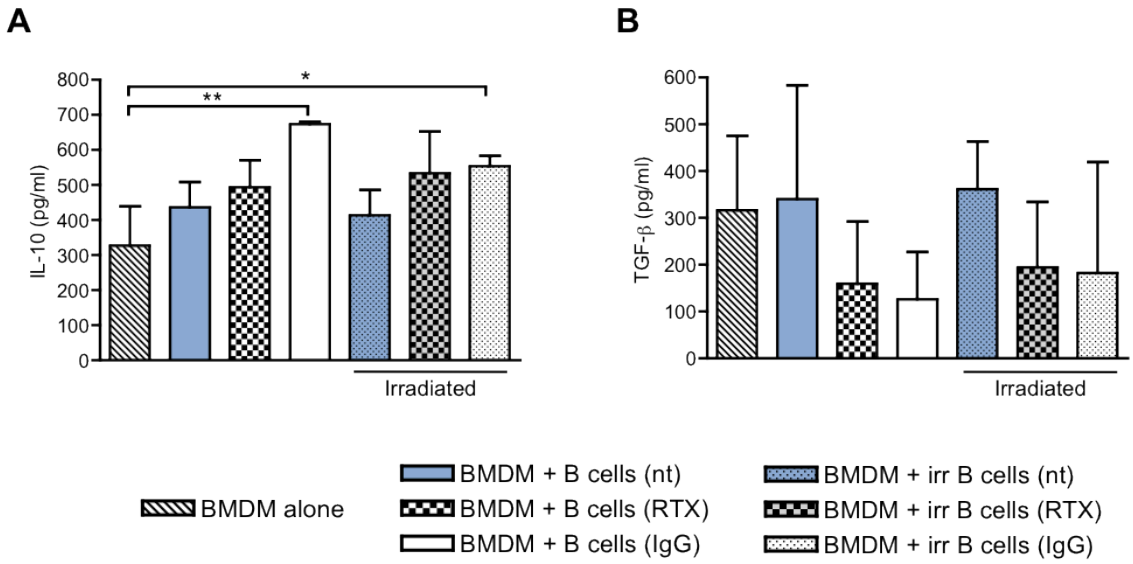

Figure 4.7 Co-culture of BMDM with RTX pre-treated B cells does not alter IL-10 or TGF-β production by BMDM

Murine L929 BMDM stimulated with 100U IFNγ and 100ng/ml LPS were co-cultured with viable or irradiated pre-treated B cells overnight, cell culture supernatants were collected, and IL-10 and TGF-β production investigated by ELISA. (**A**) Graph of pooled data showing the levels of IL-10 (pg/ml). (**B**) Graph of pooled data showing the levels of TGF-β (pg/ml). (IL-10 n=1, data from a single experiment, TGF-β n=2, data from 2 independent experiments) Statistics used: One Way ANOVA performed on each data set in (A) and (B**)**, followed by Bonferroni's post test, with * = $p<0.05$, and ** = $p<0.01$.

conditions (Figure 4.9a). Although the data indicates an increase in interaction between RTX pre-treated viable B cells and BMDM of several activation states compared to controls, only when the L929 BMDM were stimulated with LPS alone was this increase significant, with 38.8±1.5% $CFSE^+$ BMDM compared to 29.4±2% $CFSE^+$ BMDM when co-cultured with un-treated viable B cells, and 27.3±1.9% $CFSE^+$ BMDM when co-cultured with IgG pre-treated viable B cells (Figure 4.9b). The interaction of peritoneal macrophages with RTX pre-treated B cells did not differ from that of controls, however overall the peritoneal macrophages did show considerably higher levels of interaction with all B cells conditions compared to the BMDM, regardless of B cell viability or pre-treatment (Figure 4.9b and c). An overall average of 68.7±3.6% of peritoneal macrophages were $CFSE^+$ on co-culture with viable B cells, while 67.2±2.9% of peritoneal macrophages were $CFSE^+$ after co-culture with irradiated B cells.

These data demonstrate that the activation state of the BMDM used in these assays does not have an effect on the level of cell-cell interaction detected, however primary peritoneal macrophages show substantially higher levels of interaction with both un-treated and pre-treated B cells compared to L929 BMDM. Although peritoneal macrophages demonstrated differences in interaction levels, and could be argued to be a more physiologically relevant tool for investigation, the decision that BMDM would be used in further studies was made. This was primarily due to the low numbers of peritoneal macrophages that can be isolated, making large scale or repeated *in vitro* studies difficult. It was also decided to use BMDM that had not been stimulated with either IFNγ or LPS, as this additional step had no effect on the levels of interaction seen between the BMDM and pre-treated B cells.

4.2.5 Kinetics of early interactions between L929 BMDM and pre-treated B cells

Although no difference was seen in the levels of interaction between BMDM and the pre-treated B cells at the 3hr time-point, studies looking into L929 BMDM interactions with viable and apoptotic cells (Chapter 3) indicated that variations in interaction could be detected at time-points as early as 15min. Due to these findings, it was decided to look into the early kinetics of the L929 BMDM-pre-treated B cell interactions. *In vitro* assays were performed as before with un-stimulated L929 BMDM and RTX pre-treated hCD20tg B cells used, but with co-cultures set up for 15, 30 or 60min. The cell ratio used in the co-cultures was also altered to 3 B cells:1 BMDM, in at attempt to draw out any differences between the B cell pre-treatments that may not have been observable with lower B cell numbers.

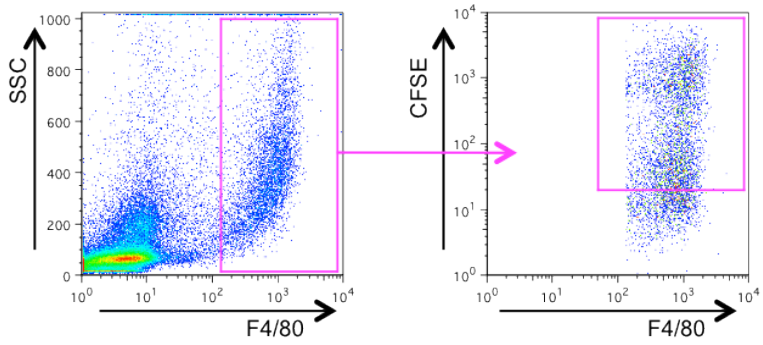

Figure 4.8 Gating strategy for analysis of CFSE$^+$ peritoneal macrophages
Primary peritoneal macrophages were isolated from WT C57BL/6 mice, co-cultured with CFSE stained pre-treated B cells and analyzed for their CFSE signal. The dot plots demonstrate the gating strategy used to define peritoneal macrophages and identify the CFSE$^+$ subset. First panel: SSC vs. FSC. Second panel: CFSE vs. F4/80.

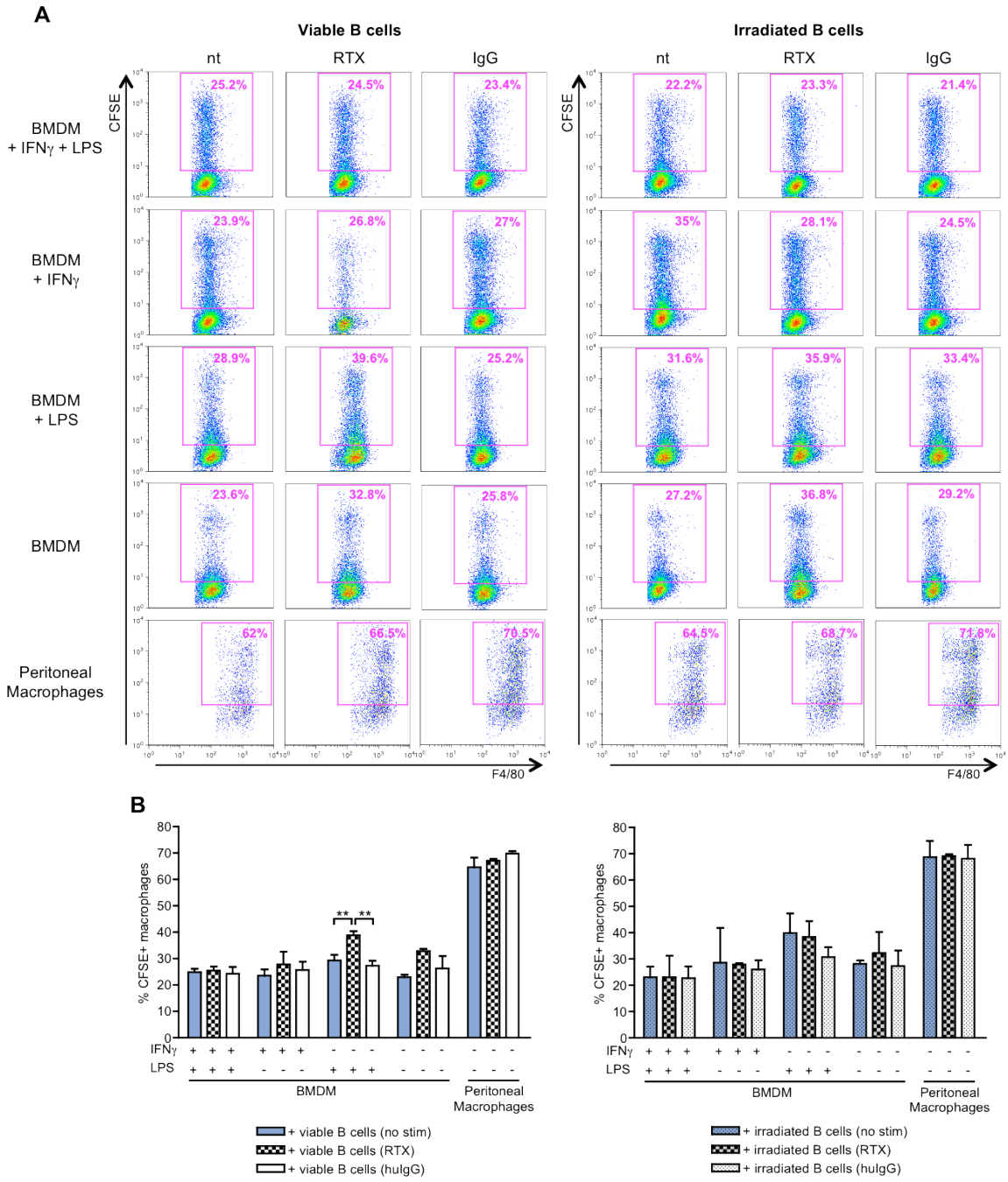

Figure 4.9 Peritoneal macrophages show substantially higher levels of interaction with pre-treated B cells compared to BMDM, regardless of activation state

Murine BMDM were grown in cRPMI supplemented with M-CSF containing L929 supernatant. On d7, adherent cells (BMDM) or freshly isolated primary murine peritoneal macrophages, were co-cultured with CFSE stained viable or irradiated pre-treated B cells, at a ratio of 1:1 for 3hr and interaction levels analyzed by flow cytometry. 100U IFNγ and/or 100ng/ml LPS was added to certain conditions, as shown. (**A**) Representative FACS plots showing levels of interaction between pre-treated, viable or irradiated B cells, and BMDM with or without IFNγ and/or LPS, or peritoneal macrophages. Panels: CFSE vs. F4/80. (**B**) Graphs of pooled data showing the percentage of $CFSE^{+}$ BMDM or peritoneal macrophages after co-culture with viable or irradiated pre-treated B cells. RTX: Rituximab. (n=1, 3 replicates) Statistics used: One-way ANOVA performed on each full data set in (B) and (C), followed by Bonferroni's post test, with ** = $p<0.01$.

In the samples tested $CFSE^{+}$ BMDM were gated on as described previously (Figure 4.6a). With the addition of a higher proportion of pre-treated B cells in the co-cultures, the percentage of $CFSE^{+}$ BMDM increased dramatically, resulting in a near completely $CFSE^{+}$ BMDM population for all co-culture conditions investigated (Figure 4.10a, b, d and e). Within these co-cultures, a distinct $CFSE^{hi}$ BMDM population became evident and an additional $CFSE^{hi}$ gate was introduced (gating rationale detailed in section 3.2.2). It can be seen that on co-culture of BMDM with viable pre-treated B cells a substantially higher level of interaction occurred between the BMDM and RTX pre-treated cells as early as 15min in culture, compared to the IgG pre-treatments (RTX pre-treatment: 75.8±1.8% $CFSE^{hi}$ BMDM vs. IgG pre-treatment: 46.4±1.6% $CFSE^{hi}$ BMDM) (Figure 4.10c). The RTX pre-treated B cells also showed a higher level of interaction with the BMDM, compared to the un-treated B cells, however with the numbers of samples looked at the increase was not significant. This pattern of enhanced interaction between RTX pre-treated B cells and BMDM continued at 30 and 60min. After 30min of co-culture with RTX pre-treated B cells 75±3.5% of BMDM were $CFSE^{hi}$, a significantly higher proportion than in the un-treated B cell co-cultures (47.5±1.7% $CFSE^{hi}$ BMDM) or the IgG pre-treated co-cultures (52.7±3% $CFSE^{hi}$ BMDM). After 60min of co-culture, BMDM interaction with RTX pre-treated B cells was still significantly higher than that of BMDM with un-treated B cells (RTX pre-treated: 59.9±3.7% $CFSE^{hi}$ BMDM v. un-treated: 46.3±2.8% $CFSE^{hi}$ BMDM). The BMDM also showed a higher level of interaction with the RTX pre-treated B cells compared to the IgG pre-treated B cells, however this increase was not significant.

When co-cultured with irradiated pre-treated B cells, the BMDM showed significantly higher levels of cell-cell interaction with the RTX pre-treated B cells, compared to controls, at all early time-points investigated (Figure 4.10f), although overall interaction levels were lower than those seen for BMDM with viable B cells. After 15min, 37.5±3.7% of BMDM co-cultured with RTX pre-treated irradiated B cells were $CFSE^{hi}$, compared to 11.3±3.1% of BMDM cultured with un-treated irradiated B cells and 13.8±3.4% of BMDM cultured with IgG pre-treated irradiated B cells. After 30min interaction levels stayed consistent, with the BMDM showing significantly higher levels of interaction with the RTX pre-treated irradiated B cells (48.2±0.1% $CFSE^{hi}$ BMDM), compared to those with either un-treated (13.3±1%), or IgG pre-treated (19.4±3.7%), B cells. This pattern also continued after 60min of co-culture (RTX pre-treated: 39.4±4.1% $CFSE^{hi}$ BMDM vs. un-treated: 23.2±0.7% $CFSE^{hi}$ BMDM and IgG pre-treated: 26.2±2.1% $CFSE^{hi}$ BMDM).

To further explore the interactions going on between the L929 BMDM and pre-treated B cells, and whether surface cell-cell adhesion or B cells internalization was occurring, fluorescent microscopy was utilized. CFSE stained, pre-treated viable B cells, were co-

cultured with CellTracker Violet labelled L929 BMDM for 15, 30 or 60min. The cells were then fixed to slides using a cytospin and visualized using a Zeiss ApoTome. The type of interaction the B cells were undergoing was categorized as either no interaction, surface cell-cell interactions or internalization (Figure 4.11), with the categories defined as follows: no interaction – the B cell is not in contact with any BMDM; cell-cell interaction – the B cell is in contact with one or more BMDM with the cytoplasm of the BMDM seen to be interacting with the B cell; internalization – the B cell is >80% surrounded by BMDM cytoplasm.

After 15min of co-culture, the nature of the interaction between the B cells and L929 BMDM was not influenced by B cell pre-treatment, with the majority of B cells from all pre-treatments undergoing cell-cell surface interactions (un-treated: 70±14.6%, RTX pre-treated: 88.2±6.9%, IgG pre-treated: 69.2±10.4%) (Figure 4.12a). After 30min of co-culture, the predominant form of BMDM-B cells interaction was still surface cell-cell interactions for all B cell pre-treatments (un-treated: 79.9±6.3%, RTX pre-treated: 71.3±10.7%, IgG pre-treated: 84.5±1.8%), however a notably larger proportion of RTX pre-treated B cells had been taken up by the BMDM (18±2.1%), compared to both the un-treated B cells (1.7±3), and the IgG pre-treated B cells (4.2±2.7%) (Figure 4.12b). After 60min of co-culture, the majority of un-treated and IgG pre-treated B cells were undergoing cell-cell interactions with the BMDM (79.1±12% and 60.9±12.9%, respectively), however far fewer RTX pre-treated B cells were undergoing this type of interaction (37.3±16.4%) (Figure 4.12c). At this later time-point, the majority of the RTX pre-treated cells were internalized by the BMDM, with a significant increase in the internalization of RTX pre-treated B cells seen over the time points investigated (15min: 4.3±5.5%, vs. 60min: 47.9±18.5%).

These results confirm the earlier findings in this chapter that RTX pre-treatment of B cells affects the way viable and apoptotic B cells interact with L929 BMDM. RTX pre-treatment of B cells results in a higher levels of overall BMDM-B cell interaction and increased uptake of B cells by BMDM. These data also show that this increased interaction happens soon after L929 BMDM encounter the RTX pre-treated B cells, with cell-cell interactions seen within 15min of co-culture.

4.2.6 Comparison of ingestion of pre-treated B cells by GM-CSF and L929 BMDM

As discussed in the previous chapter (section 3.2.8), multiple methods of *in vitro* maturation can be used to generate murine BMDM, with considerable variability seen in the resultant macrophage phenotype. BMDM generated using L929 cell supernatant are

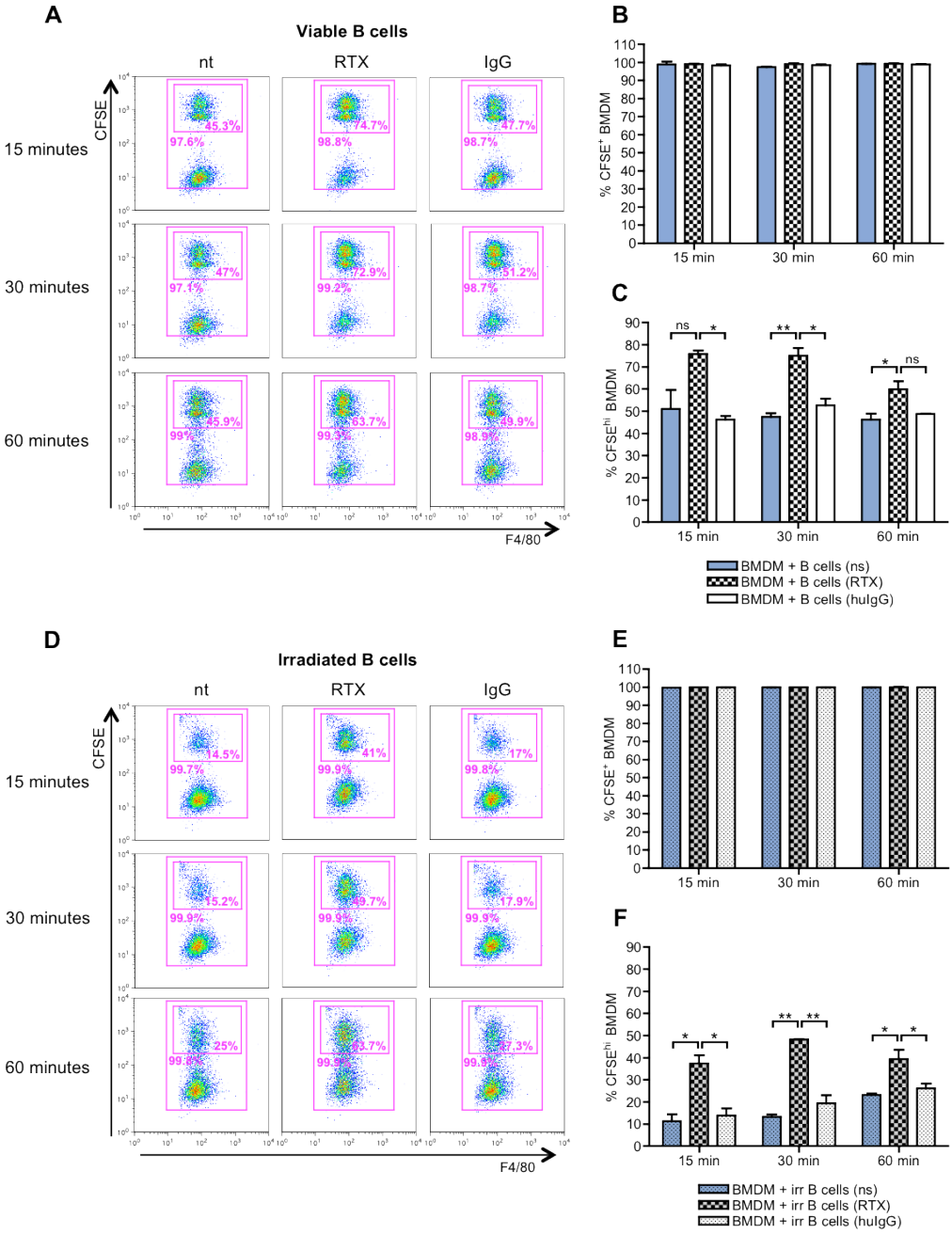

Figure 4.10 Viable and irradiated RTX pre-treated B cells show a significantly higher level of interaction with L929 BMDM

Murine BMDM were grown in cRPMI supplemented with M-CSF containing L929 supernatant. On d7 adherent cells were co-cultured with CFSE stained viable or irradiated pre-treated primary B cells 15, 30 or 60min, at a ratio of 1 BMDM:3 B cells. Interaction levels were analyzed by flow cytometry. (**A**) Representative FACS plots showing the levels of interaction seen between L929 BMDM and viable pre-treated viable B cells, co-cultured for either 15, 30 or 60min. Panels: CFSE vs. F4/80. (**B**) Graph of pooled data showing the percentage of $CFSE^{+}$ BMDM after co-culture with viable pre-treated viable B cells. (**C**) Graph of pooled data showing the percentage of $CFSE^{hi}$ BMDM after co-culture with viable pre-treated viable B cells. (**D**) Representative FACS plots showing the levels of interaction seen between L929 BMDM and irradiated pre-treated B cells, co-cultured for either 15, 30 or 60min. Panels: CFSE vs. F4/80. (**E**) Graph of pooled data showing the percentage of $CFSE^{+}$ BMDM after co-culture with viable pre-treated irradiated B cells. (**F**) Graph of pooled data showing the percentage of $CFSE^{hi}$ BMDM after co-culture with irradiated pre-treated viable B cells. (n=1, 3 replicates) Stats used: One Way ANOVA performed on each full data set in (B) (C) (E) and (F), followed by Bonferroni's post test, with * = $p<0.05$, and ** = $p<0.01$.

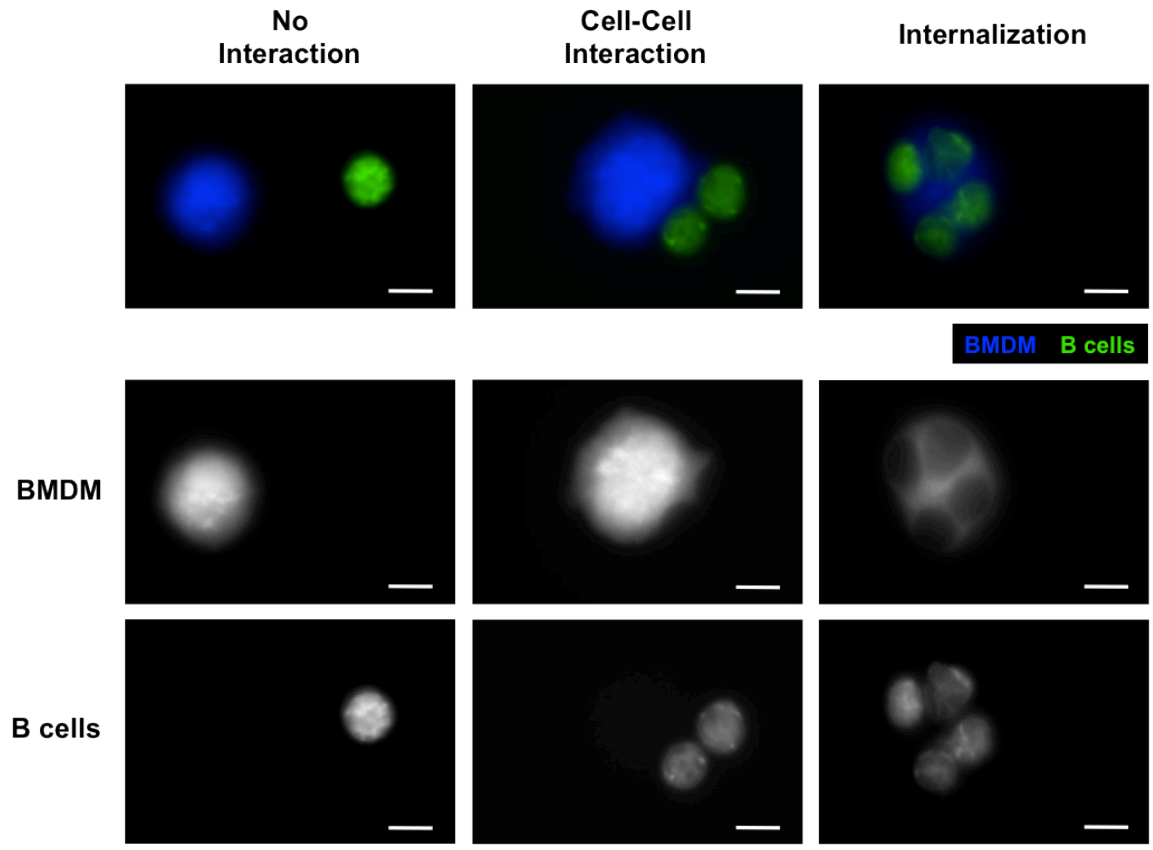

Figure 4.11 Scoring guide for L929 BMDM - B cell interactions
Murine BMDM were grown in cRPMI supplemented with M-CSF containing L929 supernatant. On d7, adherent cells were stained with CellTracker violet and co-cultured for 15, 30 or 60min with pre-treated primary hCD20tg B cells labelled with CFSE. The cells were fixed to slides using a cytospin and visualized using a Ziess ApoTome (magnification x63). Interactions between pre-treated B cells and BMDM were visualized and the type of interaction the B cells were undergoing was categorized as either: no interaction, surface cell-cell interactions or internalization. The categories were defined as follows: no interaction – the B cell is not in contact with any BMDM; cell-cell interaction – the B cell is in contact with one or more BMDM with the cytoplasm of the BMDM seen to be interacting with the B cell; internalization – the B cell is >80% surrounded by BMDM cytoplasm. First row: composite images, with CellTracker violet stained BMDM in blue and CFSE stained B cells in green. Second row: CellTracker violet stained BMDM. Third row: CFSE stained B cells. Scale bar = 10μm.

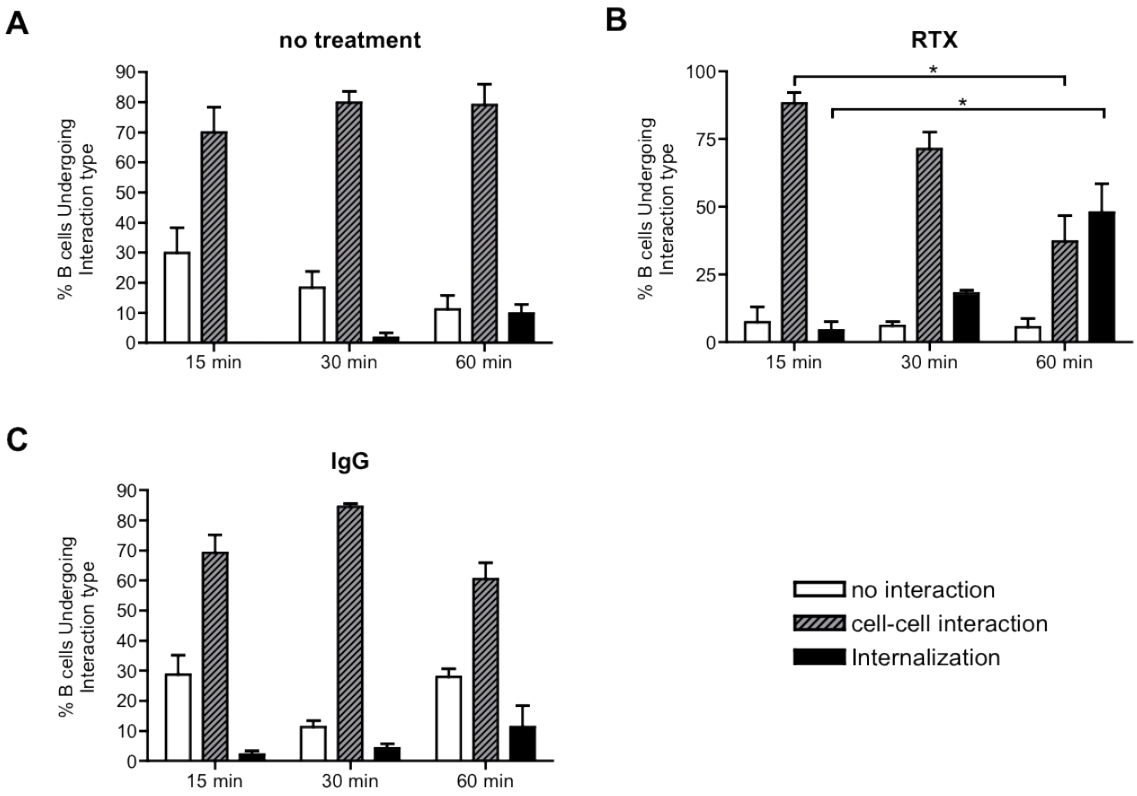

Figure 4.12 Categorizing L929 BMDM interactions with pre-treated B cells
Pre-treated primary hCD20tg B cells were labelled with CFSE, and co-cultured with CellTracker violet stained L929 BMDM for 15, 30 or 60min. The cells were fixed to slides using a cytospin and visualized using a Ziess ApoTome (magnification x63). (**A**) Graph showing the percentage of un-treated B cells undergoing no interactions, cell-cell interactions or internalization at 15, 30 and 60min. (**B**) Graph showing the percentage of RTX pre-treated B cells undergoing no interactions, cell-cell interactions or internalization at 15, 30 and 60min. (**C**) Graph showing the percentage of IgG pre-treated B cells undergoing no interactions, cell-cell interactions or internalization at 15, 30 and 60min. (n=1) Statistics used: One-way ANOVA (Kruskal Wallis) performed on each interaction category for each treatment group over time, with *= $p<0.05$.

considered to resemble non-inflammatory, regulatory macrophages found *in vivo*, while BMDM generated using GM-CSF and IL-3 are considered to be a more inflammatory population of macrophages. After observing the effect of RTX pre-treatment on B cell interactions with L929 BMDM, it was decided to investigate whether RTX pre-treatment of B cells had similar effects on their interactions with GM-CSF BMDM. To do this, the previous co-culture experiments were repeated using GM-CSF BMDM population. Mature, adherent GM-CSF BMDM were co-cultured with CFSE-stained viable or irradiated pre-treated B cells for 15min, at a ratio of 5:1 (B cells:BMDM). In the previous assays undertaken in which BMDM were co-cultured with pre-treated B cells, a cell ratio of 1:1 was initially used, with this increased to 3:1 (B cells:BMDM) in an attempt to draw out any differences between the conditions. These assay were undertaken in parallel to those done in Chapter 3, in which a 5:1 (AC:BMDM) ratio was consistently utilised. In order to bring these two sections into line, it was decided to use a ratio of 5 B cells:1 BMDM for all future co-culture assays including pre-treated B cells. 1ng/ml LPS stimulation was added to certain conditions during the co-cultures, and L929 BMDM used for comparison. As before, interaction levels were analyzed by flow cytometry.

The proportions of $CFSE^{+}$ GM-CSF BMDM were consistent throughout the conditions investigated, and so analysis was limited to the $CFSE^{hi}$ population (Figure 4.13a). A significantly greater percentage of $CFSE^{hi}$ GM-CSF BMDM could be seen on co-culture with RTX pre-treated viable B cells compared to controls (RTX pre-treatment: 19.9±2.2% vs. no-treatment: 8.6±2.1%, and IgG pre-treated: 6.6±1%) (Figure 4.13b). When co-cultured in the presence of 1ng/ml LPS, this pattern of interaction between GM-CSF BMDM and pre-treated viable B cells was unaltered, with significantly more interaction seen between the GM-CSF BMDM and the RTX pre-treated viable B cells (20.8±3%), compared to the levels seen on co-culture with either the un-treated B cells (13.8±1.9%) or the IgG pre-treated B cells (8.4±2.6%). When irradiated B cells were used in the co-cultures conditions with GM-CSF BMDM, RTX pre-treatment again significantly increased the proportion of $CFSE^{hi}$ GM-CSF BMDM, both in the presence of LPS (RTX pre-treatment: 22.3±3.6% vs. un-treated: 10.8±1.7% and IgG pre-treated: 9.8±1.2%) and the absence (RTX pre-treatment: 21.8±3% vs. un-treated: 8.2±1.5% and IgG pre-treated: 8.7±1.3%) (Figure 4.13c).

As with the previous co-culture studies undertaken utilizing L929 BMDM, the overall proportion of $CFSE^{+}$ L929 BMDM was consistent throughout all conditions (Figure 4.14a), however enhanced cell-cell interactions were seen between the L929 BMDM and RTX pre-treated B cells ($CFSE^{hi}$ L929 BMDM). Significantly higher proportions of $CFSE^{hi}$ L929 BMDM could be seen on co-culture with RTX pre-treated B cells, compared to controls, when either viable or irradiated B cells were used for co-culture, and the presence of

LPS did not alter this pattern of interaction (viable B cells - RTX pre-treated: 55.1±3.7% vs. un-treated: 36±4.5% and IgG pre-treated: 38.5±3%, irradiated B cells - RTX pre-treated: 57.3±5.6% vs. un-treated: 35.8±6.7% and IgG pre-treated: 36.2±4.9%) (Figure 4.14b and c).

Although the same pattern of interaction was seen on co-culture of BMDM and pre-treated B cells, regardless of the method of BMDM generation (GM-CSF vs.L929), differences were seen in the relative proportions of the BMDM population undergoing interactions. When co-cultured with RTX pre-treated viable B cells in the absence of LPS, 19.9±2.2% of GM-CSF BMDM were $CFSE^{hi}$, while 55.1±3.7% of L929 BMDM stained $CFSE^{hi}$, with considerably lower percentages of $CFSE^{hi}$ BMDM consistently observed in all conditions containing GM-CSF BMDM, compared to the equivalent co-culture condition containing L929 BMDM.

To determine whether cell-cell interactions between BMDM and RTX pre-treated B cells had an effect on the BMDM phenotype, the levels of IL-10 and IL-12 in the cell culture supernatants were investigated. The relative levels of production of these cytokines can give an indication of the phenotype of the macrophages present, with M1 cells producing high levels of IL-12 and minimal IL-10, while M2 cells produce moderate to high levels of IL-10, and very little IL-12 [17]. On culture of GM-CSF BMDM alone or with either viable or irradiated pre-treated B cells in the absence of LPS, no IL-10 could be detected for any of the conditions investigated (Figure 4.15a). On addition of LPS, the GM-CSF BMDM produced moderate levels of IL-10, however co-culture with pre-treated viable B cells did not alter the levels compared to GM-CSF BMDM cultured alone (179±18pg/ml IL-10), with GM-CSF co-cultured with un-treated B cells producing 127±12pg/ml, with RTX pre-treated B cells producing 147±40pg/ml IL-10 and those co-cultured with IgG pre-treated B cells producing 126±27pg/ml IL-10 (Figure 4.15a, left panel). Co-culture with irradiated pre-treated B cells in the presence of LPS also did not alter the amounts of IL-10 secreted by the GM-CSF BMDM compared to those cultured alone (un-treated irradiated B cells: 170±63pg/ml IL-10, RTX pre-treated irradiated B cells: 171±76pg/ml IL-10, and IgG pre-treated irradiated B cells: 176±50pg/ml) (Figure 4.15a, right panel). As with the GM-CSF BMDM, no IL-10 production by L929 BMDM could be detected in the absence of LPS (Figure 4.15b). On addition of LPS, the L929 BMDM produced high levels of IL-10 (1065±202pg/ml), however the addition of pre-treated B cells, either viable or irradiated, did not alter IL-10 production by the BMDM. When IL-12 production by GM-CSF BMDM was investigated, it was seen that on culture of the BMDM alone, in the absence of LPS minimal levels of this cytokine were produced (36±11pg/ml), and that co-culture with either viable or irradiated pre-treated B cells had no effect on IL-12 production (Figure 4.15c). On addition of LPS, the amount of

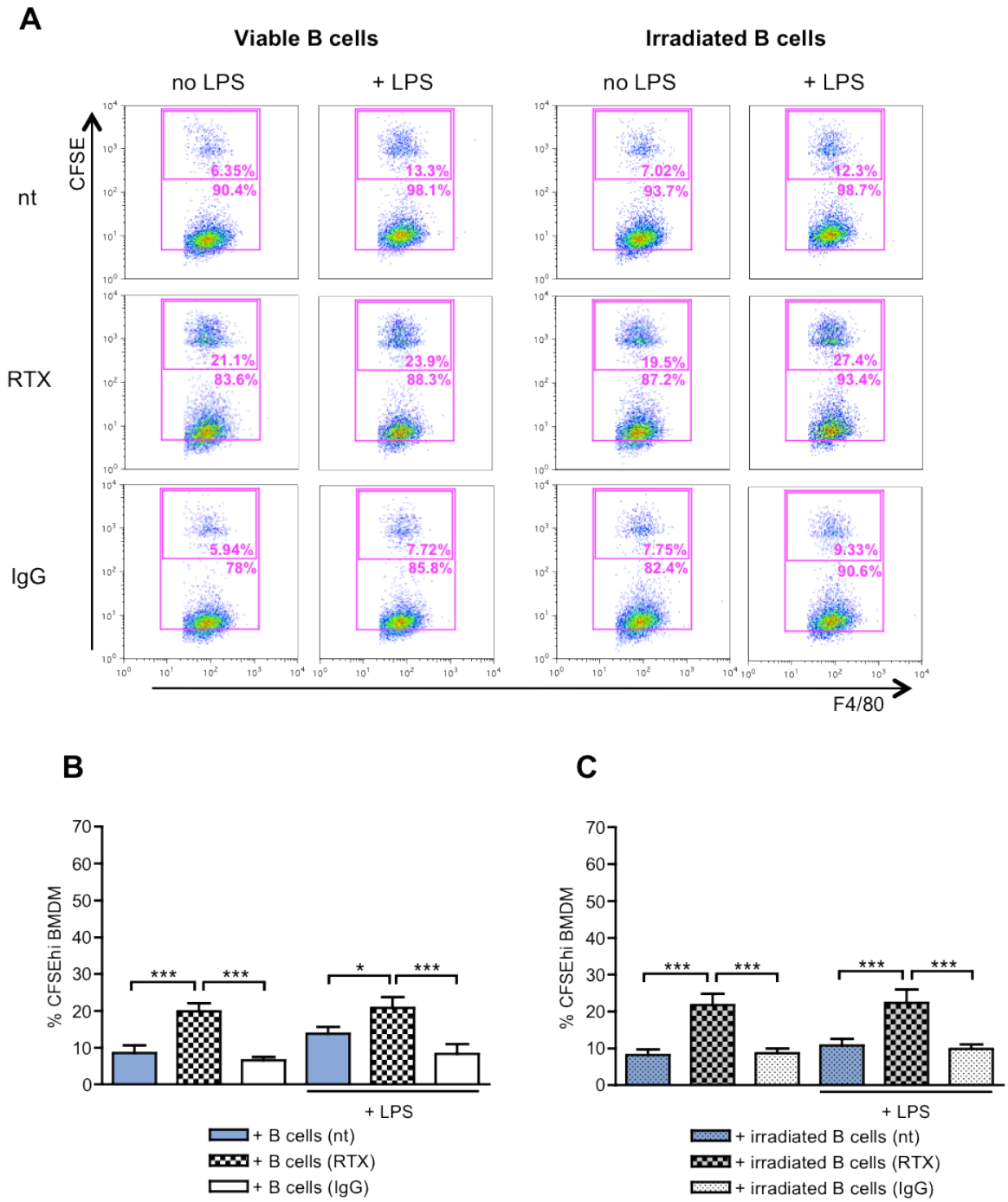

Figure 4.13 Viable and irradiated RTX pre-treated B cells show a significantly higher level of interaction with GM-CSF BMDM in the presence or absence of LPS

Murine BMDM were grown in cRPMI supplemented with GM-CSF and IL-3. On d7 adherent cells were co-cultured with CFSE stained viable or irradiated, pre-treated primary B cells for 15min, at a ratio of 1 BMDM:5 B cells, in the presence or absence of 1ng/ml LPS. Interaction levels were analyzed by flow cytometry. (**A**) Representative FACS plots showing the levels of interaction seen between GM-CSF BMDM and viable pre-treated B cells, co-cultured for either 15, 30 or 60min. Panels: CFSE vs. F4/80. (**B**) Graph of pooled data showing the percentage of $CFSE^{hi}$ GM-CSF BMDM after co-culture with viable pre-treated B cells. (**C**) Graph of pooled data showing the percentage of $CFSE^{hi}$ GM-CSF BMDM after co-culture with irradiated pre-treated B cells. (Viable B cells n=1, irradiated B cells n=2) Statistics used: One Way ANOVA performed on each full data set in (B) and (C), followed by Bonferroni's post test, with *** = p<0.001.

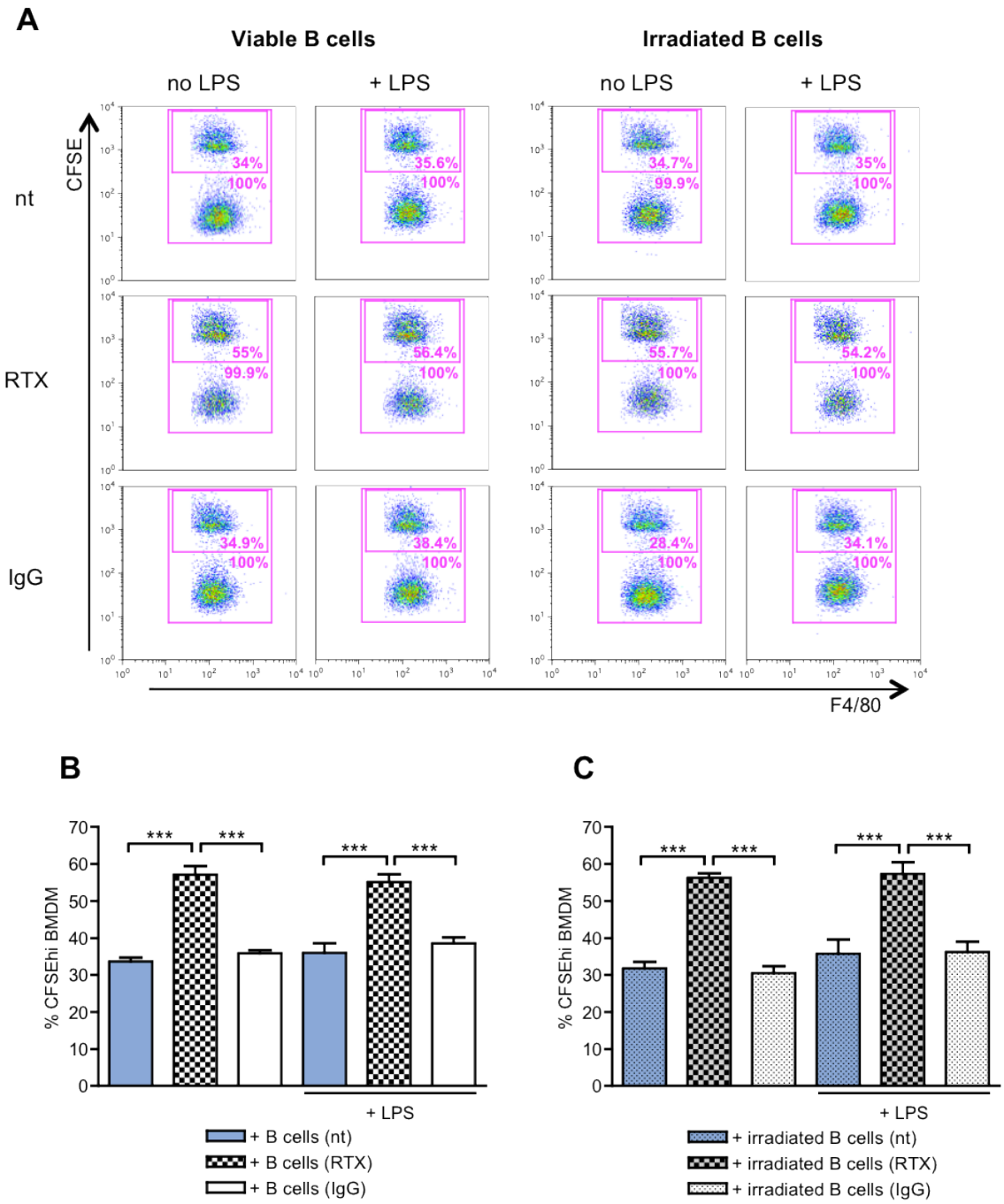

Figure 4.14 Viable and irradiated RTX pre-treated B cells show a significantly higher level of interaction with L929 BMDM in the presence or absence of LPS

Murine BMDM were grown in cRPMI supplemented with M-CSF containing L929 supernatant. On d7 adherent cells were co-cultured with CFSE stained viable or irradiated pre-treated primary B cells for 15min, at a ratio of 1 BMDM:5 B cells, in the presence or absence of 1ng/ml LPS. Interaction levels were analyzed by flow cytometry. (**A**) Representative FACS plots showing the levels of interaction seen between L929 BMDM and viable pre-treated B cells, co-cultured for either 15, 30 or 60min. Panels: CFSE vs. F4/80. (**B**) Graph of pooled data showing the percentage of $CFSE^{hi}$ L929 BMDM after co-culture with viable pre-treated B cells. (**C**) Graph of pooled data showing the percentage of $CFSE^{hi}$ L929 BMDM after co-culture with irradiated pre-treated B cells. (n=1) Statistics used: One Way ANOVA performed on each full data set in (B) and (C), followed by Bonferroni's post test, with *** = $p<0.001$.

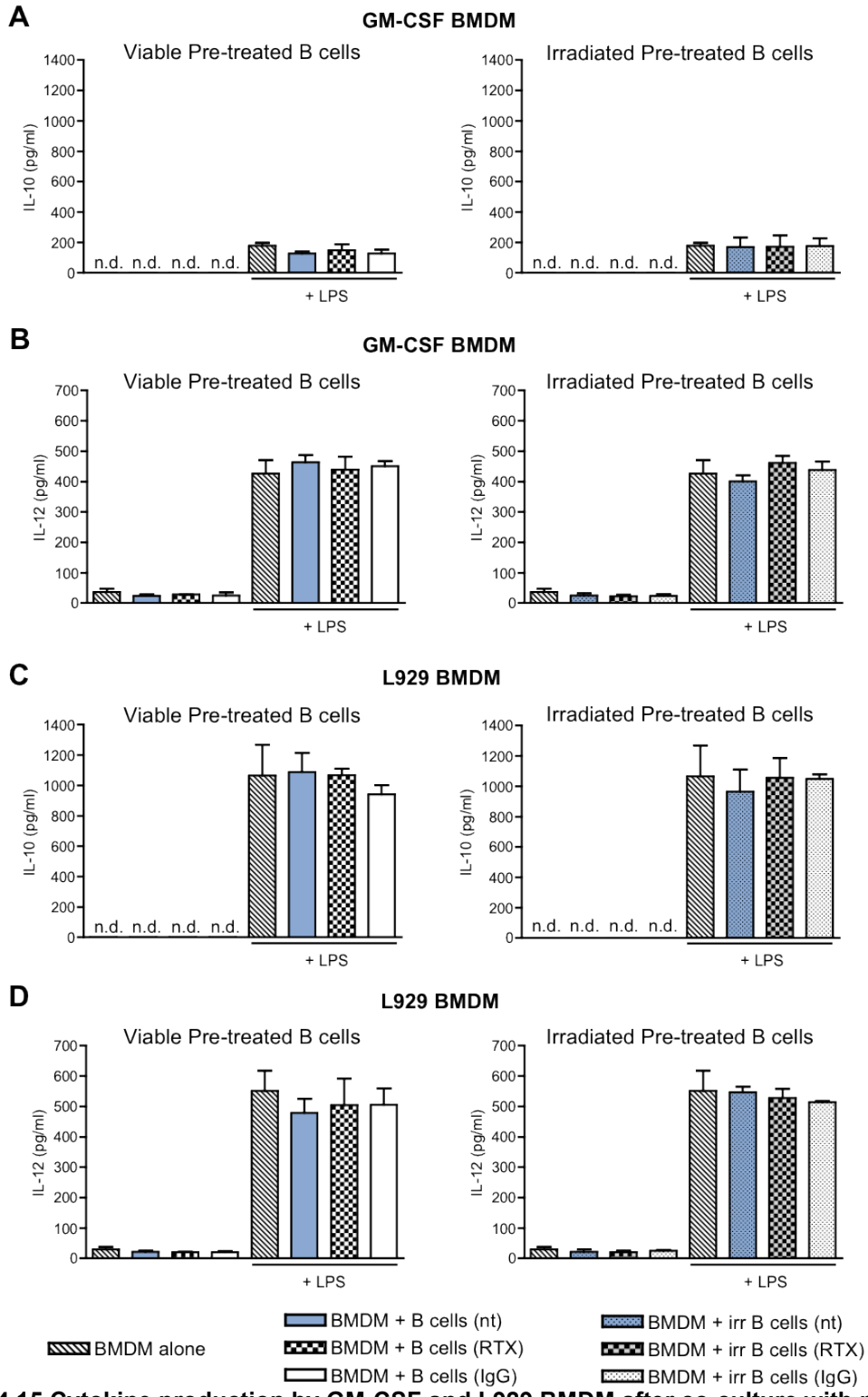

Figure 4.15 Cytokine production by GM-CSF and L929 BMDM after co-culture with pre-treated B cells

Un-stimulated and 1ng/ml LPS stimulated murine GM-CSF BMDM or L929 BMDM were co-cultured with viable or irradiated pre-treated B cells overnight, cell culture supernatants collected, and IL-10 and IL-12 production quantified by ELISA. (**A**) Graph showing IL-10 production by GM-CSF BMDM after co-culture with viable or irradiated pre-treated B cells, in the presence and absence of LPS. (**B**) Graph showing IL-12 production by GM-CSF BMDM after co-culture with viable or irradiated pre-treated B cells, in the presence and absence of LPS. (**C**) Graph showing IL-10 production by L929 BMDM after co-culture with viable or irradiated pre-treated B cells, in the presence and absence of LPS. (**D**) Graph showing IL-12 production by L929 BMDM after co-culture with viable or irradiated pre-treated B cells, in the presence and absence of LPS. (n=1, 3 replicates)

IL-12 secreted by GM-CSF BMDM cultured alone increased markedly to 426±44pg/ml. Co-culture of GM-CSF BMDM with either viable or irradiated pre-treated B cells in the presence of LPS did not alter the levels of IL-12. Similar levels of IL-12 were produced by L929 BMDM cultured in the presence of LPS, with 551±66pg/ml IL-12 detected (Figure 4.15d). No difference in the levels of IL-12 produced by L929 BMDM were observed on co-culture with either viable or irradiated pre-treated B cells, in the presence of LPS.

Together these findings show that in this experimental set up, GM-CSF BMDM undergo lower levels of interaction with B cells than L929 BMDM, however both L929 and GM-CSF BMDM experience enhanced cell-cell interaction with RTX pre-treated B cells. It was also established that in both inflammatory and non-inflammatory conditions, the increased interactions observed between the BMDM and RTX pre-treated B cells had no effect on the levels of IL-10 or IL-12 produced, indicating that the increased interaction does not affect the phenotype of either population of BMDM.

4.2.7 Effects of type-I and type-II anti-CD20 antibody pre-treatment on the interaction of B cells with BMDM

Anti-CD20 antibodies are defined as either type-I or type-II antibodies, dependent on their ability to redistribute CD20 into lipid rafts upon binding, with type-I antibodies, such as RTX, able to induce this redistribution of CD20. Type-II antibodies, such as Tositumomab (B1), do not have this effect on CD20, and it has been shown that binding of B cells by type-II antibodies results in far less modulation of CD20 from cell surface, compared to type-I anti-CD20 antibodies [251]. We wanted to explore whether the ability of RTX to redistribute CD20 played a role in the increased interactions observed between L929 BMDM and RTX pre-treated B cells. To do this, the previous BMDM co-culture assay was repeated, with viable CFSE-stained B cells incubated with either the type-I murine RTX antibody (mRTX), the type-II murine Tositumomab antibody (mB1), murine polyclonal IgG (mIgG) or left un-treated. These pre-treated B cells were then co-cultured with L929 BMDM for 15min, at a 5:1 ratio (B cells:BMDM) and the resultant interaction levels analyzed by flow cytometry.

The proportions of $CFSE^{+}$ L929 BMDM were consistent throughout the conditions investigated, and so analysis was limited to the population of L929 BMDM undergoing elevated levels of B cell interaction – the $CFSE^{hi}$ BMDM population (Figure 4.16a). As seen throughout the chapter with standard RTX, co-culture of L929 BMDM with mRTX treated B cells resulted in a significantly larger proportion of $CFSE^{hi}$ BMDM, compared to those co-cultured with either un-treated or IgG pre-treated B cells (Figure 4.16b) (mRTX pre-treated: 44.7±2.3% $CFSE^{hi}$ BMDM vs. un-treated: 28.6±8.8% $CFSE^{hi}$ BMDM and IgG pre-

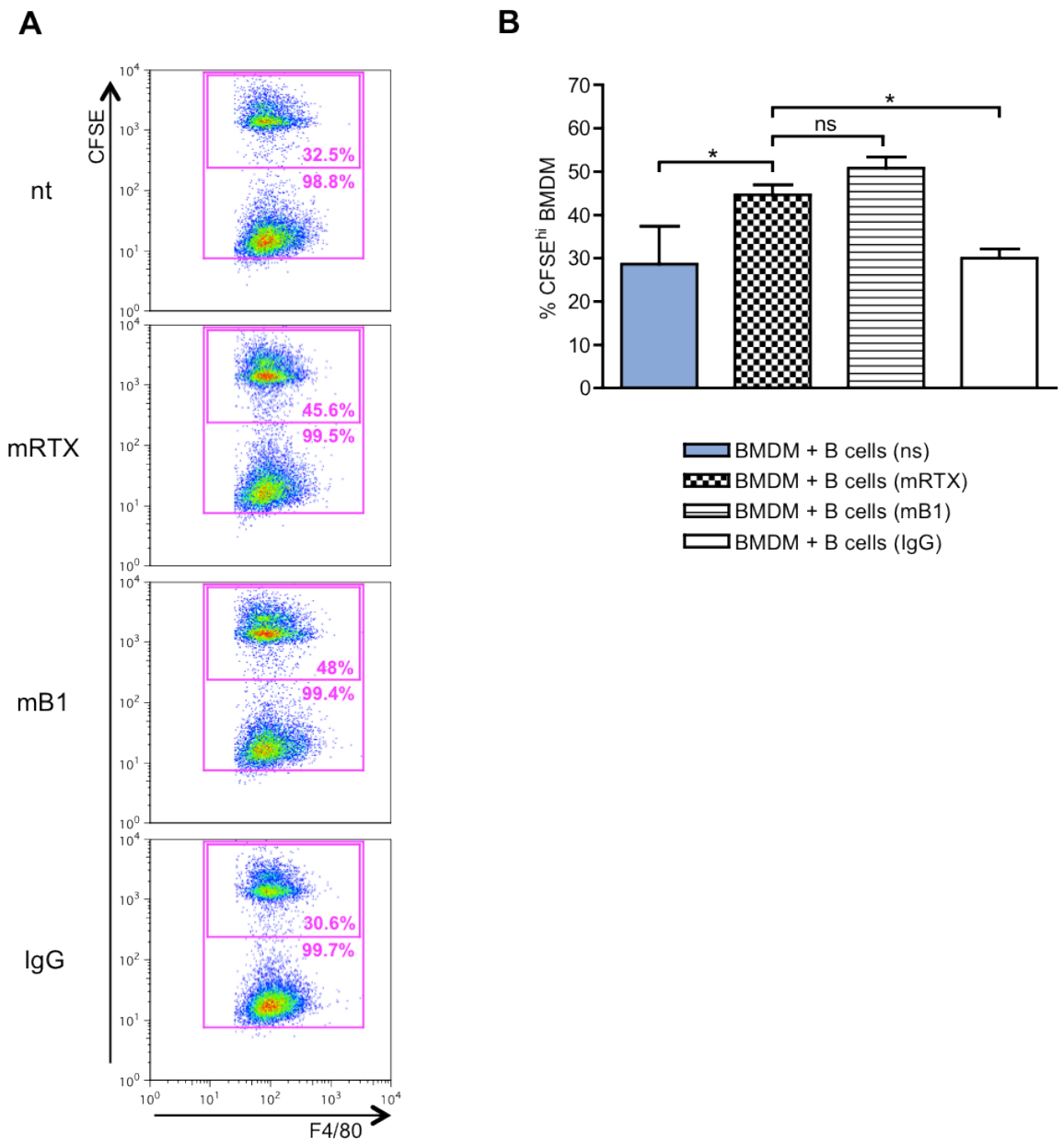

Figure 4.16 Comparison of the effects of type-I and type-II anti-CD20 antibodies on the interaction of BMDM and pre-treated B cells
Murine BMDM were grown in cRPMI supplemented with M-CSF containing L929 supernatant. On d7 adherent cells were co-cultured with CFSE stained viable pre-treated primary B cells for 15min at a ratio of 1 BMDM:5 B cells. Interaction levels were analyzed by flow cytometry. (**A**) Representative FACS plots showing the levels of interaction seen between L929 BMDM and viable B cells either given no pre-treatment (nt) or pre-treated with murine RTX (mRTX), murine Tositumomab (mB1) or murine polyclonal IgG (IgG). Panels: CFSE vs. F4/80. (**B**) Graph of pooled data showing the percentage of $CFSE^{hi}$ L929 BMDM after co-culture with pre-treated B cells (n=1) Statistics used: One Way ANOVA performed on complete data set, followed by Bonferroni's post test, with a value of $p<0.05$ considered significant and * = $p<0.05$.

treated: 30±2.2% $CFSE^{hi}$ BMDM) Co-culture of L929 BMDM with mB1 treated B cells resulted in a significantly larger proportion of $CFSE^{hi}$ BMDM (50.8±2.5%), compared to those co-cultured with either un-treated or IgG pre-treated B cells. However, no difference was seen in the proportion of L929 BMDM with B cells pre-treated with either mRTX or mB1.

This study demonstrates that in this assay system, both type-I and type-II anti-CD20 antibody pre-treatment of B cells have the ability to enhance their interactions with L929 BMDM, and that the type of anti-CD20 antibody used does not influence these interactions.

4.3 Discussion

- In this chapter we went on to investigate the ability of RTX treatment to alter B cell interactions with other cells prior to depletion, and the possibility that these altered interactions could regulate responses by macrophages.
- RTX pre-treated B cells underwent increased levels of interaction with BMDM, resulting in the enhanced phagocytosis of RTX-coated B cells. This increased interaction and uptake did not affect BMDM function, as determined by cytokine production.
- These findings show that RTX bound B cells do not modulate BMDM cytokine responses. Investigation of a wider range of BMDM functional outcomes would enable us to determine whether other biologically relevant changes are occurring after these interactions.

For the *in vitro* assays primary B cells isolated from our in-house colony of hCD20tg C57BL/6 mice were used. Work by Beers et al has shown that hCD20tg B cells internalize surface hCD20 on binding of an IgG2a version of Rituximab (Rit-m2a), resulting in an accumulation of internalized antibody, with approximately 50% of their surface hCD20 internalized after 2hr in culture, and around 80% internalized by 6hr [100]. However, work by Beum and colleagues utilizing the standard IgG1 form of RTX and the 38C13-$CD20^+$ B cell line demonstrated a far slower rate of internalization, with less than 25% of surface RTX having undergone internalization after 2hr, as determined by flow cytometry [252]. Due to the discrepancies seen in RTX internalization between different $CD20^+$ cell populations, and the variations in protocols used, the details of RTX internalization by hCD20tg B cells were investigated prior to co-culture assays being undertaken.

Flow cytometry was used to examine the RTX-mediated internalization of CD20 from the surface of hCD20tg B cells, with a fluorescently labeled conjugate comprising of the standard IgG1 form of RTX and AlexaFluor488, utilized. After incubation of hCD20tg B cells with RTX-488, quenching of cell surface fluorescence allowed differentiation of the signal from internalized RTX-488 from that of total RTX-488, allowing the signal from the surface bound RTX to be calculated, giving relative values for internal vs. surface bound RTX. To enable this type of analysis, removal of cell surface fluorescence is required. Trypan blue quenching [246-248,253,254], and acid stripping protocols [249,250,255-257] were investigated on a range of commercially available FACS antibodies. Trypan quenching resulted in very little decrease in the signal of the antibodies tested, with acid stripping protocols showing moderate to high success in the removal of cell surface fluorescence. However, before attempted optimization of the acid stripping protocol was pursued, a specific AlexaFluor-488 quenching antibody was tested [180]. Incubation of RTX-488 labeled B cells with the anti-488 antibody resulted in the dramatic reduction of AF488 MFI, with no detrimental effect on cell viability, and so it was decided to utilize this approach of removal of AF488-specific cell surface fluorescence in the RTX internalization studies.

On incubation of hCD20tg B cells with the standard IgG1 form of RTX, a similar rate of RTX internalization was observed compared to that seen by Beers et al on incubation of hCD20tg B cells with the IgG2a form of RTX [100]. With the conditions used for the current study, maximal surface binding of hCD20 by RTX was not achieved until after 1hr of culture, as evidenced by the increasing total MFI seen up to this time. The decrease in the percentage of B cells measuring RTX-488^{+} after treatment with the anti-488 antibody at 0–30min indicates that at these time points a significant proportion of B cells had not yet internalized any fluorescently labeled RTX, while from the 1hr time-point onwards, the percentage of RTX-488^{+} B cells was consistent before and after treatment with anti-488 antibody, implying that after this time some level of RTX internalization had occurred in all B cells. After one hour in culture the majority of bound RTX was still present on the surface of the hCD20tg B cells, however from 3hr onwards >75% had been internalized. A small decrease in internal fluorescence was seen at 24hr, indicating that degradation of the RTX-488 conjugate may have begun. Fluorescent microscopy confirmed the flow cytometric data, illustrating the increase in total RTX-488 binding observed over the first 30min of culture.

Along with ADCC and CDC, one of the mechanisms of RTX-mediated B cell depletion is the direct induction of apoptosis in B cells. If the *in vitro* incubation of hCD20tg B cells with RTX resulted in an increased number of apoptotic B cells compared to controls, any differences seen in the interactions of BMDM and RTX pre-treated B cells could

theoretically be attributed to the increased apoptotic cells present, rather than to the RTX pre-treated B cells. Previous work by Kamburova et al has shown that addition of RTX alone to *in vitro* cultures of human B cells does not increase the occurrence of cell death, with the presence of complement proteins as well as RTX required for cell death to occur [245]. In the present cultures of hCD20tg B cells no increase in B cell death observed in cultures incubated with RTX compared to controls, with the majority of cells still viable after 8hr in culture, in line with previous findings.

Once the interaction of hCD20tg B cells with RTX was elucidated, *in vitro* B cell-BMDM co-culture assays were undertaken. It has previously been shown that RTX stimulation alters B cell interaction with T cells, resulting in the skewing of T cell populations to more Th2-like [245] and less Th17-like [244] phenotypes, as well changing the subclass of immunoglobulin produced by B cells [244]. With the current assay we wanted to explore whether RTX binding to B cells has an effect on their interactions with macrophages, with BMDM used as the model macrophage.

In the co-culture assays undertaken, when cultured at a BMDM-B cell ratio of 1:1, increased interaction between L929 BMDM and CFSE-labeled RTX pre-treated B cells was evident compared to controls, but not necessarily significant. The levels of interaction between peritoneal macrophages and pre-treated B cells were also investigated, with peritoneal macrophages showing a far greater level of B cell interaction compared to that of the L929 BMDM. Mouse peritoneal macrophages are comprised of two main subsets: an 'immature' population that are $F4/80^+$, express high levels of FcRs and demonstrate an elevated phagocytic capacity; and a smaller 'mature' population, with a reduced expression of F4/80 and FcRs, and a diminished phagocytic capacity [258]. Although all cells isolated from the peritoneal cavity were included in the co-culture conditions, analysis was limited to the $F4/80^+$ population to exclude skewing of the results by non-macrophage cell types. However, by focusing on the $F4/80^+$ population, the analysis was concentrated on the 'immature', highly phagocytic peritoneal macrophage subset, which could explain the increased levels of $CFSE^+$ macrophages seen compared to the BMDM investigated. Comparison of murine $F4/80^+$ peritoneal macrophages to murine splenic macrophages has also highlighted the enhanced phagocytic capacity of this macrophage population. In a study by Liu et al, the ability of peritoneal macrophages to take-up red blood cells and T cells during *in vitro* co-culture was significantly greater than splenic macrophages [259]. These peritoneal macrophages were shown to express lower levels of MHC II and co-stimulatory molecules, but higher levels of the pattern recognition receptors TLR2 and TLR4, compared to the splenic macrophages [259]. These results indicate that peritoneal macrophages may be specialized for the recognition and clearance of pathogens and other stimuli, while

other subsets of macrophages, such as splenic macrophages, are more proficient at the presentation of antigen and stimulation of effector responses. Although in the present *in vitro* assay, the interactions of peritoneal macrophages were being compared to BMDM, this previous work demonstrates the enhanced phagocytic capacity of peritoneal macrophages compared to other macrophage subsets.

Another explanation for the increased interaction seen between the peritoneal macrophages and B cells, compared to that of the L929 BMDM and B cells is the differing origin of these cell populations. Macrophages express a wide array of PRRs allowing detection of AC, with different macrophage populations expressing different combinations of these receptors. Much work is still needed to fully understand the relative contribution of these receptors to AC uptake and their influence on subsequent cellular responses, however recent work however has shown that tissue-resident and monocyte-derived macrophages express different PS receptors [260], with tissue-resident macrophages more efficient at clearing AC in a murine model of thioglycollate-induced peritonitis [260]. Tissue-resident macrophages have also been shown to sequester bridging molecules required for AC uptake by inflammatory monocyte-derived macrophages, effectively limiting their contribution to AC clearance [260]. This difference in AC uptake was proposed by the authors to be a 'sorting system' for AC, helping to maintain tolerance by encouraging non-inflammatory AC uptake by M2-like tissue-resident macrophage populations, rather than immunogenic uptake by inflammatory macrophage populations. Murine $F4/80^{+}$ peritoneal macrophages have been shown to be tissue-resident self-renewing cells, and the population is maintained independent of circulating monocytes [15]. L929 BMDM, on the other hand, are generated from bone marrow precursors, following the MPS model of development, and more closely emulate inflammatory monocyte-derived macrophages found *in vivo*. As such, the increased level of interaction seen in co-cultures containing the peritoneal macrophages may not be due to their maturation state, but rather due to their role as tissue-resident macrophages, predominantly focused around tissue homeostasis and repair [reviewed in [261], and including the enhanced uptake of AC.

When the peritoneal macrophages were co-cultured with the various pre-treated B cells conditions no difference in the interaction levels was observed, however this may have been due to the small numbers of repeats undertaken. Isolating substantial numbers of peritoneal macrophages proved to be challenging, and although a difference may have emerged with further investigation, it was decided to move away from the use of this primary cell population. This study also highlighted that IFNγ and/or LPS stimulation of the BMDM, and therefore the activation state of the BMDM, had no effect on the levels of interaction seen in the vast majority of conditions. This confirmed previous work by

Leidi et al, in which it was shown that IFNγ and LPS treatment of human monocyte-derived macrophages had no effect on the uptake of RTX pre-treated B-CLL (B-chronic lymphocytic leukemia) cells by this macrophage population [227].

In an effort to enhance any differences between the pre-treatments, the ratio of B cells to BMDM in the co-cultures was increased. When higher ratios of B cells to L929 BMDM (3:1 or 5:1) were used, the majority of BMDM from all conditions were $CFSE^{+}$ after co-culture, indicating some level of B cell interaction had occurred in all conditions. However in these higher ratio co-cultures a distinct $CFSE^{hi}$ population also became apparent, as seen in the co-culture assays undertaken in Chapter 3. The $CFSE^{lo}$ population of BMDM in these higher ratio cultures was postulated to be due to the transfer of CFSE via tunneling nanotubes, although this cannot conclusively be stated without further investigation. As the rational for this theory was presented in depth in Chapter 3 (section 3.3), it will not be discussed here. However, as a result of this theory, it was decided that in these cultures the $CFSE^{hi}$ BMDM population would more accurately represent the BMDM undergoing prolonged, and therefore potentially more influential, cell-cell interactions, or those with ingested B cells, and as such it is the $CFSE^{hi}$ population that has been focused on for analysis.

A significant increase in the proportion of $CFSE^{hi}$ L929 BMDM was consistently observed when co-cultured with RTX pre-treated B cells, compared to controls, with this increase seen over a variety of time-points, ranging from 15min - 3hr of co-culture. To expand on the data acquired by flow cytometry, fluorescent microscopy was utilized to visualize the early interactions between the L929 BMDM and pre-treated B cells, and explore whether the enhanced interaction of RTX pre-treated B cells with BMDM observed was due to increased cell-cell adhesion, or whether increased phagocytosis of B cells was also involved. No differences were seen between conditions at the earliest time point, however by 30min of co-culture a substantial increase in the percentage of phagocytosed RTX pre-treated B cells was visible compared to the other B cell conditions, with this increase in uptake also apparent at the 60min time-point. The enhanced phagocytosis observed may be a RTX-specific event, however it could also be due to the opsonization of the B cells by RTX, regardless of RTX specificity or function. Cells can undergo opsonization by antibodies of a range of specificities, as well as complement components, with this coating of the cell targeting it for clearance by phagocytes. Macrophages express a variety of cell surface receptors to allow them to detect these opsonized cells, including members of the Fcγ family of receptors, which bind the Fc portion of IgG molecules, promoting the uptake and subsequent destruction of antibody opsonized cells. Antibodies of the IgG1 and IgG3 subclasses are the most

efficient for promoting phagocytosis, with RTX an IgG1 antibody. Therefore, along with any specific signals that may arise from RTX binding to B cells, the cell will also be detected as an opsonized cell by phagocytes. As the IgG used for the control B cell pre-treatment was a polyclonal IgG preparation, it would not bind to the B cells in any substantial amount due to the mix of antibody specificities present in the preparation, and as a result these cells should not become opsonized. The RTX internalization studies undertaken in this chapter demonstrate that on B cell incubation with RTX, the majority of bound RTX is present on the surface of the cell at all time-points from 15min – 1hr, effectively opsonizing the cell. By the 3hr time-point almost 75% of the bound RTX was internalized by the B cell, however the amount of surface RTX remaining may have been enough to allow recognition as an opsonized cell by the BMDM. The kinetics of phagocytosis observed in the present microscopy study fits with that of opsonized cells, with almost no B cell uptake by L929 BMDM at 15min, low levels at 30min, and an substantial proportion seen after 60min of co-culture.

In an attempt to dissect whether this increased phagocytosis of RTX pre-treated B cells was a RTX-specific effect or was just due to antibody opsonization, the monoclonal antibody Tositumomab (B1) was used as an additional B cell pre-treatment. Tositumomab is a type-II anti-CD20 antibody, and does not cause the redistribution of CD20 into lipid rafts, as opposed to type-I anti-CD20 antibodies, such as RTX. In a range of *in vitro* cellular assays using human peripheral blood cells and a variety of B cell lines, Tositumomab has been shown to be a potent inducer of ADCC, compared to RTX, but less capable of stimulating CDC [240] and shown to be ineffective at recruiting complement components [262]. In SCID mice adoptively transferred with the EHRB B cell line, complement depletion prior to antibody infusion had no effect on B1-mediated B cell depletion, whereas RTX-mediated depletion was markedly reduced in the absence of complement proteins [262]. Although RTX and B1 are both anti-CD20 antibodies, the different mechanisms of B cell clearance that result from RTX and B1 treatment indicates these mAbs have differing modes of action within the body. On comparison of L929 BMDM interaction with RTX and B1 pre-treated B cells it could be seen that pre-treatment with either antibody resulted in significantly more interaction with BMDM versus the untreated or IgG pre-treated B cells. However, no difference was seen between the levels of interaction resulting from RTX or B1 pre-treatment, demonstrating that the increased BMDM-RTX pre-treated B cell interactions are likely not a result of a RTX-specific effect. These results indicate that the enhanced interactions may be due to B cell opsonization, however they may due to a CD20-mediated effect. As both RTX and B1 are anti-CD20 antibodies, it is possible that the binding of these antibodies to their target molecule induces a change in the B cell, enhancing its ability to interact with the BMDM. The addition of a further co-culture

condition, containing B cells pre-treated with an antibody specific for different B cell surface marker, such as CD19, would help to dissect whether this is the case, or whether B cell opsonization by any specificity of antigen would have the same effect on interaction levels.

To investigate whether RTX pre-treated B cells also undergo enhanced interaction with a more inflammatory population of macrophages, the interaction of pre-treated B cells with GM-CSF BMDM and L929 BMDM was compared. There is substantial variability in macrophage phenotypes associated with the various methods of BMDM generation, with a large body of work looking into the phenotype and function of these different subsets, while generation of BMDM using recombinant GM-CSF produces an M1-like population of macrophages, which resemble the classically activated, inflammatory cell population found *in vivo*. Generation of BMDM using L929 supernatant results in a more regulatory, M2-like population of macrophages.

As with L929 BMDM, the M1-like GM-CSF BMDM undergo enhanced cell-cell interactions with RTX pre-treated B cells compared to controls. However, in the *in vitro* assay undertaken, lower levels of interaction were seen between B cells and the GM-CSF BMDM. The M2-like L929 BMDM have previously been shown to be highly phagocytic in comparison to GM-CSF BMDM [227], and as such, reduced uptake of B cells during co-culture by GM-CSF BMDM could be attributed to intrinsic cell characteristics, rather than a consequence of the assay.

Interestingly, at the 15min time-point, co-culture of either GM-CSF or L929 BMDM with irradiated pre-treated B cells did not alter the levels of cell-cell interaction observed, when compared to co-culture with viable pre-treated B cells. Only during the 3hr co-cultures of L929 BMDM and pre-treated B cells was an increase in BMDM interaction with irradiated pre-treated B cells observed, compared to that seen in the equivalent viable pre-treatment conditions. One of the chief roles of macrophages *in vivo* is the rapid clearance of apoptotic cells from the system, and as apoptosis of the B cells is the outcome of irradiation, it might be expected that the interaction levels seen between BMDM and the irradiated B cells would consistently be greater than those between BMDM and viable B cells. The comparable levels of interaction seen after short-term co-culture are not restricted to viable/apoptotic B cells, as work in the previous chapter looking into BMDM–AC interactions also demonstrates comparable levels of interaction between BMDM and viable or apoptotic T cells, and viable or apoptotic thymocytes. Although these findings initially seem to disagree with previous work in the apoptotic field, this is not necessarily the case. At the early 15min time-point, BMDM and viable B cells underwent surface interactions, as detailed by the fluorescent microscopy study

undertaken in this chapter, however these interactions would not necessarily lead to phagocytosis of these B cells. Work by Brown et al has demonstrated that THP-1 macrophages will bind both viable and apoptotic neutrophils through homotypic adhesion of CD31 expressed on the surface of the cells, however subsequent CD31-mediated signalling results in active detachment of the viable, but not apoptotic neutrophils [151]. These results demonstrate that macrophage recognition of a cell as either viable or apoptotic occurs through surface interactions, prior to the ingestion of those cells that are detected as being apoptotic.

Cell adhesion molecules (CAMs) could also mediate the interactions seen between viable B cells and BMDM. CAMs are surface expressed proteins responsible for cell-cell interactions, as well as leukocyte migration and homing *in vivo*. Adhesion molecules can be classified into three main groups: selectins, integrins and the immunoglobulin superfamily; and are classified depending on their molecular structure. B cells and macrophages express various integrins and immunoglobulin superfamily members, with many of these molecules acting as ligands for one another. For example, the immunoglobulin superfamily member ICAM-3 (intercellular adhesion molecule-3) is constitutively expressed by all leukocytes [reviewed in [148], and is able to interact with LFA-1 (leukocyte functional antigen-1) expressed by both B cells and macrophages. Another immunoglobulin superfamily member, ICAM-1, is expressed at low levels by resting B cells and macrophages, however on activation with inflammatory cytokines its expression is up-regulated, whereupon it can interact with LFA-1 [263], as well as the integrin Mac-1 ($\alpha_M\beta_2$) [264], expressed by macrophages.

This initial stage of cell recognition by macrophages could account for the equivalent BMDM interaction levels with viable and apoptotic B cells seen after 15min of co-culture, but the increased BMDM interaction with apoptotic B cells seen after 3hr. Very few studies into apoptotic cells directly compare the rate or amount of AC interaction to that of viable cells, with none found looking at as early a time-point, however the increased interaction of BMDM and apoptotic B cells after 3hr of co-culture fits with the previous literature found [125,151]. However, as discussed in Chapter 3, these results may potentially be explained by the BMDM interacting with contaminating apoptotic B cells in the 'viable' B cell conditions. If this is indeed the case, a multitude of receptors could be involved with the BMDM-B cell interactions seen. On apoptosis, cells expose a variety of neo-epitopes collectively termed ACAMPs, with phagocytes able to recognize these directly through PRRs, or indirectly through adaptor molecules (Figure 1.2).

In an attempt to ascertain whether the increased cell-cell interactions observed had any functional outcome, ELISAs were undertaken to investigate the levels of pro- and anti-inflammatory cytokines produced by the BMDM after overnight co-culture. We hypothesize that one of the mechanisms of action of RTX may be the re-introduction of a temporary tolerance to the immune system through indirect effects of RTX-mediated B cell depletion on other cells of the immune system, such as an effect on the interactions of RTX-bound B cells prior to their clearance from the system. To re-introduce tolerance, an anti-inflammatory environment would need to be established as a result of RTX treatment in order to halt the already present systemic inflammation seen in RA. Macrophages are hugely plastic cells, and are able to alter their phenotype in response to different environmental stimuli, with the anti-inflammatory cytokines IL-10 and TGF-β both produced by macrophages under certain conditions, contributing the resolution of inflammation. Quantification of cytokine secretion, in combination with the identification of specific surface markers, can also be used to categorize macrophages into particular subgroups, with the levels of IL-10 and IL-12 secreted commonly used to help in the identification of macrophage subsets. Each subset produces different ratios of these mediators: classically activated, inflammatory macrophages are known to produce high levels of pro-inflammatory IL-12 and low levels of IL-10; whereas regulatory macrophages produce high levels of the anti-inflammatory cytokine IL-10, while down-regulating their production of IL-12; and wound-healing macrophages produce low levels of both IL-10 and IL-12 [reviewed in [17]. By quantifying the levels of cytokines produced by the BMDM in response to RTX pre-treated B cells, it is possible to start to discern whether RTX binding to B cells alters the signals received by BMDM on cell-cell interaction, and alterations in the production of these mediators could indicate a skewing of the BMDM to a more anti-inflammatory phenotype.

The levels of IL-10 and IL-12 produced by the GM-CSF and L929 BMDM cultured alone in the presence of LPS were in line with those expected. The M1-like GM-CSF BMDM produced minimal levels of IL-10 and high levels of IL-12, while the M2-like L929 BMDM produced high levels of IL-10, with comparatively low levels of IL-12. However, no change in IL-10, IL-12 or TGF-β production could be seen on co-culture of either BMDM population with RTX pre-treated B cells, compared to BMDM cultured alone, and this was true when either viable or irradiated B cells were used for the co-cultures. Although not conclusive, the data generated from these cytokine ELISAs indicates that the interaction of RTX pre-treated B cells with BMDM does not enhance anti-inflammatory functions by the macrophages, or induce a change in phenotype in these cells.

There is some disparity in the literature as to whether RTX treatment has a widespread effect on cytokine levels. In a study looking at the response to a single dose of RTX by dialysis-dependent renal failure patients, levels of serum TGF-β were seen to increase after treatment in patients receiving high-dose RTX, although the results were highly variable and a small sample size used. Moreover, an increase in the pro-inflammatory cytokine IL-6 was also documented in the majority of these patients [265]. A longer-term study in RA patients, looking at serum cytokine levels after B cell depletion therapy, showed that multiple rounds of RTX treatment progressively reduced serum levels of the inflammatory cytokines IL-15 and IL-17A [266]. Findings by Bouaziz and colleagues however, show that B cell depletion in C57BL/6 mice using anti-murine CD20 antibodies does not alter serum cytokine levels [267]. Levels of IL-1, IL-2, IL-4, IL-5, IL-6, IL-10, IL-12, IL-13, IL-17, TNFα, IFNγ, GM-CSF, and TGF-β1 were measured for 7 days post RTX treatment, and compared to serum collected from the mice prior to depletion, with no change seen in the levels of any cytokine investigated [267]. Recent work in which a single intra-operative dose of RTX was given to renal transplant patients, supported the finding of a lack of systemic effect of B cell depletion on cytokine production by immune cells [268]. In this study, the amounts of IL-1β, IL-6, IL-17, IL-22, TNFα, and IFNγ produced *ex vivo* by peripheral blood mononuclear cells isolated before or after RTX-treatment were investigated, with levels unchanged up to one month after treatment [268]. Although these papers highlight the variation in the literature as to the effects of RTX-mediated B cell depletion on serum cytokine production, the work in this chapter shows that co-culture of RTX pre-treated B cells and BMDM does not modulate the production of IL-10, IL-12 or TGF-β under the experimental conditions used.

Interestingly, apoptotic B cells had no effect on cytokine production by BMDM, regardless of RTX pre-treatment. The immunosuppressive effects of AC on cytokine production have repeatedly been demonstrated under a range of conditions [157,171,218,232,248]. None of the studies in the literature utilize B cells as the model AC, however work from Chapter 3 of this thesis demonstrates that BMDM interactions with AC of different origins do not greatly differ, and so it can be assumed that these results could be extrapolated to apoptotic B cells. As such the finding that apoptotic B cells had no effect on BMDM was unexpected; however it is a finding replicated in previous work from this thesis (Chapter 3). As this has been a consistent finding with the co-culture assay used, regardless of the origin of AC, it can be classified as an artefact of the particular experimental protocol utilized, rather than an intrinsic trait of apoptotic B cells.

In summation, these findings demonstrate that RTX pre-treatment of B cells results in increased levels of interaction with both GM-CSF and L929 BMDM at early time-points, leading to enhanced phagocytosis of RTX-coated B cells compared to un-treated B cells. This increased interaction does not affect BMDM phenotype or function as determined by the production of IL-10, IL-12 and TGF-β. However, the possibility of alterations in BMDM phenotype and function not detected by the particular assays utilized cannot be ruled out.

Chapter 5: Secondary Presentation of Antigens

5.1 Introduction

In order for a protein antigen to be recognized by T cells it must first be broken down into its composite peptides, and these peptides presented on an MHC (major histocompatbility complex) molecule expressed on the surface of another cell, ready for recognition by antigen-specific T cells. There are two different types of MHC molecule: MHC I molecules, expressed by nearly all nucleated cells of the body, with the highest levels expressed on lymphocytes; and MHC II molecules, expressed primarily on APCs. Presentation of a peptide in the context of MHC I results in peptide recognition by T cells expressing the CD8 co-receptor [30,31], known as cytotoxic T cells, while presentation in the context of MHC II results in recognition by T cells expressing the CD4 co-receptor [32], known as T helper (Th) cells, with these different subclasses of T cell having distinct effector mechanisms and roles within the immune response.

MHC I molecules predominantly present cytosolic peptides, these being either endogenous peptides arising from proteins found within the cell, or proteins resulting from cytosolic pathogens such as viruses. Peptides from the cytosol are transported into the endoplasmic reticulum, where those that are of the correct size and express the appropriate binding motifs are loaded onto newly synthesized MHC I molecules. Once a stable peptide:MHC I complex is formed, it is transported to the cell surface and presented, ready for recognition by antigen-specific $CD8^+$ T cells. Although classically known for the presentation of peptides deriving from the cytosol of a cell, MHC I molecules are also able to present antigens originating from other cells, a process known as cross-presentation [reviewed in [269]. Proteins taken up into vesicles from the cells surroundings can undergo retrograde transport, whereby they are actively transported into the cell cytosol from an enclosed vesicle. Once in the cytosol the proteins are degraded into peptides by the proteosome, and transported back in to the ER ready for loading onto MHC I molecules and subsequent presentation.

MHC II molecules primarily present exogenous antigen located within an APC's vesicular system, such as antigens that have been taken up by phagocytosis, endocytosis or macropinocytosis, or pathogens that reside and replicate within the vesicles of cells. Once these proteins are enclosed in intracellular vesicles, called endosomes, they are degraded by proteases, which become activated on acidification of the early endosome. The acidified peptide-containing endosome then binds to a lysosome containing MHC II molecules, to form the MHC II compartment, and it is within this compartment that it is thought peptide loading takes place. With the help of accessory molecules, stable peptide:MHC II complexes are formed, and these complexes are transported to the cell surface where they are presented, ready for recognition by $CD4^+$ T cells. MHC II

molecules can also undertake a form of cross-presentation, in which endogenous cytosolic proteins and organelles are delivered to the lysosomes for degradation via the process of autophagy, ultimately resulting in their presentation by MHC II molecules [reviewed in [270]. Autophagy is a constitutive process, however it is enhanced in response to cellular stress, and functions to enhance cell survival through the re-use of nutrients already present in the cell, as well as broadening the spectrum of responses to intracellular pathogens.

Antigen presentation by MHC molecules is a crucial step in both the activation and tolerization of the adaptive immune response, and it is the expression of co-stimulatory molecules on the APC that define the outcome of antigen recognition by adaptive immune cells. On the binding of a T cell to its specific antigen in the context of self-MHC, the cell becomes primed, but it is only once it has received a second signal from activatory co-stimulatory molecules expressed by the APC, in the presence of specific cytokines, that it will become activated and differentiate into an effector cell. This interaction induces T cells to differentiate into effector cells by increasing IL-2 production resulting in enhanced cellular proliferation, as well as inducing the up-regulation of cell surface molecules involved in the resultant T cell differentiation. MHC I restricted $CD8^+$ T cells become cytotoxic T cells, capable of rapid clonal expansion in response to activation and the direct killing of malignant or infected cells [reviewed in [271]. Depending on the cytokine milieu present at the time of activation, $CD4^+$ T cells can develop into either Th1, Th2, Th17 or Tregs. Each subset has distinct effector functions and roles within the immune response, and can be characterized based on the production of signature cytokines. Th1 cells are known to produce a range of pro-inflammatory cytokines, such as IFNγ, and are involved in cell-mediated immunity, via the activation of macrophages, and induce IgG production by B cells, while Th2 cells secrete the cytokines IL-4, IL-5, IL-6, IL-10 and IL-13 and are predominantly involved in non-inflammatory immune responses and the clearance of parasites [reviewed in [33]. Th17 cells are the most recently characterized $CD4^+$ T cell subset, and are often the first to be generated in response to infection, producing cytokines, such as IL-17, that activate local cells and recruit neutrophils [34,272]. Regulatory T cells that develop in the periphery from naïve $CD4^+$ T cells in the presence of TGF-β and IL-10 are termed inducible Tregs (iTregs) [35], as opposed to natural Tregs (nTregs), which develop in the thymus. These iTregs are able to inhibit pro-inflammatory immune responses, both by direct cell-contact mechanisms, and the production of anti-inflammatory cytokines.

If the second co-stimulatory signal is not given, or inhibitory rather than activatory co-stimulation molecules are bound, tolerance to the specific antigen results. CTLA-4 is an inhibitory receptor expressed on the surface of T cells, and has a high affinity for the co-stimulatory molecules CD80/CD86. Ligation of CD80/CD86 by CTLA-4 blocks the interaction of these activatory molecules with CD28 expressed on the T cell surface, resulting in the T cell encountering cognate antigen in the absence of further activatory signals. If antigen is recognised by T cells in the absence of co-stimulatory signals, the recognising T cell will either undergo clonal deletion, via activation-induced cell death, or become anergic, a state in which the cell can no longer be stimulated by cognate antigen. Both of these mechanisms act to induce a state of peripheral tolerance toward the antigen in question.

This control of activation vs. tolerance at the time of antigen recognition is vital to the maintenance of peripheral tolerance to harmless self-antigen. When this control mechanisms breaks down, the result is an active, highly detrimental response toward self, leading to the development of autoimmune disorders. Systemic lupus erythematosus (SLE) is a chronic autoimmune disease in which increased levels of apoptotic lymphocytes [273], coupled with defects in the clearance of apoptotic cells [156], results in the release of cell material ultimately leading to a break in tolerance to intracellular self-antigens. Autoantibodies directed toward double stranded DNA are characteristic of SLE, and are implicated in the pathogenesis of disease. Type I diabetes, another common autoimmune disease, results from a loss of tolerance toward antigens expressed by the pancreatic β-cells [274], the insulin producing cells of the body, resulting in their immune-mediated destruction [reviewed in [275].

The presentation of both self and non-self antigens happens continually, throughout the body, and is a well-characterized process. The majority of studies looking into antigen presentation focus on the ‘direct’ presentation of antigens, i.e. those that derive from proteins the cell has directly encountered, either through infection or uptake, or those that are constitutively expressed within the cell. The aim of the work in this chapter was to investigate whether an APC could present antigen it has not directly encountered, but derives from a protein taken up by another cell prior to that cell being phagocytosed by the APC, a process we have termed ‘secondary presentation’.

We hypothesize that Rituximab may re-introduce temporary tolerance to the immune system. If on treatment with Rituximab apoptosis of B cells is caused, the B cells will be phagocytosed by APCs in a non-inflammatory context. As previously discussed, apoptosis occurs regularly as a normal part of tissue turnover and homeostasis, and in order to prevent autoimmunity, the immune system is tolerized against antigens found on the

surface of apoptotic cells, with AC having been shown repeatedly to have immunosuppressive effects on the immune system [158,166-169]. The phagocytosed B cell, and any antigens it has internalized, will be degraded, and the resultant peptides presented by the APC in a tolerogenic context. If the B cell had previously taken up self-antigen, specifically the putative self-antigen the RA response is directed toward, presentation of this arthritogenic antigen in a non-inflammatory, tolerizing environment, may result in the re-introduction of temporary tolerance to a system in the midst of chronic inflammation.

As a step to understanding the integrity of this hypothesis, we wanted to examine whether APCs are able to achieve secondary presentation of antigen previously taken up by B cells. To do this, an *in vitro* assay was developed involving BMDM, primary hCD20tg B cells and transgenic OVA-specific primary T cells [276], with OVA used as the model antigen. As hCD20tg B cells are polyclonal, B cell receptor (BcR) mediated uptake of OVA will not occur in the majority of these cells, and so a way to ensure uptake of sufficient amounts of OVA by B cells was needed. It has been shown by Beers et al that RTX is internalized by B cells after binding to CD20 [100], and so to overcome this problem, the immunodominant $OVA_{323-339}$ peptide [277] was chemically conjugated to rituximab (RTX:OVA) (as described in section 1.3.4.). By conjugating the OVA peptide to RTX, the OVA will be taken up on internalization of RTX, resulting in an accumulation of peptide inside early endosomes within the B cells. This internalized OVA could then potentially by taken up by the macrophages on phagocytosis of the B cells, and presented to the OVA-specific T cells, by these BMDM. Activation of the T cells, isolated from OTII T cell receptor (TcR) transgenic mice, can then be used as a read out of successful secondary antigen presentation by the BMDM, with Figure 5.1 giving an overview of the assay protocol.

Chapter objectives:

- To develop an *in vitro* assay to investigate whether BMDM are able to achieve secondary presentation of antigen previously taken up by B cells
- To explore the functional effect of this secondary presentation on antigen-specific T cells

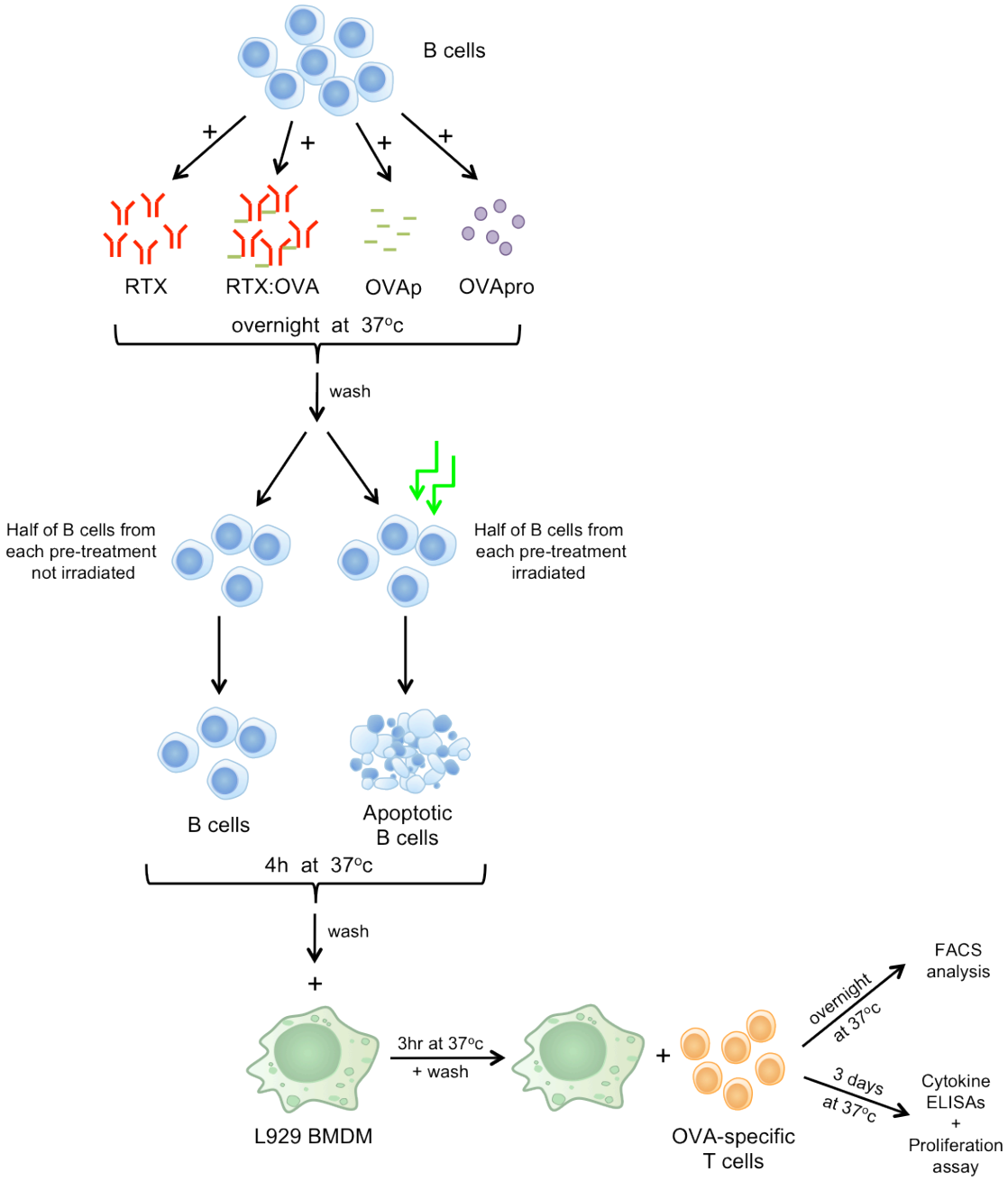

Figure 5.1 Schematic of the secondary presentation assay
An overview of the *in vitro* assay used to assess whether BMDM can successfully present antigen previously taken up by B cells. BMDM were generated and co-cultured for 3h with primary hCD20tg B cells, which had been pre-treated with 30μg/ml of RTX, RTX conjugated to OVA peptide (RTX:OVA), OVA peptide alone (OVAp), or OVA protein (OVApro). The BDMD were washed, to remove the B cells, and co-cultured overnight with OVA-specific T cells. T cell activation was used as a measure of successful antigen presentation, and was assessed by flow cytometry. Cytokine production, and cellular proliferation after co-culture were also examined.

5.2 Results

5.2.1 Activation of T cells by secondary presentation of antigen by BMDM

In vitro assays were performed to assess whether macrophage phagocytosis of B cells that have previously encountered antigen can result in the successful presentation of this antigen. To do this, primary hCD20tg B cells were cultured with 30μg/ml of RTX chemically conjugated to OVAp (RTX:OVA), with un-treated B cells, and those cultured with either RTX alone or $OVA_{323-339}$ peptide (OVAp) alone included as negative controls. The conditions containing un-treated B cells, or B cells cultured with RTX, do not contain OVA at any stage, and therefore no OVA-specific T cell activation should occur.

In the conditions containing B cells cultured with OVAp, no interaction was expected between the polyclonal B cell population and the peptide, and therefore the peptide should not be available for the BMDM to present to the OVA-specific T cells later in the assay. Half of the cells from each pre-treatment were irradiated to induce apoptosis, and all B cells incubated for 4hr, before extensive washing to remove free antigen, and co-cultured with BMDM for 3hr. The BMDM were washed to remove any un-bound B cells, and co-cultured overnight with OVA-specific OTII T cells to allow activation to occur. CD69 up-regulation by OTII T cells was used as a measure of T cell activation, as assessed by flow cytometry.

In the cell samples tested, viable lymphocytes were gated on using FSC and SSC, and within this population T cells were defined as $CD3^+CD4^+$ cells, with CD69 expression on this population quantified (Figure 5.2a). The level of T cell activation observed in the un-treated B cell condition (BMDM+B(nt)) was used as a measurement of background activation. No OVA was present at any point in this condition and no T cell activation, or subsequent up-regulation of CD69, should take place in the absence of OVA. When OTII T cells were co-cultured with BMDM incubated with B cells pre-treated with RTX:OVA (BMDM+B(RTX:OVA)), the data indicates an increased expression of CD69 by the T cells (17.1±3.6% $CD69^+$), with the 2 separate peaks seen in the FACS histograms for CD69 (Figure 5.2b) demonstrating the presence of two T cell populations with distinct CD69 expression profiles. On addition of RTX alone into the secondary presentation assay, no T cell activation above background was seen, with only 4.2±0.2% of OTII T cells co-cultured with BMDM+B RTX pre-treated B cells (BMDM+B(RTX)) expressing CD69. Surprisingly, when co-cultured with BMDM incubated with B cells pre-treated with OVAp (BMDM+B(OVAp)), 75.4±4.1% of OTII T cells expressed CD69 on their surface (Figure 5.2b). This was a sizable increase compared to the T cells from the

BMDM+B(nt) condition, in which only 5.1±0.3% of OTII T cells expressed CD69 after co-culture. On co-culture of OVA-specific T cells with BMDM incubated with irradiated apoptotic B cells (BMDM+apopB) pre-treated with RTX:OVA (BMDM+apopB(RTX:OVA)) an up-regulation of CD69 by the T cells was also seen, with 16.4±0.6% of T cells expressing CD69, compared to background expression levels of 5.9±0.5% in the BMDM+apopB(nt) group (Figure 5.2c). No up-regulation of CD69 by the OTII T cells was observed in the BMDM+apopB(RTX), compared to background levels. As with the condition containing viable B cells pre-treated with RTX:OVA, co-culture of OTII T cells with BMDM incubated with apoptotic B cells pre-treated with OVAp resulted in an up-regulation of CD69 by the T cells, with 85.6±4% staining positive for CD69.

Within the $CD69^+$ OTII T cell population, the level of surface CD69 expression was investigated. The MFI of CD69 showed an increase above background for both the BMDM+B(RTX:OVA) and BMDM+apopB(RTX:OVA) groups (Figure 5.3a and b). CD69 MFI for the BMDM+B(RTX:OVA) T cells was 358±122, compared to 91±0.1 in the BMDM+B(nt) condition, and 287±67 for the BMDM+apopB(RTX:OVA) T cells, compared to background levels of 101±18 on the T cells from the BMDM+apopB(nt) group. Substantial increases in OTII T cell CD69 MFI were also seen in both the BMDM+B(OVAp) and BMDM+apopB(OVAp) groups (Figure 5.3a and b), with a CD69 MFI of 989±61 and 716±103, respectively.

For this preliminary study, both irradiated and non-irradiated B cells were utilized as the antigen supply for the BMDM. Substantial activation of T cells was seen when co-cultured with BMDM previously incubated with irradiated B cells pre-treated with 30µg/ml RTX:OVA (BMDM+apopB(RTX:OVA)) (Figure 5.2c), as well as when non-irradiated, viable, B cells with the same pre-treatment were used as the BMDM antigen supply (Figure 5.2b). The levels of surface CD69 expressed on $CD69^+$ T cells from these treatment groups was also similar, with a CD69 MFI of 287±67 for the T cells from the BMDM+apopB(RTX:OVA) group, and a CD69 MFI of 358±122 on those from the BMDM+B(RTX:OVA) group (Figure 5.3a and b).

These data indicate that OVA-specific OTII T cells can be activated by the addition of RTX:OVA into the secondary presentation assay system, with this activation occurring when either viable or irradiated B cells are utilized. As a result of these findings, it was decided to remove the irradiated B cell groups from any further assays undertaken, as this additional condition did not add anything to the understanding of the system. Contrary to expectations, the addition of OVAp into this *in vitro* system also induced substantial activation of OTII T cells.

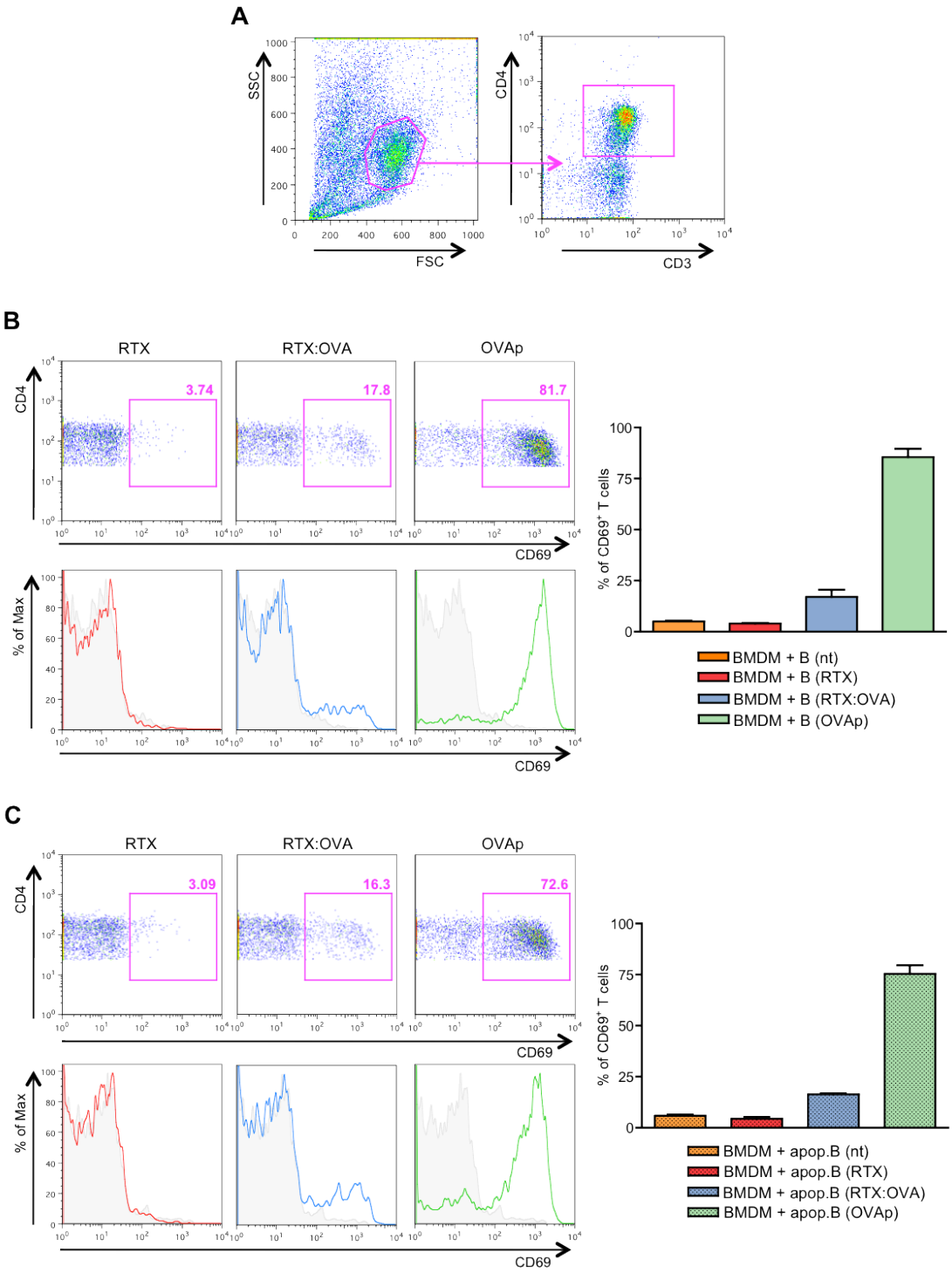

Figure 5.2 Activation of T cells by secondary presentation of antigen by BMDM
OTII T cells were co-cultured overnight with BMDM, which had been incubated with pre-treated viable or apoptotic B cells. Cells were then stained for flow cytometry, and analyzed using a FACSCalibur, with CD69 expression used as a marker of T cell activation. (**A**) The gating strategy used to identify T cells. First panel: SSC vs. FSC. Second panel: CD4 vs. CD3. (**B**) Representative FACS plots (CD4 vs. CD69) and histograms (% of Max vs. CD69) showing levels of OTII T cell activation after co-culture with BMDM previously incubated with pre-treated viable B cells (BMDM + B), and graph of pooled data showing the percentage of $CD69^+$ T cells after co-culture. Grey histogram = co-cultures with BMDM previously incubated with un-treated B cells. (**C**) Representative FACS plots (CD4 vs. CD69) and histograms (% of Max vs. CD69) showing levels of OTII T cell activation after co-culture with BMDM previously incubated with pre-treated apoptotic B cells (BMDM + apop.B), and graph of pooled data showing the percentage of $CD69^+$ T cells after co-culture. nt: no pre-treatment, RTX: Rituximab, RTX:OVA: RTX conjugated to OVA peptide, OVAp: OVA peptide. (n=1, 3 replicates)

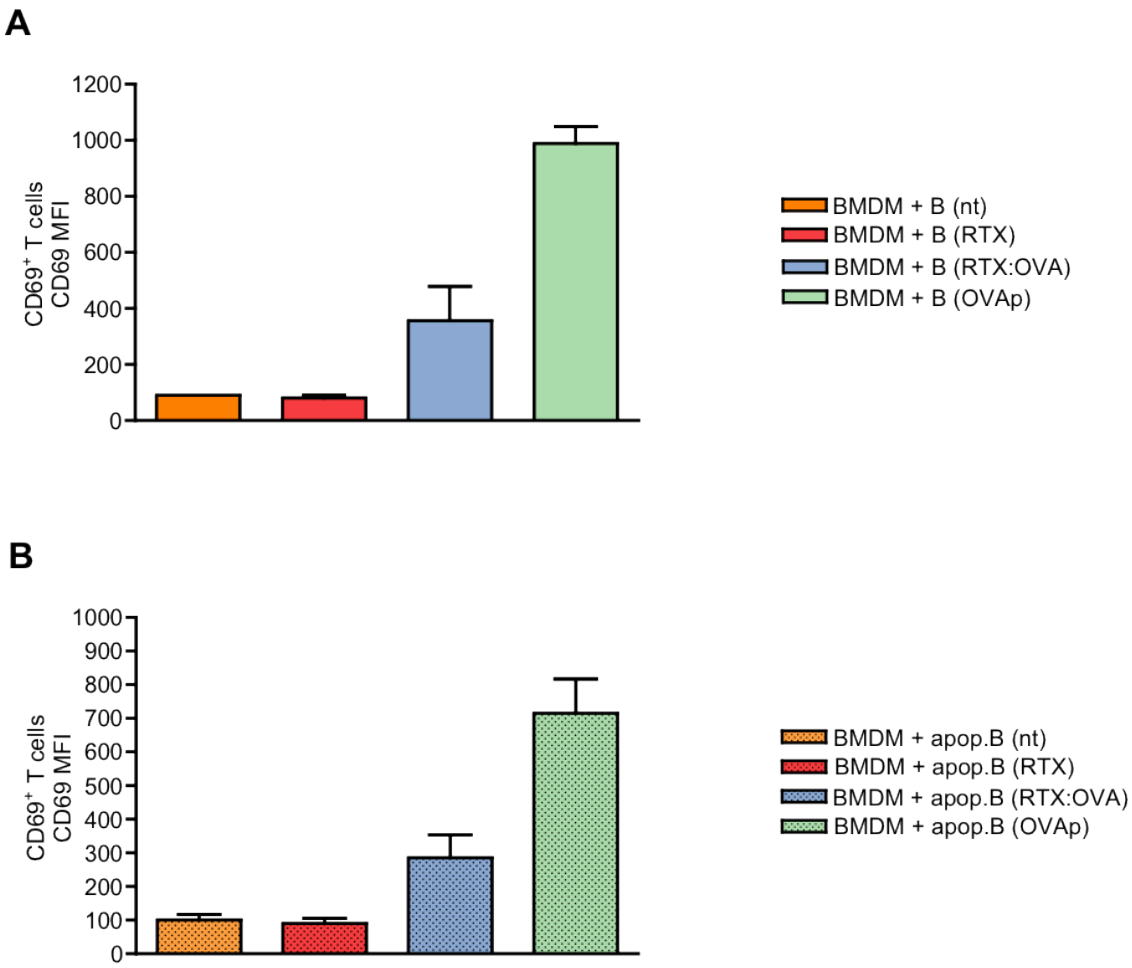

Figure 5.3 Level of activation of T cells after secondary presentation of RTX:OVA by BMDM
OTII T cells were co-cultured overnight with BMDM, which had been incubated with pre-treated viable or apoptotic B cells. Cells were then stained for flow cytometry, and analyzed using a FACSCalibur, with CD69 expression used as a marker of T cell activation. (**A**) Graph of pooled data showing the CD69 MFI of $CD69^+$ OTII T cells after co-culture with BMDM previously incubated with pre-treated viable B cells (BMDM + B). (**B**) Graph of pooled data showing the CD69 MFI of $CD69^+$ OTII T cells after co-culture with BMDM previously incubated with OVAp pre-treated apoptotic B cells (BMDM+ apop.B). nt: no pre-treatment, RTX: Rituximab, RTX:OVA: RTX conjugated to OVA peptide, OVAp: OVA peptide. (n=1, 3 replicates)

5.2.2 *Activation of OTII T cells after secondary presentation of differing concentrations of RTX:OVA by BMDM*

To assess whether increased OTII T cell activation could be achieved by the addition of higher concentrations of RTX:OVA into the secondary presentation assay, the previous assay was repeated with some minor changes. Non-irradiated hCD20tg B cells were used in co-cultures with BMDM, and these B cells were pre-treated with RTX:OVA at either 30μg/ml or 100μg/ml. Un-treated B cells and those pre-treated with OVA peptide (OVAp) at either 15μg/ml or 30μg/ml were again included, with an additional B cell pre-treatment of OVA protein (OVApro) at either 30μg/ml or 100μg/ml included as a further control group. OVA-specific T cells only become activated on recognition of the immunodominant peptide fragment of the OVA protein in the context of the correct MHC II molecule, and therefore in the conditions containing OVApro, processing of the protein would need to occur before successful presentation can result. No uptake of the protein by the polyclonal B cell population would be expected, and as such no peptide fragments should be available for the BMDM to present to the OVA-specific T cells later in the assay. After initial co-culture of pre-treated B cells with BMDM, the BMDM were washed to remove any un-bound B cells, and co-cultured overnight with OVA-specific OTII T cells, as done previously. Again, CD69 up-regulation was quantified by flow cytometry, as outlined in Figure 5.2a.

A similar level of background T cell activation was seen in the BMDM+B(nt) group for this study as in the preliminary experiment, with 9.5±1.2% of T cells expressing CD69 after co-culture, with an MFI of 102±3 (Figure 5.4b). When used at 30μg/ml, no significant activation above background was seen on T cells from the BMDM+B(RTX:OVA) condition, with 15.4±2.7% expressing CD69. However, the levels of expression of CD69 on these cells was significantly increased compared to the BMDM+B(nt) group (MFIs: 294±12 vs. 102±3, respectively). OVApro pre-treatment of B cells was included as an additional control (BMDM+B(OVApro)), and when used at 30μg/ml no significant activation of T cells was seen, with 22.6±0.4% expressing CD69, and an MFI of 203±17. As with the previous assay, significant up-regulation of CD69 was seen in the BMDM+B(OVAp) group, with 83.9±1.8% of T cells positive for CD69, and an MFI of 878±105. When used at 100μg/ml, the RTX:OVA pre-treatment resulted in significant activation of OTII T cells compared to the BMDM+B(nt) group, with 26.9±3.4% of T cells from the BMDM+B(RTX:OVA) condition expressing CD69, with an MFI of 437±29. Interestingly, when B cells were pre-treated with 100μg/ml OVApro, comparable levels of T cells activation were seen in the BMDM+B(OVApro) condition as were seen in the BMDM+B(RTX:OVA) condition, with 37.9±2.9% of T cells from the BMDM+B(OVApro) CD69 positive, and an MFI of 301±13. This activation is reflected in the 2 distinct populations

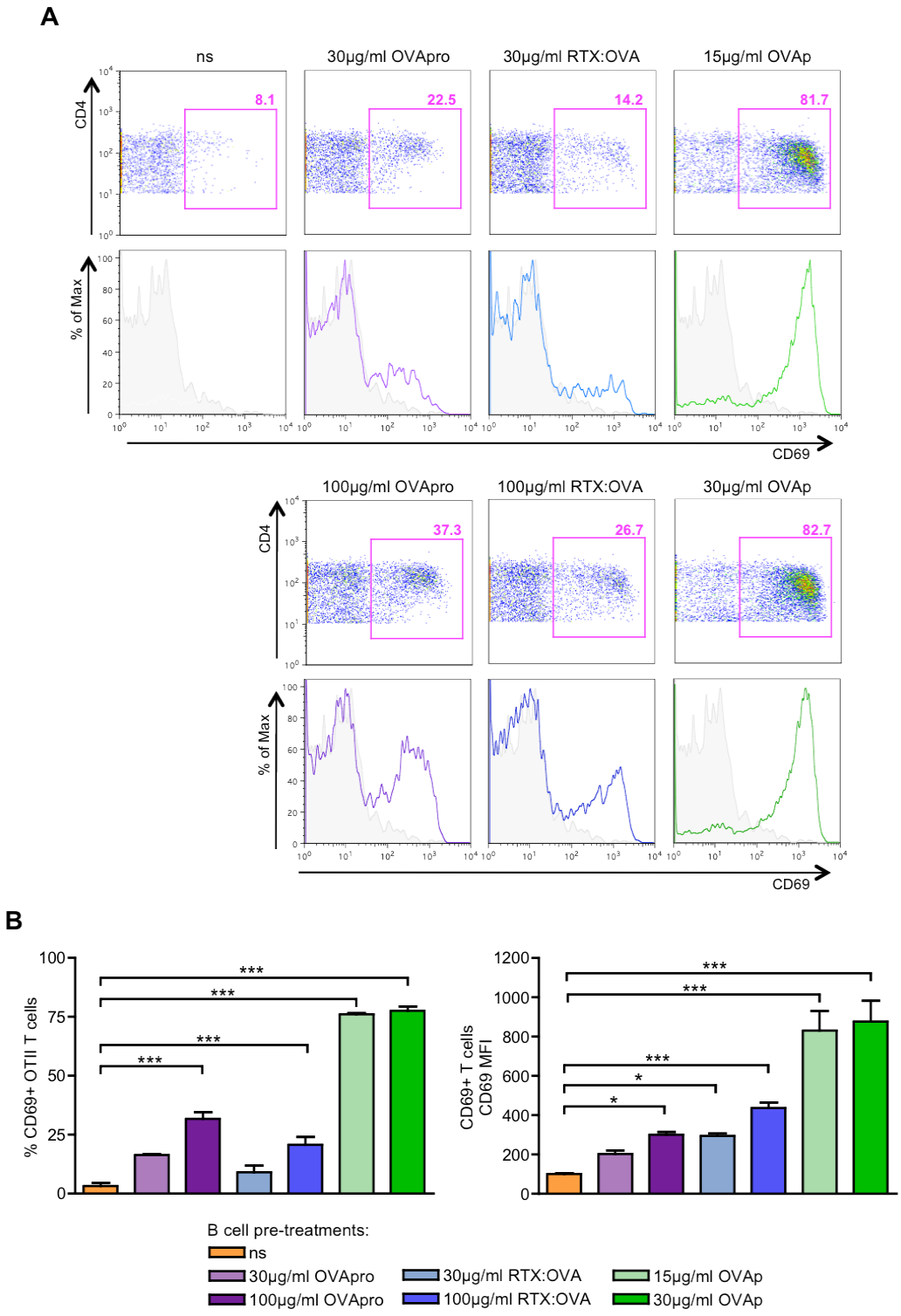

Figure 5.4 Activation of OTII T cells after secondary presentation of differing concentrations of RTX:OVA by BMDM

OTII T cells were co-cultured overnight with BMDM, which had been incubated with viable B cells pre-treated with different concentrations of a Rituximab-OVA peptide conjugate (RTX:OVA), or controls. Cells were then stained for flow cytometry, and analyzed using a FACSCalibur, with CD69 expression used as a marker of T cell activation. (**A**) Representative FACS plots (CD4 vs. CD69) and histograms (% of Max vs. CD69) showing OTII T cell activation after co-culture with BMDM previously incubated with pre-treated viable B cells. (**B**) Graphs of pooled data showing the percentage of $CD69^+$ T cells after co-culture, and the MFI of CD69 on $CD69^+$ T cells. (n=1, 3 replicates) Statistics used: One-way ANOVA performed on each compete data set (% and MFI), followed by Bonferroni's post test, with * = $p<0.05$, and *** = $p<0.001$.

seen in the FACS histograms for both of these conditions (Figure 5.4a). A lesser dose of 15μg/ml OVAp pre-treatment was also included in the study. Even with this reduced concentration of OVAp used for B cell pre-treatment, activation of OTII T cell was seen, with 82.3±0.6% expressing CD69 and an MFI of 831±98.

These data show that OVA-specific T cells can be activated by addition of a RTX:OVA conjugate into this *in vitro* assay system, indicating that successful presentation of OVA derived from the RTX:OVA conjugate by BMDM is occurring. Interestingly, in this system OVA-specific T cells can also be activated by pre-treatment of the hCD20tg B cells with OVAp or OVApro, indicating that this polyclonal B cell population must be taking up OVA in sufficient amounts for subsequent secondary presentation by BMDM to occur.

5.2.3 Comparison of activation of OVA-specific T cells after secondary presentation of RTX:OVA by B cells or BMDM

To investigate whether the activation of OVA-specific T cells by RTX:OVA in this assay system was due to successful secondary antigen presentation by BMDM, or was actually due to the direct presentation of antigen by any residual pre-treated B cells still present in the system, additional B cells only controls were added. For this revised assay, non-irradiated primary hCD20tg B cells were pre-treated overnight with: RTX:OVA at either 30μg/ml or 100μg/ml; OVApro at either 30μg/ml or 100μg/ml; OVAp at either 15μg/ml or 30μg/ml; or left un-treated. These B cells were then either incubated with BMDM for 3h, or incubated alone. As before, all conditions were washed, and the remaining BMDM co-cultured overnight with OVA-specific OTII T cells. CD69 up-regulation by the T cells was used as a measure of T cell activation as assessed by flow cytometry, with T cell proliferative responses and cytokine production also quantified.

In the cell samples tested, lymphocytes were gated on using FSC and SSC, and within this population the T cells were defined as $CD3^+CD4^+$ cells. The expression of CD69 on this cell population was then investigated (Figure 5.5). In the conditions that did not have BMDM added, no activation of T cells was detected by flow cytometry in any pre-treatment group compared to the un-treated B cell group (B(nt)) (Figure 5.6a and c). In the T cell co-cultures with BMDM that had been incubated with pre-treated B cells, significant increases in the levels of $CD69^+$ T cells were observed when B cells were pre-treated with 100μg/ml of the RTX:OVA conjugate (100μg/ml BMDM+B(RTX:OVA) - 44±8.6% $CD69^+$ T cells, MFI: 443±81), when compared to the BMDM+B(nt) group (12.1±6% $CD69^+$ T cells, MFI: 99±4) (Figure 5.6b and c). A significant increase in $CD69^+$ T cells was also seen in both the 30μg/ml and 15μg/ml BMDM+B(OVAp) group (30μg/ml – 74.3±18.8% $CD69^+$ T cells, MFI: 856±362, 15μg/ml - 58.4±32.2% $CD69^+$ T cells, MFI: 781±439). When

comparisons were made between the BMDM+B co-cultures in which significant T cell activation occurred, and the equivalent pre-treatment groups from the B cell only conditions, the proportion of T cells expressing CD69, as well as the levels of CD69 up-regulation, were significantly higher in the BMDM+B co-cultures (Figure 5.6c).

To determine if the up-regulation of CD69 on the OVA-specific T cells was a good reflection of the levels of activation taking place within this population, T cell proliferative responses were investigated. The cytokine IL-2 functions as a T cell growth factor, and is produced in an autocrine manner by T cells on the binding of antigen to the TcR, or by activation with mitogens [278]. IL-2 binding by T cells induces the up-regulation of the IL-2 receptor, resulting in a positive feedback loop stimulating the growth and proliferation of T cells [279,280]. In view of this, IL-2 production by T cells can be used as an indirect measurement T cell proliferation. Cell culture supernatants were collected after either BMDM–T cell co-culture, or B cell-T cell co-culture, and ELISAs used to quantify the levels of IL-2 present. A significant increase in IL-2 concentration was seen in the 100µg/ml BMDM+B(RTX:OVA) T cell co-cultures (42±6pg/ml), compared to the BMDM+B(nt) group (2±1pg/ml) (Figure 5.7a). Significant increases in IL-2 levels were also seen in both the 30µg/ml and 15µg/ml BMDM+B(OVAp) groups, with 374±15pg/ml and 347±3pg/ml of IL-2 detected, respectively. In the B cell-T cell co-cultures, no significant increase in IL-2 was observed in the B(RTX:OVA) conditions compared to the B(nt) co-cultures (2±1pg/ml). A significant increase in IL-2 production was observed in the 100µg/ml B(OVAp) group (111±61pg/ml), however the levels of IL-2 production were notably lower than those detected for the equivalent pre-treatment in which BMDM were present (111±61pg/ml IL-2 vs. 374±15pg/ml IL-2).

T cell proliferative responses were also measured directly by quantifying the incorporation of radioactive tritiated-thymidine (^{3}H-thymidine) into newly synthesized cells over a set time-period. In the BMDM+B conditions, significantly more proliferation was seen in T cells that had been co-cultured with BMDM incubated with B cells pre-treated with 100µg/ml RTX:OVA (7948±4558 CPM), compared to those from the BMDM+B(nt) group (221±208 CPM) (Figure 5.7b). In the direct B cell-T cell co-cultures, significant proliferation was seen only in T cells from the 30µg/ml B(OVAp) group (1289±565 CPM) compared to the T cells co-cultured with B cells that had received no pre-treatment (36±24 CPM). Although T cell proliferation did occur in co-cultures not containing BMDM, the maximal response seen in the direct B cell co-cultures was far less than that observed in the BMDM containing co-cultures (30µg/ml B(OVAp): 1289±565 CPM; vs. 100µg/ml BMDM+B(RTX:OVA): 7948±4558 CPM), indicating a lower level of T cell activation in these conditions.

In an attempt to characterize the specific T cell response resulting from secondary antigen presentation in this assay, the levels of IFNγ, IL-10 and IL-17A in the cell culture supernatants were investigated. Naïve $CD4^+$ T cells can differentiate into several distinct effector cell subsets, and these subsets can be distinguished based on their pattern of cytokine expression. IFNγ was used as a marker of Th1 cells [281], IL-10 as a marker of iTregs [35], and IL-17 for Th17 [34,272]. No significant increases in either IFNγ or IL-10 production were seen in any BMDM-T cell co-culture condition (Figure 5.8a and b). The data indicates increased IFNγ levels in the 100µg/ml BMDM+B(RTX:OVA) group (293±22pg/ml), however this was not significant when compared to the BMDM+B(nt) co-culture (185±32pg/ml). No IFNγ or IL-10 was detectable in any of the direct B cell-T cell co-cultures, regardless of the B cell pre-treatment (data not shown). A significant increase in the level of IL-17A was seen on co-culture of the OVA-specific T cells with 100µg/ml BMDM+B(RTX:OVA) compared to the BMDM+B(nt) group, with 55±7pg/ml IL-17A vs. 28±9pg/ml IL-17A (Figure 5.8c). No change in IL-17A levels were detected in any of the B cell-T cell co-cultures, with baseline levels similar to those detected in the BMDM-T cell co-cultures (B(nt): 30±10pg/ml IL-17A; BMDM+B(nt): 28±9pg/ml IL-17A).

With the experimental protocol used, BMDM are able to successfully present antigens to T cells that they themselves have not directly taken up. BMDM presented OVA, derived from a B cell ingested RTX:OVA conjugate, to OVA-specific T cells resulting in the activation of these cells as evidenced by their up-regulation of CD69, increased production of IL-2, and enhanced cellular proliferation. BMDM were also able to present immunogenic OVA epitopes to T cells, with these epitopes derived from OVApro taken up by B cells that were subsequently engulfed by BMDM. This presentation resulted in the activation of these OVA-specific T cells as evidence by their up-regulation of CD69, however, no change in the levels of IL-2 or cellular proliferation were detected.

5.3 Discussion

- An *in vitro* assay was developed in order to investigate whether self-antigen taken up by autoreactive B cells could be presented by other APCs after phagocytosis of the B cells.
- We found that successful secondary presentation of antigen by BMDM was possible.
- These findings are a first step toward understanding this type of antigen presentation and demonstrate that this is an interesting line of investigation to pursue, with further work allowing us to answer the question of whether tolerance or activation would result from such antigen presentation *in vivo*.

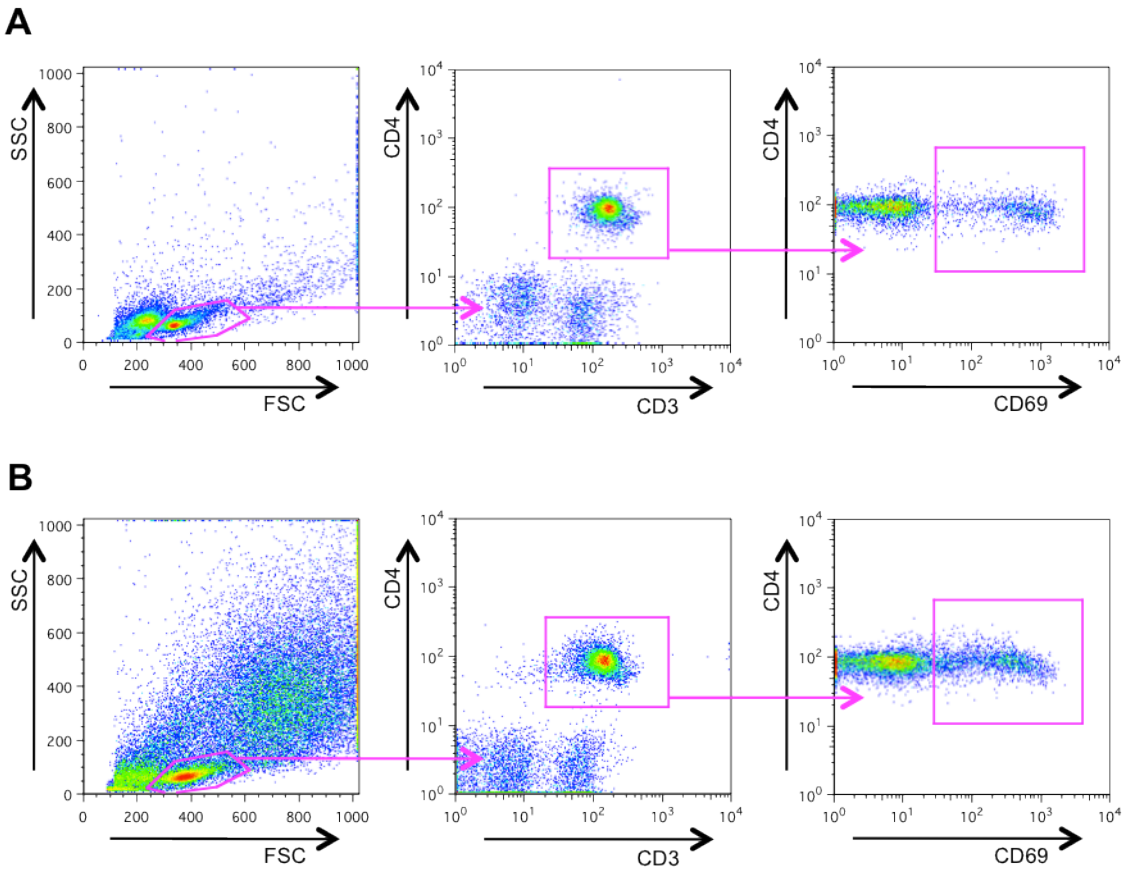

Figure 5.5 Gating strategy for analysis of CD69 up-regulation on OTII T cells
Primary T cells were isolated from OTII mice, co-cultured overnight with B cells or BMDM pre-incubated with B cells, and their surface expression of CD69 analysed via flow cytometry. (**A**) Representative dot plots demonstrating the gating strategy used to define total T cells and $CD69^+$ T cells in T cell-B cell co-cultures. First panel: SSC vs. FSC. Second panel: CD4 vs. CD3. Third panel: CD4 vs. CD69. (**B**) Representative dot plats demonstrating the gating strategy used to define total T cells and $CD69^+$ T cells in T cell-BMDM co-cultures. First panel: SSC vs. FSC. Second panel: CD4 vs. CD3. Third panel: CD4 vs. CD69.

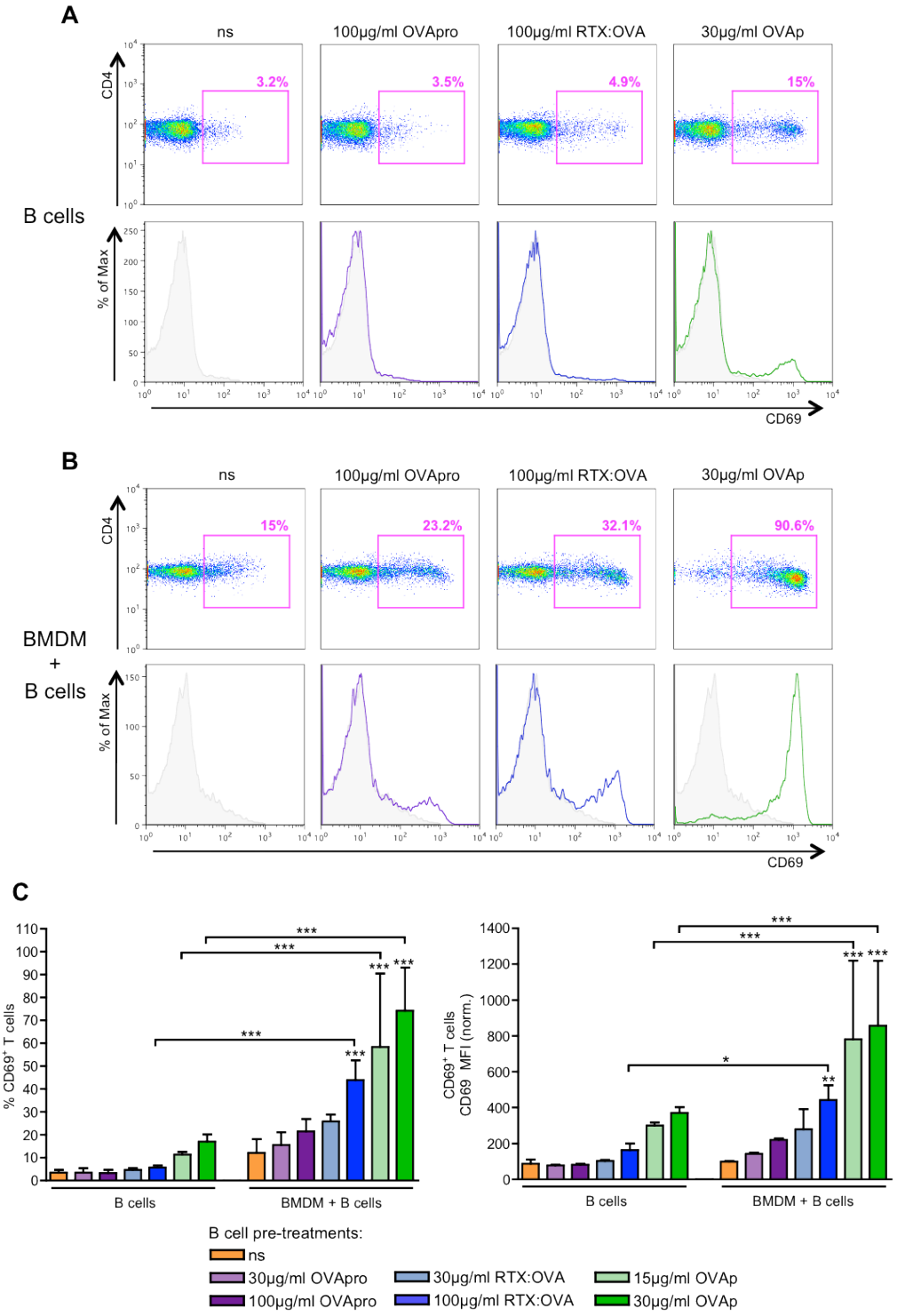

Figure 5.6 Comparison of activation of OVA-specific T cells after direct presentation of RTX:OVA by B cells, or secondary presentation by BMDM

Primary OTII T cells were co-cultured overnight with pre-treated B cells, or BMDM incubated with pre-treated B cells. Cells were then stained for flow cytometry, and analyzed using a FACSCalibur, with CD69 expression used as a marker of T cell activation. (**A**) Representative FACS plots (CD4 vs. CD69) and histograms (% of Max vs. CD69) showing levels of OTII T cell activation after co-culture with pre-treated B cells. (**B**) Representative FACS plots (CD4 vs. CD69) and histograms (% of Max vs. CD69) showing levels of OTII T cell activation after co-culture with BMDM incubated with pre-treated B cells. (**C**) Graphs of pooled data showing the percentage of $CD69^+$ T cells after co-culture, and the MFI of CD69 on $CD69^+$ T cells. (n=2, from 2 independent experiments) Statistics used: One-way ANOVA performed on each complete data set (% and MFI), followed by Bonferroni's post test, with * = $p<0.05$, and *** = $p<0.001$.

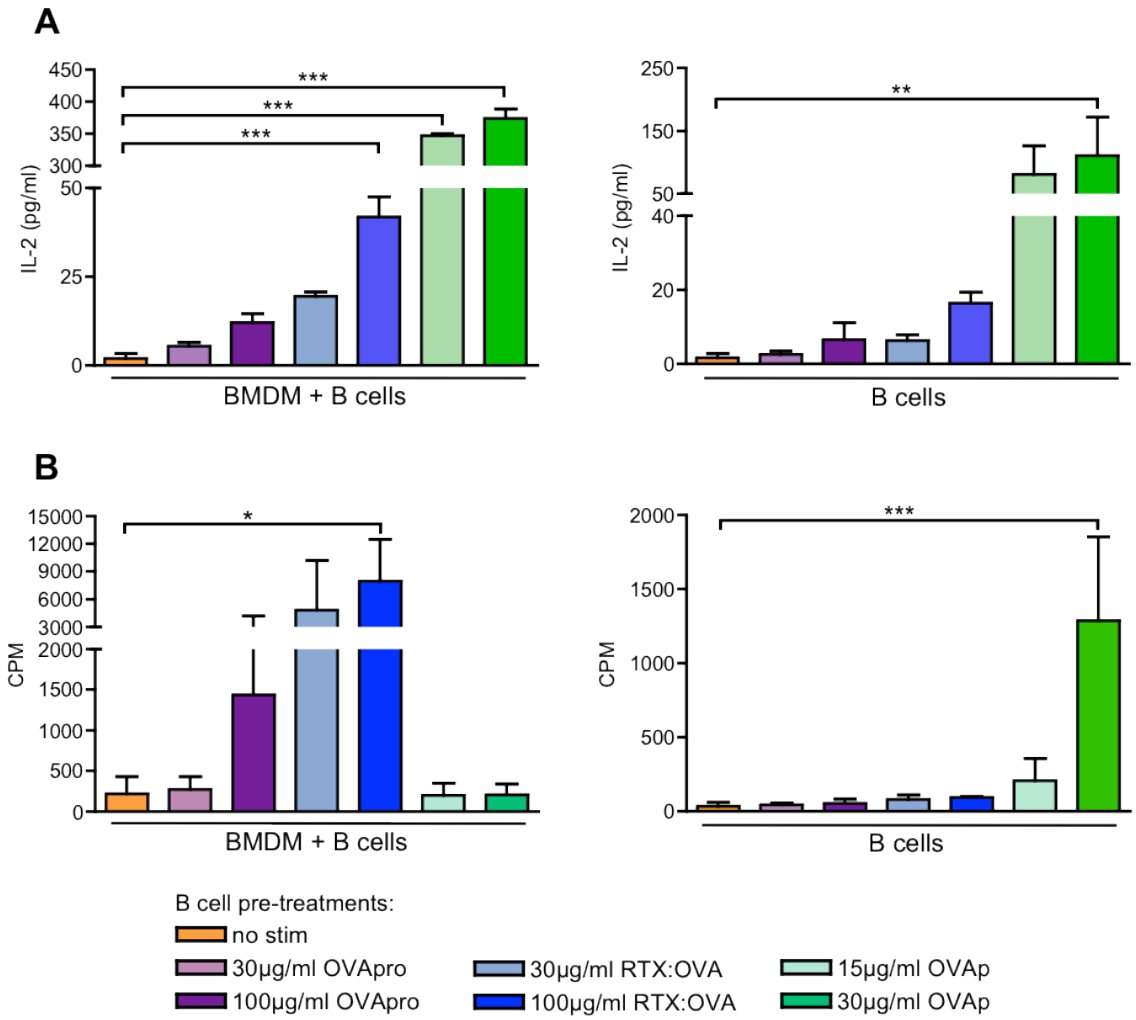

Figure 5.7 Proliferative responses of OTII T cells after direct presentation of RTX:OVA by B cells, or secondary presentation by BMDM

OTII T cells were co-cultured with pre-treated B cells, or BMDM incubated with pre-treated B cells for 72hr. (**A**) Graphs showing IL-2 production (pg/ml) after co-culture, as determined by ELISA. (**B**) Graphs showing cellular proliferation, as quantified by the incorporation of ^{3}H-thymidine into newly synthesized cells after co-culture. CPM = counts per minute. (IL-2 ELISA n=1, proliferation assay n=2 with data from 2 independent experiments) Statistics used: One-way ANOVA performed on each complete data set (BMDM+B cells IL-2 production, B cells IL-2 production, BMDM+B cells proliferation, B cell proliferation) followed by Bonferroni's post test, with * = $p<0.05$, ** = $p<0.01$, and *** = $p<0.001$.

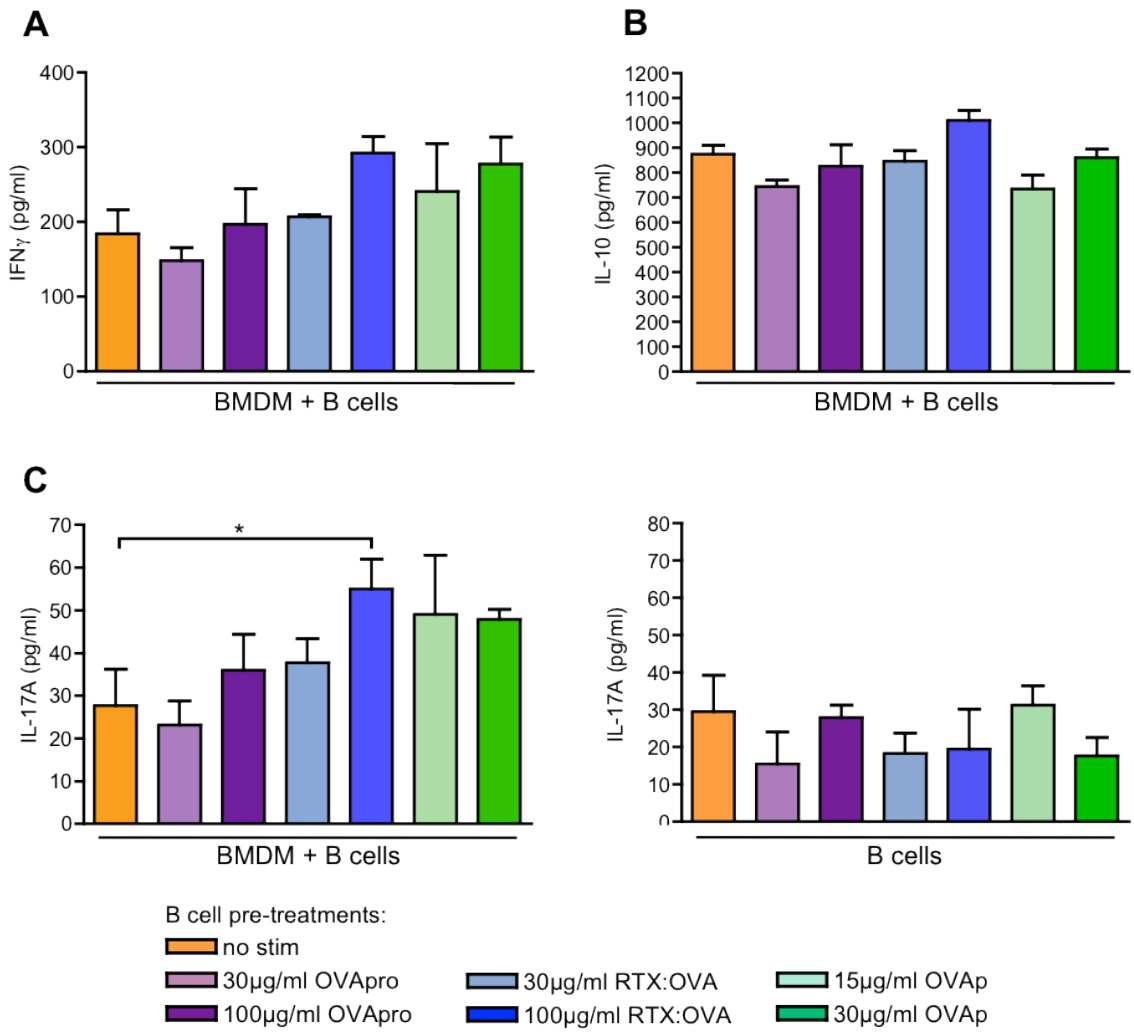

Figure 5.8 T cell responses to secondary presentation of RTX:OVA by BMDM
OTII T cells were co-cultured directly with pre-treated B cells, or BMDM incubated with pre-treated B cells for 72hr. Cell culture supernatants were then collected and cytokine production investigated by ELISA. (**A**) Graph showing the levels of IFNγ production (pg/ml) after co-culture with BMDM incubated with pre-treated B cells. (**B**) Graph showing the levels of IL-10 production (pg/ml) after co-culture with BMDM incubated with pre-treated B cells. (**C**) Graph showing the levels of IL-17A production (pg/ml) after co-culture with BMDM incubated with pre-treated B cells (left panel) or after direct co-culture with pre-treated B cells (right panel). (n=1) Statistics used: One-way ANOVA performed on each complete data set (BMDM+B cells IFNγ production, BMDM+B cells IL-10 production, BMDM+B cells IL-17A production, B cells IL-17A production), followed by Bonferroni's post test, with * = $p<0.05$, and ** = $p<0.01$.

Many hypotheses have been put forward to explain how RTX treatment exerts its beneficial effects in RA, however a definitive answer has yet to be reached, and it is probable that there will not be one mechanism alone. We hypothesize that one of the potential mechanisms of action is that RTX re-introduces temporary tolerance to the immune system. If APCs are able to present antigen that they themselves have not directly taken up, this could lead the presentation of self-antigen endocytosed by auto-reactive B cells, prior to RTX-mediated depletion, by APCs in an anti-inflammatory setting after ingestion of antigen-containing auto-reactive B cells undergoing apoptosis as a result of RTX treatment.

In our assay, hCD20tg B cells were pre-treated with a RTX:OVA conjugate as way to ensure the internalization of OVA by a large proportion of the polyclonal B cell population. These cells were then incubated with BMDM, which were subsequently co-cultured with OVA-specific T cells, with the activation and proliferation of the transgenic T cells used as a read out of successful antigen presentation.

OVA peptide (OVAp) was used as a control throughout the secondary presentation assays, with OVA protein (OVApro) also used in the majority of assays. hCD20tg B cells are polyclonal, and therefore only a fraction of the cells isolated from a naïve hCD20tg mouse will be specific for OVA. As such, it was expected that sufficient amounts of either OVAp or OVApro would not be taken up by the B cells to allow substantial secondary presentation by BMDM, and therefore these conditions were intended as negative controls. When OVAp was used as the B cell pre-treatment, extremely high levels of OVA-specific T cell activation after BMDM-T cell co-culture were consistently observed for both concentrations of peptide tested. These results could not be attributed to an unusually high proportion of OVA-specific B cells within the B cell populations used, as the same B cell preparations were utilized for all conditions within an experiment. Therefore, if a particularly high percentage of OVA-specific B cells were present, this would be reflected in the activation rates seen with OVA protein pre-treatment, and this was not the case. A possible explanation for the increase of T cell activation in response to B cell pre-treatment with OVAp is that empty MHC molecules expressed on the surface of the B cells directly bound the immunogenic OVA peptide present in the culture media. Each MHC molecule has the ability to bind to multiple different peptides containing the correct anchor residues [282] and as such, the OVAp could be bound by a much higher proportion of B cells, including non-OVA-specific B cells within the population. It has previously been shown that empty MHC I [283] and MHC II [284] molecules are able to directly bind extracellular peptides, with work by Santambrogio et al demonstrating that immature DCs express numerous empty MHC class II molecules on their surface, and that these are capable of loading antigen

directly from the extracellular medium and presenting it to T cells *in vitro* [285]. It is thought that this mechanism of antigen binding by APCs may allow a more diverse range of peptides to be presented to T cells, without the need for intracellular antigen processing. Although direct peptide binding by MHC has been demonstrated *in vitro*, it is not thought to readily occur in B cells under physiological conditions, with MHC II molecules that are not antigen loaded in the endosomal compartment retained within the cell, and subsequently degraded [286]. It would also not be expected that B cells would express substantial numbers of empty class I molecules, as it has been shown that although empty MHC I molecules expressed on the cell surface are able to directly bind peptide *in vitro*, these empty molecules are unstable, with a very short half life at physiological temperatures [287]. Antigen binding induces a conformational change stabilizing the molecule, resulting in prolonged expression of the MHC:peptide complex on the cell surface [287]. Although this is the case under physiological conditions, work by Hidde Ploegh's group has revealed that at a range of reduced, non-physiological temperatures there is an increase in the levels of empty MHC I molecules expressed by cells [288,289]. In these studies, using the murine lymphoma cell lines RMA and RMA-S, it was found that culturing both cell lines at temperatures ranging from 19-33^{o}C resulted in a marked increase in the expression of correctly folded class I molecules, and that on addition of exogenous influenza-derived peptide to the cultures the cells could be sensitized to antigen-specific cytotoxic T cell-mediated killing [289]. At reduced temperatures these empty class I molecules were stably expressed, however, if the cells were subsequently incubated at 37^{o}C the expressed empty class I molecules rapidly lost their peptide binding capacity and disappeared from the cell surface, with only those molecules that had formed MHC:peptide complexes remaining [288]. These findings could explain the ability of the hCD20tg B cells to directly bind OVAp, as prior to their incubation with antigen the B cells are kept at room temperature during certain initial stages of the assay. As room temperature in a lab is generally regulated to be ~20-25^{o}C, this would fall well within the temperature range shown to induce expression of empty class I molecules on the surface of cells, and therefore could result in MHC I up-regulation on the surface of the B cells. Although the cultures were promptly transferred to 37^{o}C for overnight incubation after addition of antigen, direct binding of peptide by empty MHC I in lower temperature cultures has been shown to be a rapid process, with addition of peptide to RMA-S cells immediately before transfer to 37^{o}C sufficient to rescue surface MHC molecules from destruction [288]. Therefore, the overnight incubation of B cells at 37^{o}C would not interfere with the direct binding of OVAp by expressed empty MHC, resulting in the presence of sufficient peptide during the B cell-BMDM co-cultures to allow subsequent secondary presentation to OVA-specific T cells.

Another possible explanation for the interaction of the polyclonal B cells with OVAp is its uptake by macropinocytosis. Unlike other APCs, which take up antigens non-specifically from their surrounding environment, B cells take up antigen for presentation via antigen-specific B cell receptor (BcR) mediated endocytosis [290], enabling them to focus the immune response to specific targets. Although this method of antigen uptake seems to be the most relevant in a physiological setting, it has been shown that B cells are also able to ingest antigen non-specifically, via macropinocytosis [290]. In the present culture system, the uptake of OVAp by polyclonal hCD20tg B cells could be due to a non-specific, fluid-phase uptake process, such as macropinocytosis. When pre-treated with high enough concentrations of OVAp, these B cells are able to undergo sufficient levels of this non-specific antigen uptake to allow subsequent secondary presentation by BMDM.

When 30µg/ml OVApro was used as the B cell pre-treatment, no activation of OVA-specific T cells was seen above background levels, as detected by flow cytometry, IL-2 ELISA and proliferation assay. On 100µg/ml OVApro B cell pre-treatment, fairly consistent levels of moderate T cell activation were seen after BMDM-T cell co-culture. In the present culture system, it is proposed that the uptake of OVApro by polyclonal hCD20tg B cells is due macropinocytosis, as discussed in regard to OVAp uptake.

Presentation of OVA peptide derived from the RTX:OVA conjugate was observed in this assay system when B cells were pre-treated with 100µg/ml RTX:OVA prior to incubation with BMDM, with this successful presentation demonstrated by the up-regulation of the early activation marker CD69 [291] on OVA-specific T cells after BMDM-T cell co-culture. The levels of T cell activation detected in the RTX:OVA conditions were expected to be substantially greater than those observed in the OVApro conditions, however this was not the case, and comparable CD69 up-regulation by T cells was detected. The RTX:OVA conjugate was developed as a delivery mechanism to target OVA into the hCD20tg B cells, allowing the use of this population of polyclonal B cells in the system. However, after undertaking the assay it was clear that secondary presentation of OVA resulted when B cells were pre-treated with either RTX:OVA or OVApro, raising the question of whether this delivery mechanism was indeed necessary. In the BMDM+B conditions, increases in CD69 expression by OVA-specific T cells resulted from B cell pre-treatment with either RTX:OVA or OVApro, however out of the two conditions, only with the use of RTX:OVA was significant T cell proliferation, IL-2 production or IL-17A production detected. These differences indicate that the presentation of OVA derived from RTX:OVA or OVApro resulted in different responses by the OVA-specific T cell population. This difference may have been due to the relative amounts of OVA presentation in these conditions. Processing of both RTX:OVA and OVApro would need to

occur before presentation of the immunogenic OVA peptide could take place. If the RTX:OVA conjugate is easier to process than the complete OVA protein, this could result in an increase in the amount of processed OVA peptide present in the BMDM. With more processed peptide available for presentation, enhanced expression of MHC:OVAp complexes on the BMDM surface and a subsequent increase in OVA-specific T cell activation may result. If this is indeed the case, then increasing the concentration of OVApro used in the B cell pre-treatment would result in comparable levels of T cell activation and cytokine production, compared to those from the RTX:OVA conditions, negating the need for the conjugate protein delivery mechanism. However, the differences observed between these conditions may be due to the different processing and presentation of these antigens by the BMDM, although without further investigation this cannot be known. It is also unclear at this stage whether a potential difference in the processing/presentation of OVAp derived from these two sources would have any relevance to the process currently under investigation, and therefore even if inherent differences did exist, the use of the RTX:OVA conjugate may still be unnecessary in this particular setting.

After the initial secondary presentation assays were undertaken, the question was raised as to whether the T cell activation observed after BMDM-T cell co-culture was due to secondary presentation of antigen by the BMDM, or whether residual B cells remained in the culture system at the time of co-culture, and the activation seen was a result of direct presentation by these contaminating B cells. In an attempt to clarify the route of presentation taking place, B cell only controls were set up. BMDM were not added to these conditions, but in all other respects they were treated in the exact same way as the counterpart BMDM+B conditions, with the resultant T cell activation quantified after T cell co-culture, as before. No significant T cell activation detected in any of the B cell only controls, regardless of the pre-treatment used, indicating that the activation seen in the BMDM+B conditions is indeed due to secondary antigen presentation by the BMDM, rather then direct B cell presentation. Although this control does not conclusively rule out direct presentation by B cells, as non-internalized B cells bound to the surface of adherent BMDM in the BMDM+B conditions may be responsible for some of the activation seen in these cultures via direct antigen presentation, it does strongly indicate this is the case.

Several reasons for the lack of direct presentation seen in the B cell only conditions can be suggested, depending on the B cell pre-treatment in question. If working under the assumption that OVAp interacts with the polyclonal B cell population by being directly bound by empty MHC molecules expressed on the surface of the B cells, minimal direct presentation by B cells may seem to conflict with this idea. However, the apparent lack

of T cell activation in these conditions could be explained within the context of this theory. Some level of T cell activation is seen in the OVAp pre-treated B cell-T cell cultures, with an increase in CD69 expression, IL-2 production and T cell proliferation observed, it is just in comparison to the BMDM co-cultures that this level of activation appears minimal. Resting B cells are known to be poor antigen presenting cells [292], and although the direct binding of antigen to B cell MHC was not investigated in these studies, the disparity in T cell activation levels in the secondary presentation assay may purely reflect the intrinsic antigen presenting capacity of B cells versus macrophages. Another potential cause of this reduced level of direct presentation of OVAp may be to do with the MHC restriction of the OVA-specific T cells used in the assay. If on culture in reduced temperatures, the B cells up-regulate MHC I molecules rather than MHC II molecules, and these class I proteins directly bind OVAp present in the media, the resultant MHC:peptide complex will only be detectable by MHC I-restricted $CD8^+$ T cells [30,31]. As the OVA-specific T cells used for the secondary presentation assays were isolated using a $CD4^+$ T cell isolation kit, there will be no $CD8^+$ T cells in the assay to detect this antigen presentation, and therefore even if OVAp-expressing B cells were present in this condition, $CD4^+$ T cell activation would not occur. In contrast, in the BMDM conditions the uptake of B cells and any bound OVAp would result in their targeting to the exogenous antigen processing pathway, leading to the presentation of OVAp on MHC II molecules, and allowing its recognition by $CD4^+$ OVA-specific T cells.

In the context of either OVAp or OVApro uptake by macropinocytosis, the reduced direct presentation observed may be due to the route of peptide uptake. Antigen that has been taken up by B cells via macropinocytosis rather than BcR-mediated endocytosis may not enter the antigen processing pathway, therefore inhibiting subsequent peptide presentation by the B cells. This does not seem to be the case however, with work by Chesnut et al demonstrating that uptake of the KLH antigen by polyclonal B cells can result in the activation of KLH-specific T hybridoma cells, as demonstrated by increase T cell production of IL-2 [293]. Although demonstrating that successful peptide presentation by B cells is possible after macropinocytosis of antigen, this study highlights the reduced capacity of B cells to induce T cell activation after this form of antigen uptake, compared to other populations of APCs. In the secondary presentation assays utilized in this chapter, all cells were cultured at a 1:1 ratio, and this low number of B cells:T cells in the direct co-culture conditions may explain the lack of T cell activation. Potentially, if the number of OVAp or OVApro pre-treated B cells included in the co-cultures were increased, higher levels of T cells activation would be detected. Another possible explanation focuses on the viability of the B cells. In the initial secondary presentation assays undertaken, conditions containing both non-irradiated and irradiated B cells were included. On examination of the results it was

seen that similar levels of T cell activation were seen in the corresponding pre-treatments regardless of which B cell group was included in the assay, and so it was decided that only non-irradiated B cells would be used in future. Although the B cells used for the remainder of the assays had not undergone irradiation, B cells do not survive well in culture without the addition of specific survival factors. After overnight antigen pre-treatment in the absence of survival factors, the majority of B cells would be either apoptotic or dead in both the irradiated and non-irradiated conditions, with only a small percentage of viable cells present, as demonstrated in Chapter 3, Figure 3.1. As such, even if the numbers of OVAp or OVApro pre-treated B cells included in the B cell-T cell co-cultures was sufficient to theoretically result in T cell activation, the B cells may not have been healthy enough to successfully present antigen.

In order to fully dissect the contribution of direct antigen presentation by B cells in this assay system, further studies would need to be undertaken. The addition of a B cell marker into the FACS panel used to gauge T cell activation would enable the detection of contaminating B cells remaining in the BMDM+B conditions. Internalized B cells would not be accessible to antibody without prior cell permeabilization, and therefore any B cell staining seen could be attributed to un-ingested, surface bound B cells with the potential to directly present antigen. Microscopy could also be used to visualize the specific cell-cell interactions going on, either by labelling each cell population with a different stain, such as CFSE, prior to their use in the assay, or by utilizing antibodies specific for distinct cell surface markers before visualization. These approaches would both help to characterize the cell populations present in the final co-culture stages of the assay, and their involvement in the interactions taking place. Use of a fluorescently labelled antigen, coupled with visualization of cells via microscopy, could be used to directly trace the route of antigen presentation, and conclusively define the contributions of direct vs. secondary presentation on the activation of OVA-specific T cells.

Although it cannot be conclusively stated that secondary antigen presentation is fully responsible for all the T cells activation seen in the BMDM+B conditions, it is reasonable to conclude that this presentation mechanism is involved in this system when B cells are pre-treated with the RTX:OVA conjugate. On binding of the RTX to hCD20 expressed on the B cell, the conjugate will be taken up via the CD20 internalization pathway, rather than by BcR-mediated internalization, the usual route for antigen-specific endocytosis by B cells [294]. It has been shown in a variety of B cell lines that internalization of CD20:RTX complexes results in their trafficking to early endosomes and subsequently lysosomes, as visualised by confocal microscopy [100]. The fusion of acidified endosomes with lysosomes is a key step in the processing pathway of exogenous

antigens, exposing them to lysosomal proteases and resulting in the generation of peptides [295], which can then to be loaded onto newly synthesized MHC II molecules. Theoretically, once located in B cells lysosomes, the RTX:OVA conjugate could be broken down into its constituent peptides, where it may encounter and be loaded onto empty class II molecules to be presented on the cell surface. However, there is no direct evidence that the RTX internalization pathway intersects the exogenous antigen-processing pathway at any stage. The movement and fusion of endosomes and lysosomes within the cell is highly regulated, and is dependent on the expression of specific Rab and SNARE (soluble NSF attachment protein receptor) proteins on the surface of the endosome [reviewed in [296]. Endosomes express different members of the Rab and SNARE families of proteins dependant on their role within the cell, and their final target destination [reviewed in [297]. It is thought that peptide loading onto class II molecules occurs in the MIIC compartment, a particular type of MHC II containing lysosome, however this has not yet been clearly defined [reviewed in [298]. Thus, although it is known that CD20:RTX complexes traffic into lysosomes where they are degraded and MHC II molecules reside in lysosomes prior to antigen loading, until the specific lysosomes involved are defined, or the potential intersection of these pathways is directly studied, it cannot be said whether empty MHC II molecules would encounter the internalized RTX:OVA conjugate. Although direct presentation of the constituent OVA peptide by the B cell after this form of internalization is theoretically possible, it seems unlikely to have occurred. In the B cell only conditions pre-treated with RTX:OVA no indication of any T cell activation was observed at either concentration investigated. In the BMDM+B conditions, any RTX:OVA contained within the B cell or bound to its surface will be digested by the phagocyte in the same manner as all other exogenous antigens on phagocytosis of the B cell, and therefore will be easily accessible for loading on to MHC II molecules and subsequent presentation. Because of this, it seems reasonable to conclude that successful secondary presentation by BMDM has occurred in this assay system, and that the T cell activation seen could not be solely attributed to direct antigen presentation by possible contaminating B cells.

Although the concept of secondary antigen presentation has not previously been investigated in its own right, published work looking into varying aspects of the immune response touches on this presentation pathway, providing further evidence that this may be a naturally occurring mechanism of antigen presentation. In a study looking into cross-presentation of exogenous antigens to $CD8^+$ T cells by dendritic cells (DC), Alfaro et al demonstrate that DC can successfully present OVA protein contained within neutrophils, to both $CD4^+$ and $CD8^+$ OVA-specific T cells [299]. In this study murine neutrophils were cultured *in vitro* with OVA protein, followed by co-culture with murine DCs. The DCs were then exposed to OVA-specific OTI ($CD8^+$) and OTII ($CD4^+$) T cells.

T cell proliferation, as measured by CFSE dilution 72hr later, was used as a marker of successful OVA presentation, with cell division observed in both the $CD4^+$ and $CD8^+$ T cells co-cultured with DC that had been incubated with neutrophils preloaded with OVA, indicating secondary presentation had occurred in this system. The authors also go on to examine whether this type of secondary presentation can result in successful T cell activation in an *in vivo* setting. To do this, C57BL/6 mice were injected with CFSE stained OTI T cells, and the following day injected in the footpad with H-2^d neutrophils either preloaded with OVA or untreated, and H-2^b DCs. As OTI T cells can only see OVA peptide in the context of H-2^b, the use of neutrophils from a H-2^d background removed the possibility of direct presentation of OVA to the transgenic T cells by the preloaded neutrophils. Draining lymph nodes and spleens were harvested 72 hours later, and T cell proliferation was measured by CFSE dilution as detected by flow cytometry. Only OTI T cells isolated from mice that had been injected with DC and neutrophils that had phagocytosed OVA showed signs of proliferation above background levels, demonstrating that secondary presentation can also occur in a more physiologically relevant setting.

Work by Kambayashi et al looking in to the involvement of mast cells in antigen-specific T cell responses has shown that antigen taken up via Fc receptor-mediated endocytosis can also undergo secondary presentation by APC [300]. Murine mast cells were incubated first with anti OVA-IgE to allow binding of the IgE by surface Fcε receptors expressed by the mast cells, followed by incubation with OVA protein. This resulted in opsonisation of the OVA protein by the Fcε receptor-bound anti OVA-IgE, leading to intracellular uptake of the antigen. These preloaded mast cells were then co-cultured with unsorted splenocytes from OTII mice, and the activation of OTII OVA-specific T cells assessed by flow cytometry. Activation was determined by CD69 up-regulation on the OTII T cells, with increased expression observed on T cells originating from the co-cultures involving OVA preloaded mast cells, but not from co-cultures involving untreated mast cells. When OVA preloaded mast cells were cultured with purified OTII T cell populations, minimal levels of T cell activation were seen, demonstrating that the T cell CD69 up-regulation observed in the mast cell-splenocyte co-cultures did not result from direct antigen presentation by the mast cells, but was the result of presentation by APCs within the splenocyte population. This was confirmed by addition of DCs to preloaded mast cell-OTII T cell co-cultures, resulting in enhanced CD69 expression by the T cells. This secondary presentation model was then further tested in an *in vivo* setting. This was done by the injection of CFSE labelled OTII T cells and OVA preloaded mast cells into C57BL/6 mice. The spleens and draining lymph nodes were harvested from the mice 5 days later, and analysed via flow cytometry for proliferation of the CFSE stained T cells as measured by CFSE dilution. Proliferation of the OTII T cells was

observed in mice injected with OVA preloaded mast cells, but was not in mice injected with untreated mast cells. This finding demonstrates that mast cells that have previously taken up antigen by receptor-mediated endocytosis can serve as a source of antigen for presentation to T cells *in vivo*.

These studies, along with the work presented in this chapter, serve to illustrate that successful secondary presentation of antigen is indeed possible in a variety of settings. The up-regulation of CD69 by OVA-specific T cells, along with the cellular proliferation and IL-2 production observed, demonstrate that successful antigen presentation has occurred. However, these results do not indicate the nature of the T cell response in this setting. Although CD69 is generally considered an early activation marker, work by Sancho et al. in CD69-deficient mice has highlighted a potential role for this molecule as a negative regulator of immune responses [301,302]. In addition, T cell proliferation does not necessarily imply the generation of effector cell populations. Activation-induced cell death is a process in which activation through the T cell receptor results in a period of cell proliferation followed by apoptosis of the T cell [303], with exposure of T cells to IL-2 shown to be critical to this form of induced cells death [304]. Due to this, it cannot be conclusively stated that the T cell activation seen in this assay will result in the generation of effector populations.

To start to dissect the impact of secondary OVA presentation in this assay, the generation of specific T cell subsets in response to this secondary presentation was investigated. Cytokine ELISAs were undertaken, with the levels of IFNγ, IL-17A and IL-10 investigated, as $CD4^+$ T cell subsets can be identified by their production of signature cytokines [reviewed in [305]. IFNγ production is indicative of the presence of pro-inflammatory Th1 cells [281], and in the BMDM+B conditions no significant change in the levels of IFNγ were seen compared to the un-treated BMDM+B controls, for any of the B cell pre-treatments used. These results indicate that antigen presentation did not result in the generation of a substantial population of Th1 cells under these conditions. Levels of the anti-inflammatory cytokine, IL-10, also did not change for any of the B cell pre-treatments used compared to the BMDM+B(nt) group. IL-10 can be produced by a variety of immune cells, in the case of T cells it is most commonly associated with the Treg subsets [35], and acts on APCs to suppress their antigen presenting capacity [306] and inhibit the production of pro-inflammatory cytokines [307]. Generation of a population of iTregs could have been a mechanism of tolerance induction, however this lack of a change in IL-10 concentration indicates that secondary presentation in this system did not generate a significant regulatory population. IL-17A, is characteristic of the Th17 cell subset [34,272], and a significant increase in IL-17A production was seen in the

BMDM+B(RTX:OVA) compared to the BMDM+B(nt) group. These data indicate that under the conditions used, the secondary presentation of OVA resulted in expansion of the Th17 cell population, with no corresponding effects in the Th1 cell or iTreg populations.

The generation of an inflammatory Th17 population in response to antigen presentation in this system may not be a result of the method of secondary presentation, but rather a reflection of the broader assay conditions used. Before co-culture with B cells, the BMDM were stimulated overnight with IFNγ and then treated with LPS. This stimulation protocol mimics a pro-inflammatory environment, resulting in a pool of activated macrophages expressing the co-stimulatory molecules required to initiate T cell responses. This *in vitro* treatment could be said to better reflect the inflammatory RA environment, however we hypothesize that on RTX-treatment *in vivo,* APCs will obtain antigen from apoptotic B cells. The immunomodulatory signals from the large number of apoptotic B cells would potentially be able to overcome the inflammatory environment. Although B cells will constitutively undergo apoptosis at low levels within the body, this sudden increase in the number of apoptotic B cells present in the system may be enough to tip the balance toward an anti-inflammatory environment, and combined with the potential increased levels of secondary presentation, could be enough to result in tolerance to the arthritogenic auto-antigen. In this version of the assay, non-irradiated B cells were used, rather than those that had been irradiated to induce apoptosis. As mentioned previously, B cells in culture have a very short life span without the addition of growth factors, and therefore a proportion of the B cells present in culture would be expected to be apoptotic or undergoing apoptosis, however the number of apoptotic cells present in the assay system may not have been enough to override the inflammatory stimulus given to the macrophages, resulting in an active immune response toward OVA. Also, as previously shown in this thesis and by previous studies, the response of macrophages to AC differs depending on the macrophage subset (Chapter 3, sections 3.2.7 - 3.2.9) and the inflammatory milieu present at the time of uptake (Chapter 3, section 3.2.2) [175]. This suggests that different outcomes would result from the inclusion of different macrophage populations, or different activatory stimuli, something that would be interesting to investigate in more detail.

In light of earlier work in this thesis looking into the interaction of AC and BMDM, and the finding that in certain culture conditions viable cells seem to have the same immunomodulatory capacity as AC, it would be interesting to include a group of truly viable B cells into the secondary presentation assay. This is something that could be done by the addition of B cell survival factors, such as IL-4 or a CD40L-CD8α fusion protein [308], into the overnight pre-treatment stage. Another potential alteration to

the assay would be the inclusion of a control conjugate at the B cell pre-treatment stage. If the modified OVA peptide used in the RTX:OVA conjugate was instead conjugated to a RTX isotype, this would control for the uptake mechanism of the OVA in this condition. However, with the questions raised as to whether the RTX:OVA conjugate is needed for this assay to work, or whether the use of OVApro is sufficient, this control may not be of use.

Together these results demonstrate that successful secondary presentation of OVA by BMDM is possible in this assay system, and that with the conditions used this presentation may result in the generation of a Th17 cell population. Although these results cannot definitively state whether tolerance or activation would result from such antigen presentation *in vivo*, they are first step toward understanding this interaction and encourage the pursuit of this line of investigation.

Chapter 6: Human CD20 Transgenic Mice

6.1 Introduction

Transgenic mice are valuable tools for biomedical research, and are extensively used in the study of autoimmune diseases. Human CD20 transgenic (hCD20tg) mice specifically express the human CD20 molecule on the surface of their B cells. The amino acid sequence of CD20 is well conserved between humans and mice [309], however human-specific anti-CD20 antibodies do not detect the mouse homologue. The transgenic expression of hCD20 on the surface of murine B cells enables the study of human-specific anti-CD20 monoclonal antibodies (mAbs), such as RTX, in animal models of disease. Rituximab was originally developed for the treatment of B cell lymphomas [310], but its use in the clinic has now spread to encompass the treatment of autoimmune disorders such as SLE [311], and RA [80], and is being considered for use in Multiple Sclerosis (MS) [312-314]. As use of these biologics increases, and as the search for improved efficacy continues, hCD20tg mice are a vital tool to facilitate the study of the complex interaction between anti-CD20 monoclonal antibodies and B cells, as well as the significant consequences B cell depletion has on the immune system as a whole.

CD20, previously known as the B1 molecule [315], is a transmembrane protein belonging to the MS4A family, sharing structural similarities with the β chain of the Fc receptor FcεRI, found on mast cells [316]. It is a stable B cell-specific marker, with expression lost on terminal differentiation of cells into plasma cells [317]. It is thought that CD20 is involved in B cell proliferation, with binding of CD20 by anti-CD20 antibodies resulting in the inhibition of cell cycle progression following activation [318], and extensive cross-linking of CD20 leading to apoptosis [235]. It has also been suggested that CD20 may have a role in the generation of optimal B cell responses [319]. Several studies have highlighted a role for CD20 in the regulation of the transmembrane movement of calcium in B cells. In the 1993 paper by Bubien et al, it was demonstrated that the binding of CD20 by anti-CD20 antibodies results in enhanced transmembrane calcium conductance [320]. In this same paper, the authors went on to show that transfection of CD20 cDNA into a variety of human and murine cells also results in an increased transmembrane Ca^{2+} conductance [320]. Despite these findings, the endogenous ligand for CD20 is still currently unknown, and B cells in CD20 knockout mice develop and function normally [321].

The hCD20tg colonies maintained at the University of Glasgow were originally established from mice obtained from Dr. Mark Shlomchik (Yale University School of Medicine). The hCD20tg founder lines were generated by the introduction of a bacterial artificial chromosome (BAC) carrying the gene for human CD20 into the pronuclei of mouse embryos. BAC inserts have been used to produce a variety of transgenic mouse

strains since the late 1990s [322], and are highly stable, allowing the introduction of genomic inserts up to 300kb in length [reviewed in [323].

Several groups have previously characterized hCD20 expression in hCD20tg mice [242,324,325], however the animals used in the current work were from a separately maintained colony, with a new hCD20tg DBA strain created from the original hCD20tg C57BL/6 strain via backcrossing and therefore it was decided to validate these mice in-house prior to their use.

Chapter objectives:

- To confirm the expression of hCD20 by B cells in the blood and secondary lymphoid organs
- To characterize the ability of RTX to bind to hCD20 expressed by hCD20tg mice
- To investigate the ability of RTX to deplete B cells in hCD20tg mice

6.2 Results

6.2.1 Genotyping of hCD20tg mice

It has been previously noted in other hCD20tg colonies that hCD20tg female mice do not breed well, and so breeding pairs at the University of Glasgow have been consistently set up using wild-type (WT) females and hCD20tg males. As this type of mating results in both hCD20tg heterozygous offspring and WT littermates, all pups were genotyped by PCR prior to use. Two sets of primers were used to ensure the presence of the transgene in the animals: one that amplifies part of the un-translated exon 2 region within the hCD20 gene; and one that amplifies a sequence near the end of the BAC. A band of 100kbp for *5'Bac*, and 400kbp for *Exon 2*, indicated the presence of the hCD20 transgene [324].

The hCD20 transgene could be readily detected in a proportion of the pups bred from both the C57BL/6 and DBA colonies. In no samples tested was a positive result detected for one primer but not the other, with all pups either showing bands for both the *Exon 2* and *5' Bac* primers, or no bands at all, as can be seen in Figure 6.1. Mice expressing the transgene were termed hCD20tg, while those with no expression were termed WT littermates.

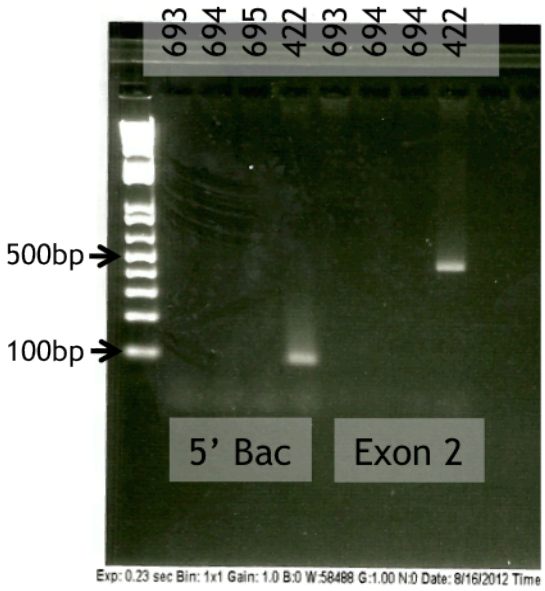

Figure 6.1 Genotyping of hCD20tg mice using primers for the 5' Bac region and Exon 2 of the *hCD20* gene
PCR was performed on DNA extracted from tail tips taken from 3-4 week old pups. The numbers across the top of the gel represent the identification numbers of various pups. A band of 100kbp for *5'Bac*, and 400kbp for *Exon 2*, indicated the presence of the hCD20 transgene.

6.2.2 2H7 anti-hCD20 antibody titration

To verify the presence of the hCD20 protein on the surface of B cells in those mice that tested positive for the hCD20 transgene flow cytometry was used.

A variety of anti-hCD20 antibodies are commercially available for use in flow cytometry, with the majority of these coming from the 2H7 clone. The ability of a selection of these antibodies to detect hCD20 was investigated. Peripheral blood mononuclear cells (PBMCs) were separated from human buffy coats and stained for lineage specific markers, along with various amounts of either anti-hCD20 FITC, anti-hCD20 PE, anti-hCD20 PerCPCy5 or anti-hCD20 APC, all clone 2H7. Analysis of hCD20 expression in this context was performed on $CD3^{-}CD19^{+}$ B cells (Figure 6.2a).

When used at 2.5µl/test, all the anti-hCD20 antibodies tested could detect a similar quantity of $hCD20^{+}$ peripheral blood B cells (Figure 6.2b). For all antibodies, the percentage of B cells seen to be expressing hCD20 increased as the amount of antibody used per test increased, up to 10µl/test. For both the anti-hCD20 FITC and anti-hCD20 PE, using 15µl/test did not increase the percentage of $hCD20^{+}$ B cells detected above the 10µl/test level, however for the anti hCD20-PECy5 and anti-hCD20 APC 15µl/test increased the levels of detection still further.

The amount of hCD20 detected on the surface of $hCD20^{+}$ human B cells by the various antibodies was also looked at (Figure 6.2c). The MFI value was noticeably higher for all antibodies tested when used at 15µl/test compared to when used at 10µl/test (FITC MFI: 230 vs. 295 respectively; PE MFI: 98 vs. 129; PECy5 MFI: 213 vs. 390; and APC MFI: 159 vs. 251, respectively), indicating that a greater level of hCD20 was detected on the cell surface when the anti-hCD20 antibodies were used at this higher concentration. Although the MFI value was consistently highest for each antibody at 15µl/test, the MFI values varied greatly between the different conjugated antibodies at this concentration (MFI range: 129 – 390). It was decided that anti-hCD20 PECy5 would be used for phenotypic characterization of the hCD20tg colonies, as although all antibodies tested bound similar proportions of B cells, the strength of the PECy5 signal was considerably greater than that for either FITC, PE or APC.

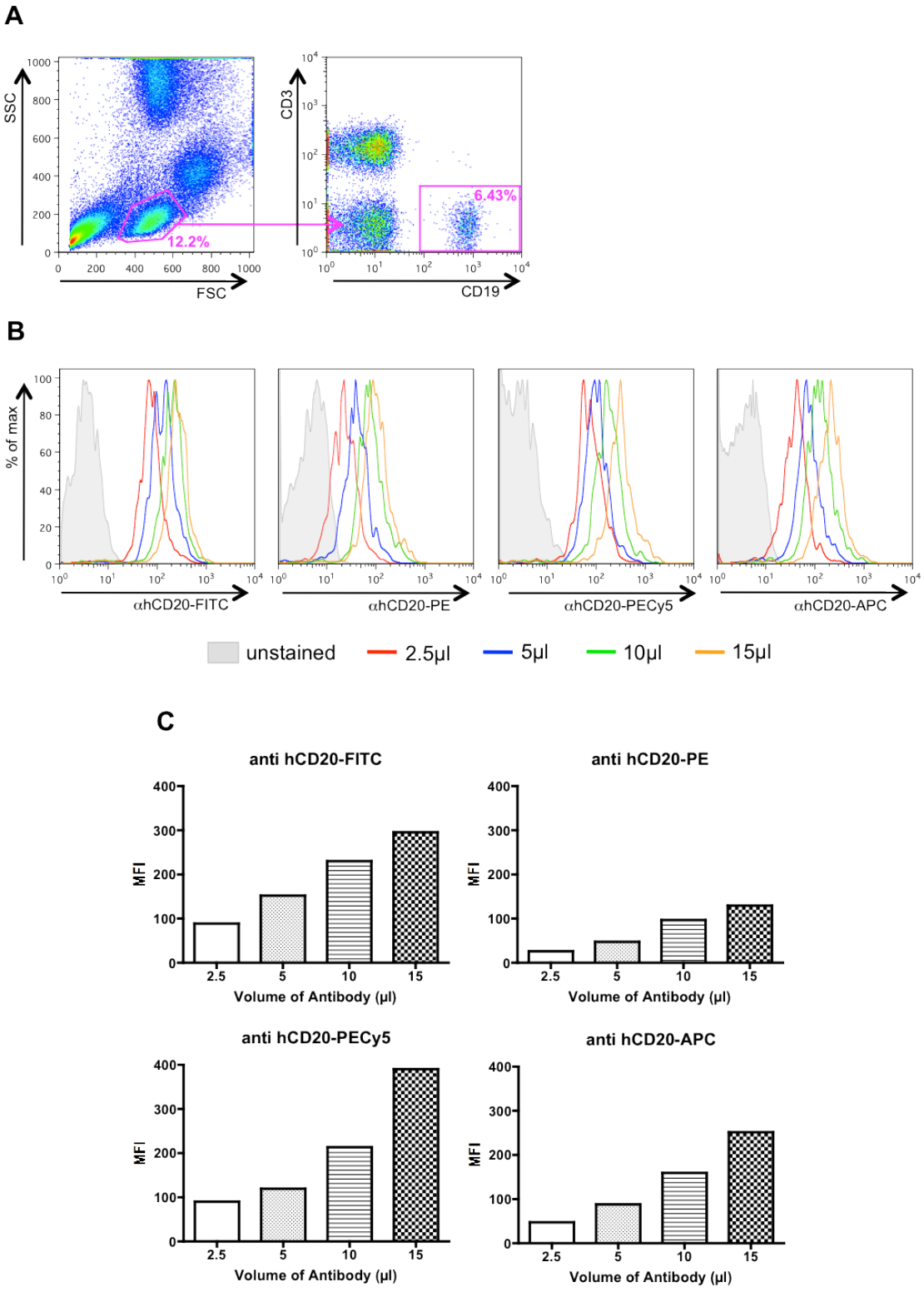

Figure 6.2 Titration of 2H7 anti-hCD20 antibodies
PBMCs were separated from human buffy coats and stained for lineage specific markers, and either anti-hCD20 FITC, anti-hCD20 PE, anti-hCD20 PerCPCy5 or anti-hCD20 APC, all clone 2H7. (**A**) Representative dot plats demonstrating the gating strategy used to define B cells. First panel: SSC vs. FSC. Second panel: CD3 vs. CD19. (**B**) Representative FACS histograms showing hCD20 detection by each anti-hCD20 antibody when used at 2.5, 5, 10 or 15µl per test. Panels: % of Max vs. hCD20. (**C**) Graphs showing the hCD20 MFI for each of the anti-hCD20 antibodies at all the concentrations tested. (n=1)

6.2.3 Phenotypic characterization using 2H7 anti-hCD20 antibodies

To investigate the expression of hCD20 on the surface of cells from hCD20tg mice, tail bleeds were performed on hCD20tg C57BL/6 mice in which the presence on the hCD20 transgene had been verified by PCR. WT littermates were used as controls. Cells were stained with cell lineage markers, along with anti-hCD20 PECy5 (clone 2H7), and analyzed using flow cytometry.

In the blood samples tested, viable cells were gated on using FSC and SSC, and within this population B cells were defined as $CD3^{-}CD19^{+}$ cells (Figure 6.3a). hCD20 could not be detected on B cells from either the hCD20tg mice or the WT littermates using the 2H7 anti-hCD20 (Figure 6.3b). This result was unexpected, as B cells from the hCD20tg mice were expected to express hCD20 on the surface of their mature B cells. The level of hCD20 expression on T cells and monocytes was also investigated for comparison. Within the viable cell population T cells were defined as $CD3^{+}CD19^{-}$, and monocytes as $CD11b^{+}$ (Figure 6.3a). As expected, neither population expressed detectable levels of hCD20 (Figure 6.3b).

This lack of hCD20 staining on transgenic B cells could be due to a lack of expression of hCD20 on the surface of these cells, or it could be a result of an inability of the 2H7 anti-hCD20 antibody used to detect transgenic hCD20. Although in the previous binding tests for this antibody staining of cell surface hCD20 was observed, these tests were performed on human B cells, not transgenic murine cells.

6.2.4 Comparison of transgenic hCD20 staining by 2H7 and L27 anti-hCD20 antibodies

The anti-hCD20 2H7 antibody did not detect hCD20 expression on B cells from hCD20tg mice. To try to verify if this was an accurate representation of the levels of hCD20 on the surface of these transgenic B cells, or if this finding was simply a result of a lack of compatibility of the 2H7 anti-hCD20 antibody with transgenic hCD20, another antibody clone, L27, was used. As it was seen with the 2H7 clone that the ability of an anti-CD20 antibody to detect hCD20 in human samples did not correlate to detection of transgenic hCD20 in murine samples, the L27 antibody was not validated on human cells prior to use on hCD20tg B cells.

Tail bleeds were performed on mice in which the presence on the hCD20 transgene had been verified by PCR. WT littermates were used as controls. Samples were stained with antibodies to lineage specific markers, and either the 2H7 anti-hCD20 antibody, or the

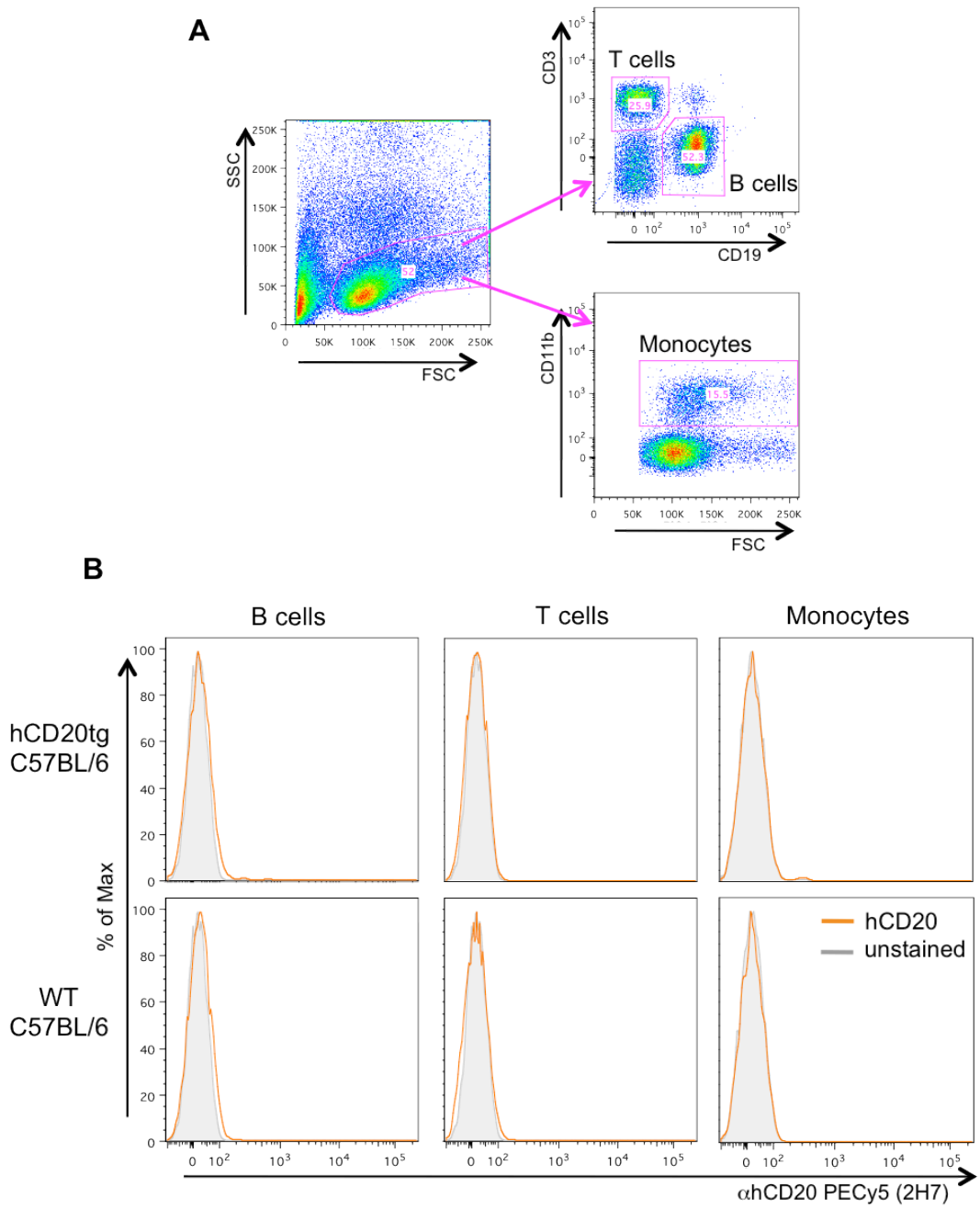

Figure 6.3 hCD20 expression cannot be observed in hCD20tg C57BL/6 mice with the 2H7 anti-hCD20 antibody clone

Tail bleeds were performed on WT and hCD20tg C57BL/6 mice. Blood samples were stained with 2H7 anti-hCD20 PECy5 along with cell lineage markers, and analyzed using a FACSCalibur. (**A**) Representative FACS plots showing the gating strategy used to identify the B cell, T cell and monocyte populations. Left panel: SSC vs. FSC. Top right panel: CD3 vs. CD19. Bottom right panel: CD11b vs. FSC. (**B**) Representative FACS histograms showing hCD20 expression by hCD20tg mice as detected by 2H7 anti-hCD20 PECy5. WT littermates are shown for comparison. Panels: % of Max vs. hCD20. (n=4, data from a single experiment)

L27 anti-hCD20 antibody. Stained samples were subsequently analyzed by flow cytometry. Viable $CD3^{-}CD19^{+}$ B cells were gated on (Figure 6.4a), and the expression of hCD20 in this population evaluated.

Nominal levels of B cells stained positive for hCD20 in both hCD20tg and WT littermates with the 2H7 anti-hCD20 antibody (Figure 6.4b). However, at the same concentrations, the L27 anti-hCD20 antibody was able to detect hDC20 expression in blood samples from the same transgenic animals, with 72.9±3.4% of hCD20tg B cells staining positive for hCD20, compared to 1.9±0.7% of B cells from wild-type littermates (Figure 6.4b and Figure 6.4c). Minimal levels of hCD20 staining could be seen on B cells from non-transgenic WT littermates, however once non-specific background staining was deducted from the results using values obtained from FMO (fluorescence minus one) tests, it could be concluded that C57CL/6 WT littermates mice do not express hCD20 on the surface of their B cells, while hCD20tg C57BL/6 express hCD20 on the majority of their circulating B cells (Figure 6.4b, d).

Although both clones of anti-hCD20 antibody are seen to bind endogenous CD20 in human samples [326,327], these results demonstrate that the 2H7 clone is unable to detect the transgenic hCD20 expressed in this colony of hCD20tg mice. As an outcome of this, L27 anti-hCD20 antibodies were utilized for all further flow cytometric analyses undertaken.

6.2.5 Phenotypic characterization using L27 anti-hCD20 antibodies

6.2.5.1 Evaluation of hCD20 expression in the blood and secondary lymphoid organs of hCD20tg mice

Once an antibody able to detect hCD20 in hCD20tg mice was identified, a more in depth investigation of the pattern of hCD20 expression in these transgenic mice was undertaken. Spleens, peripheral LNs and blood were isolated from hCD20tg C57BL/6 mice and single cell suspensions made. Cells were then stained with L27 anti-hCD20 along with cell lineage markers, and analyzed using a MACSQuant.

Viable cells were gated on using FSC and SSC. Within this population B cells were defined as $CD19^{+}$ cells, and T cells as $CD3^{+}$ cells. Within the $CD19^{+}$ B cell population, B cell subsets were further classified on the basis of their CD21 and CD24 expression, allowing the differentiation of follicular (Fo) B cells, Transitional 1 (T1) B cells and Transitional 2/Maginal Zone (T2-MZ) B cells, as shown in Figure 6.5a. Viable neutrophils and monocytes were defined as $CD45^{+}$ viable cells, with high levels of CD11b expression, and were distinguished from one another by their expression of GR1 and Ly6C. Monocyte

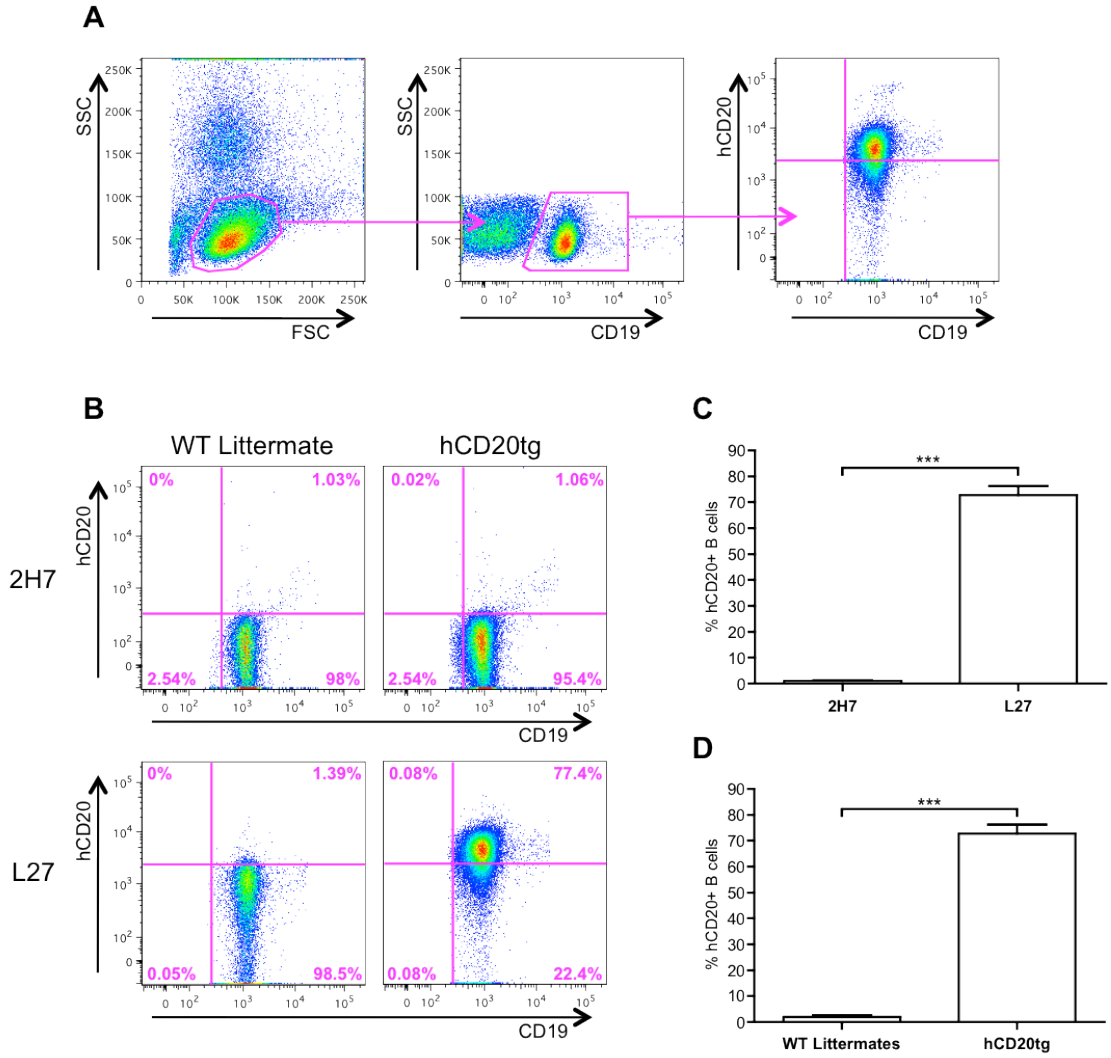

Figure 6.4 L27 anti-hCD20 antibody is able to detect hCD20 in hCD20tg mice
Tail bleeds were performed on hCD20tg C57BL/6 mice and WT littermates. Blood samples were stained for lineage specific markers, and either 2H7 anti-hCD20 or L27 anti-hCD20. $CD3^{-}CD19^{+}$ cells were gated on, and the expression of hCD20 in this population analyzed. (**A**) Representative FACS plots demonstrating the gating strategy used to define total B cells and $hCD20^{+}$ B cells. First panel: SSC vs. FSC. Second panel: SSC vs. CD19, Third panel: hCD20 vs. CD19. (**B**) Representative FACS plots showing the detection of hCD20 by the 2H7 anti-hCD20 antibody and the L27 anti-hCD20 in WT littermates and hCD20tg mice. Panels: hCD20 vs. CD19. (**C**) Graph of pooled data showing the percentage $hCD20^{+}$ B cells as detected by the 2H7 and L27 anti-hCD20 antibodies. (**D**) Graph of pooled data showing the percentage of $hCD20^{+}$ B cells in WT littermates and hCD20tg C57BL/6 mice. (WT littermate n=3, hCD20tg n=4, data from a single experiment) Statistics used: Unpaired t-tests performed on (C) and (D), with *** = $p<0.001$.

could then be further distinguished into Ly6C negative (Ly6C^{neg}), Ly6C intermediate (Ly6C^{int}) and Ly6C high (Ly6C^{hi}) monocyte subsets (Figure 6.5b).

The majority of B cells in the spleen, regardless of their subset, expressed hCD20 on their surface (Total B cells 62±8.8%; Fo B cells 59.9±10.3%; T1 B cells 55.6±10.7%; T2-MZ B cells 76.7±7% hCD20^{+}) (Figure 6.6a – left and middle panels). Overall, very low levels of hCD20 expression were seen in all other cell types investigated, with 3.4±0.5% of T cells, 4.7±0.1% of neutrophils, and 10.6±4.3% of monocytes in the spleen staining positive for hCD20 (Figure 6.6a, left panel). When the monocyte subsets were examined individually, it could be seen that a notable percentage of the Ly6C^{neg} monocyte subset showed hCD20 expression (25.4±8.5% hCD20^{+}) (Figure 6.6a, right panel), however the levels of surface hCD20 expression on this cell subset was considerably lower than that on B cells in the same tissue (mean MFIs of 117 and 245, respectively) (Figure 6.6d, e).In the peripheral LN 50.1±0.8% of B cells expressed hCD20, with minimal staining on T cells (4.9±0.8%) in this tissue (Figure 6.6b). Similar patterns of hCD20 expression were seen in the blood, with B cells expressing high levels of hCD20 on their surface (63.8±9%), and all other cell types expressing minimal hCD20 overall (<10% hCD20^{+}) (Figure 6.6c, left panel). The Ly6C^{neg} monocyte subset in the blood also showed a greater percentage of hCD20 expression than the other subsets, with 15.8±6.3% of the population staining positive for hCD20 (Figure 6.6c, right panel). The levels of surface expression of hCD20 on B cells and Ly6C^{neg} monocytes also showed the same pattern as in the spleen (mean MFIs of 256 and 81, respectively) (Figure 6.6d and e).

Together this data confirms that mice genotyped as being hCD20tg express hCD20 on the surface of their B cells, and indicates that this expression is mostly limited to B cell populations in the tissues tested. However Ly6C^{neg} monocytes, in both the spleen and blood, seemed to have an unexpected, moderate hCD20 surface expression. These results may accurately reflect the levels of hCD20 seen on surface of hCD20tg Ly6C^{neg} monocytes, however, it is important to note that due to the technical aspects of the study this positive population could be B cell contamination in the Ly6C^{neg} monocyte gate. No B cell marker was used in the monocytes staining panel and thus it cannot categorically ruled out that B cells are not part of the Ly6C^{neg} subset.

6.2.5.2 Evaluation of hCD20 expression in the Ly6C^{neg} monocyte population after B cell exclusion

To allow a full understanding of the expression of hCD20 in hCD20tg mice, and whether the Ly6C^{neg} monocyte subset aberrantly express hCD20 in these transgenic animals, a new monocyte FACS panel was developed with an additional B cell marker added to

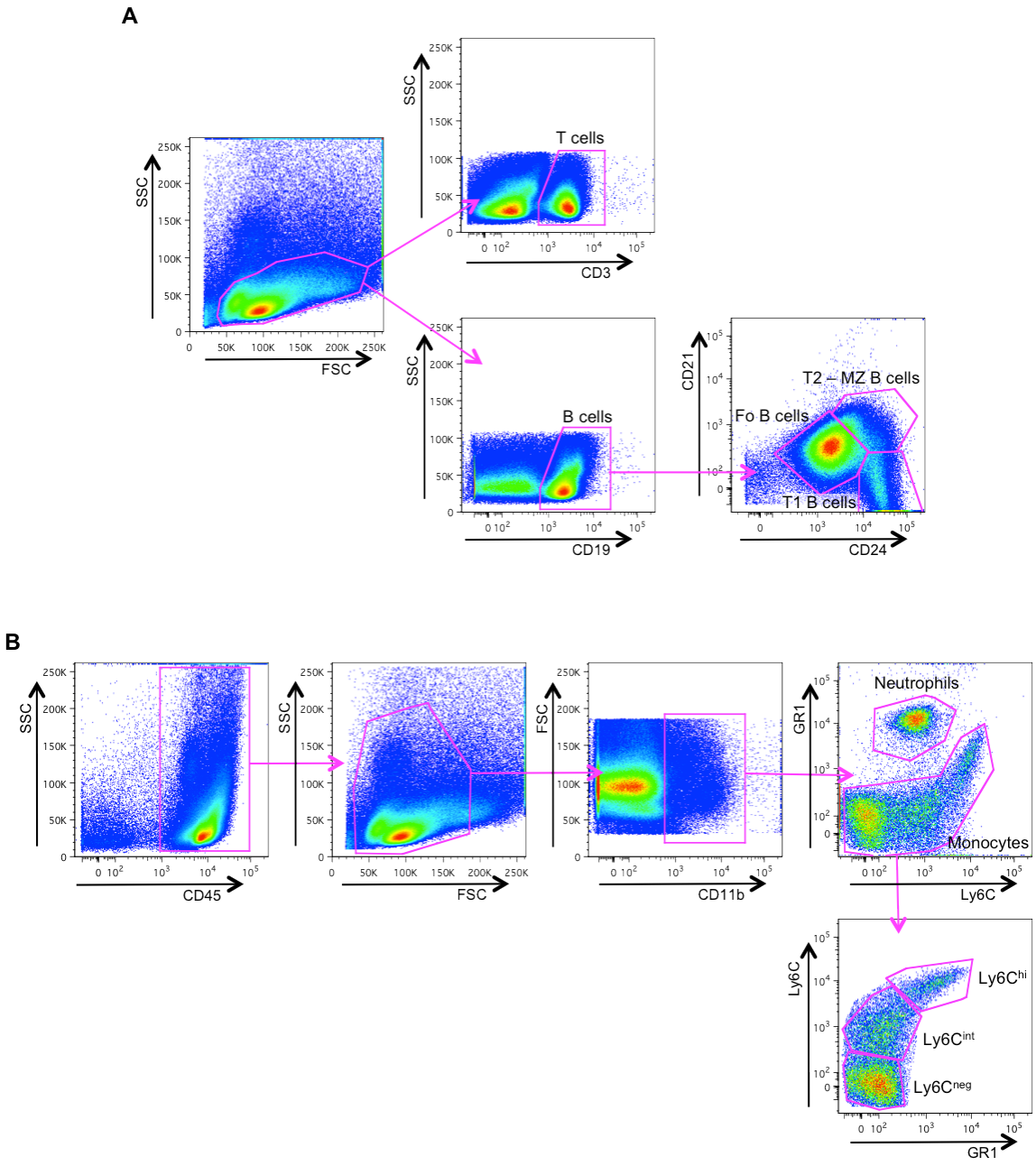

Figure 6.5 Gating strategy for analysis of hCD20 expression in hCD20tg mice
Spleen, LN and blood were isolated from hCD20tg C57BL/6 mice, and analysed by flow cytometry, with the expression of hCD20 investigated using a L27 anti-hCD20 antibody. (**A**) Representative dot plots demonstrating the gating strategy used to define total T cells, total B cells and the Follicular (Fo), Transitional 1 (T1) and Transitional 2/Marginal zone (T2-MZ) B cell subsets. Left panel: SSC vs. FSC. Top middle panel: SSC vs. CD3. Bottom middle panel: SSC vs. CD19. Bottom right panel: CD21 vs. CD24. (**B**) Representative dot plots detailing the gating strategy used to define total neutrophils, total monocytes and the Ly6C high ($Ly6C^{hi}$), Ly6C intermediate ($Ly6C^{int}$) and Ly6C negative ($Ly6C^{neg}$) monocyte subsets. First panel: SSC vs, CD45. Second panel: SSC vs. FSC. Third panel: FSC vs. CD11b. Fourth panel: GR1 vs. Ly6C. Fifth panel: Ly6C vs. GR1.

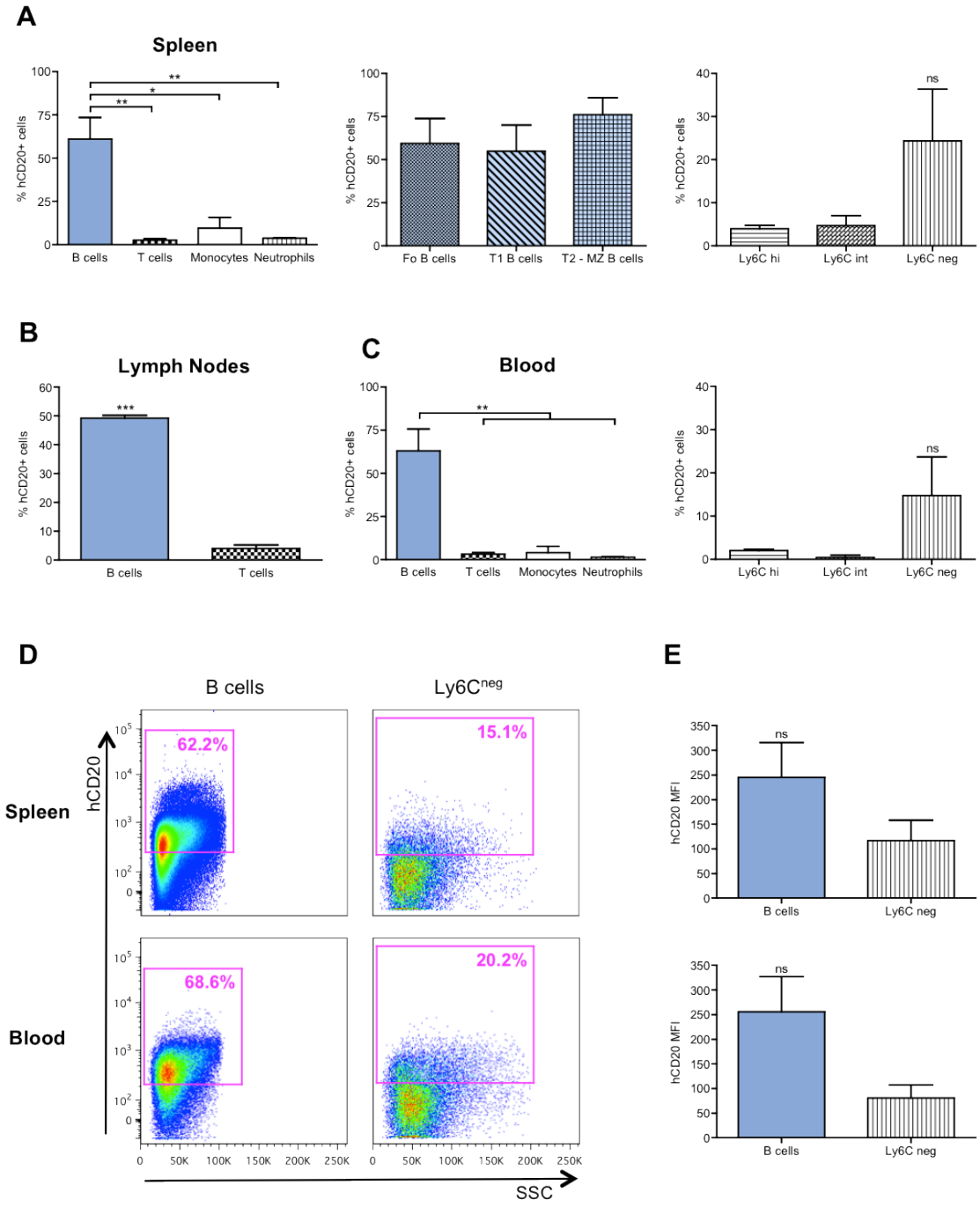

Figure 6.6 Expression of hCD20 by hCD20tg C57BL/6 mice
Tissues were isolated from hCD20tg C57BL/6 mice and single cell suspensions made. Cells were then stained with anti-hCD20 v450 (L27) along with cell lineage markers and analyzed using a MACSQuant. (**A**) Graphs showing the percentage of hCD20^{+} cells within different cell populations in the spleen. (**B**) Graph showing the percentage of hCD20^{+} B cells and T cells in the peripheral lymph nodes (LN). (**C**) Graphs showing the percentage of hCD20^{+} cells within different cell populations in the blood. (**D**) Representative FACS plots showing hCD20 expression by B cells and Ly6C^{neg} monocytes in the spleen and blood. Panels: hCD20 vs. SSC. (**E**) Graphs of pooled data showing the hCD20 MFI of B cells and Ly6C^{neg} monocytes in the spleen (top) and blood (bottom) on hCD20tg C57BL/6 mice. (n= 3, data from 2 independent experiments) Statistics used: For (B) and (E) students T test; all others, One way ANOVA performed on each complete data set (splenic cell populations, splenic B cell subsets, splenic monocyte subsets, blood cell populations, blood monocyte subsets) followed by Bonferroni's post test, with * = $p<0.05$, ** = $p<0.01$ and *** = $p<0.001$.

allow definite exclusion of this population before further analysis. A hCD20tg DBA strain has been generated in house from the original hCD20tg C57BL/6 strain, and once the issues with the staining panel had been amended the expression of hCD20 was investigated in both populations.

Cells isolated from the spleens, peripheral LNs and blood of both hCD20tg C57BL/6 and DBA mice were analyzed. T cells, total B cells and the Fo, T1 and T2-MZ B cell subsets were gated as previously shown (Figure 6.5). The neutrophil/monocyte-staining panel was expanded, and the gating strategy modified to reflect this (Figure 6.7). In detail, viable cells within the $CD45^+$ population were identified and then gated for CD19 expression. $CD19^-$ cells were selected, to ensure removal of any B cell contamination from the final analysis, and the $CD11b^+$ cells within this population considered to be a mix of neutrophils and monocytes. These populations were then distinguished by their differential expression of GR1 and Ly6C. The monocyte population can be then further subdivided into $Ly6C^{neg}$, $Ly6C^{int}$, and $Ly6C^{hi}$ subsets for analysis.

In the spleens of hCD20tg C57BL/6 mice the majority of B cells express hCD20 (66.1±7.7%). WT littermates do not express hCD20, and as such were included in the study to allow discrimination of true hCD20 expression from non-specific background staining, with B cells from WT littermates demonstrating minimal levels of hCD20 staining (4.8±0.3%) (Figure 6.8a and b). In the hCD20tg mice, no hCD20 staining above background was detected in the splenic T cells (hCD20tg: 5.6±2.9%; WT littermates: 4.3±0.5%), monocyte (hCD20tg: 0.1±0.2%; WT littermates: 0.01±0.01%) or neutrophil (hCD20tg: 1.3±0.3%; WT littermates: 1±0.4%) populations (Figure 6.8a and b). When the B cell subsets in the spleen were investigated further, a large proportion of the Fo, T1 and T2-MZ B cells subsets could be seen to express hCD20, with no differences found in the percentage of cells expressing hCD20 in each of these three groups (Figure 6.8c). However the data indicates that with a larger sample pool an increased proportion of $hCD20^+$ cells may be found with within the T2-MZ subset (68±9.6%) compared to the Fo and T1 subsets (51.1±10.4% and 51.8±8.7%, respectively). Again, low-level background staining was seen in the B cell subsets investigated in WT littermates (Fo: 0.9±0.9%; T1: 1.7±0.7%; T2-MZ: 2.4±1.3%). The exclusion of B cells from the monocyte-staining panel considerably reduced the amount of hCD20 expression detected within the $Ly6C^{neg}$ monocyte subset in the spleen (Figure 6.8d). With the previous panel 25.4±8.5% of $Ly6C^{neg}$ monocytes were positive for hCD20 expression in hCD20tg C57BL/6 mice, however with the new panel, only 0.1±0.2% of this subset were positive for hCD20 staining, which is equivalent to the background levels of hCD20 staining seen in this subset in WT littermates (0.2±0.4%).

The cells isolated from the peripheral LN and blood of hCD20tg C57BL/6 mice show similar levels of hCD20 expression as their counterparts in the spleen. The majority of LN B cells from hCD20tg C57BL/6 mice express hCD20 (55.1±5.5%). Very few hCD20tg T cells stain as $hCD20^+$ (5±1.2%) (Figure 6.9a), with comparable levels in WT littermate T cells (4±0.9%) indicating this staining is an artifact of the assay, rather than actual expression of hCD20. Significantly less WT littermate B cells stained positive for hCD20 (5±0.4%), with only minimal non-specific staining seen compared to hCD20tg B cells. In the blood of hCD20tg C57BL/6 mice, 50±13.8% of B cells express hCD20, with only background staining of 3.7±1.1% in WT littermate B cells (Figure 6.9b). The T cell, monocyte and neutrophil populations from both hCD20tg mice and WT littermates show background staining only (<5%), as do all monocyte subsets investigated, with no hCD20 expression detected.

The expression of hCD20 in hCD20tg DBA mice was also investigated using the revised FACS panels. As with the C57BL/6 transgenic mice, a significant proportion of B cells from the spleen (65.6±9.6% - Figure 6.10a and b), LN (59±9.3% - Figure 6.11a) and blood (49.9±14.8% - Figure 6.11b) express hCD20 on their surface compared to the background levels of staining seen in WT littermates (spleen: 4.4±0.3%, LN: 7.6±2.5% and blood: 3.9±0.7% $hCD20^+$) (Figures 6.10b, 6.11a and 6.11b, respectively). In the hCD20tg DBA mice, the T cell, monocyte and neutrophil populations in these tissues did not show any hCD20 staining above the levels seen in the WT littermates, with extremely low percentages of $hCD20^+$ cells (<5%) in all populations. The majority of all splenic B cell subsets investigated in the hCD20tg DBA mice expressed hCD20 (Figure 6.10c), with no notable difference in the expression levels between subsets (Fo: 60.9±28.3%; T1: 57.5±18%; T2-MZ: 61.9±27.7%), although the hCD20 staining in these populations showed a higher level of variation than in others looked at. WT littermates had minimal background hCD20 staining for all splenic B cell subsets (Fo: 2.1±0.6%; T1: 2.8±0.6%; T2-MZ: 1.7±0.3%). No expression of hCD20 by monocyte subsets in the spleens of hCD20tg DBA animals was seen, with comparable levels of hCD20 staining seen as in the WT littermates (hCD20tg: 1.6±0.4% of $Ly6C^{hi}$, 3.6±1.1% of $Ly6C^{int}$ and 1.7±1.5% of $Ly6C^{neg}$, vs. WT littermates: 1.3±0.4% of $Ly6C^{hi}$, 4.8±0.1% of $Ly6C^{int}$ and 1.5±1.3% of $Ly6C^{neg}$). Unfortunately, due to a technical issue, the monocyte subsets in the blood of the DBA hCD20tg mice could not be investigated. However, due to the similarities seen in the expression pattern of hCD20 by the monocyte subsets of the spleen and blood in the hCD20tg C57BL/6 mice, and the comparable levels of hCD20 seen on all populations of cells investigated in the hCD20tg C57BL/6 mice and the hCD20tg DBA mice, it can be supposed that all monocyte subsets in the blood of hCD20tg DBA mice would not express hCD20 on their surface.

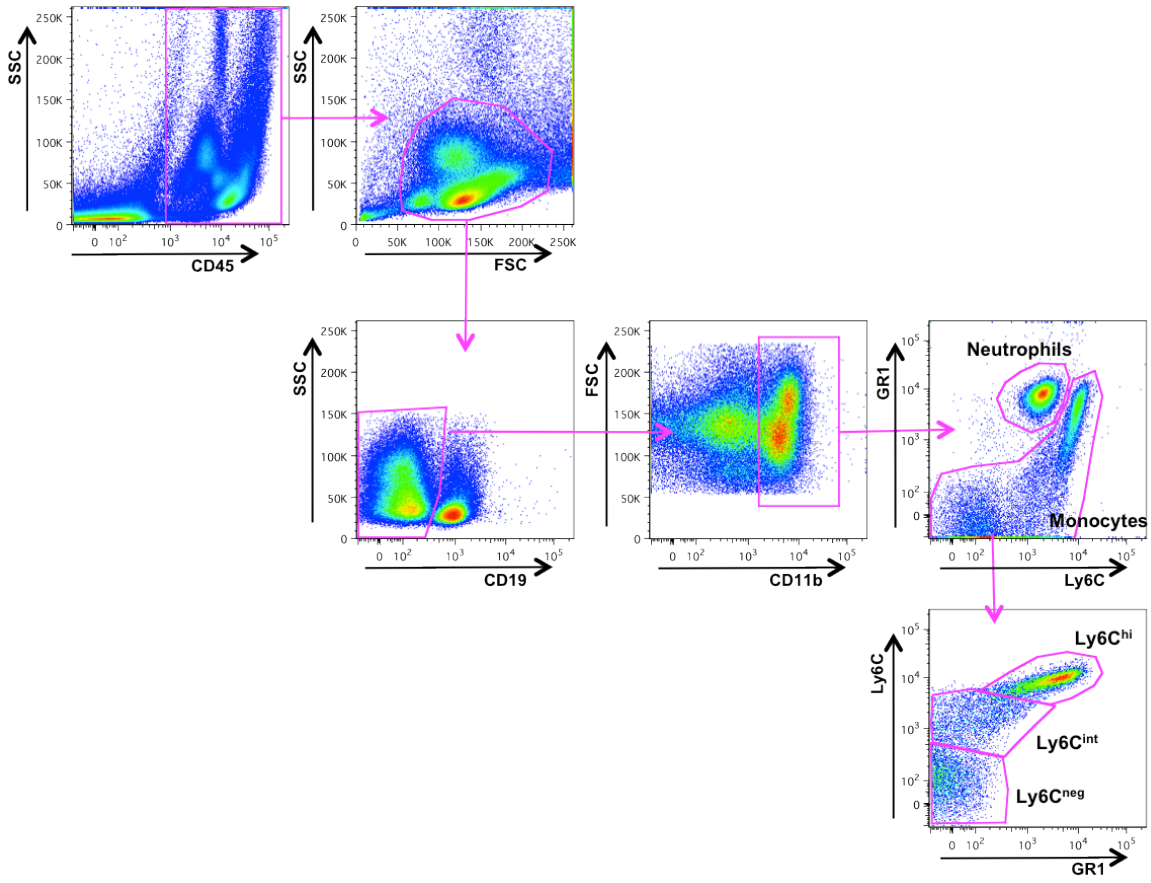

Figure 6.7 Revised monocyte gating strategy for analysis of hCD20 expression in hCD20tg mice

Spleen, LN and blood were isolated from hCD20tg mice, and analysed by flow cytometry, with the expression of hCD20 investigated using a L27 anti-hCD20 antibody. Representative dot plots are shown, detailing the gating strategy used to define total neutrophils, total monocytes and the Ly6C high ($Ly6C^{hi}$), Ly6C intermediate ($Ly6C^{int}$) and Ly6C negative ($Ly6C^{neg}$) monocyte subsets, with an additional $CD19^-$ gating step added. First panel: SSC vs, CD45. Second panel: SSC vs. FSC. Third panel: FSC vs. CD19. Fourth panel: FSC vs. CD11b. Fifth panel: GR1 vs. Ly6C. Sixth panel: Ly6C vs. GR1.

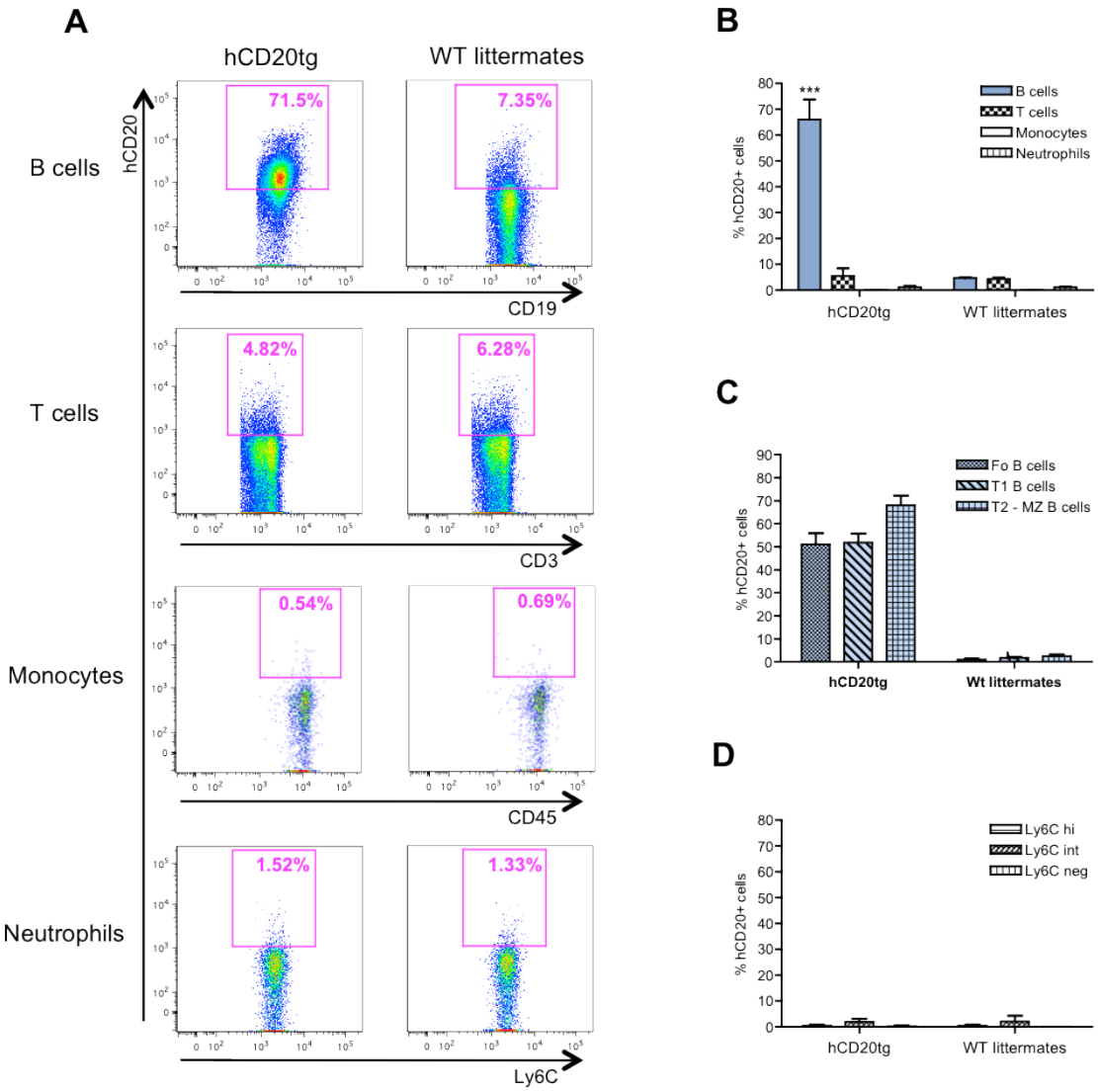

Figure 6.8 Transgenic hCD20 is expressed on splenic B cells from hCD20tg C57BL/6 mice
Spleens were isolated from hCD20tg C57BL/6 mice and WT littermates, and single cell suspensions made. Cells were then stained with L27 anti-hCD20 along with cell lineage markers and analyzed using a MACSQuant. (**A**) Representative FACS plots showing hCD20 staining on each splenic cell population investigated. B cell panels: hCD20 vs. CD19. T cell panels: hCD20 vs. CD3. Monocyte panels: hCD20 vs. CD45. Neutrophil panels: hCD20 vs. Ly6C. (**B**) Graph of pooled data showing the percentage of $hCD20^{+}$ B cells, T cells, monocytes and neutrophils in the spleens of hCD20tg mice and WT littermates. (**C**) Graph of pooled data showing the percentage of $hCD20^{+}$ follicular (Fo), transitional-1 (T1) and transitional-2/marginal zone (T2-MZ) B cells in the spleens of hCD20tg mice and WT littermates. (**D**) Graph of pooled data showing the percentage of $hCD20^{+}$ $Ly6C^{hi}$, $Ly6C^{int}$ and $Ly6C^{neg}$ monocytes in the spleens of hCD20tg mice and WT littermates. (hCD20tg n=5, WT littermates n=3, data from a single experiment) Statistics used: One way ANOVA performed on each complete data set (splenic cell populations, B cell subsets, monocyte subsets) followed by Bonferroni's post test, with *** = $p<0.001$.

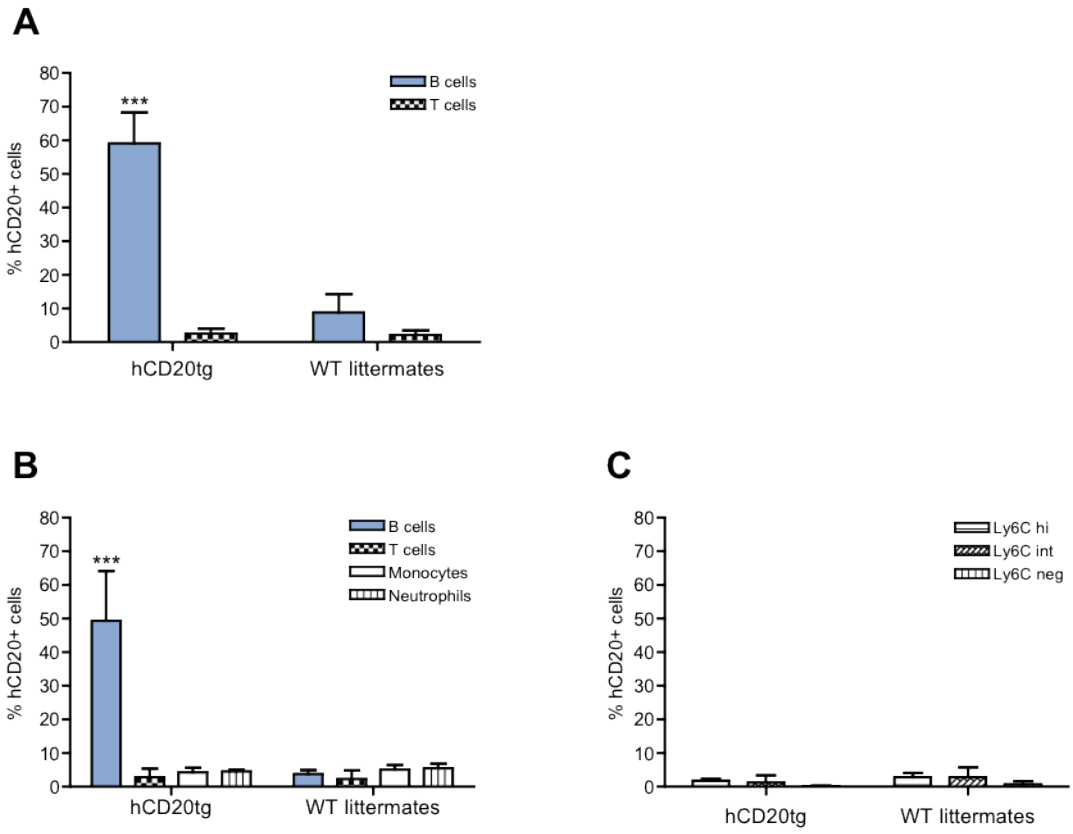

Figure 6.9 Transgenic hCD20 is expressed on B cells from the lymph nodes and blood of hCD20tg C57BL/6 mice

Tissues were isolated from hCD20tg C57BL/6 mice and WT littermates, and single cell suspensions made. Cells were then stained with L27 anti-hCD20 along with cell lineage markers and analyzed using a MACSQuant. (**A**) Graph of pooled data showing the percentage of $hCD20^+$ B cells and T cells in the peripheral lymph nodes of hCD20tg mice and WT littermates. (**B**) Graph of pooled data showing the percentage of $hCD20^+$ B cells, T cells, monocytes and neutrophils in the blood of hCD20tg mice and WT littermates. (**C**) Graph of pooled data showing the percentage of $hCD20^+$ $Ly6C^{hi}$, $Ly6C^{int}$ and $Ly6C^{neg}$ monocytes in the blood of hCD20tg mice and WT littermates. (hCD20tg n=5, WT littermates n=3, data from a single experiment) Statistics used: lymph nodes - unpaired T test; blood - One way ANOVA performed on each complete data set (splenic cell populations, monocyte subsets) followed by Bonferroni's post test, with *** = $p<0.001$.

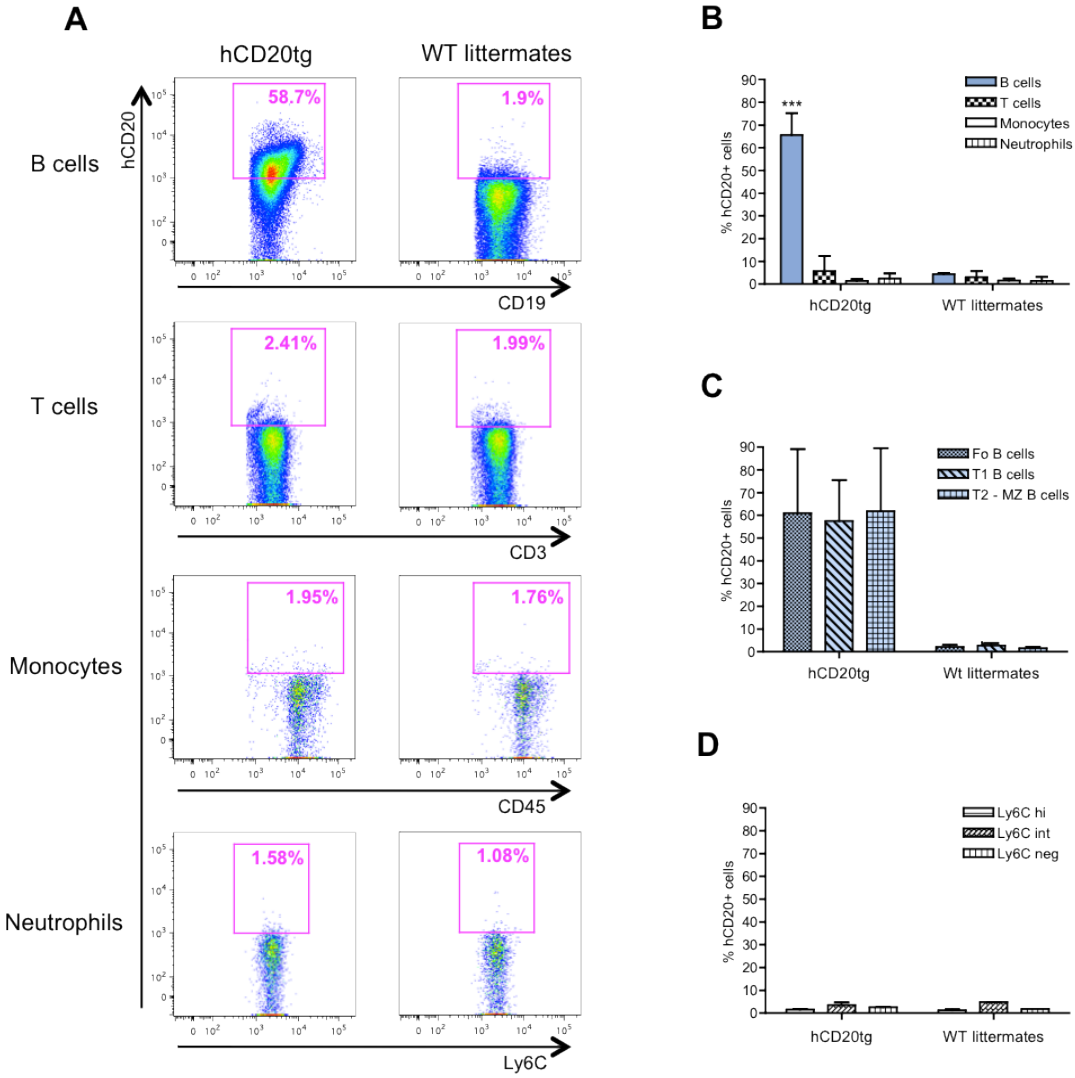

Figure 6.10 Transgenic hCD20 is expressed on splenic B cells from hCD20tg DBA mice
Spleens were isolated from hCD20tg DBA mice and WT littermates, and single cell suspensions made. Cells were then stained with L27 anti-hCD20 along with cell lineage markers and analyzed using a MACSQuant. (**A**) Representative FACS plots showing hCD20 staining on each splenic cell population investigated. B cell panels: hCD20 vs. CD19. T cell panels: hCD20 vs. CD3. Monocyte panels: hCD20 vs. CD45. Neutrophil panels: hCD20 vs. Ly6C. (**B**) Graph of pooled data showing the percentage of $hCD20^+$ B cells, T cells, monocytes and neutrophils in the spleens of hCD20tg mice and WT littermates. (**C**) Graph of pooled data showing the percentage of $hCD20^+$ follicular (Fo), transitional-1 (T1) and transitional-2/marginal zone (T2-MZ) B cells in the spleens of hCD20tg mice and WT littermates. (**D**) Graph of pooled data showing the percentage of $hCD20^+$ $Ly6C^{hi}$, $Ly6C^{int}$ and $Ly6C^{neg}$ monocytes in the spleens of hCD20tg mice and WT littermates. (n=3, data from a single experiment) Statistics used: One way ANOVA performed on each complete data set in (B) (C) and (D), followed by Bonferroni's post test, with *** = $p<0.001$.

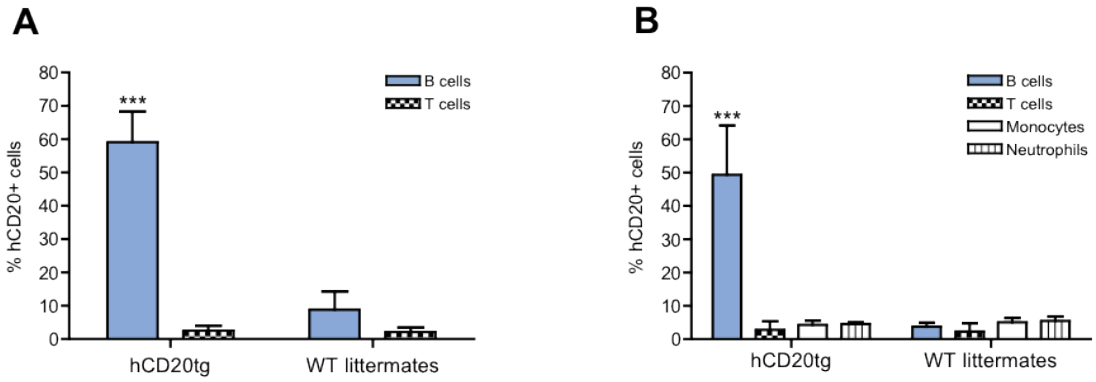

Figure 6.11 Transgenic hCD20 is expressed on B cells from the lymph nodes and blood of hCD20tg DBA mice

Tissues were isolated from hCD20tg DBA mice and WT littermates, and single cell suspensions made. Cells were then stained with L27 anti-hCD20 along with cell lineage markers and analyzed using a MACSQuant. (**A**) Graph of pooled data showing the percentage of $hCD20^+$ B cells and T cells in the peripheral lymph nodes of hCD20tg mice and WT littermates. (**B**) Graph of pooled data showing the percentage of $hCD20^+$ B cells, T cells, monocytes and neutrophils in the blood of hCD20tg mice and WT littermates. (n=3, data from a single experiment) Statistics used: lymph nodes - unpaired T test; blood - One way ANOVA performed on the complete data set, followed by Bonferroni's post test, with *** = $p<0.001$.

Together this data supports the previous FACS data showing that C57BL/6 hCD20tg mice express significant levels of hCD20 on the surface of their B cells, and that this expression is limited to the B cell populations in all tissues tested. It also clarifies the pattern of expression of hCD20 on monocytes in both the spleen and blood, showing that the previous hCD20 expression seen in the Ly6C^{neg} monocyte populations was indeed due to B cell contamination during analysis, rather than a true reflection of the expression by these cells. The characterization of the DBA hCD20tg strain confirms that these mice also express significant levels of hCD20 on the surface of their B cells, although the proportion of hCD20 expressing cells varies more than in the original hCD20tg C57BL/6 colony, and this expression is specific to the B cell populations in the tissues tested.

6.2.6 Binding of Rituximab to hCD20tg B cells

RTX is a chimeric anti-hCD20 antibody, derived from the murine parent 2B8 clone (C2B8). After the discovery that anti-CD20 antibodies of different clones vary greatly in their ability to bind transgenic hCD20, studies were undertaken to confirm the ability of RTX to bind B cells from hCD20tg mice. To do this, RTX was conjugated to the fluorochrome AlexaFluor-488 (RTX-488), allowing detection of the monoclonal antibody by flow cytometry.

An initial comparison of RTX binding to total splenocytes from hCD20tg mice and WT littermates was undertaken (Figure 6.12). Cells were stained with CD19 to allow detection of B cells and incubated with the RTX-488 conjugate. While no notable RTX-488 staining was observed in WT littermates (2.1% of CD19$^+$ cells), 97.5% of CD19$^+$ splenocytes in hCD20tg mice were RTX-488 positive.

Once it was seen that the RTX-488 conjugate was indeed able to bind to CD19$^+$ hCD20tg cells, a comparison between the binding of RTX-488 and the commercially available anti-hCD20 antibodies was made (Figure 6.13a). Cells were stained with cell lineage markers, and either 2H7 anti-hCD20, L27 anti-hCD20, or RTX-488. Significantly more hCD20$^+$ B cells were detected with RTX-488 than either commercially available antibody in both the spleens and peripheral LNs of hCD20tg C57BL/6 mice (Figure 6.13b). When using RTX-488 (1µg/test), 96.1±0.9% of splenic CD19$^+$ B cells stained positive for hCD20, while only 51.9±7.6% and 0.6±0.2% of B cells were hCD20$^+$ with the L27 and 2H7 anti-hCD20 antibodies, respectively. A similar level of hCD20$^+$ B cells was detected using 2µg of RTX-488 per test (hCD20tg C57BL/6, spleen: 96.1±0.9% vs. 97.2±0.7%). In the LNs of C57BL/6 hCD20tg mice, 98±0.1% of B cells were positive for hCD20 when using RTX-488 staining (1µg/test), compared to 40.9±6.7% with L27 anti-hCD20 and 1.24±0.3% with 2H7 anti-hCD20. In DBA hCD20tg mice a similar staining pattern was observed (Figure 6.13c),

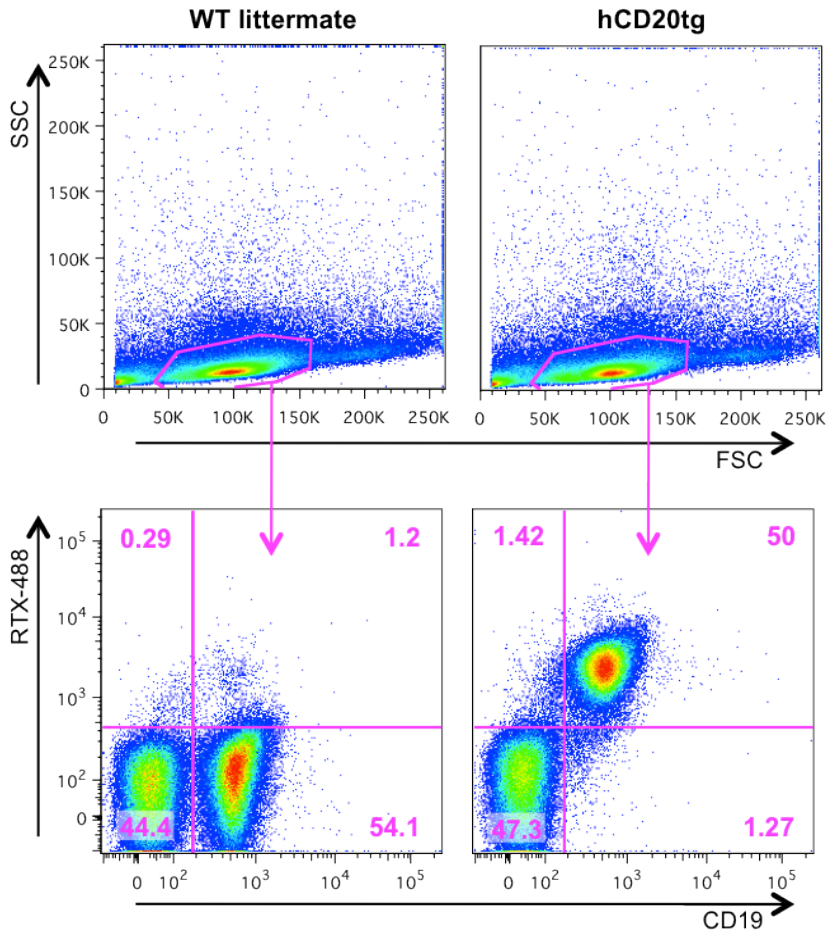

Figure 6.12 Rituximab-488 binds to B cells in hCD20tg mice but not WT littermates
Spleens were harvested from hCD20tg DBA mice and WT littermates. Total splenocytes were stained for lineage specific markers and RTX-488, and analyzed using a MACSQuant. Representative FACS plots showing the binding of RTX to lymphocytes in the spleens of WT littermates and hCD20tg mice. Top panels: SSC vs. FSC. Bottom panels: RTX-488 vs. CD19. (n=1)

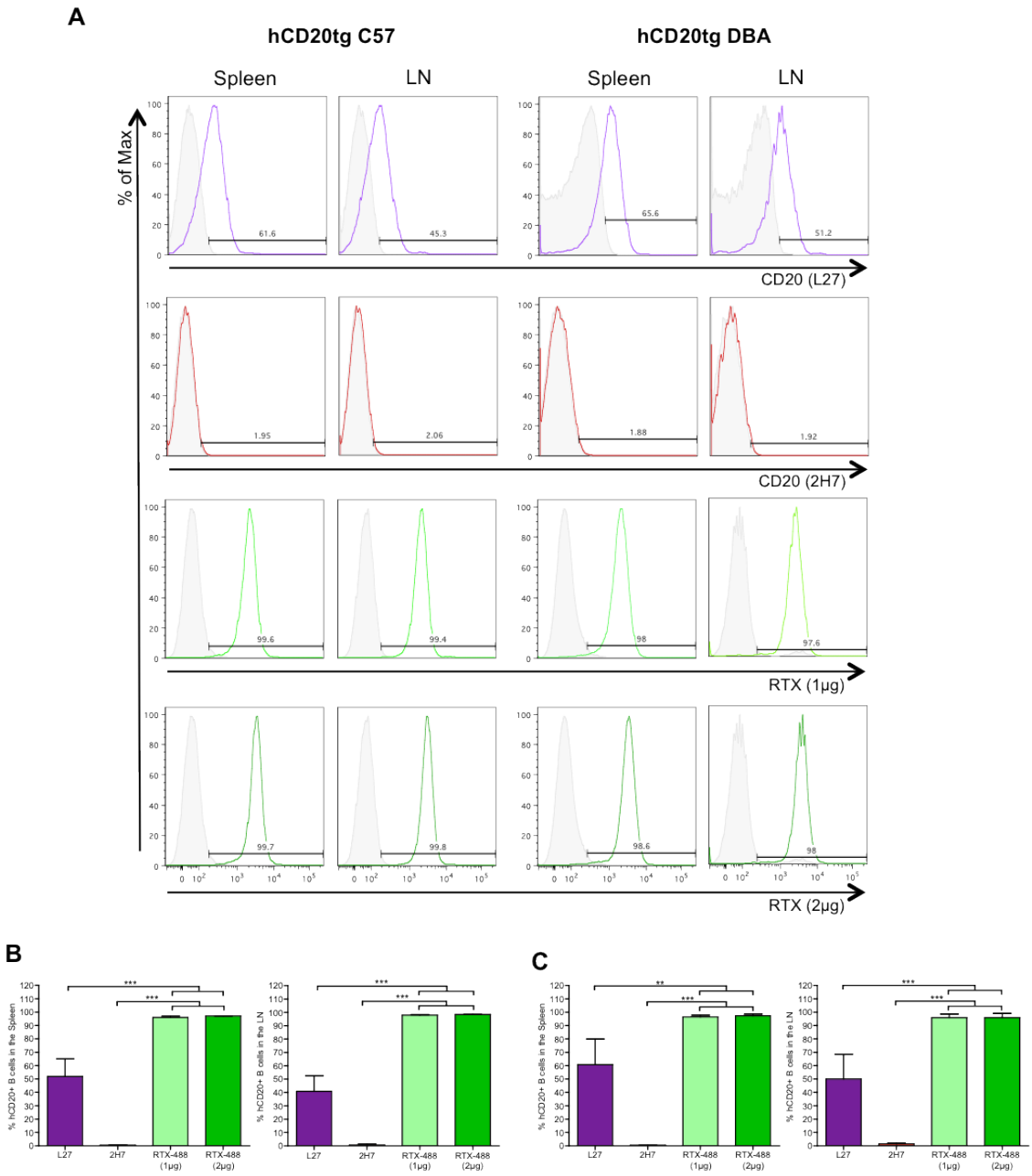

Figure 6.13 A greater percentage of hCD20$^+$ B cells can be detected in hCD20tg mice using RTX-488, compared to both L27 and 2H7 antibodies

Tissues were isolated from hCD20tg mice and single cell suspensions made. Cells were then stained for lineage specific markers, and either L27 anti-hCD20, 2H7 anti-hCD20, or RTX-488, and analyzed by flow cytometry. CD3$^-$CD19$^+$ cells were gated on, and the staining of hCD20 evaluated. (**A**) Representative FACS histograms showing staining of hCD20 on B cells isolated from spleens and LNs of hCD20tg mice. Coloured lines represent the anti-hCD20 antibody used, with grey histograms representing FMO staining. First row panels: % of Max vs. L27 anti-hCD20, Second row panels: % of Max vs. 2H7 anti-hCD20. Third row panels: % of Max vs. RTX-488 (1ug/test). Fourth row panels: % of Max vs. RTX-488 (2µg/test). (**B**) Graphs of pooled data showing the percentage of hCD20$^+$ B cells in the spleen (left) and LN (right) of hCD20tg C57BL/6 mice. (**C**) Graphs of pooled data showing the percentage of hCD20$^+$ B cells in the spleen (left) and LN (right) of hCD20tg DBA mice. (hCD20tg C57BL/6 n=3, hCD20tg DBA n=4, data from a single experiment) Stats used: One way ANOVA performed on each complete data set (hCD20tg C57BL/6 spleen, hCD20tg C57BL/6 LN, hCD20tg DBA spleen, hCD20tg DBA LN) followed by Bonferroni's post test, with ** = p<0.01 and *** = p<0.001.

with 96.5±0.7% of splenic B cells staining positive for hCD20, compared to only 60.7±9.6% and 0.5±0.07% with L27 and 2H7 anti-CD20, respectively. RTX-488 was also able to detect far greater levels of $hCD20^+$ B cells in peripheral LN samples from DBA hCD20tg mice, with 96±1.3% of B cells staining positive for hCD20 compared to 50±9.2% with L27 anti-hCD20 and 1.5±0.2% with 2H7 anti-hCD20.

Together this data confirms that RTX is able to bind to B cells from both hCD20tg C57BL/6 and DBA hCD20tg mice, and that this binding is specific for transgenic hCD20, as minimal RTX binding was detected on B cells from WT littermates.

6.2.7 RTX-mediated B cell depletion in hCD20tg mice

Once the ability of RTX to bind B cells from hCD20tg mice had been confirmed, the ability of RTX to deplete B cells in hCD20tg mice was investigated. To do this, healthy animals were injected i.v. with 100µg RTX or control IgG. On day 6 mice were bled from the tail vein, red blood cells lysed, and the samples stained for flow cytometry and analysed on a FACSCalibur. On day 7 the mice were sacrificed, and the spleens, peripheral lymph nodes, mesenteric lymph nodes, and peyers patches harvested and single cell suspensions made. All tissue samples were stained for lineage markers and run on a FACSCalibur. Results were normalized and expressed as a ratio of B cells:T cells in the relevant tissue.

RTX treatment resulted in a varying degree of depletion of B cells, with significant levels of depletion seen in all tissues tested, bar the spleen. In the spleen, no significant B cell depletion was detected, with RTX-treated animals having 0.62±0.1 B cells to every T cell, compared to 0.92±0.01 in the control animals. Significant B cell depletion was seen the peripheral LNs, mesenteric LNs and peyers patches. In RTX-treated mice 0.13±0.04 B cells:1 T cell were seen in the peripheral LNs, compared to 0.26±0.04 B cells:1 T cell in the control animals, in the mesenteric LN, RTX-treated animals had 0.09±0.01 B cells:1 T cell, compared to 0.41±0.09, and in the peyers patches treated mice had 0.68±0.07 B cells:1 T cell, compared to 1.78±1 B cell:1 T cell. The greatest level of B cell depletion was seen in the blood, with a reduction from 2.1±0.34 B cells:1 T cell in control animals to 0.21± 0.01 B cells:1 T cell.

These results demonstrate that RTX effectively depletes B cells in the blood of hCD20tg mice, with significant depletion also seen in the majority of secondary lymphoid organs investigated.

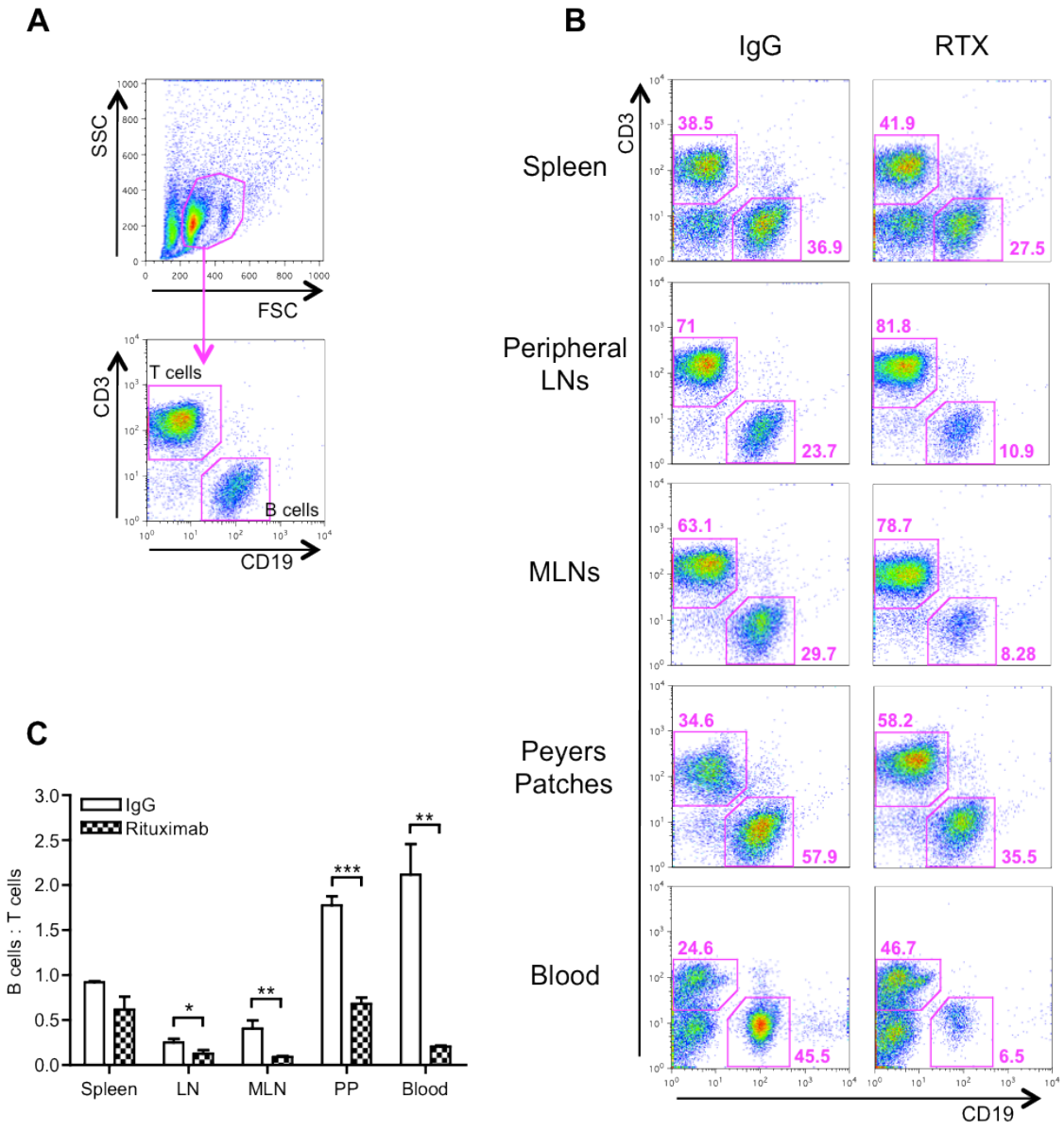

Figure 6.14 RTX-mediated B cell depletion in hCD20tg mice
Healthy hCD20tg C57BL/6 mice were injected i.v. with either 100µg RTX or 100µg IgG on day 0. On day 6 mice were bled from the tail vein, and on day 7 sacrificed, with spleens, peripheral lymph nodes (LNs), mesenteric lymph nodes (MLNs), and peyers patches (PP) harvested and single cell suspensions made. All tissue samples were stained for lineage markers and run on a FACSCalibur on the day of collection. (**A**) Representative FACS plots demonstrating the gating strategy used to define total B cells and total T cells. Top panel: SSC vs. FSC. Bottom panel: CD3 vs. CD19. (**B**) Representative FACS plots showing the levels of B cells depletion in various tissues of the body. Panels: CD3 vs. CD19. (**C**) Graph of pooled data showing the ratio of B cells:T cells in the spleen, LN, MLN, PP and blood of RTX-treated and IgG-treated mice. (n=3, data from a single experiment) Statistics used: Unpaired t-test (RTX-treated vs. IgG-treated), with * = $p<0.5$, ** = $p<0.01$ and *** = $p<0.001$.

6.3 Discussion

- The in-house colonies of hCD20tg C57BL/6 and DBA mice were characterised in order to determine their suitability for use in RTX-mediated depletion studies.
- Both hCD20tg strains express hCD20 on the surface of their B cells, with RTX able to bind this transgenic hCD20 resulting in B cell depletion in the peripheral blood and secondary lymphoid organs.
- These results demonstrate that the hCD20tg C57BL/6 and DBA strains are suitable for use in studies employing RTX-mediated B cell depletion.

To allow the use of Rituximab in our experiments, rather than a mouse specific anti-CD20 antibody, transgenic C57BL/6 mice expressing hCD20 on the surface of their B cells have been obtained and bred in house. From this parent strain a hCD20tg DBA strain has also been generated. To do this, the MAX-BAX^{sm} (Marker-Assisted Accelerated Backcrossing) program of speed congenics from Charles River was utilized to backcross the founder line to DBA/1J over 9 generations. With this method, the genetic background of each offspring was determined by microsatellite analysis, allowing the percentage congenicity to be assessed throughout backcrossing, resulting in the rapid production of the DBA congenic strain.

In the majority of the literature utilizing hCD20tg mice the 2H7 clone of anti-hCD20 antibody has been used. All 2H7 antibodies tested for their ability to bind hCD20 in human buffy coat samples were able to detect hCD20 expression, with the percentage of B cell identified as hCD20^{+} increasing with the amount of antibody used. However, when using 2H7 anti-hCD20 antibodies on samples from hCD20tg mice, transgenic hCD20 was detected in very low levels, if at all, on the surface of primary hCD20tg B cells. This finding caused some concern initially as it indicated the hCD20tg mice might not express the hCD20 protein on the surface of their B cells even though the transgene was present. Once it was determined that this result was not due to the concentration of antibody or the particular vial of antibody used (results not shown), an anti-hCD20 antibody of clone L27 was evaluated. The L27 antibody was able to detect considerable hCD20 on the surface of B cells isolated from hCD20tg mice, indicating that the previous lack of detection was due to the clone of antibody used, and not a lack of hCD20 expression.

Although the expression of hCD20 on transgenic B cells was detected after this reagent change, the lack of binding of transgenic hCD20 by the 2H7 antibodies raises some questions about the molecule expressed by the hCD20tg mice, and its similarity to endogenous hCD20. Three isoforms of CD20 are expressed on the surface of human

B cells, with the 33,000 M_r isoform accounting for 75-80% of surface CD20 [328,329]. Although the commercially available anti-hCD20 antibodies do not specify a target CD20 isoform, it may be the case that certain clones are more readily able to detect one isoform over the others, and that the prominent isoform expressed by hCD20tg mice differs from that expressed in humans. SDS-polyacrylamide gel electrophoresis was originally utilized to identify the relative expression of the different hCD20 isoforms on human B cells, and this technique could also be employed to identify the specific isoform/s of hCD20 expressed by hCD20tg mice. Another explanation for the lack of binding could be related to the fact that different clones of antibody of the same specificity will detect different epitopes on the target molecule. Potentially, the transgenic expression of hCD20 on murine B cells somehow alters epitopes on the molecule, resulting in a loss or masking of the epitope 2H7 antibodies bind. The gene encoding endogenous murine CD20 is not disrupted on insertion of the hCD20-containing BAC, and therefore is expressed alongside hCD20 on the surface of the transgenic B cells [242]. As such it is possible that some level of steric hindrance between the two forms of CD20 is occurring. 2H7 anti-hCD20 antibodies are structurally similar to RTX [330], with almost identical core contact regions [85], however studies have shown that differences in the H3 loop of the two antibodies result in a lower affinity of 2H7 for hCD20 and fewer binding interactions when compared to RTX [330]. On investigation of the binding of RTX to transgenic hCD20 it could be seen that RTX was capable of binding the vast majority of transgenic B cells. In the tests undertaken, a RTX-488 conjugate bound over 90% of primary hCD20tg B cells from both the spleen and peripheral LNs of C57BL/6 and DBA hCD20tg mice, a far higher percentage than either the 2H7 or L27 antibodies. RTX binding was not seen in WT littermates, confirming that RTX was binding to the hCD20 and not endogenous CD20 on murine B cells. These results highlights the fact that although the percentage of $hCD20^+$ detected using the L27 antibody was far greater than that with the 2H7 clone, it was still far less able to bind to transgenic hCD20 than RTX. Titration of the L27 antibody was not undertaken, and so the reduced levels of binding seen with this antibody compared to RTX may be an intrinsic trait of the antibody, however it could potentially be due to the use of sub-optimal concentrations during staining. The ability of RTX to bind transgenic hCD20 on the surface of the vast majority of transgenic B cells, along with the, albeit reduced, ability of the L27 clone, indicates that the lack of binding of 2H7 is due to the antibody, rather than a lack of hCD20 expression.

The L27 anti-hCD20 antibody was used to undertake a more in depth investigation of the pattern of hCD20 expression in hCD20tg C57BL/6 mice. Some issues with the staining panel used were highlighted during analysis, specifically the inability to fully gate out B cells from the $Ly6C^{neg}$ monocyte population, and as a result modifications to the

monocyte-staining panel were made. Using this revised staining panel, the hCD20tg C57BL/6 and hCD20tg DBA strains were characterized, with cells from the spleens, peripheral LNs and blood from these animals analyzed by flow cytometry. In both the hCD20tg C57BL/6 and hCD20tg DBA bred in-house, it could be seen that the majority of B cells in the spleen, LNs and blood expressed hCD20, and this expression was consistent across all B cell subsets investigated. All other cell types looked at (T cells, neutrophils and monocytes) showed minimal hCD20 expression, including the Ly6C^{neg} monocyte population, confirming that the previously detected hCD20 expression was due to transgenic B cell contamination within this gate, rather than aberrant expression by this monocyte subset. Work by Mark Shlomchik's group has previously shown that hCD20tg MRL/*lpr* mice, hCD20tg BALB/c mice and hCD20tg MRL+/+ mice all express high levels of transgenic hCD20 on the surface of their B cells as detected by flow cytometry [324]. The expression of hCD20 in these mice is first seen in the bone marrow at the late pre-B cell stage, with only background levels of hCD20 staining detected on the non-B cell populations tested [324]. Flow cytometric characterization of splenocytes from hCD20tg NOD mice has also confirmed expression of hCD20 on the surface of B cells, with this expression occurring from the pre-B cell stage to mature B cells [325]. B cell function in these hCD20tg NOD mice was shown to be unaffected by hCD20 expression compared to WT NOD mice, with no difference in CD40 and CD86 up-regulation seen after stimulation with either anti-Ig or anti-CD40 antibodies [325]. The levels of natural IgA, IgG1 and IgG2 in the serum of hCD20tg and WT NOD mice were also found to be comparable, as detected by ELISA [325]. The hCD20 expression patterns seen in the in-house hCD20tg C57BL/6 and hCD20tg DBA colonies are in line with the characterizations of numerous hCD20tg strains previously undertaken by other researchers, and confirm the expression patterns expected in these strains.

The ability of RTX to deplete B cells in hCD20tg C57BL/6 mice was then investigated. Some level of B cell depletion was detected in all tissues investigated, however the extent of depletion varied between tissues. It has been previously been documented that in patients, B cell depletion in solid tissues shows considerable variation between individuals and is frequently not complete [108,331-333], with work in primate models showing that increasingly higher doses of anti-CD20 mAbs are needed to deplete B cells in the bone marrow, LNs and spleen [92]. Interestingly, previously work has generally indicated that splenic B cells are cleared more readily by RTX-mediated depletion than LN B cells [241], however in the present study that was found not to be the case. Although some differences arose in the pattern of B cell depletion seen in the hCD20tg mice compared to other work, depletion was in line with that expected, and as such it was decided that the hCD20tg strain would be an appropriate model for RTX-depletion studies.

These results show that transgenic mice bred from our C57BL/6 and DBA hCD20tg colonies can be readily detected via PCR, and that these mice express the hCD20 molecule on the surface of their B cells in the spleen, peripheral LNs and blood. This expression is restricted to the B cell population, and not seen in transgene-negative WT littermates. The hCD20 molecule expressed by both the C57BL/6 and DBA hCD20tg mice can be bound by RTX, with no binding of endogenous murine CD20 seen in WT littermates. RTX treatment of hCD20tg mice resulted in the depletion of vast majority of B cells from the blood, and substantial numbers from secondary lymphoid organs. Together, these data demonstrate that the hCD20tg mice are a suitable model to use for studies into RTX-mediated B cell depletion.

Chapter 7: Modelling Inflammatory Responses *In Vivo*

7.1 Introduction

Due to the complexity of the processes involved in autoimmune diseases, animal models are widely used to facilitate their study, and have been instrumental in countless advances within the field of RA research.

Many rodent models of arthritis have been developed over the years. Some models utilize genetically manipulated animals that spontaneously develop arthritis over the course of their lifetime, such as the K/BxN mouse model. These mice express transgenic TcR receptors that recognize peptides deriving from a ubiquitously expressed protein, resulting in a severe, chronic arthritis, which typically develops at 4-5 weeks of age [reviewed in [334]. More commonly, models rely on the induction of disease either through the administration of an inducing agent, such as type-II collagen (CII) [335] aggrecan [336], or the soluble auto-antigen G6PI (glucose-6-phosphate isomerase) [337], or the passive transfer of disease via autoantibody transfer [338].

Collagen induced arthritis (CIA) was first described in the late 1970s [339], and is one of the most prevalent models of rheumatoid arthritis in use today. This model relies on the immunization of genetically susceptible strains of mice [340] with an emulsion of heterologous type-II collagen (CII) and Complete Freund's Adjuvant (CFA) to initiate disease, followed by a CII challenge on day 21. Clinical symptoms normally begin to present 21-28 days after initial disease induction, and can be evaluated by both clinical arthritis scoring systems and paw and ankle measurements [335]. Sub-clinical disease parameters can also be assessed, with CII-specific T cell proliferative responses and titres of serum CII-specific IgG subclasses often investigated.

CIA is characterized by synovial hyperplasia and the progressive destruction of cartilage and bone, with disease induction requiring both T cell and B cell activation, as well as the infiltration of joint tissue by populations of inflammatory cells. Genetic susceptibility to CIA is associated with the expression of particular MHC II haplotypes, with mice expressing H-2A^q readily susceptible to disease induction. This MHC II association highlights the role of CD4$^+$ T cells in disease pathology, with a dominant Th1 response established early on in disease and characterized by the production of IFNγ during the onset of arthritis [341]. This early T cell response is vital to CIA development, with administration of monoclonal antibodies toward CD4 [342], the TcR [343], or MHC II molecules [344] at the time of disease induction able to suppress disease pathogenesis. However, a direct role for T cells in mediating disease pathology is uncertain. The Th1 response initiates inflammation by recruiting polymorphonuclear cells, to the joint and providing B cell help. Infiltrating polymorphonuclear cells

produce a range of pro-inflammatory cytokines including TNFα [345], IL-1β [346] and IL-6 [347]. TNFα induces the up-regulation of adhesion molecules on the endothelium, further enhancing the infiltration of inflammatory cells, with IL-1β promoting neutrophilia and the production of collagenases, the enzymes responsible for the break down of collagen. IL-6 stimulates myelopoiesis, and is involved the development of activated B cells, with the production of anti-CII antibodies by B cells a hallmark of CIA pathogenesis. In DBA mice, the Th1-associated IgG2a subclass is the predominant pathogenic isotype, with a positive correlation seen between the serum levels of CII-specific IgG2a and clinical pathology [348]. These CII-specific autoantibodies are considered to be the primary mechanism of disease immunopathogenesis, binding to articular cartilage and initiating the complement cascade [349]. Activation of complement contributes to the recruitment of innate immune cells, such as neutrophils and macrophages, further promoting joint inflammation. Innate cell infiltration eventually leads to the development of oedema and synovial hyperplasia [350], with subsequent pannus formation at the synovium-cartilage interface. On disease progression a down-regulation of IFNγ production results in a skewing of the immune response toward a Th2 phenotype, with an associated increase in the Th2 cytokines IL-10 and IL-4 [341]. CIA is a transient model of arthritis, with this increase in IL-10 production helping to down-regulate the pathogenic inflammatory response, and resulting in eventual disease remission.

The pathogenesis of CIA shares multiple features with human disease, such as the development of synovial hyperplasia, autoantibody production by B cells [351], and joint infiltration by inflammatory cells [350]. However, differences between CIA and human arthritis are also apparent. Disease progresses far more rapidly in CIA, and, unlike RA, is of a transient nature. The pattern of joint involvement also differs between the diseases, and periostial reactions are common in the mouse model but not in human arthritis. Despite the various differences, CIA is a valuable tool for understanding the pathogenesis of human disease, as well as for testing the efficacy of new therapies [352] and better understanding the mode of action of those already in use [353].

Along with the study of specific diseases, animal models can be utilized to explore varying aspects of the immune response to particular antigens. Delayed-type hypersensitivity (DTH) assays are used to investigate antigen-specific, cell-mediated immunity in response to a chosen antigen, and have been frequently used in studies of oral tolerance [354-357], as well as in those looking into the re-introduction of systemic tolerance in autoimmune disorders [182,358].

To induce DTH responses, mice are systemically immunized with the selected antigen, followed by a challenge 14-21 days later, in either the ear pinna [359] or footpad [183]. Local swelling is assessed 24 hours post challenge, with antigen-specific T cell responses [182] and serum antibody levels also commonly examined. DTH responses are dependent on local T cell-mediated responses to the model antigen [360], leading to cellular infiltration and oedema at the site of antigen challenge, with tolerance in this model defined as a lack of inflammation in response to this controlled re-exposure.

In this chapter both the CIA and DTH models have been utilized in an effort to dissect the complex interactions taking place on RTX-mediated B cell depletion in RA.

Chapter objectives:

- To investigate whether apoptotic B cells are able to ameliorate disease symptoms in a murine model of CIA
- To investigate whether RTX treatment of hCD20tg mice can improve disease outcome in a murine model of CIA
- To set up a DTH model in the lab for future use to explore tolerance induction after RTX treatment

7.2 Results

7.2.1 Prophylactic treatment of CIA with apoptotic B cells

Rituximab treatment causes the depletion of CD20-expressing B cells in the blood and lymphoid tissues of the body in both humans and mice [81,361]. This depletion is thought to occur through several mechanisms including, but not limited to, direct apoptosis of B cells [238]. There is a vast body of literature demonstrating the immunosuppressive effects of apoptotic cells on the immunes system, and it has previously been shown by Gray et al that apoptotic thymocytes protect mice from CIA [172]. The current study aimed to investigate the effect of apoptotic B cells on arthritis. To do this, either $5x10^6$ or $0.5x10^6$ apoptotic B cells were adoptively transferred via the tail vein into WT DBA mice on day 0, with control mice receiving PBS only or $5x10^6$ viable B cells. CIA was induced with chicken CII in all mice on day 0, and boosted on day 21, following the protocols outlined in section 2.4.3, and disease progression and severity was evaluated. Using this protocol to induce arthritis, disease is not generally seen before the boost on day 21, and so clinical scoring, ankle, and paw measurements, were not started before this time.

Similar levels of general inflammation, as measured by the 16-point clinical scoring system (Chapter 2, Table 2.1), could be detected in all groups (Figure 7.1a), with average cumulative scores of 12±12 for the PBS treated group, 22±26 for the group that received $5x10^6$ B cells, 18±22 for the group that received that $5x10^6$ apoptotic B cells, and 15±21 for the group that received $0.5x10^6$ apoptotic B cells. The general inflammation scores of individual animals were also investigated on d39 and d42 (Figure 7.1b), and it can be seen that in both groups receiving apoptotic B cells the average score is brought up by only one or two highly arthritic animals, in comparison to the PBS and B cell groups which contain a greater proportion of highly arthritic animals. Joint inflammation scores followed the same pattern of progression as the general inflammation scores (Figure 7.1c), with no differences detected between any of the groups. Again, the joint inflammation scores of individual animals were investigated on d39 and d42 (Figure 7.1d). With this mode of visualisation it can be seen that as with the general inflammation scores, both groups receiving apoptotic B cells contain only one or two highly arthritic animals, in comparison to the PBS and B cell groups which contain a greater proportion of highly arthritic animals.

Ankle size changed little over the course of the experiment (Figure 7.2a), and no difference was observed between treatment groups. A greater variation in paw size was seen, although again, no difference was detected between any group (Figure 7.2b). Averaging 52±6%, the incidence of disease was considerably lower than expected (Figure 7.2c), with incidence levels of 80-100% anticipated in DBA mice [335].

The general-inflammation and joint-inflammation scores, along with paw and ankle measurements, allow quantification of clinical disease, however there may be sub-clinical disease in animals that do not present with visible symptoms. To allow investigation of this potential sub-clinical disease, blood was collected from all mice on day 42 and ELISAs undertaken to quantify total serum titres of IgG and IgG1, as well as relative levels of CII-specific IgG1 and IgG2a. No difference was seen in the concentration of either total IgG (Figure 7.3a) or total IgG1 (Figure 7.3b) between the treatment groups. Titres of CII-specific IgG1 and IgG2 were also comparable in all groups (Figure 7.3c and d, respectively).

To determine whether the scoring of paw inflammation was accurately representing sub-clinical disease in the mice, the correlation between maximal joint score and CII-specific antibody titres was investigated. The groups receiving $5x10^6$ B cells, and $5x10^6$ apoptotic B cells showed a significant correlation between maximal joint score and CII-specific IgG1 levels, with serum antibody titres increasing with increased score (Figure 7.4a). The groups administered either PBS or $0.5x10^6$ apoptotic B cells did not show any

correlation between clinical score and CII-specific IgG1. No correlation between joint inflammation scores and serum CII-specific IgG2a was seen in any treatment group (Figure 7.4b).

As an additional read out of sub-clinical disease, T cell proliferation in response to re-stimulation with collagen was measured by quantifying the incorporation of radioactive tritiated-thymidine (^{3}H-thymidine) into newly synthesized cells (Figure 7.5). LN cells were harvested from all mice on day 42, and cells cultured *in vitro* with collagen protein for 72-96hr, before pulsing with ^{3}H-thymidine. Significantly more proliferation was seen in the T cells from mice receiving $5x10^6$ B cells, compared to those given PBS regardless of the concentration of CII re-stimulation. However, this increased proliferation was not significant when compared to either of the other treatment groups. There was also an increase in proliferation of cells from mice given $5x10^6$ apoptotic B cells compared to PBS controls, when cultured with 60µg/ml of collagen. Again, this increase was not significant when compared to the proliferation levels of the other groups when cultured with 60µg/ml collagen.

With the experimental protocol used, no effect of apoptotic B cell administration on CIA progression or severity could be detected, as measured by either clinical scores or serum CII-specific antibody levels. However, unexpectedly, an increase in collagen-induced T cell proliferation was seen in cells from mice that received 5x106 apoptotic B cells compared to PBS control animals.

7.2.2 Effects of hCD20tg B cell transfer and subsequent RTX treatment on CIA severity and progression

In parallel to this study, the effects of RTX-mediated B cell apoptosis on CIA were investigated. It is known that RTX treatment directly induces apoptosis in a proportion on the B cell population [235-237], and this is a potential mechanism by which RTX exerts its beneficial effects. A strain of hCD20tg DBA mice have been generated in-house to allow the use of RTX in an animal model of arthritis, however at this point in time our hCD20tg DBA colony was not fully established and therefore not available in the numbers required for disease models. As an interim solution, it was decided to adoptively transfer hCD20tg DBA B cells into WT DBA mice, allowing apoptosis to be induced in this defined B cell population. The adoptive transfer of hCD20tg B cells and subsequent RTX treatment took place on day 0, with induction of CIA using chicken CII undertaken later the same day. This allowed the study of the effects of RTX-mediated B cell apoptosis specifically, rather than an alternate method of B cell apoptosis.

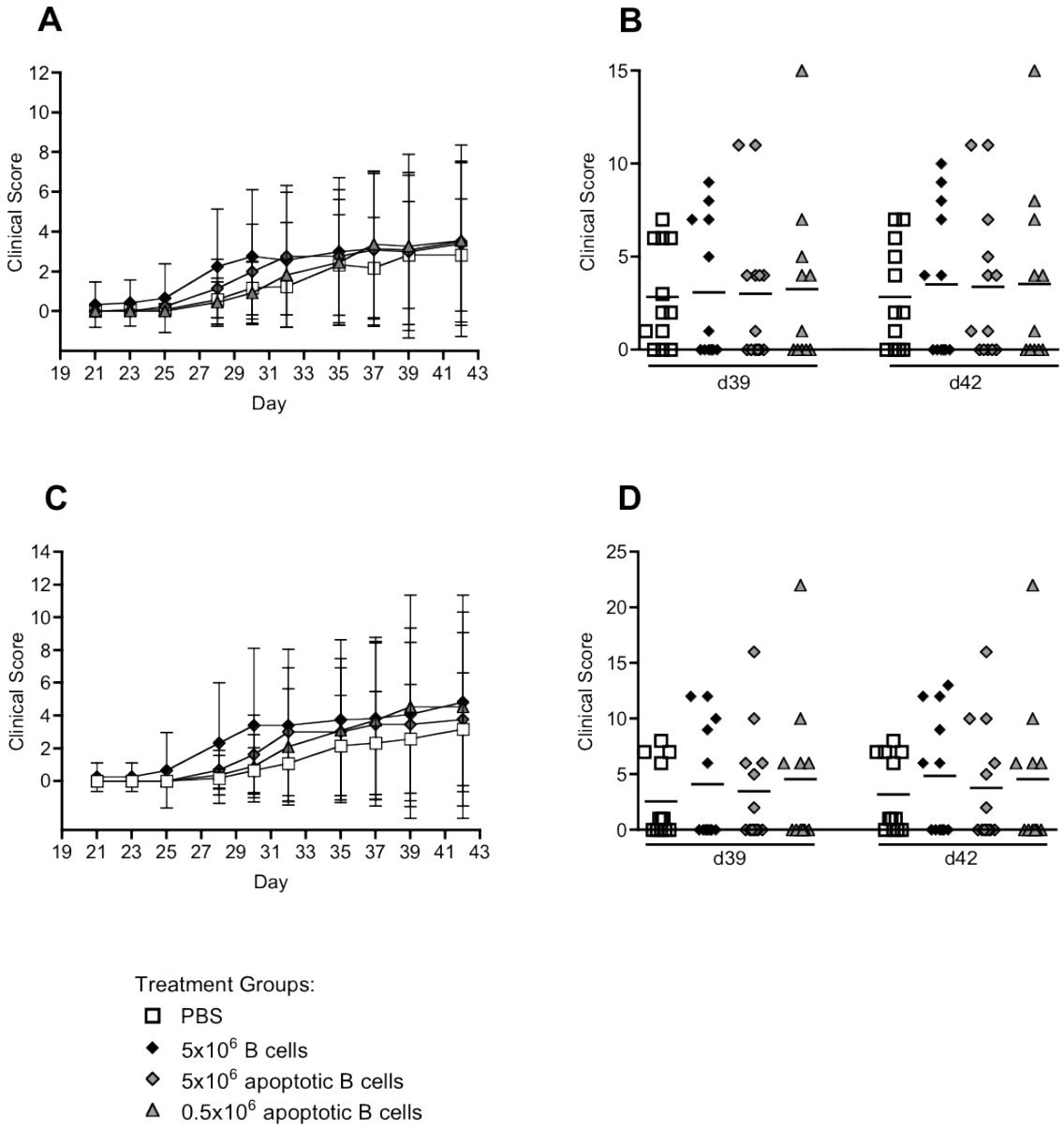

Figure 7.1 Clinical scores of collagen induced arthritis in WT DBA mice adoptively transferred with apoptotic B cells

On day 0 WT DBA mice were adoptively transferred with either: $5x10^6$ B cells (◆); $5x10^6$ apoptotic B cells (◆); or $0.5x10^6$ apoptotic B cells (▲) via the tail vein. Control mice received PBS only (□). CIA was then induced in these animals. (**A**) Graph showing the general inflammation scores (16-point scoring system) for all treatment groups. (**B**) Scatter graph showing the general inflammation scores for each animal on days 39 and 42. (**C**) Graph showing the joint inflammation scores (24-point scoring system) for all treatment (**D**) Scatter graph showing the joint inflammation scores for each animal on days 39 and 42. (n=13, data from 2 independent experiments) Statistics used: Two-way ANOVA, followed by Bonferroni's post-test, with $p<0.05$ considered statistically significant.

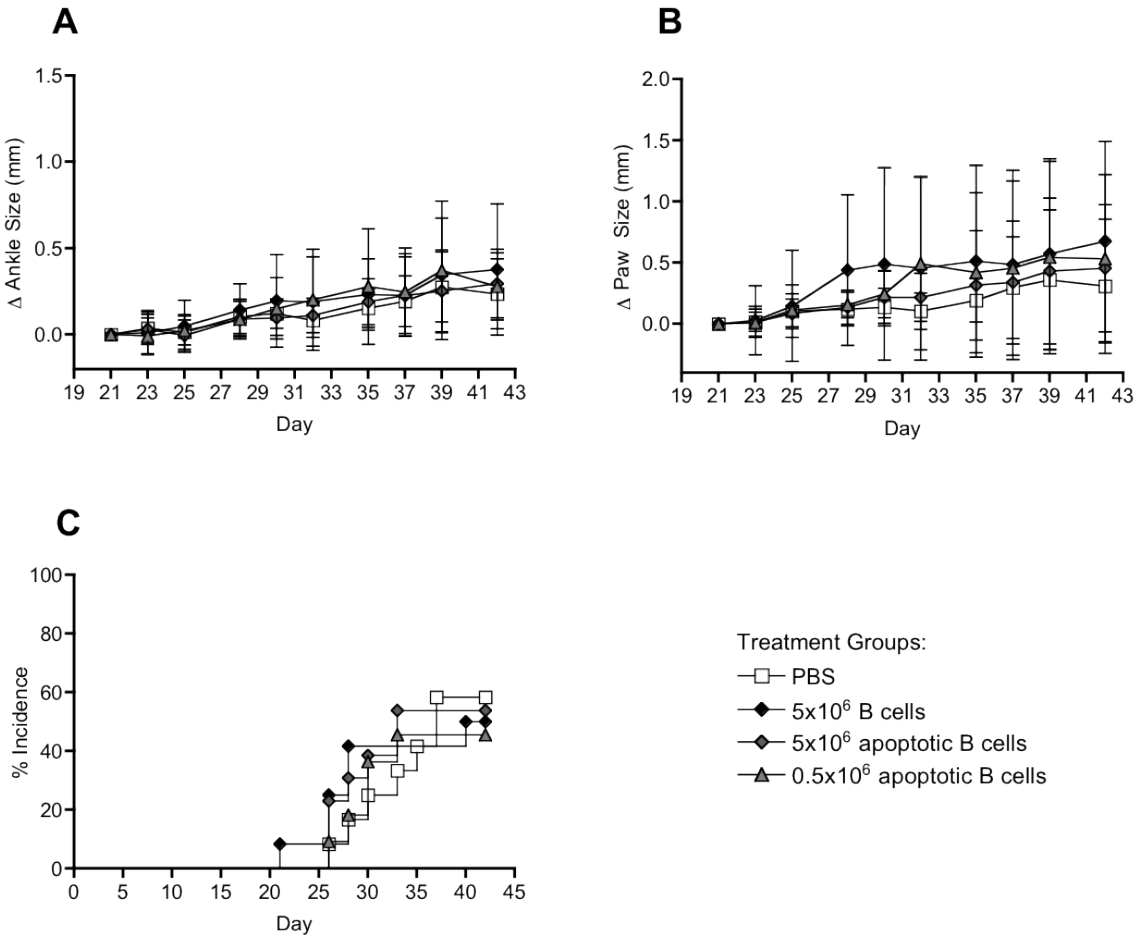

Figure 7.2 Swelling and incidence of collagen induced arthritis in WT DBA mice adoptively transferred with apoptotic B cells

On day 0 WT DBA mice were adoptively transferred with either: $5x10^6$ B cells (◆); $5x10^6$ apoptotic B cells (◆); or $0.5x10^6$ apoptotic B cells (▲) via the tail vein. Control mice received PBS only (□). CIA was then induced in these animals. (**A**) Graph showing the change in ankle size for all treatment groups. (**B**) Graph showing the change in paw size for all treatment groups. (**C**) Graph showing the incidence of disease in all treatment groups. (n=13, data from 2 independent experiments) Statistics used: Two-way ANOVA performed on complete data sets in (A) (B) and (C), with $p<0.05$ considered significant.

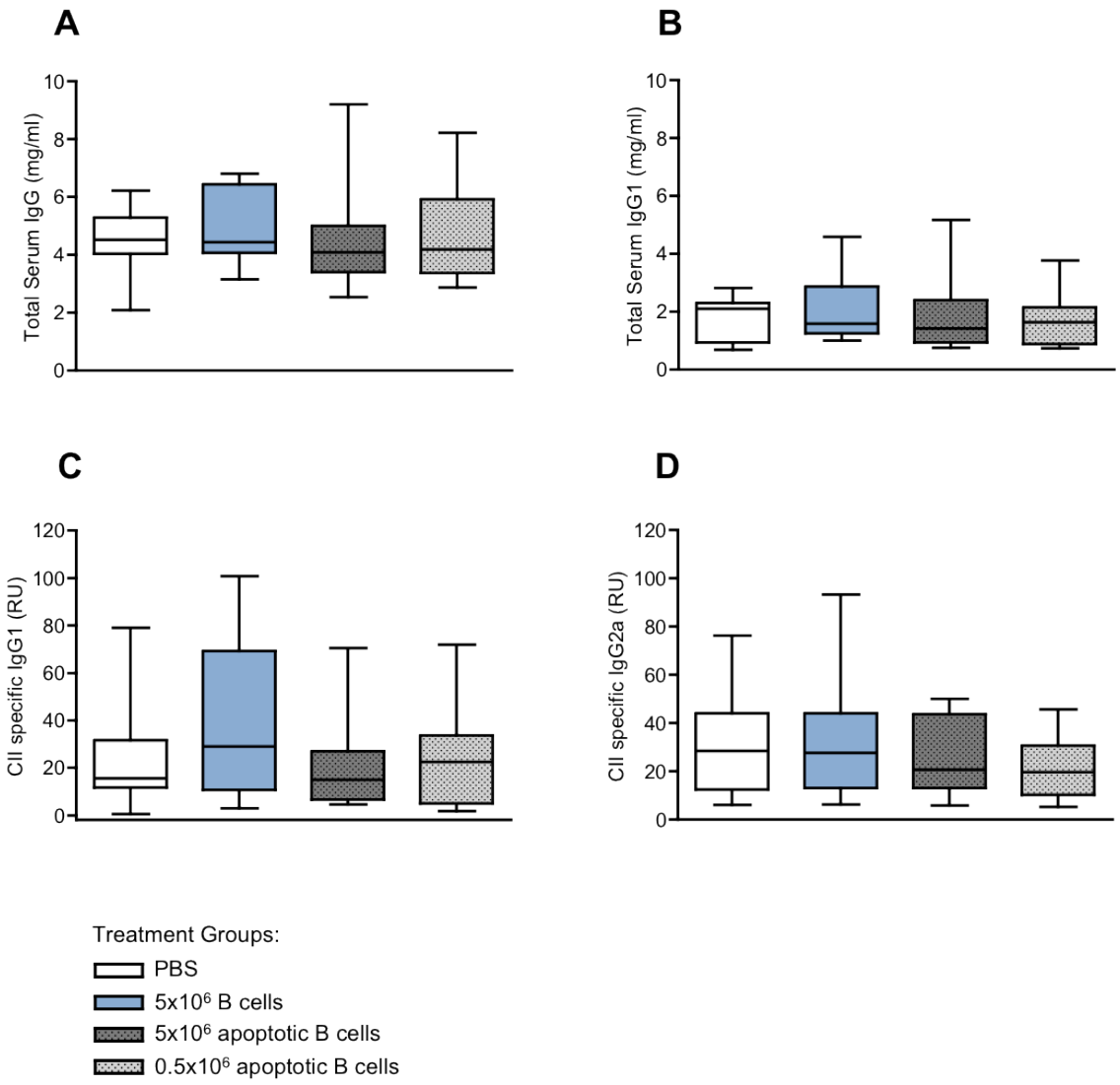

Figure 7.3 Serum antibody titres in WT DBA mice adoptively transferred with apoptotic B cells

Mice were culled on d42, blood samples collected and serum IgG titres quantified by ELISA. (**A**) Graph showing the concentration of total serum IgG (mg/ml) for all treatment groups (**B**) Graph showing the concentration of total serum IgG1 (mg/ml) for all treatment groups. (**C**) Graph showing the concentration of CII-specific serum IgG1 (RU = relative units) for all treatment groups. (**D**) Graph showing the concentration collagen type-II specific IgG2a (RU = relative units) for all treatment groups. (n=13, data from 2 independent experiments) Statistics used: One-way ANOVA performed on the complete data sets in (A) (B) (C) and (D), followed by Bonferroni's post-test, with $p<0.05$ considered statistically significant.

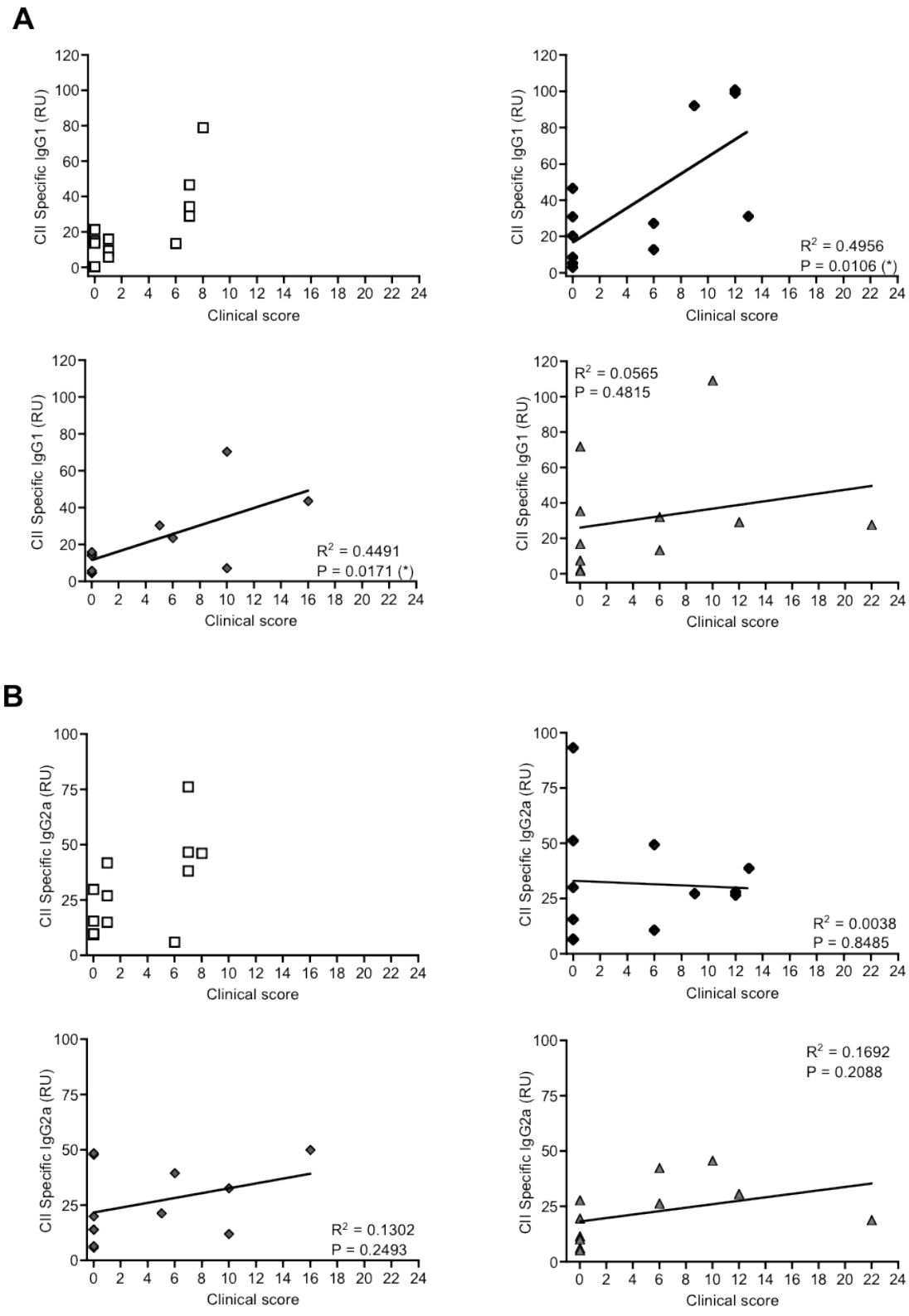

Figure 7.4 Correlation of maximal joint inflammation score with serum titre of collagen-specific IgG1 or IgG2a

(**A**) Graphs showing the correlation of maximal joint inflammation score (24-point clinical score) and CII-specific IgG1 for each treatment group. (**B**) Graphs showing the correlation of maximal joint inflammation score and CII-specific IgG2a for each treatment group. (PBS only ☐ (n=12); $5x10^6$ B cells ◆ (n=12); $5x10^6$ apoptotic B cells ◆ (n=12); or $0.5x10^6$ apoptotic B cells ▲ (n=11, data from 2 independent experiments). Statistics used: Linear regression and Spearman r tests where shown , with * = $p<0.05$.

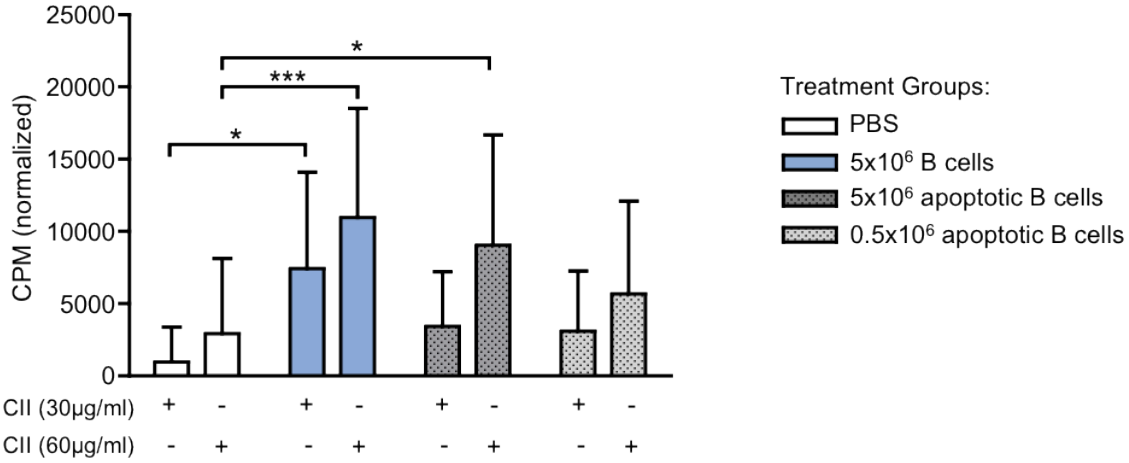

Figure 7.5 Collagen re-stimulation responses
Mice were culled on d42 and peripheral LNs were harvested to allow the investigation of cellular proliferation in response to collagen re-stimulation was investigated. LN cells were cultured *in vitro* with ^{3}H-thymdine and either 30µg/ml or 60µg/ml collagen protein to look at specific proliferation responses. Values are normalized to media only controls. CPM = counts per minute. ($0.5x10^6$ apoptotic B cells: n=6, all other groups: n=7, data from a single experiment) Statistics used: One-way ANOVA performed on complete data set, followed by Bonferroni's post-test, with * = $p<0.05$, and *** = $p<0.001$.

No difference was seen in the levels of either general inflammation or joint specific inflammation between the treatment groups (Figure 7.6a and b, respectively). The general and joint inflammation scores of individual animals was also plotted, to attempt to visualise any differences between the treatments groups (Figure 7.6b and d). All groups, except the hCD20 B cell + RTX group, show a clear separation between a highly arthritis group and a minimally arthritis group, however the numbers of responders and non-responders did not differ between groups. The hCD20 B cell + RTX group show a more uniform spread of scores, which could indicate that the treatment was able to reduce the clinical score of animals which would have otherwise become highly arthritic. However, it may also be a sign of a more consistent disease induction within this group, and without further work would be needed to discern the cause. A more severe arthritis was seen in this run of CIA compared to the runs undertaken in which irradiated apoptotic B cells were adoptively transferred into WT DBA mice, with average cumulative scores of: 27±28 for mice receiving hCD20tg B cells + RTX; 23±25 for mice receiving RTX alone: 27±23 for mice receiving hCD20tg B cells + IgG; and 25±19 for mice receiving IgG alone. An increase in both ankle and paw size was observed in all groups after day 37, however the levels of swelling did not differ between the treatment groups (Figure 7.7a and b). Disease incidence averaged 83±14% for the run, falling within the range expected for DBA/1 mice [335] (Figure 7.7c).

In the IgG treated group a significantly higher concentration of total serum IgG was found compared to the RTX treated group (Figure 7.8a), with this groups also having a significantly higher concentration of total serum IgG1 compared to all other treatment groups (Figure 7.8b). No difference in the levels of total IgG or total IgG1 was seen between any of the other treatment groups. Relative levels of serum CII-specific IgG1 and IgG2a were unchanged between the groups (Figure 7.8c and d, respectively).

The correlation between maximal joint inflammation score and serum levels of CII-specific IgG1 and IgG2a was investigated (Figure 7.9). A significant positive correlation was seen between maximal inflammatory score, and both CII-specific IgG1 and IgG2a subclasses, in the mice given hCD20tg B cells + RTX. A significant correlation was also seen in the IgG control group between maximal joint inflammation score and levels of CII-specific IgG2a, with higher levels of IgG2a seen as maximal scores increased.

T cell proliferation in response to re-stimulation with collagen was also measured. Significantly more proliferation was seen in T cells from mice receiving IgG alone, than those receiving either hCD20tg B cells + IgG, or RTX alone, when cultured with 60μg/ml of CII (Figure 7.10). No other variation in the levels of T cells proliferation was seen

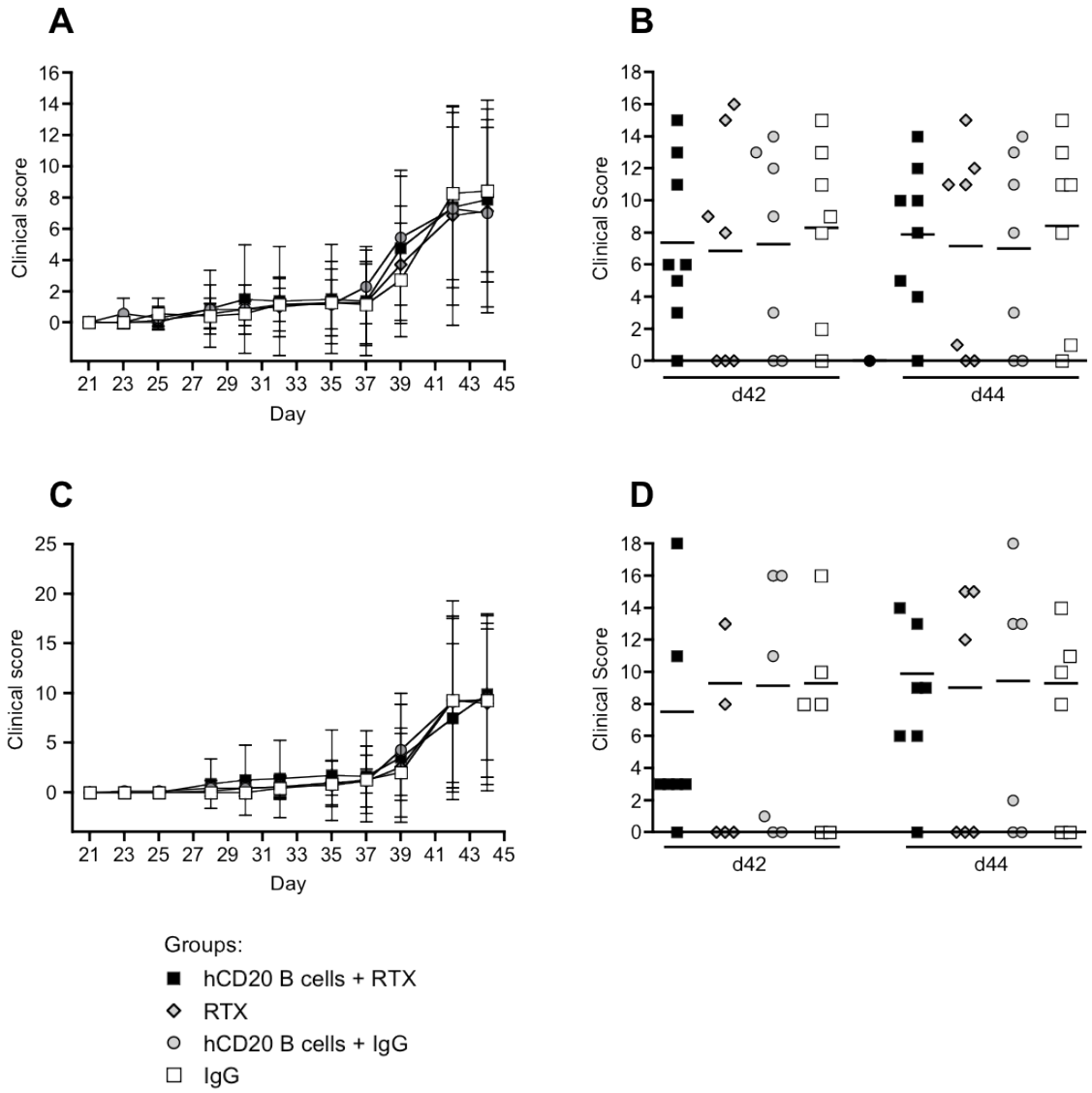

Figure 7.6 Clinical scores of collagen induced arthritis in WT DBA mice adoptively transferred with hCD20tg B cells and treated with Rituximab

On day 0, hCD20tg B cells were adoptively transferred into WT DBA mice via the tail vein, which were then given a single dose of RTX (■), or hIgG (●). Further control mice received RTX of hIgG only (◆ and □, respectively). CIA was then induced in these animals the same day. (**A**) Graph showing the general inflammation scores (16-point scoring system) for all groups. (**B**) Scatter graph showing the general inflammation scores for each animal on days 42 and 42. (**C**) Graph showing the joint inflammation scores (24-point scoring system) for all groups. (**D**) Scatter graph showing the joint inflammation scores for each animal on days 42 and 44. (hCD20tg B cells + RTX group: n=8, for all other groups: n=7, data from a single experiment) Statistics used: Two-way ANOVA performed on complete data sets in (A) and (C), with $p<0.05$ considered statistically significant.

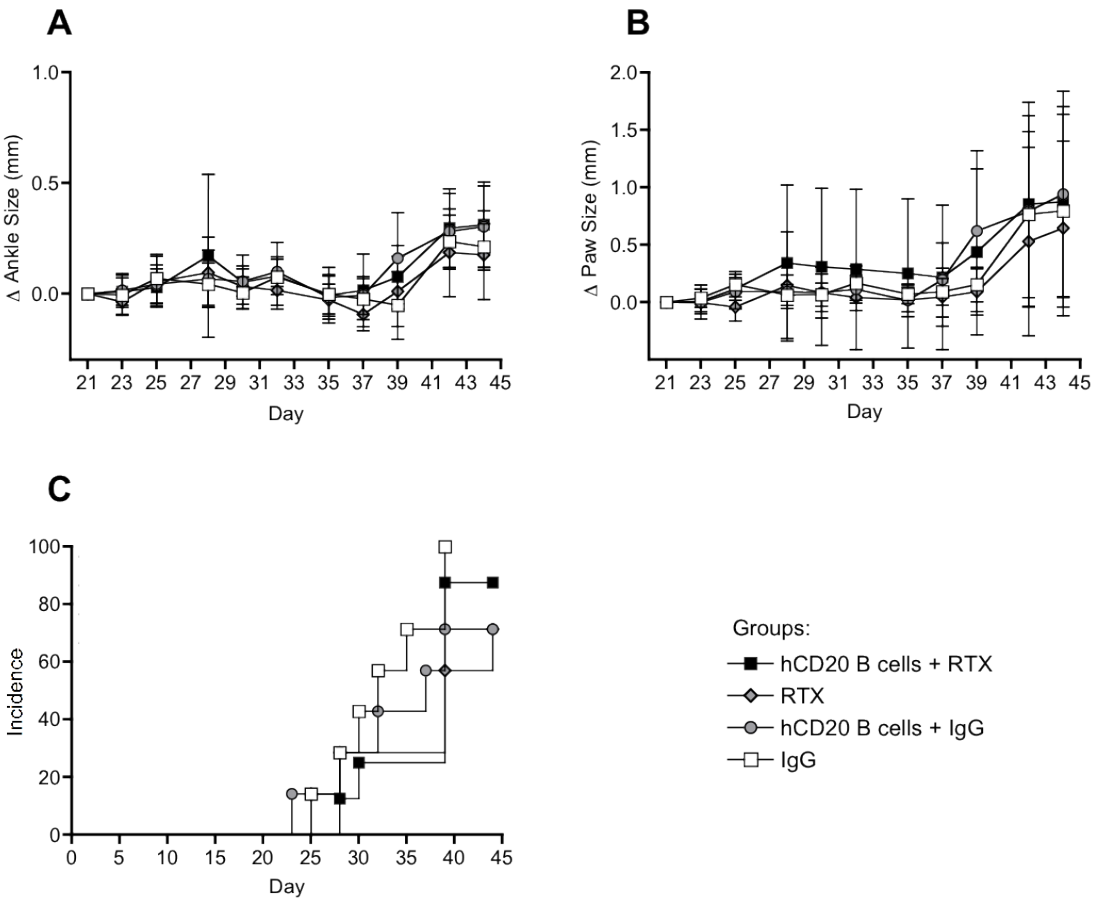

Figure 7.7 Swelling and incidence collagen induced arthritis in WT DBA mice adoptively transferred with hCD20tg B cells and treated with Rituximab
On day 0, hCD20tg B cells were adoptively transferred into WT DBA mice via the tail vein, which were then given a single dose of RTX (■), or hIgG (●). Further control mice received RTX of hIgG only (◆ and □, respectively). CIA was then induced in these animals the same day. (**A**) Graph showing the change in ankle size for all groups. (**B**) Graph showing the change in paw size for all groups. (**C**) Graph showing the incidence of disease in all treatment groups. (hCD20tg B cells + RTX group: n=8, for all other groups: n=7, data from a single experiment) Statistics used: Two-way ANOVA performed on complete data sets in (A) (B) and (C), with $p<0.05$ considered statistically significant.

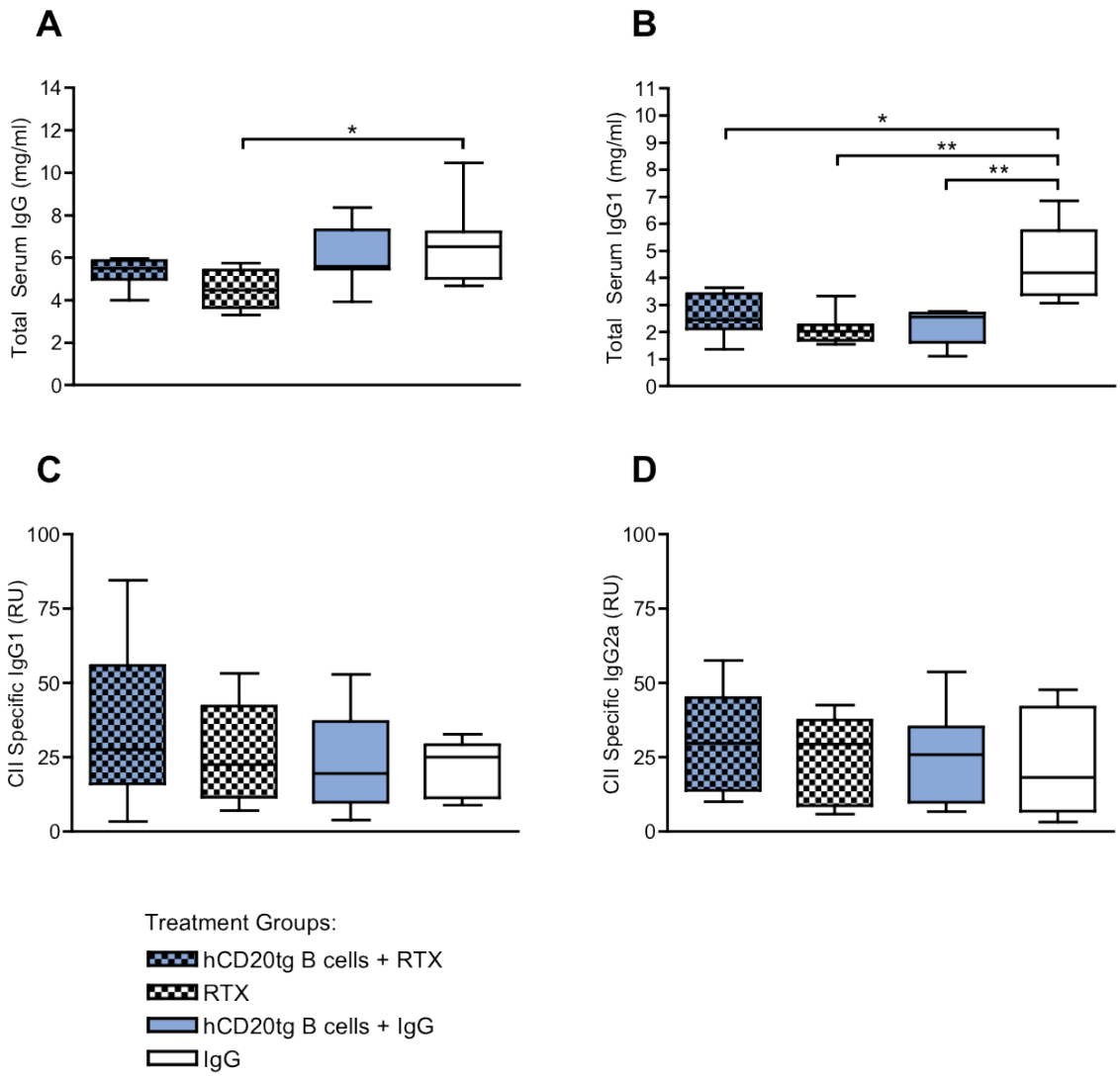

Figure 7.8 Serum antibody titres in WT DBA mice adoptively transferred with hCD20tg B cells and treated with RTX

Mice were culled on d44, blood samples taken and serum IgG titres quantified by ELISA. (**A**) Graph showing the concentration of total serum IgG (mg/ml) for all treatment groups (**B**) Graph showing the concentration of total serum IgG1 (mg/ml) for all treatment groups. (**C**) Graph showing the concentration of CII-specific serum IgG1 (RU = relative units) for all treatment groups. (**D**) Graph showing the concentration collagen type-II specific IgG2a (RU) for all treatment groups. (hCD20tg B cells + RTX group: n=8, for all other groups: n=7, data from a single experiment) Statistics used: One-way ANOVA performed on each complete data set in (A) (B) (C) and (D), followed by Bonferroni's post-test, with * = $p<0.05$, ** = $p<0.01$, and *** = $p<0.001$.

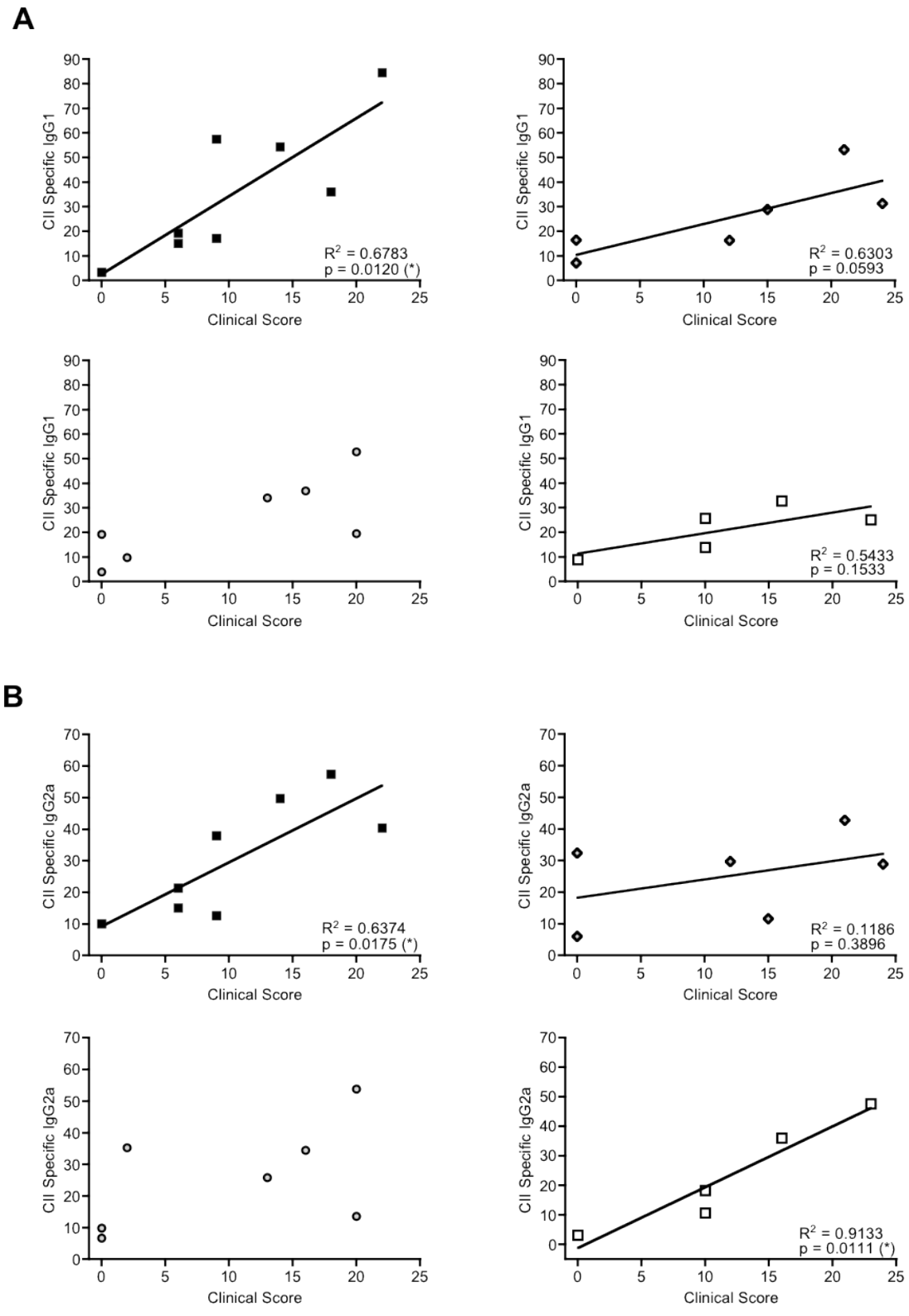

Figure 7.9 Correlation of maximal joint inflammation score with serum titre of collagen-specific IgG1 or IgG2a

(**A**) Graphs showing the correlation of maximal joint inflammation score (24-point clinical score) and CII-specific IgG1 for each group. (**B**) Graphs showing the correlation of maximal joint inflammation score and CII-specific IgG2a for each group. (hCD20tg B cells + RTX ■ (n=8); RTX only ◇ (n=6); hCD20tg B cells + IgG **O** (n=7); IgG only □ (n=5), data from a single experiment). Statistics used: Linear regression and Spearman r tests where shown, with * = $p<0.05$.

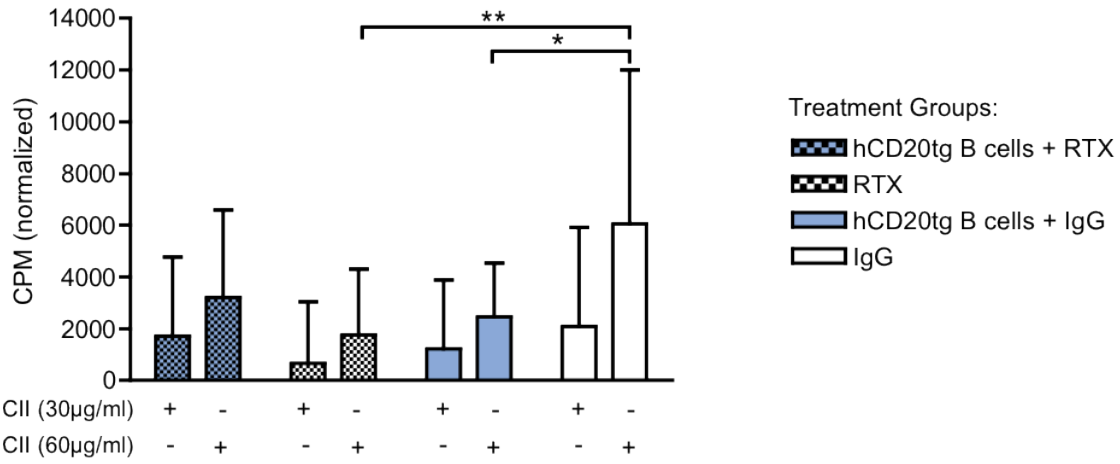

Figure 7.10 Collagen re-stimulation responses
Mice were culled on d42 and peripheral LNs were harvested to allow the investigation of cellular proliferation in response to collagen re-stimulation was investigated. LN cells were cultured *in vitro* ^{3}H-thymdine and varying concentrations of collagen protein to look at specific proliferation responses. Values are normalized to media only controls. CPM = counts per minute. (hCD20tg B cells + RTX group: n=8, for all other groups: n=7, data from a single experiment) Statistics used: One-way ANOVA performed on complete data set, followed by Bonferroni's post-test, with * = $p<0.05$, and ** = $p<0.01$.

between the groups when cells were cultured with 60µg/ml CII, and no differences in proliferation could be detected when the cells were cultured with 30µg/ml of CII.

In this model system, RTX-mediated B cell apoptosis had no effect on the symptoms of CIA as determined by clinical scoring of general- and joint specific inflammation, as well as measurement of ankle- and paw swelling. In the IgG control group, an increase in T cell proliferation was seen, as well as higher levels of total serum IgG and IgG1, however no difference was detected in levels of CII-specific antibodies between any of the groups investigated.

7.2.3 Rituximab treatment of CIA in hCD20tg DBA mice

Once the hCD20tg DBA colony was established, the effects of RTX-mediated B cell depletion on CIA was investigated in this transgenic mouse model. hCD20tg mice have previously been used to explore RTX-mediated B cell depletion in a range of *in vivo* disease models [324,325,358], however this transgenic strain has not yet been used to study RTX-mediated B cell depletion in the context of arthritis. To do this, hCD20tg DBA mice were given a single dose of RTX on day 0, with CIA induced later the same day. WT littermates were included in the run for comparison of disease kinetics.

General inflammation of the paws was detected from day 28 (Figure 7.11a), with joint inflammation being observed from the same time-point (Figure 7.11c). The severity of this inflammation increased over the course of the experiment in all treatment groups. The level of inflammation seen in the hCD20tg mice + IgG was lower than in the other groups, however this difference was not significant. The general inflammation scores and joint inflammation scores of individual animals were also investigated on d40 and d42 (Figure 7.10b, d). All groups contain both high and low responders, with no great difference seen in the numbers between the groups for either scoring system.

Ankle size fluctuated in all groups (Figure 7.11a), with a significant increase in the ankle size of the WT littermates + RTX group seen on day 33, compared to that of the hCD20tg mice + IgG, and on d37 compared to both hCD20tg groups. Paw size peaked on day 37, with the WT littermates + RTX group having significantly more paw swelling than the hCD20tg mice + IgG on days 33, 35, 37 and 40 (Figure 7.11b). Again, the hCD20tg + IgG group were seen to have the least evidence of disease. Although there was no significant differences in disease incidence between the groups, the data indicated that disease incidence may be higher in WT littermates than in hCD20tg mice, with 86% of WT littermates showing signs of arthritis compared to 63% in the hCD20tg mice, falling below the expected levels for DBA mice (Figure 7.11c).

Serum was collected from all mice on day 42, and the absolute concentration of total polyclonal IgG and IgG1 assessed. Relative levels of CII-specific IgG1 and CII-specific IgG2a were also measured. No difference was detected in the concentration of total IgG or total IgG1 between any of the groups (Figure 7.12a, b). Collagen-specific IgG1 and IgG2a levels also showed no difference between groups, however the titres of CII-specific IgG2a seen were more varied in both WT littermate groups compared to the groups consisting of hCD20tg mice (Figure 7.12d).

In order to compare the clinical disease observed in the mice with any sub-clinical pathology the correlation between maximal clinical score for joint inflammation and CII-specific serum antibodies was examined (Figure 7.13). A significant positive correlation was seen between clinical score and CII-specific IgG1 levels in the WT littermates treated with IgG. No other group showed a significant correlation between these parameters.

As a further measurement of sub-clinical disease, post-mortem x-rays were taken of the left hind paw to determine the level of radiographic pathology incurred during the model. Images were captured using a Kodak Fx Pro, and were scored for radiological bone damage. Figure 7.15a shows an overview of the joints included in the scoring system, as well as representative x-rays of a healthy and an arthritic mouse paw. With this scoring system, a score of 1 assigned for evidence of erosions, osteopenia, periostial reactions and loss of joint space in various joints of the paw, and a score of 0 in the absence of evidence of each parameter. A maximal score of 27 was possible. Radiographic scores did not differ between the groups (Figure 7.15b), and no correlation was seen between the radiographic scores and the maximal joint inflammation scores for any of the groups in the run (Figure 7.15c).

From these data it can be concluded that with the treatment regimen used, RTX-mediated B cell depletion in hCD20tg had no effect on CIA severity or progression.

7.2.4 Rituximab treatment prior to induction of CIA in hCD20tg DBA mice

B cell depletion studies have been undertaken in multiple murine models of arthritis, each utilizing a different treatment regimen, with both the dosing and timing of anti-CD20 mAbs administration varying [71,362-364]. In studies using the murine anti-CD20 mAb MB20-16, Yanaba et al showed that B cell depletion before induction of CIA in DBA mice resulted in a different disease course and severity, compared to animals treated after disease onset [362]. We wanted to investigate whether the timing of RTX

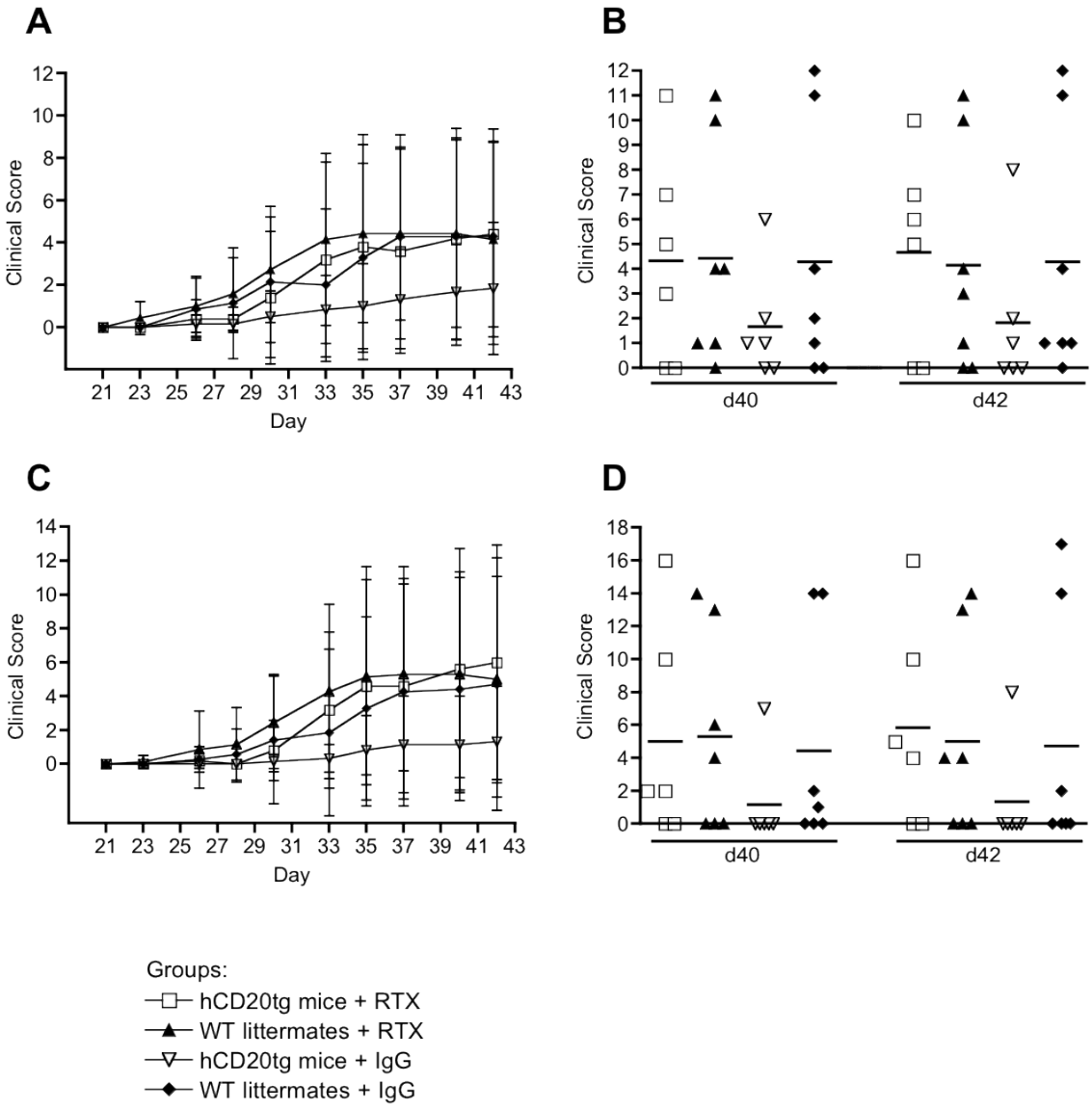

Figure 7.11 Clinical scores of collagen induced arthritis in hCD20tg DBA mice and WT littermates treated with Rituximab

CIA was induced in hCD20tg DBA mice and WT littermates on day 0. The RTX treated hCD20tg and WT littermate groups were given an i.v. injection of RTX on day 0 (□ and ▲, respectively), while control hCD20tg and WT littermate groups received IgG only (▽ and ◆, respectively). (**A**) Graph showing the general inflammation scores (16-point scoring system) for all treatment groups. (**B**) Scatter graph showing the general inflammation scores for each animal on days 40 and 42. (**C**) Graph showing the joint inflammation scores (24-point scoring system) for all treatment groups. (**D**) Scatter graph showing the joint inflammation scores for each animal on days 40 and 42. (hCD20tg + RTX n=5. hCD20tg + IgG n=6, WT littermate groups: n=7, data from a single experiment) Statistics used: Two-way ANOVA performed on complete data sets in (A) and (C), followed by a Bonferroni's post-test, with * = $p<0.05$, and ** = $p<0.01$.

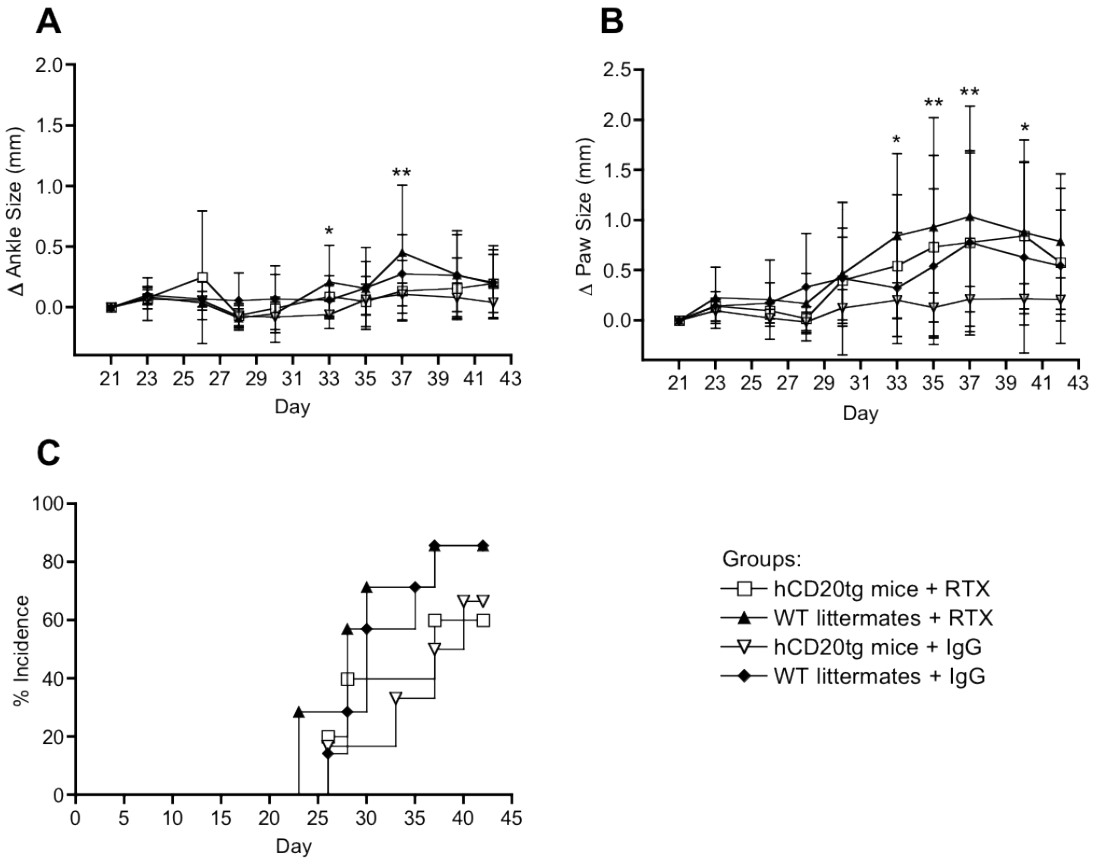

Figure 7.12 Swelling and incidence of collagen induced arthritis in hCD20tg DBA mice and WT littermates treated with Rituximab

CIA was induced in hCD20tg DBA mice and WT littermates on day 0. The RTX treated hCD20tg and WT littermate groups were given an i.v. injection of RTX on day 0 (□ and ▲, respectively), while control hCD20tg and WT littermate groups received IgG only (▽ and ◆, respectively). (**A**) Graph showing the change in ankle size for all treatment groups. (**B**) Graph showing the change in paw size for all treatment groups. (**C**) Graph showing the incidence of disease in all treatment groups. (hCD20tg + RTX n=5. hCD20tg + IgG n=6, WT littermate groups: n=7, data from a single experiment) Statistics used: Two-way ANOVA performed on complete data sets in (A) (B) and (C), followed by Bonferroni's post-test, with * = $p<0.05$ and ** = $p<0.01$.

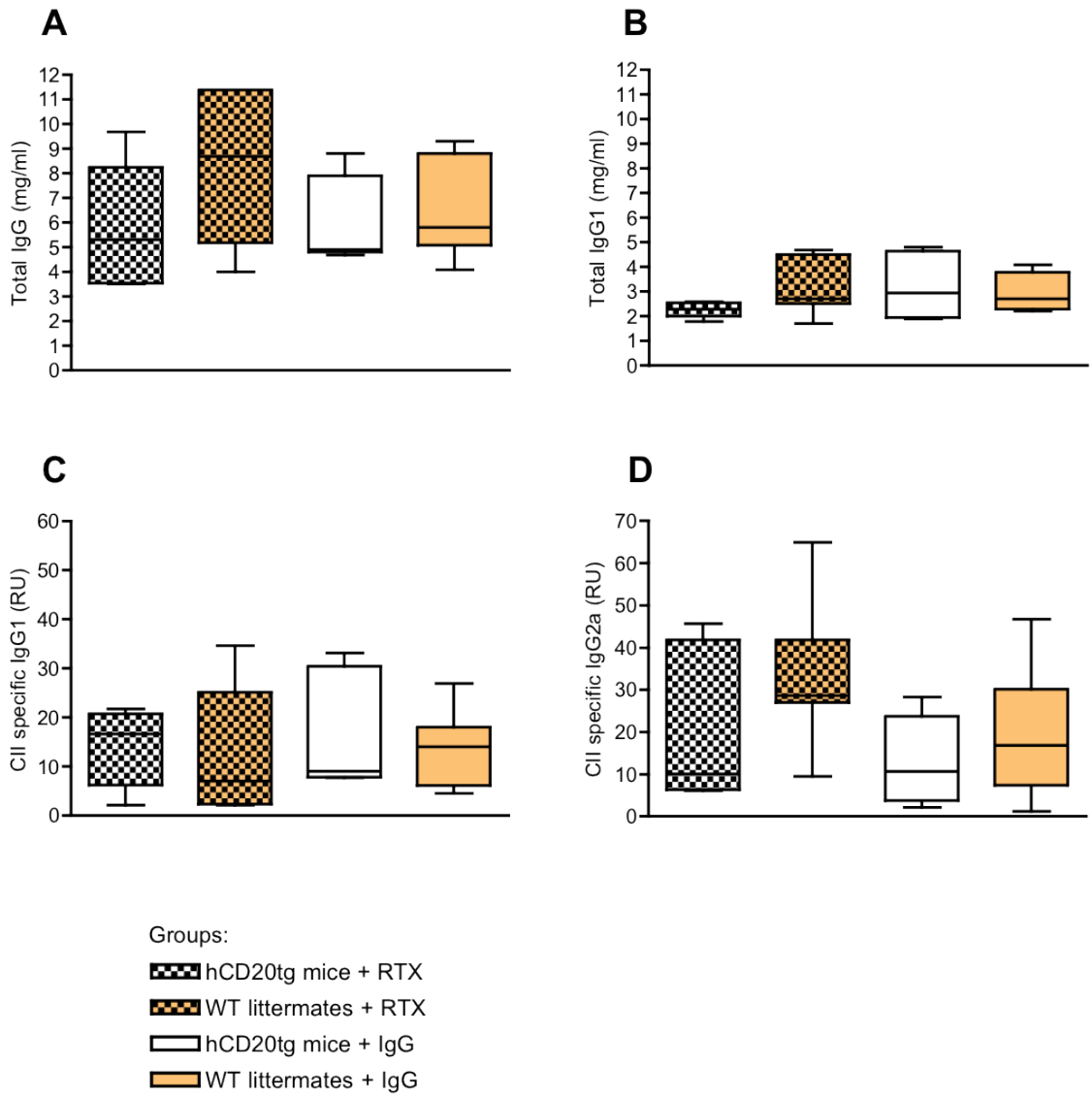

Figure 7.13 Serum IgG antibody titres in hCD20tg DBA mice and WT littermates treated with Rituximab

Mice were culled on d42 and blood samples collected to assay for serum IgG titres by ELISA. (**A**) Graph showing the serum titres of total serum IgG (mg/ml) for all groups. (**B**) Graph showing the serum titres of total serum IgG1 (mg/ml). (**C**) Graph showing the serum titres of CII-specific IgG1 (RU = relative units) (**D**) Graph showing the serum titres of CII-specific IgG2a (RU) (hCD20tg + RTX n=5. hCD20tg + IgG n=6, WT littermate groups: n=7, data from a single experiment) Statistics used: One-way ANOVA, performed on each complete data set in (A) (B) (C) and (D), with $p<0.05$ considered statistically significant.

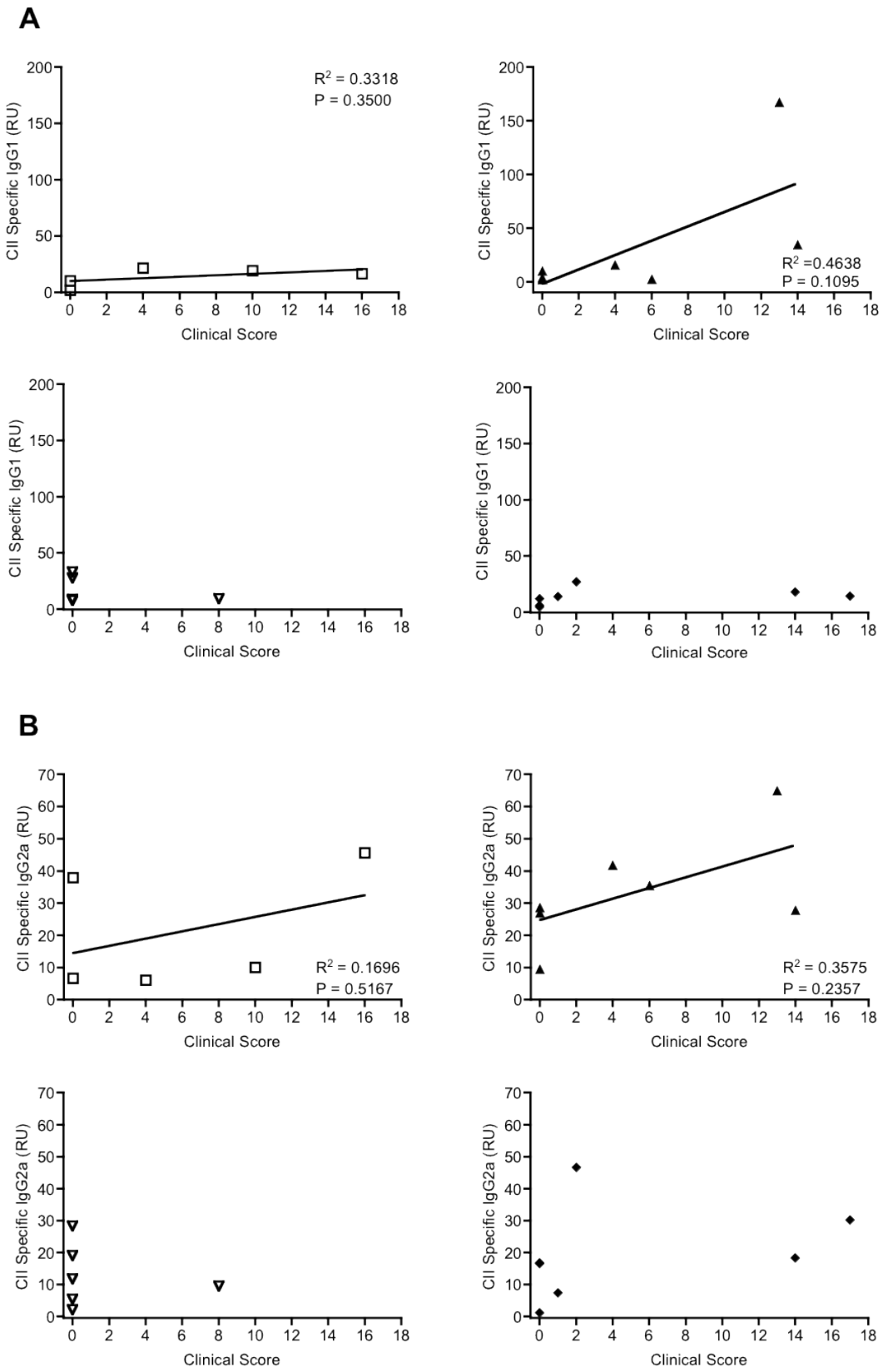

Figure 7.14 Correlation of maximal joint inflammation score and serum titre of collagen-specific IgG in hCD20tg mice and WT littermates

(**A**) Graphs showing the correlation of maximal joint inflammation score (24-point clinical score) and CII-specific IgG1 for each group. (**B**) Graphs showing the correlation of maximal joint inflammation score and CII-specific IgG2a for each group. (hCD20tg mice + RTX (□) n=5, WT littermates + RTX (▲) n=7, hCD20tg mice + IgG (▽) n=6 and WT littermates + IgG (◆) n=7). Statistics used: Linear regression and Spearman r tests where shown, with * = $p<0.05$.

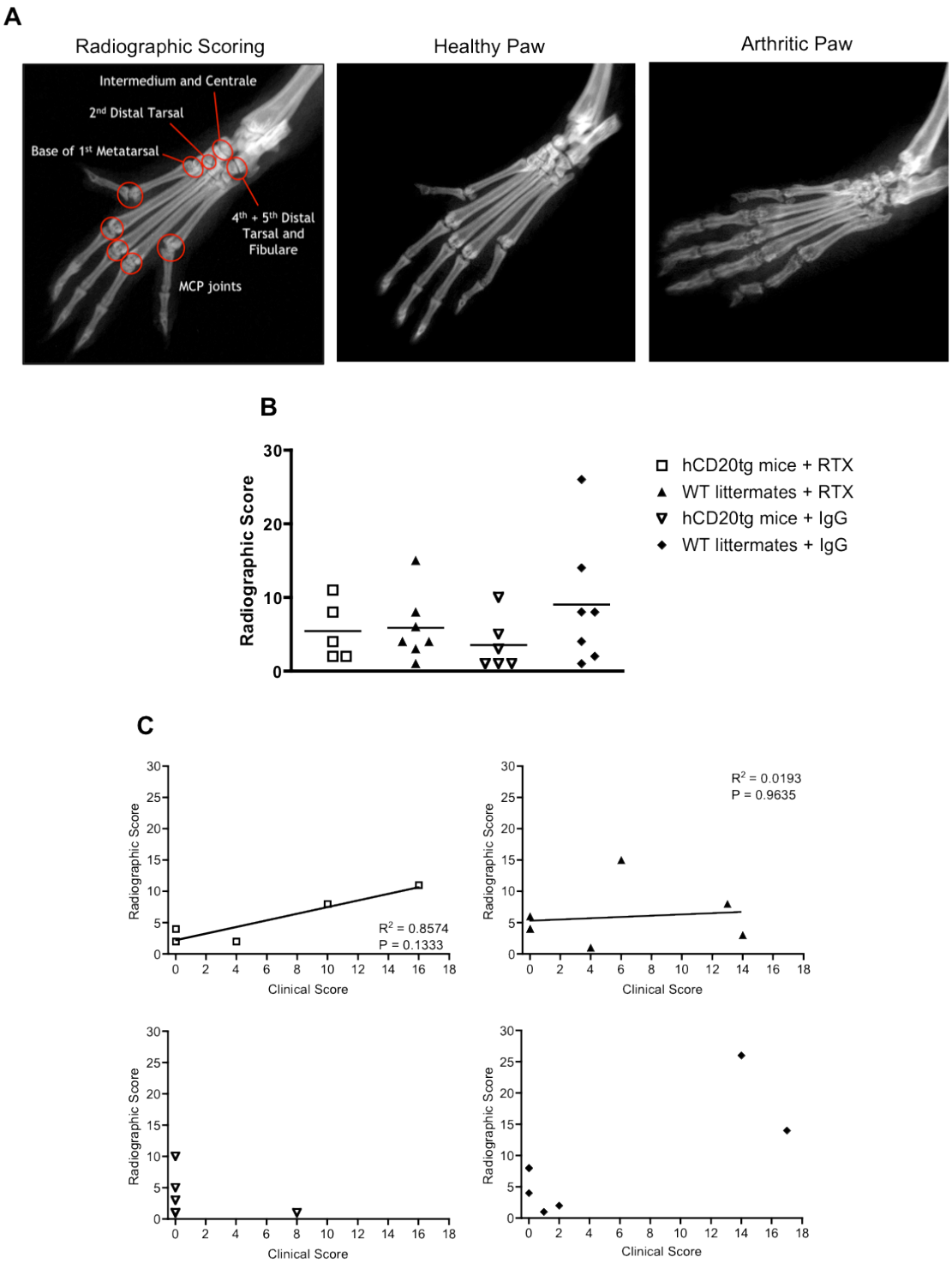

Figure 7.15 Radiographic pathology in hCD20tg mice and WT littermates treated with Rituximab

Mice were culled on d42 and the left hind leg fixed in formalin for 2 weeks. After fixation, legs were x-rayed using a Kodak In-Vivo FX PRO. (**A**) A hind paw x-ray with the joints used for scoring highlighted, followed by a representative x-ray of a healthy animal and an animal with arthritis. (**B**) Graph showing the radiographic scores for each of the experimental groups. (**C**) Graphs showing the correlation of radiographic score and maximal joint inflammation score (24-point clinical scores) for each of the four experimental groups, with the legend shown in (B). (hCD20tg + RTX: n=5, hCD20tg + IgG: n=6, WT littermate groups: n=7) Statistics used: One-way ANOVA performed on complete data set in (B); linear regression and Spearman r tests where shown in (C), with a value of $p<0.05$ considered statistically significant.

treatment would affect the outcome of B cell depletion in CIA. To do this, hCD20tg mice were given a single dose of RTX, four days prior to CIA induction using bovine CII.

Unfortunately, for these runs of CIA the levels of disease incidence was so low in both the treatment group and the control groups that no conclusions about the effectiveness of the treatment regimen could be made. Between the groups an average incidence of only 23% was seen (Figure 7.16e), and no paw swelling detected by either the scoring systems used or measurements taken (Figure 7.16a-d).

After speaking to colleagues about the minimal disease incidence level seen with the initial study undertaken using bovine CII in hCD20tg mice, it was decided to modify the induction protocol used. Previously, mice had been given one single injection of CII/CFA at the base of the tail, while awake. For the second study using this treatment regimen, mice were given the same total amount of CII/CFA but over two injection sites, while anaesthetized. However, this modification did not affect incidence levels seen.

Serum ELISAs were undertaken to detect any potential sub-clinical disease that may have been present in the mice (Figure 7.17), however no differences were detected in the levels of total serum IgG, total serum IgG1, CII-specific IgG1 or CII-specific IgG2a levels between the treatment groups.

With the minimal levels of disease seen in these runs, no conclusions could be made about the effectiveness of RTX-mediated B cell depletion prior to CIA induction in hCD20tg mice.

7.2.5 Effect of the species and supplier of collagen on CIA Induction

In standard CIA protocols available, bovine CII is used for CIA induction in DBA/1 mice, with incidence rates of 80-100% expected [335], while chicken CII is generally only used for disease induction in the less susceptible C57BL/6 mouse strain [365]. For the initial runs of CIA undertaken as part of this project, chicken CII was used due to its availability in the lab. It was then decided to replace this with bovine CII, in an attempt to keep our experiments in line with those previously undertaken by other groups, allowing for a more direct comparison of results. On the transition to bovine CII incidence rates fell dramatically, and so it was decided to more closely examine the effect of the species and supplier of collagen on CIA induction in hCD20tg mice. CIA was induced in hCD20tg mice using either chicken CII, bovine CII from MD Bioscience, or bovine CII from Sigma. Over the two runs undertaken with this variation in disease induction, virtually no disease was seen with only one animal included in the study

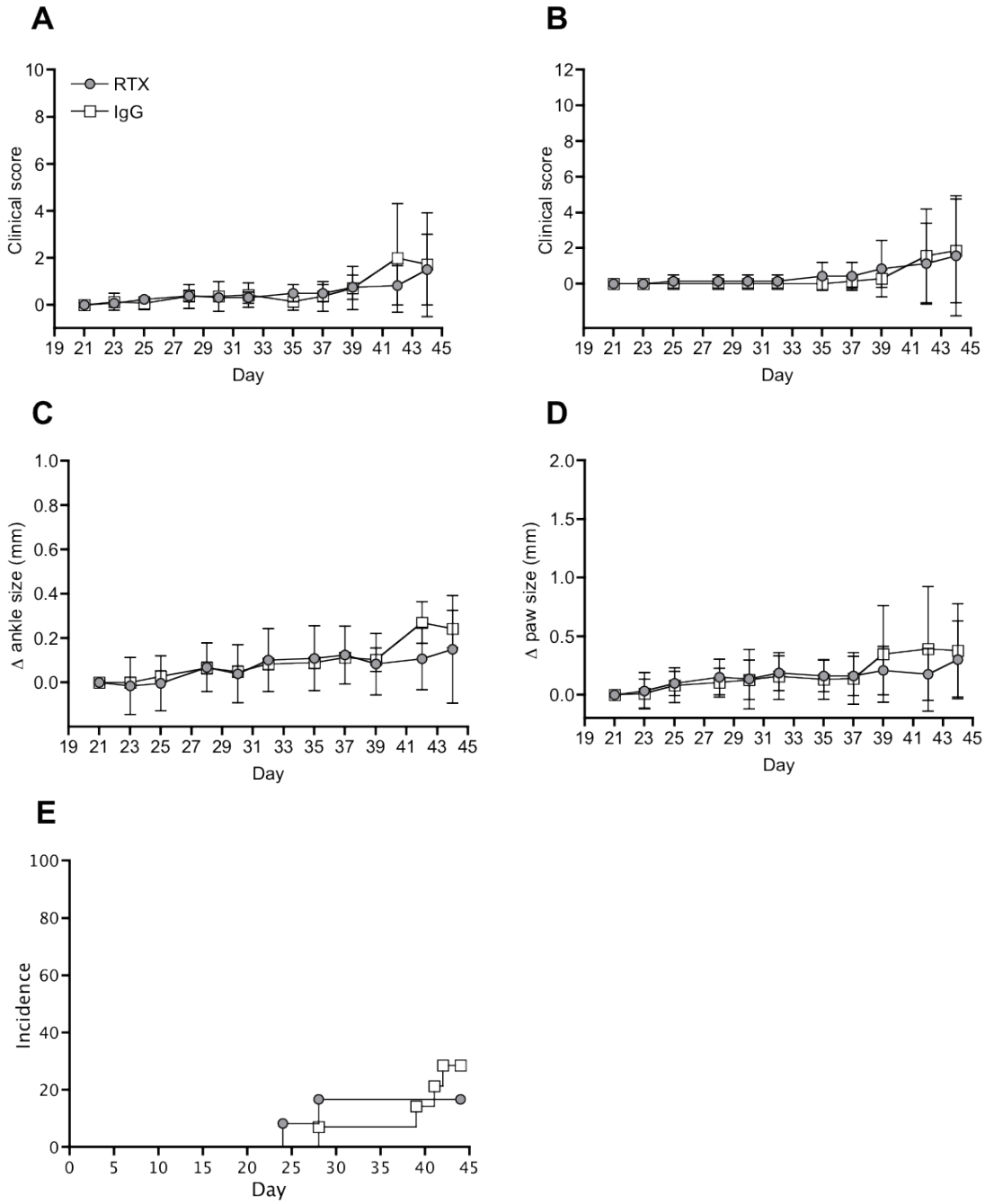

Figure 7.16 Collagen induced arthritis in hCD20tg mice treated with a single dose of Rituximab prior to disease induction

On day -4, hCD20tg DBA mice given a single dose of 100µg of RTX (●), while control mice received polyclonal hIgG (□), and CIA induced in these animals on day 0. (**A**) Graph showing the general inflammation scores (16-point scoring system) for both treatment groups. (**B**) Graph showing the joint inflammation scores (24-point scoring system) for both treatment groups. (**C**) Graph showing the change in ankle size for both treatment groups. (**D**) Graph showing the change in paw size for both treatment groups. (**E**) Graph showing the incidence of disease in both treatment groups. (RTX: n=12; IgG: n=14, data from 2 independent experiments). Statistics used: Two-way ANOVA performed on each compete data set in (A) (B) (C) (D) and (E), with values of $p<0.05$ considered significant.

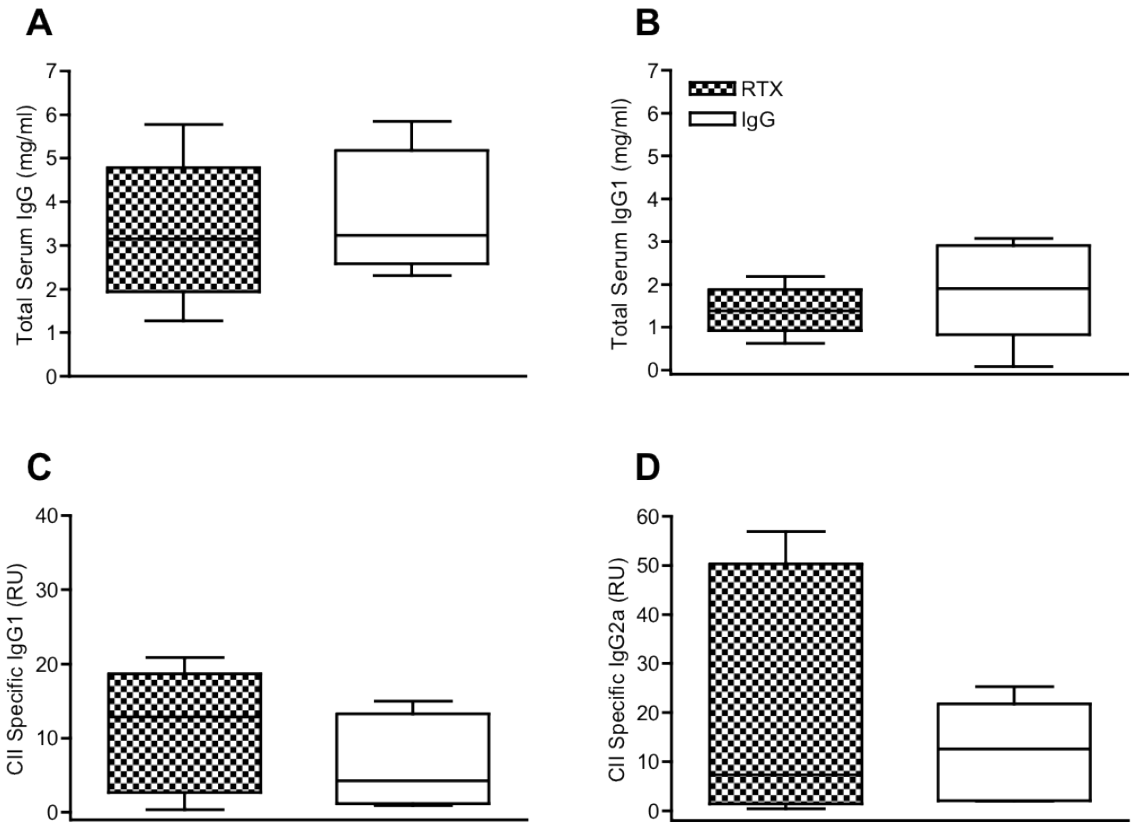

Figure 7.17 Serum antibody titres in hCD20tg mice treated with a single dose of Rituximab prior to disease induction

Mice were culled on d44 and blood samples collected, and serum IgG titres quantified by ELISA. (**A**) Graph showing the serum titres of total serum IgG (mg/ml) for all groups. (**B**) Graph showing the serum titres of total serum IgG1 (mg/ml). (**C**) Graph showing the serum titres of CII-specific IgG1 (RU = relative units) (**D**) Graph showing the serum titres of CII-specific IgG2a (RU) (n=6, data from a single experiment) Statistics used: unpaired T test (RTX-treated vs. IgG-treated) for each data set, with values of $p<0.05$ considered significant.

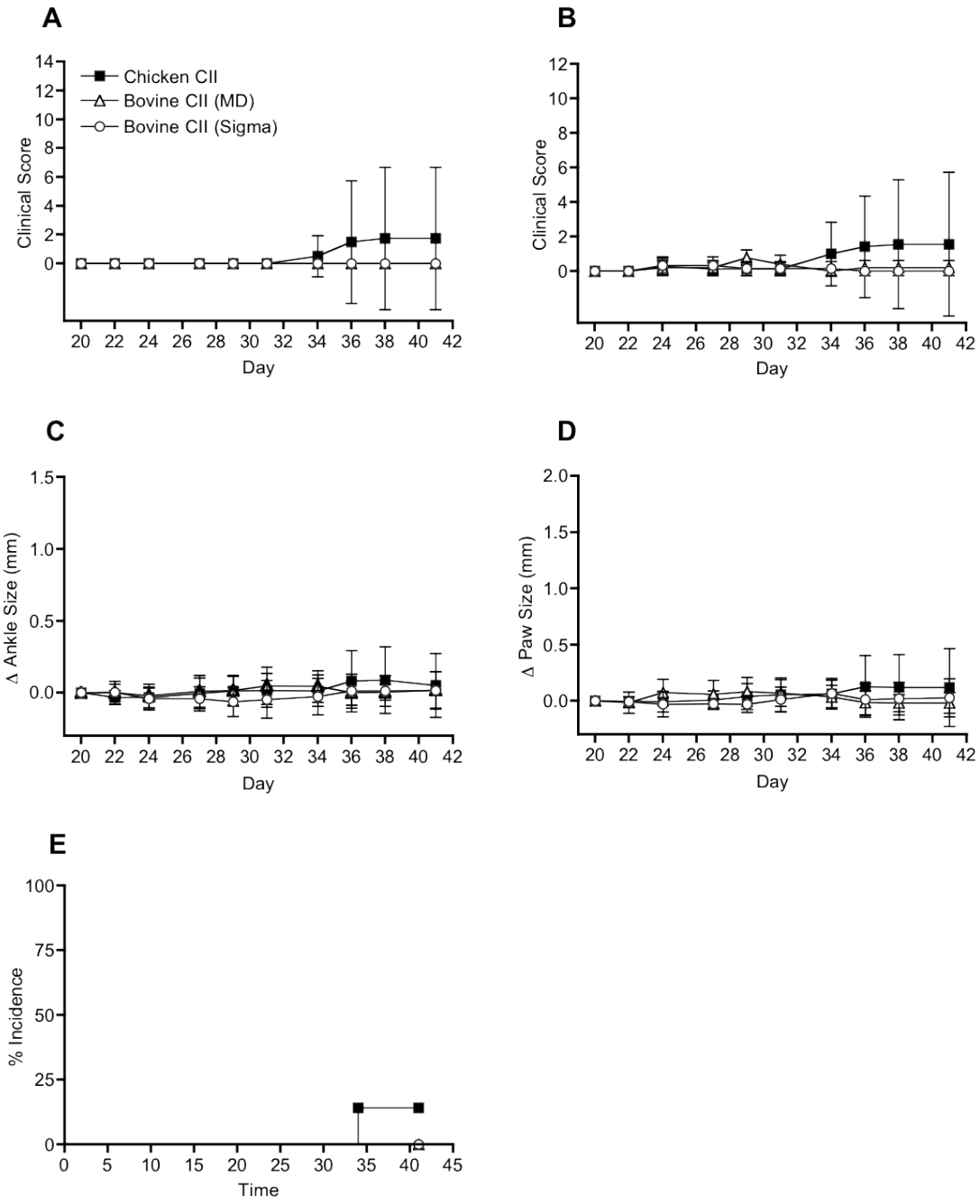

Figure 7.18 Progression of CIA induced with either chicken CII or bovine CII in hCD20tg DBA mice

CIA was induced in hCD20tg DBA mice using either chicken CII (■), bovine CII from MD Bioscience (△), or bovine CII from Sigma (○). (**A**) Graph showing the general inflammation scores (16-point scoring system) for all treatment groups. (**B**) Graph showing the joint inflammation scores (24-point scoring system) for all treatment groups. (**C**) Graph showing the change in ankle size for all treatment groups. (**D**) Graph showing the change in paw size for all treatment groups. (**E**) Graph showing the incidence of disease in all treatment groups. (chicken CII: n=8, MD bovine CII: n=5, Sigma bovine CII: n=6, data from 2 independent experiments) Statistics used: Two-way ANOVA performed on each compete data set in (A) (B) (C) (D) and (E), with values of $p<0.05$ considered significant.

showing any signs of arthritis (Figure 7.18). Between these runs, the person performing the injections was changed to a more experienced investigator to remove the possibility that sub-optimal dosing with collagen was responsible for the reduced incidence seen, however this did not have any effect on disease induction in this setting.

This continued lack of disease in hCD20tg animals induced with CIA meant that no information could be garnered from the runs, and any conclusions on the effectiveness of the various species or suppliers of CII used could not be made.

7.2.6 Comparison of disease in hCD20tg mice and WT DBA mice

In order to examine whether the limited arthritis incidence observed in hCD20tg mice could be due, at least to some extent, to an intrinsic feature of this transgenic strain. CIA was induced in hCD20tg DBA mice bred in house, and WT DBA mice bought in from Charles River, following the same general protocol as previously, with bovine CII used in both the induction and boost injections. However, the protocol used to generate the CII/CFA emulsion was altered, with the emulsion for the initial injections made the day before disease induction, stored overnight at 4^{o}C, and re-emulsified just prior to use. This protocol for emulsion preparation had been seen to increase the effectiveness of CIA induction in C57BL/6 mice (Dr. Darren Asquith, personal communication), and so the decision was made to employ this method for this run. No treatment was given to either group of mice, and no attempt was made to modify the disease course in any way.

The general inflammation scores (Figure 7.19a) and joint inflammation scores (Figure 7.19b) of both groups show very similar disease progression until day 35. After this point the data indicates an increased severity of disease in the WT DBA mice compared to the hCD20tg mice, with the cumulative general inflammation score of 12±10 for the hCD20tg mice, and 20±19 in the WT DBA mice. However due to the variability seen and group sizes used, this increase was not significant. Very little change in hind ankle size (Figure 7.19c) or hind paw size (Figure 7.19d) was observed, and these measurements did not differ between the groups. The incidence of disease was noticeably lower in hCD20tg mice, with 50% of the hCD20tg mice showing signs of arthritis, compared to 75% of the WT DBA mice, however this difference was not statistically significant.

Blood was collected from all mice on day 42 and serum ELISAs undertaken to look at the antibody response in disease. The hCD20tg mice had significantly higher levels of total serum IgG, compared to the WT DBA mice (Figure 7.20a), but levels of total IgG1 were no different between the groups (Figure 7.20b). The relative serum titres of collagen-

specific IgG1 and collagen-specific IgG2a were also investigated (Figure 7.20b and c), with concentration of CII-specific IgG1 and IgG2a similar for both groups.

The correlation of maximal joint score with serum titres of collagen-specific IgG1 and IgG2a was examined. Both hCD20tg and WT DBA mice showed an increase in CII-specific IgG1 on increased disease score (Figure 7.21a), however this correlation was only significant in the WT DBA mice. Surprisingly, in the hCD20tg mice the data indicated a decrease in CII-specific IgG2a on increased disease score, while in WT DBA there was an increase in CII-specific IgG1 on increased disease score, however neither group showed a significant correlation between maximal joint score and CII-specific and serum IgG2a (Figure 7.21b).

Collagen re-stimulation responses were also investigated. Peripheral LNs were harvested on day 42 and cultured *in vitro* in media alone or with either 30µg/ml or 60µg/ml collagen peptide. ^{3}H-thymdine was then added to the cultures and CII-specific proliferation responses quantified. There was no difference in the proliferative responses between the hCD20tg and WT DBA mice at either concentration of collagen used (Figure 7.22), and proliferation did not increase with additional CII in the culture system.

Although a lower incidence of disease in the hCD20tg DBA mice was indicated compared to the WT DBA mice, from these data it cannot be concluded whether hCD20tg DBA mice are less susceptible to CIA than WT DBA mice, with comparable clinical scores and CII-specific serum antibody levels observed in both strains.

7.2.7 T cell priming in hCD20tg mice on CIA induction

With the repeated issues experienced with collagen-induced arthritis in hCD20tg mice, we wanted to understand what may be causing this reduced response. It is known that T cells play a crucial role in disease pathogenesis in experimental arthritis [366,367], and therefore it was decided to look into the levels of T cell priming occurring in hCD20tg mice on disease induction. To do this, hCD20tg mice were injected with bovine CII/CFA on day 0, as in CIA induction, and LN harvested on day 7, with cells used for *in vitro* ^{3}H-thymidine proliferation assays.

LN cells were cultured with either 30µg/ml or 60µg/ml of CB11 CII peptide for 72hr prior to pulsing with ^{3}H-thymidine (figure 7.23). The CB11 peptide is a cyanogen bromide-cleaved fragment of CII, and it has been shown that in experimental arthritis induced with heterologous collagen, the majority of T cell responses are directed

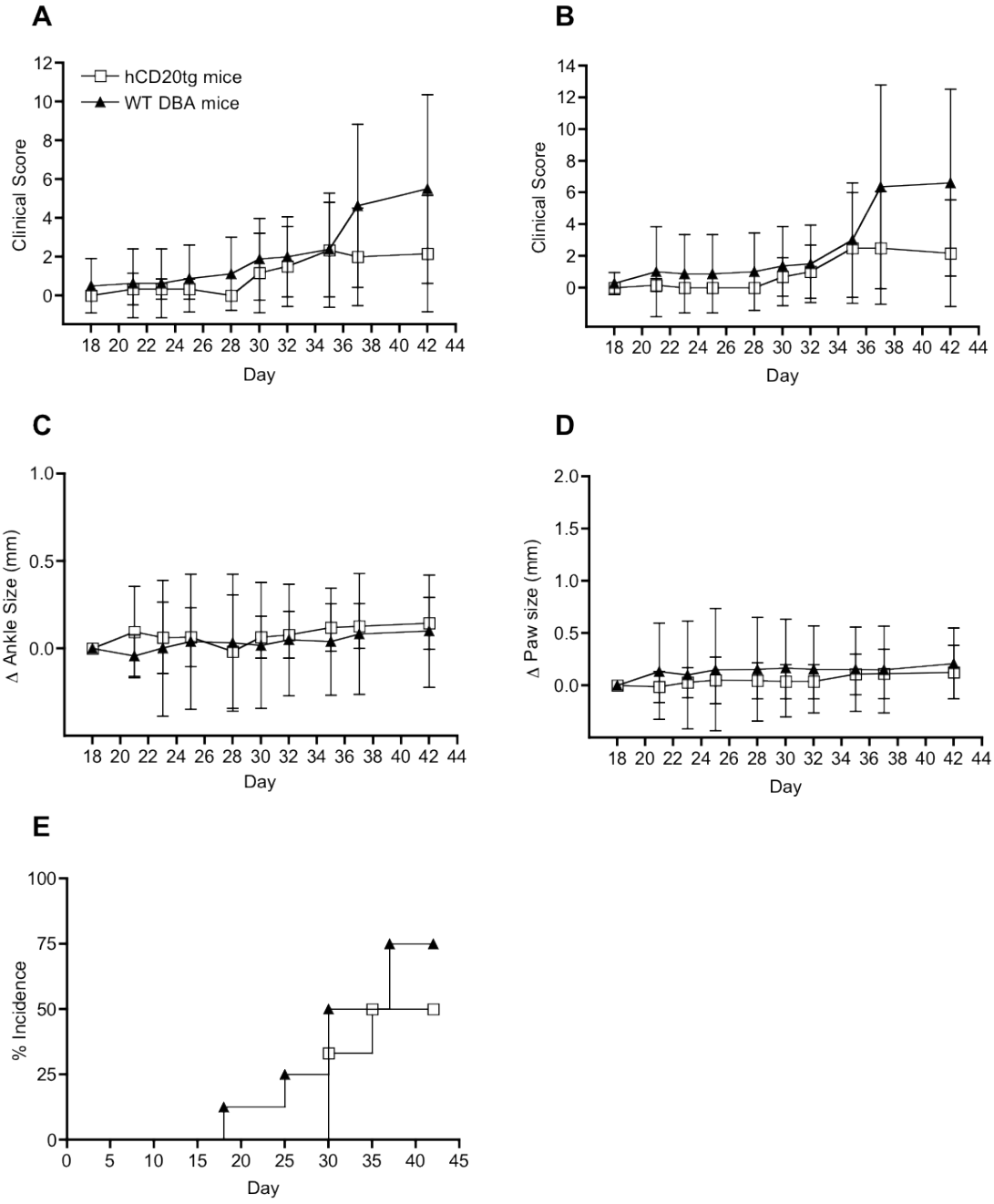

Figure 7.19 Comparison of CIA disease course in hCD20tg DBA and WT DBA mice
CIA was induced in hCD20tg DBA mice bred in-house (□) and WT DBA mice purchased from Charles River (▲). No treatment was administered to either group. (**A**) Graph showing the general inflammation scores (16-point scoring system) for both treatment groups. (**B**) Graph showing the joint inflammation scores (24-point scoring system) for both treatment groups. (**C**) Graph showing the change in ankle size for both treatment groups. (**D**) Graph showing the change in paw size for both treatment groups. (**E**) Graph showing the incidence of disease in both treatment groups. (hCD20tg mice n=6, WT DBA mice: n=8, data from a single experiment) Statistics used: Two-way ANOVA performed on each compete data set in (A) (B) (C) (D) and (E), with values of $p<0.05$ considered significant.

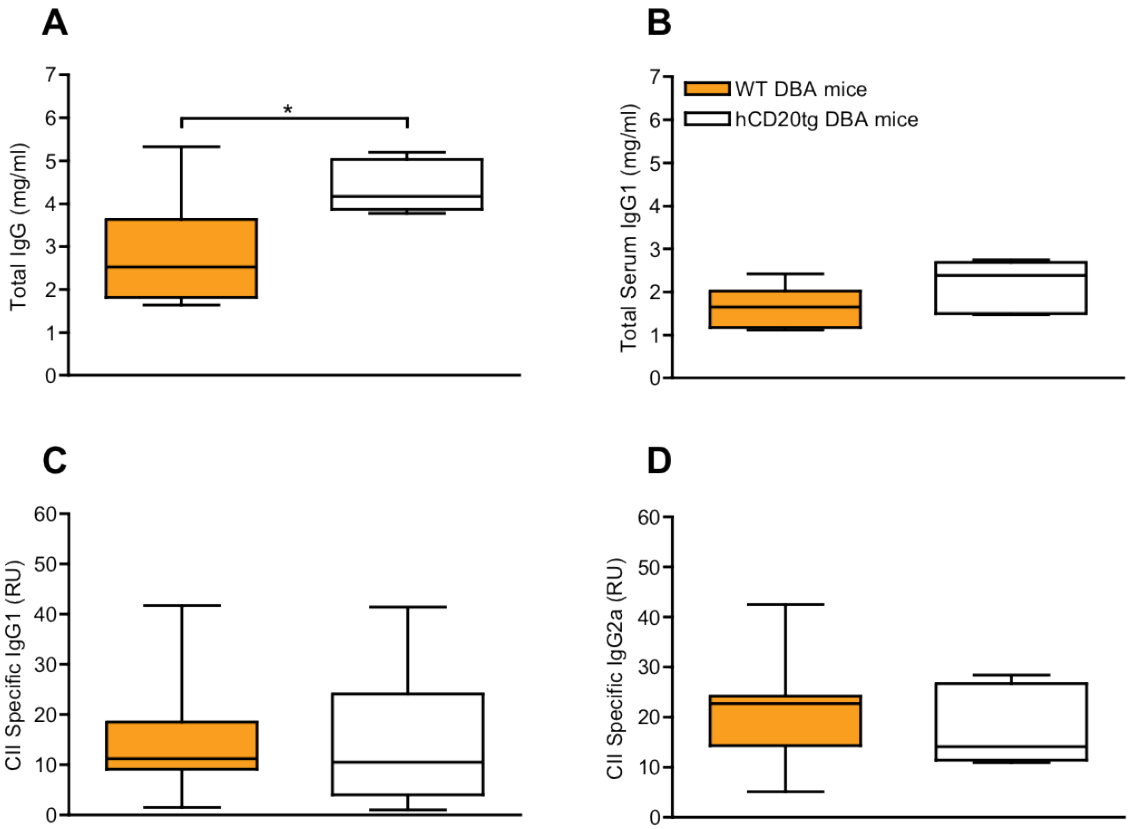

Figure 7.20 Serum antibody titres in hCD20tg DBA and WT DBA mice
Mice were culled on d42, blood samples collected and serum IgG titres quantified by ELISA. (**A**) Graph showing the titres of total serum IgG (mg/ml). (**B**) Graph showing the titres of total serum IgG1 (mg/ml). (**C**) Graph showing the serum titres of CII-specific IgG1 (RU = relative units) (**D**) Graph showing the serum titres of CII-specific IgG2a (RU). (hCD20tg mice n=6, WT DBA mice: n=7, data from a single experiment) Statistics used: unpaired T test (WT DBA vs. hCD20tg mice) on each data set, with * = $p<0.05$.

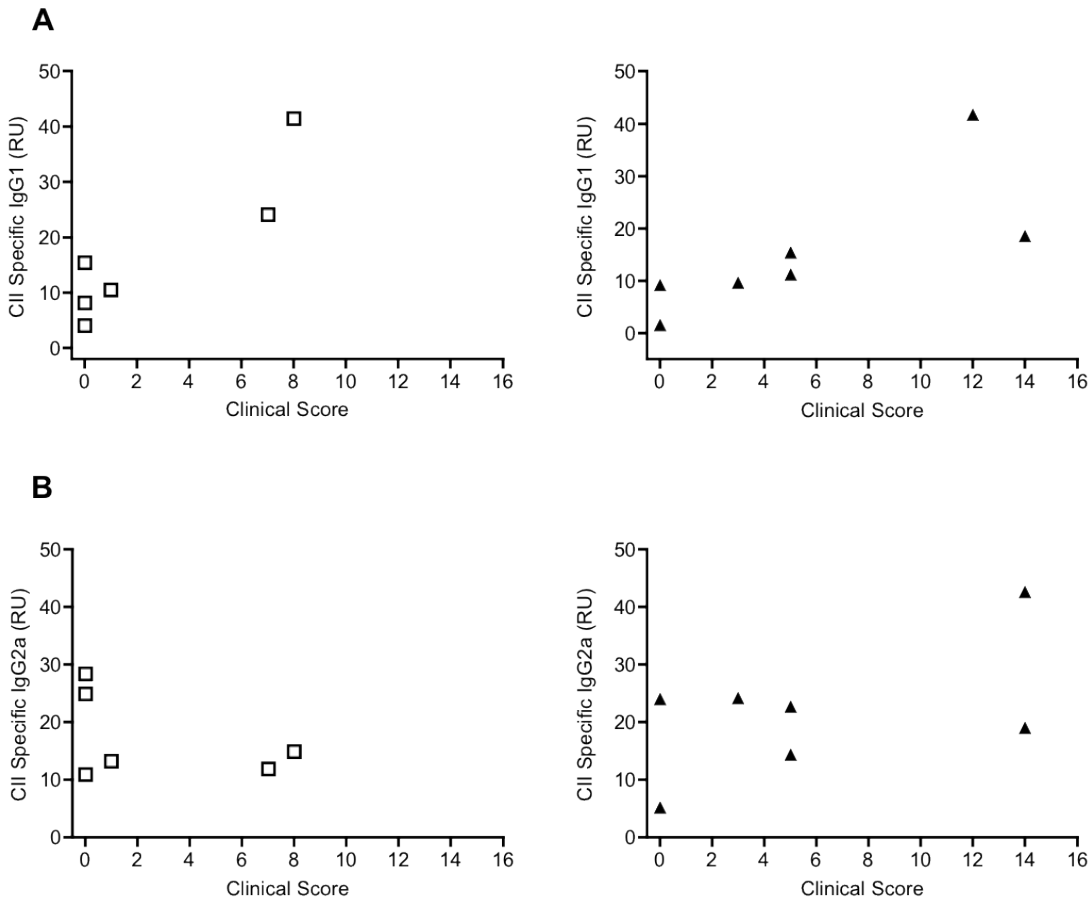

Figure 7.21 Correlation of joint inflammation scores with serum CII-specific IgG1 and IgG2a titres

(**A**) Graphs showing the correlation of maximal joint inflammation score (24-point clinical score) and CII-specific IgG1 for each group. (**B**) Graphs showing the correlation of maximal joint inflammation score and CII-specific IgG2a for each group. (hCD20tg mice (□) n=6, and WT DBA mice (▲) n=7, data from a single experiment)

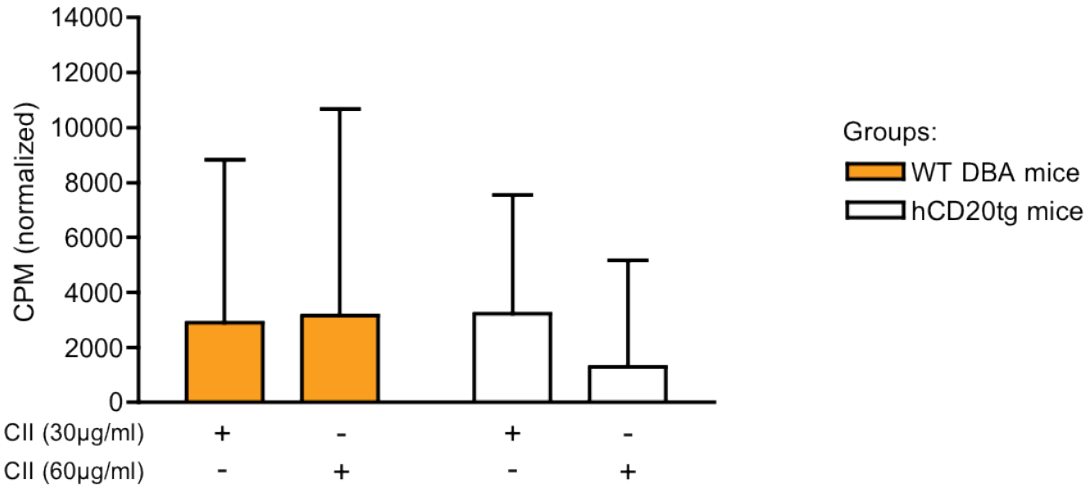

Figure 7.22 Collagen re-stimulation responses in hCD20tg DBA and WT DBA mice
Cellular proliferation in response to *in vitro* collagen re-stimulation was investigated. Peripheral LNs were harvested and cultured *in vitro* with ^{3}H-thymdine and varying concentrations of collagen protein for 72hrs to look at CII-specific proliferation responses. Values normalized to media only controls. CPM = counts per minute. (hCD20tg mice: n=6, and WT DBA mice: n=7, data from a single experiment) Statistics used: One-way ANOVA performed on complete data set, with $p<0.0.5$ considered significant.

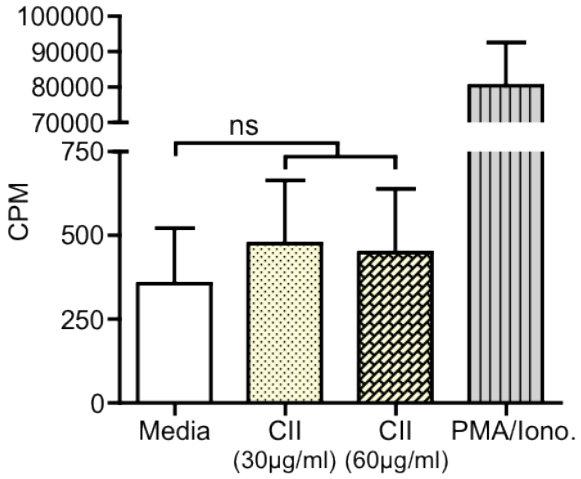

Figure 7.23 T cell recall responses after induction of CIA
CIA was induced in hCD20tg DBA mice on day 0 by i.d. injection of CII/CFA. Mice were culled on day 7, peripheral LNs collected and the LN cells cultured for 72hr with either 30µg/ml or 60µg/ml collagen type-II. Cell proliferation in response to CII-stimulation was quantified using a ^{3}H-thymidine based proliferation assay. PMA/Ionomycin stimulation was used as a positive control. CPM = counts per minute. (n=7, data from a single experiment) Statistics used: One-way ANOVA performed on complete data set, with a value of $p<0.05$ considered significant.

toward epitopes on this particular section of CII [277]. In the hCD20tg mice, no increase in T cell proliferation above background levels was seen in response to CB11 stimulation after induction of CIA (Figure 7.23). This lack of proliferation was not due to an intrinsic defect in the hCD20tg cells, as cells cultured in the presence of PMA and Ionomycin showed a 230-fold increase in proliferation, compared to those cultured in media alone.

These data show that T cell priming did not occur in the hCD20tg DBA mice on CII/CFA injection, indicating that insufficient priming may occur in this transgenic strain at the time of CIA induction. However, without directly comparing this finding with the levels of priming seen in WT DBA mice on CIA induction this cannot be conclusively stated at present.

7.2.8 Expression of MHC I-A^q in hCD20tg mice

The hCD20tg DBA colony used throughout this work was originally generated by backcrossing the hCD20 transgene from hCD20tg C57BL/6 animals onto the DBA background. It is known that susceptibility to CIA is dependant on the MHC haplotype expressed by a strain, with mice expressing either the H-2A^q or H-2A^p haplotypes susceptible to disease induction [368]. WT DBA mice express the MHC I-A^q haplotype, conferring susceptibility to CIA, while C57BL/6 mice express I-A^b. Due to the lack of T cell priming seen in the hCD20tg DBA mice, it was asked whether these transgenic animals shared the same MHC expression profile as WT DBA mice, or if they had retained an element of the original C57BL/6 MHC haplotype. To do this, WT DBA mice, hCD20tg DBA mice, WT DBA littermates and hCD20tg C57BL/6 mice were bled, and the samples analysed for cell surface expression of MHC I-A^q by flow cytometry.

In the blood of WT DBA mice, 98±0.2% of B cells expressed MHC I-A^q (Figure 7.24a and b), with a small but significant decrease in the hCD20tg DBA mice (83±3.4% of B cells MHC I-A^{q+}). A more variable expression pattern was seen in the WT littermates, and as such, the decreased expression seen in the WT littermates was not significant. hCD20tg C57BL/6 mice were included as a negative control, with minimal levels of background staining seen (0.5±0.68% of B cells MHC I-A^{q+}). Although substantial proportions of B cells from both the hCD20tg mice and WT littermates expressed MHC I-A^q, a significant and considerable decrease in the levels of surface expression of MHC I-A^q by these B cells was detected, compared to B cells from WT DBA mice (801±460) (Figure 7.24c), with an MHC I-A^q MFI of 116±18 on B cells from hCD20tg DBA and 185±134 on those from WT littermates.

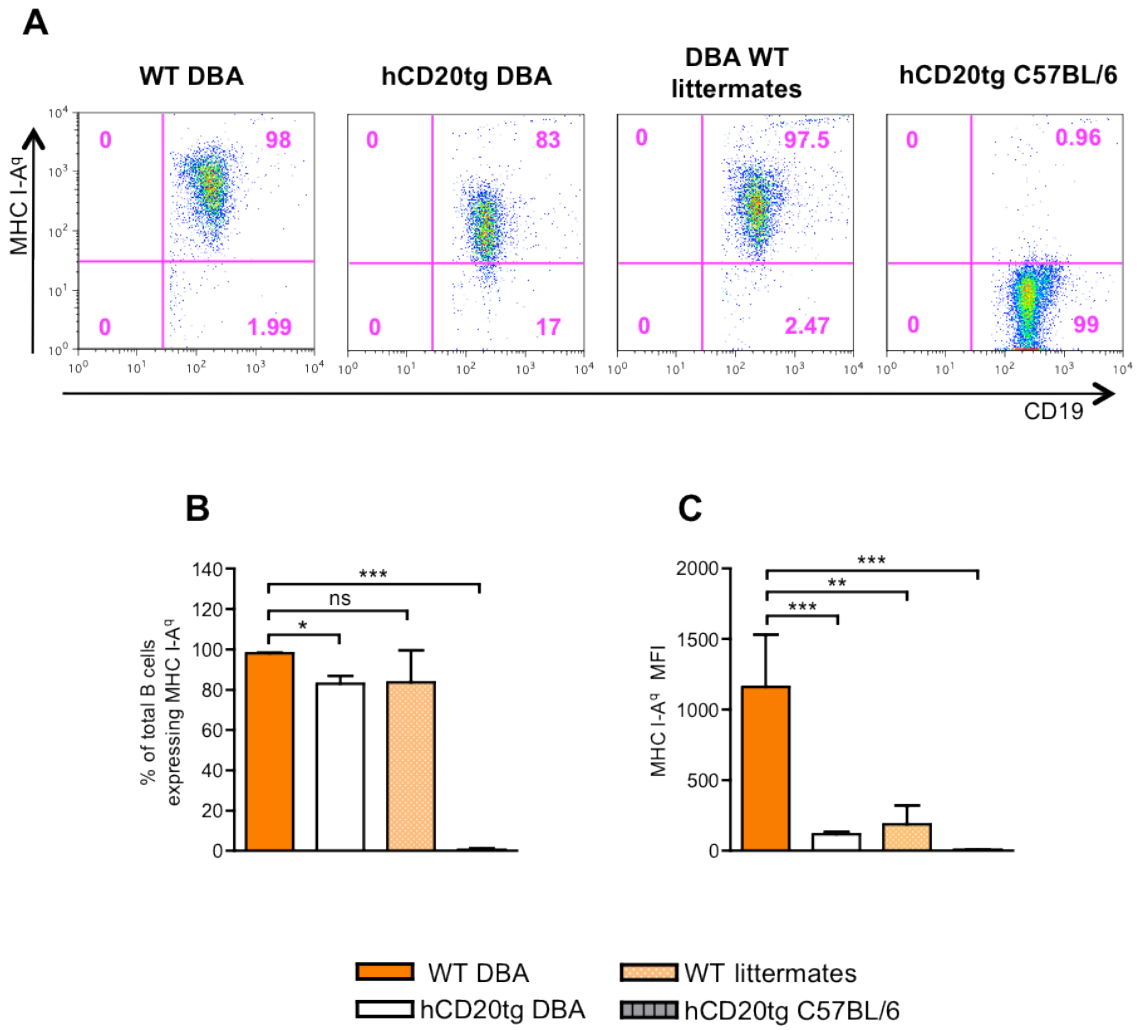

Figure 7.24 hCD20tg DBA mice and WT littermates express significantly less MHC I-A^q than WT DBA mice

Tail bleeds were performed on WT DBA mice, hCD20tg DNA mice, DBA WT littermates and hCD20tg C57BL/6 mice. Cells were stained for lineage markers and MHC I-A^q and analysed by flow cytometry. (**A**) Representative FACS plots showing the relative levels of MHC I-A^q staining in each of the four mouse genotypes. Panels: MHC I-A^q vs. CD19. (**B**) Graph of pooled data showing the percentage of total B cells expressing MHC I-A^q. (**C**) Graph of pooled data showing the relative levels of MHC I-A^q expression on MHC I-A^{q+} B cells. (WT DBA and hCD20tg DBA: n=4, WT littermates and hCD20tg C57BL/6: n=3) Statistics used: One way ANOVA performed on each complete data set in (B) and (C), followed by Bonferroni's post test, with * = $p<0.05$, ** = $p<0.01$ and *** = $p<0.001$.

These findings demonstrate that there is minimal MHC I-A^q expression in hCD20tg DBA mice compared to WT DBA mice, which could explain the poor T cell priming seen on CIA induction in this transgenic strain.

7.2.9 Delayed-type hypersensitivity responses in hCD20tg mice

Due to the challenges encountered with the induction of reliable and reproducible CIA in hCD20tg DBA mice, it was decided to explore the option of using a more general model of inflammation; a delayed-type hypersensitivity (DTH) assay. To induce a DTH response, hCD20tg DBA mice were immunized systemically with OVA/CFA in the scruff and then challenged with heat-aggregated OVA (HAO) in the left footpad 14 days later (OVA/HAO group). Before the introduction of any treatment regimens intended to modify the course of the DTH response, a basic protocol was established in the lab, with control mice receiving only the initial OVA/CFA injection (OVA/PBS group), only the HAO challenge (PBS/HAO group), or left naïve. The change in paw thickness was measured at 24 and 48hr post challenge using calipers, and cells from the draining LN harvested at the 48hr time-point and used to assess T cell cytokine production in response to OVA re-stimulation *in vitro*.

At 24hr post footpad challenge, the OVA/HAO group showed an average increase in footpad size of 0.34±0.2mm (Figure 7.25a). This increase was larger than that seen for any of the control groups (naïve: 0.05±0.13mm; PBS/HAO: 0.18±0.16mm; OVA/PBS; 0.13±0.1mm), however it did not reach significance with the number of animals used. By 48hr post challenge, paw inflammation had resolved back to baseline levels in all groups.

When cytokine production in response to *in vitro* OVA re-stimulation was investigated, it could be seen that T cells from the OVA/HAO group produced significantly more IL-2 than those from any of the control groups (Figure 7.25b), with an average IL-2 increase of 65.5±41.4pg/ml above background levels, compared to 10.1±19.9pg/ml in the naïve group, 21.1±10.7pg/ml in the PBS/HAO group and 15.3±18.8pg/ml in the OVA/PBS group.

These data demonstrate that a DTH response can be elicited in hCD20tg mice as detected by paw swelling and antigen-specific IL-2 production, however larger group sizes are needed in order to achieve significance for all parameters assessed.

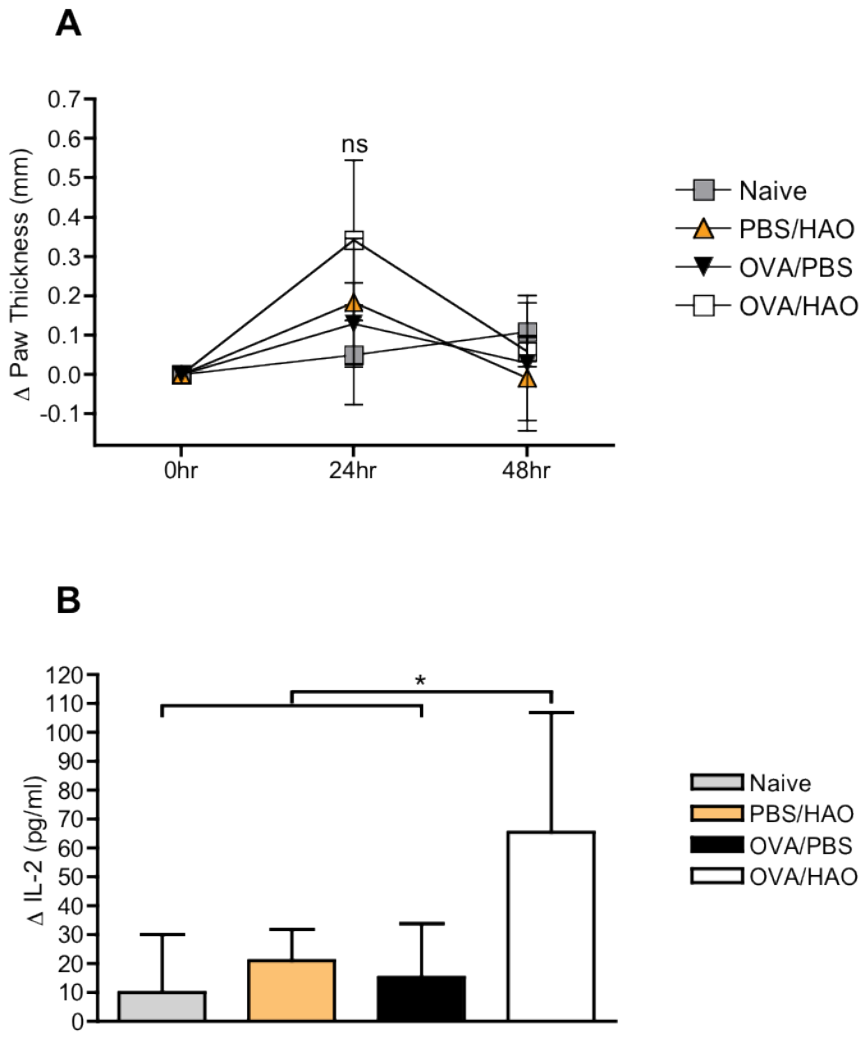

Figure 7.25 Basic DTH model in hCD20tg DBA mice
Mice were immunized with OVA/CFA s.c. in the scruff and 14 days later challenged with heat-aggregated OVA (HAO) in the left footpad. Control mice received only the initial OVA/CFA injection, only the HAO challenge, or were left naïve. Hind paw thickness was measured at 24 and 48hr post challenge using calipers. Mice were euthanized 2 days after HAO challenge, and cells from the draining lymph node harvested and used to assess *in vitro* re-stimulation responses. (**A**) OVA-specific increase in footpad thickness (mm) at baseline (0hr) and 24hr and 48hr post challenge for all groups. (**B**) IL-2 production (pg/ml) by draining LN cells after *in vitro* re-stimulation with OVA. Levels of IL-2 normalized to media only controls. (n=9, data from two independent experiments) Statistics used: One-way ANOVA performed on complete data sets in (A) and (B), followed by Bonferroni's post-test, with * = $p<0.05$.

7.3 Discussion

- To investigate our hypothesis that RTX-mediated B cell depletion introduces temporary tolerance to the immune system, *in vivo* disease models were utilised.
- Due to technical issues no conclusions could be made about the ability of apoptotic B cells or RTX treatment to ameliorate CIA, with the discovery that hCD20tg DBA mice express very little MHC I-A^q on the surface of their cells a possible explanation for this.
- These results demonstrate that although the hCD20tg DBA mice are suitable for use in RTX-mediated B cell depletion studies, due to their MHC haplotype they are not ideal for use in CIA. As such, an alternate *in vivo* model is needed for future studies, with a DTH model successfully established in the lab.

Many hypotheses have been put forward to explain how RTX treatment exerts its beneficial effects in RA, however a definitive answer has still not been reached, and it is probable that there will not be one single mechanism, but several, which when combined help to re-introduce a balance to the immune system. In this chapter, two different *in vivo* models were utilized in an attempt to investigate the complex, and potentially wide-reaching effects of RTX-mediated B cell depletion in a more physiological setting.

Treatment with RTX results in the long-lasting depletion of $CD20^+$ B cells [81], with several mechanisms involved including complement-dependent cytotoxicity (CDC), antibody-dependent cellular cytotoxicity (ADCC), and direct apoptosis of B cells [238]. It is known that apoptotic cells can have an immunosuppressive effect on the immune system [157,158], and it was this aspect of RTX-mediated B cell depletion we wanted to investigate.

It has previously been shown that apoptotic cells (AC) can modulate the immune response and have a protective effect in rodent models of arthritis. Intra-articular injection of apoptotic thymocytes prior to arthritis induction is able to inhibit the onset of immune complex-mediated arthritis in BALB/c mice [369]. This inhibition is attributed the decreased production of chemo-attractant proteins by synovial lining macrophages after ingestion of the AC, resulting in reduced immune cell infiltrates in to the joints and decreased joint inflammation. It has also been shown that systemic administration of apoptotic thymocytes can markedly suppress disease in several models of arthritis. Work by Gray et al has shown that apoptotic thymocytes, given intravenously (i.v.) up to 1 month before the induction of CIA, have a protective effect

on WT DBA mice and inhibit the development of severe arthritis in this model [172]. Systemic treatment with apoptotic thymocytes can also suppress antigen-induced arthritis in C57BL/6 mice, and it has been shown that this suppression is dependent on natural IgM [370]. In the rat model of streptococcal cell wall arthritis, intraperitoneal injection of apoptotic thymocytes at the time of arthritis induction results in decreased proinflammatory responses by macrophages, and reduced disease severity [188]. These studies demonstrate the beneficial effects of AC administration on disease severity in arthritis models, however apoptotic thymocytes are utilized as the model AC for all of these investigations. To examine whether apoptotic B cells have the same ability as apoptotic thymocytes to modulate disease course in a model of arthritis, WT DBA mice were adoptively transferred with apoptotic B cells on the day of CIA induction, and disease progression monitored.

In this experimental set up, no effect on CIA severity or progression was seen on i.v. irradiated apoptotic B cell administration. These results could indicate several things. The first, and perhaps most obvious, is that apoptotic B cells do not have the same modulatory capacity as apoptotic thymocytes in this disease model. However, we have shown in previous chapters that in an *in vitro* system, the interaction of apoptotic B cells with bone marrow derived macrophages (BMDM) has comparable effects on BMDM function as the interaction of apoptotic thymocytes with BMDM, indicating that apoptotic B cells do not differ from apoptotic thymocytes in their immunomodulatory ability. The reductionist nature of *in vitro* assays means that the results gained in these settings can differ from those seen *in vivo*, and so it could be argued that the ability of apoptotic B cells to modify BMDM is purely an artefact of the *in vitro* culture system. However, without the inclusion of an apoptotic thymocyte treatment group in the present study, it is impossible to know whether the lack of effect seen on apoptotic B cell administration is due to an inability of apoptotic B cells to modulate the immune system, or if the previous findings using apoptotic thymocytes cannot be replicated using this model in our hands.

Although several different arthritis models have been utilized previously to investigate the effects of apoptotic thymocytes on disease all with similar outcomes, the diverse findings between this and previous studies may still be explained by differences in experimental protocols. As CIA was used for the work being discussed in the current chapter, I will limit comparisons of experimental protocol to the 2007 paper by Gray et al, who also used the CIA model in DBA mice [172]. In their paper, the investigators gave a series of three injections of AC, totalling $20x10^6$ apoptotic thymocytes, with the first injection given on the day of disease induction and the others on the following 2 days. In our study, a maximum of $5x10^6$ AC were given in one single injection, just

prior to disease induction. It may be the case that the numbers of apoptotic B cells given in this study were not enough to suppress the immune response on disease induction, and that with a larger number of cells an effect would be noticeable. Giving AC in multiple injections over the course of several days, rather than in one single dose, may also increase the efficacy of this type of treatment. AC are rapidly cleared from the system, with professional phagocytes initiating uptake of AC immediately on contact, and full digestion of ingested cells occurring within 2hr of initial uptake [371]. Even in settings where professional phagocytes are overwhelmed by the number of AC present, clearance will still occur in time periods of less than 10hr as non-professional phagocytic cells are also able to ingest AC, although only after they have undergone further cell surface changes [371]. This means that when AC are administered over several days, they will be present in the system for a longer period of time, allowing more AC-immune cell interactions before clearance occurs, and therefore increasing the opportunity for immunomodulation to occur. In order to fully state whether these experimental differences could account for the variation in responses seen, a further study would need to be undertaken, modifying the present protocol to fit that of the previous work undertaken, allowing a direct comparison of the effects of apoptotic thymocytes and apoptotic B cells.

CIA is affected by environmental issues, and this sensitivity may have obscured potential findings. Within all groups included in this study, a relatively low disease incidence was observed. As previously stated, incidence levels of 80-100% are expected on induction of CIA in DBA mice [335], however in this run incidence above 60% was not seen in any treatment or control group, contributing to the variability seen in clinical inflammation scores. In those animals in which disease was observed, the severity within each group was not consistent between animals, indicating that even in those animals where induction of disease was successful, the efficiency of induction was inconsistent. It has previously been observed that serum levels of CII-specific IgG2a positively correlates with CIA pathology in both mice [372] and rats [373]. In this study, a correlation between CII-specific IgG2a serum titres and maximal inflammation score was only noted in the PBS control, with all other groups only showing a positive correlation between CII-specific IgG1 serum titres and clinical pathology. This indicates that the majority of animals included in the study did not have a pathogenic humoral response toward CII taking place, even if clinical symptoms were apparent, as although these animals showed increased levels of CII-specific IgG1, this subclass of IgG is non-pathogenic and therefore not indicative of an arthritogenic response. This general lack of correlation between CII-specific IgG2a and clinical pathology highlights the inconsistency of disease induction within this run. Together, these findings suggest that with larger treatment groups, there is the potential that differences between groups may be resolved. Due to

these concerns, drawing a firm conclusion as to the ability of apoptotic B cells to modulate the immune responses in CIA may be premature at this time.

We next went on to model the effect of RTX-mediated apoptosis of B cells in a CIA setting. To do this, B cells isolated from hCD20tg mice were adoptively transferred into WT DBA mice, which were subsequently treated with a single dose of RTX. Once cell transfer and treatment were complete, disease was induced. As shown in the previous chapter, RTX, a human-specific anti-CD20 mAb, is not able to bind murine CD20, and therefore does not bind B cells from WT littermates, or any WT mice. This model, therefore, allows selective depletion of the transferred hCD20tg B cells, while leaving the endogenous WT B cell population intact.

No differences between the treatment and control groups were seen in clinical inflammation scores or measurement of swelling, however the control groups given IgG alone had significantly higher serum levels of both total IgG and total IgG1. The half life of endogenous IgG in the serum of mice ranges from 4-8 days [374], and in humans from 7-21 days [375]. Although in this study human polyclonal IgG was administered to mice, it can be expected that the clearance of the exogenous immunoglobulin would not exceed that of endogenous IgG. The long half-life of IgG in the blood is dependant on the interaction of IgG with the neonatal Fc receptor (FcRn), with binding inhibiting the break down of IgG, and it has been shown that excess concentrations of IgG in the blood lead to saturation of available FcRn, resulting in the degradation of unbound excess IgG in the lysosomes [376,377]. In this way, elevated levels of serum IgG lead to increased IgG catabolism, and therefore a shortened half-life [378]. As serum was collected from the mice 42 days after the administration of polyclonal IgG, this increase in serum IgG levels was not likely to be due to the administration of exogenous IgG. This increase in serum IgG, as well an increased proliferative response to collagen re-stimulation, indicates that some level of sub-clinical response occurred in this group of mice after CIA induction. However, as increased levels of CII-specific IgG subclasses were not detected, it can be concluded that this response was not specifically directed at collagen, as would be expected in CIA, and was a general inflammatory response, possibly due to the continued presence of CFA at the original injection site. The lack of disease modulation in the hCD20tg B cell + RTX group indicates that RTX-mediated B cell apoptosis on this scale is not sufficient to alter the course of arthritis in WT DBA mice.

The effect of RTX treatment of CIA in hCD20tg DBA mice was then investigated. RTX treatment in this transgenic mouse strain results in depletion of the majority of B cells from the body, and is therefore a closer representation of what would occur in the

treatment of rheumatoid arthritis patients. To date, the depletion of B cells with Rituximab in CIA has not previously been undertaken. Huang et al utilized hCD20tg K/BxN mice to investigate RTX mediated B cell depletion in a spontaneous model of murine inflammatory arthritis. The hCD20tg K/BxN were given weekly doses of RTX, commencing at 5-8weeks of age, after the onset of arthritis, with treatment resulting in the depletion of short-lived CD20-expressing plasma cells, and decreased serum titres of pathogenic auto-antibodies directed toward glucose-6-phosphate isomerase, however no improvements in clinical scores and ankle swelling were seen compared to controls [364]. In all other available literature, B cells depletion studies in murine arthritis models have utilized anti-mouse CD20 antibodies [71,267,362,379], or have targeted other B cell-specific markers, such as CD22 [380]. Using RTX rather than a mouse homologue, allows the study of the interactions between this monoclonal antibody and B cells, and the resulting effects of the B cell depletion which may not be correctly represented by the use of anti mouse-CD20 antibodies. When hCD20tg DBA mice were administered a single dose of RTX on the day of CIA induction, no improvement of disease severity or progression could be detected when compared to control groups.

Previous work by Yanaba et al has shown that in mice, B cells depletion prior arthritis induction, resulting in a lack of B cells at the time of CIA initiation, will delay disease onset. However, depletion of B cells at the time of arthritis onset (day 35 in the model used) rather than on CIA induction, did not significantly ameliorate clinical disease compared to control animals [362]. Due to these findings, it was decided to modify the RTX treatment regimen used in the hCD20tg DBA mice to explore whether RTX mediated B cell depletion prior to, rather than at the time of, arthritis induction would have a beneficial effect on CIA severity. For these experiments, hCD20tg DBA mice were given a single dose of RTX on day -4, with disease induced on day 0. Unfortunately in both runs undertaken with this treatment regimen, a lack of disease incidence was seen in all groups, and therefore no conclusions could be drawn as to the effectiveness of this treatment protocol. These runs of CIA were both induced using bovine CII, rather than chicken CII, as previously used. This change in induction protocol should not have resulted in this severe drop in incidence levels, as bovine CII is the standard species used for induction of CIA in DBA mice [335], with chicken CII generally only used in the less susceptible C57BL/6 mouse strain [365] and was only chosen initially due to its availability in the lab. To investigate whether this dramatic decrease in incidence was due to the CII species used, CIA was induced in hCD20tg DBA mice using either chicken or bovine CII. As with the runs undertaken to look at RTX treatment prior to disease induction, extremely low incidence rates were observed in all of the groups, with the majority of mice showing no disease symptoms whatsoever in both test runs undertaken. As relatively good incidence levels had previously been achieved using

chicken CII in hCD20tg mice, these results were unexpected. Varying aspects of the disease induction process were altered throughout the CII test runs, as well as the runs intended to investigate RTX treatment prior to disease induction to try to figure out what was causing these problems with incidence: mice were given their initial CII dose over two i.d. injections rather than just one; mice were anaesthetised during the initial CII/CFA injection rather then left conscious; the investigator performing the injections was changed; along with the species and supplier of collagen used being altered. Mice used for all runs were of the recommended age for use in CIA models [335], and were kept on an anti-pinworm diet, as it is known that infection with helminths, such as pinworms, can alter the immune response in mice resulting in an lessening of symptoms in a variety of disease models including CIA [reviewed in [381]. However, disease induction remained minimal.

In previous runs using the chicken CII to induce CIA in both hCD20tg DBA mice and WT littermates, it was noted that the hCD20tg DBA mice tended toward a lesser severity of disease, as well as a lower disease incidence. When hCD20tg DBA mice and WT littermates were treated with RTX on the day of CIA induction, with IgG used as a control, a significant increase in both ankle and paw size was observed in the WT littermates treated with RTX, compared to the hCD20tg DBA mice treated with IgG. As these were both control groups, and neither treatment in those particular genotypes should have modified disease course in any way, this altered disease severity could be attributed to intrinsic differences between these mice. Although decreased disease severity was not evident in the group of hCD20tg DBA mice treated with RTX compared to WT littermates, the data does indicate a lower incidence of disease in both hCD20tg DBA groups compared to the WT littermate groups. Along with these findings, it was noted that all the CIA runs undertaken which resulted in minimal incidence of disease were carried out in hCD20tg DBA mice. It was decided to attempt one last run of CIA to compare arthritis induction in hCD20tg DBA mice with WT DBA mice bought in from Charles River. Bovine CII was again used for disease induction, the protocol for emulsion preparation was altered to one used by other members of the department to induce CIA in the less susceptible C57BL/6 mice (Dr Darren Asquith, personal communication). Instead of emulsifying the CII and CFA on the day of injection and using it straight away, it was prepared the day before injection and then re-emulsified just prior to use. This technique helps to ensure that a fully homogenized emulsion is prepared, reducing the chance of the components of the emulsion separating out after injection, which can result in lower disease incidence and contributes to the formation of ulcers at the site of injection. Although a large variability in disease was seen for both strains of mice, and no significant difference was seen in disease severity or incidence between the groups, the data does suggest that hCD20tg mice show a decreased severity of arthritis

and a lower incidence of disease compared to the WT mice. If repeats were undertaken to increase group sizes these differences may well become significant.

We then went on to explore possible reasons for this reduced response to CIA induction in hCD20tg DBA mice. It is known that T cell responses are vital to disease pathogenesis in rodent models of arthritis [366,367], and also play a major role in the pathogenesis and perpetuation of RA [382]. Our data show that after CII/CFA injection, T cells from hCD20tg DBA mice on do not proliferate in response to *in vitro* CII re-stimulation, indicating that insufficient T cell priming may occur on induction of CIA in this transgenic strain. T cell priming in CIA is dependent on the successful presentation of immunodominant peptides derived from CII by MHC molecules of specific haplotypes [368], with WT DBA mice expressing the MHC I-A^q haplotype, conferring susceptibility to CIA. Flow cytometry was used to investigate whether hCD20tg DBA had a reduced level of MHC I-A^q expression compared to WT DBA mice. The proportion of B cells from hCD20tg mice expressing MHC I-A^q was only slightly less than that of B cells from WT DBA mice, however when the expression levels of MHC I-A^q on these cells was investigated it could be seen that the hCD20tg B cells expressed this MHC II molecule at severely reduced levels, compared to their WT counterparts. Along with the T cell recall responses seen in hCD20tg mice, this finding points toward the possibility of there being an issue with T cell priming on CIA induction in this transgenic strain.

This lack of expression of a susceptible MHC haplotype also helps to explain the drop in incidence seen on transition from chicken CII to bovine CII in the induction protocol. Chicken CII is used to induce CIA in less susceptible C57BL/6 mice, and so the use of this species of collagen in the initial runs undertaken using the hCD20tg mice allowed a relatively good level of disease induction to be achieved. Once the collagen species was changed to the less potent bovine CII, incidence rates fell rapidly. However, when the CIA runs comparing collagen species in disease induction were undertaken, chicken CII was also unable to induce disease in hCD20tg mice. The most likely explanation for this sudden lack of disease on induction with chicken CII is that a sub-standard emulsion was prepared for the initial injections. This theory is supported by the fact that when bovine CII was used for the final CIA run comparing disease in hCD20tg and WT DBA mice, moderate arthritis was inducible in this transgenic strain when using an adapted protocol for emulsion preparation which had previously been shown to improve incidence levels in the less susceptible C57BL/6 mice.

Although an understanding of the complications involved in inducing arthritis in hCD20tg DBA mice had been reached, due to the lack of reliability and reproducibility with CIA, it was decided to move to an alternate mouse model. The model chosen was a DTH

assay, as although it is not an arthritis model, it would allow the investigation of our hypothesis in an *in vivo* model of inflammation. A basic DTH protocol was set up in the lab, with the aim of ultimately using it to investigate the potential re-establishment of tolerance after RTX treatment. A DTH response could be elicited in the hCD20tg DBA mice as detected by paw inflammation and swelling, however the change in footpad size seen was not significant compared to controls with the numbers of animals used. If a treatment group were to be included in this model, much larger group sizes would need to be used in order for any change in swelling to reach significance. To ascertain the group sizes needed, a power calculation was undertaken, with a two-sided alpha of 5%, and a power of 0.9 used. The mean value for paw swelling entered into the calculation was 0.18mm, with 0.34mm as the expected mean paw swelling after DTH, and a SD of 0.2mm. The values used were taken from the initial DTH assays undertaken. With these parameters it was calculated that a minimum of 17 mice per group would be required to detect a change in paw swelling. This means that for each DTH run undertaken, a minimum of 34 mice would be needed to allow inclusion of a treatment group plus one control group, with numbers rapidly rising with each subsequent control group deemed necessary. The hCD20tg mice used throughout this work are not commercially available, and arise from a heterozygous colony maintained in house. This means that breeding such a number of age-matched animals would be a huge undertaking, with multiple new breeding pairs needing to be set up, and a high number of unwanted WT littermates also generated alongside the desired transgenic animals. As a result, it was decided that this would not be feasible in the time frame left and no further DTH models were set up.

The aim of this chapter was to investigate our hypothesis that RTX-mediated B cell depletion may introduce a temporary tolerance to the immune system in an *in vivo* system, by utilizing animal models. The arthritis model was initially chosen for this, however after initial variability in runs, incidence levels became so low as to make the results meaningless. The reasons for this sharp decline in incidence, as well as a continued partial resistance of the hCD20tg mice to CIA induction, were explored, and the decision was made to move away from this model. DTH assays were successfully established in the lab, however due to the high number of animals needed to allow detection of significance and the time remaining in the project, this protocol was not pursued. Due to the challenges encountered while working with these animal models, no real progress was made in regards to furthering our understanding of RTX-mediated B cell depletion and the effects this has on the immune system in an *in vivo* setting. However, I was able to gain extensive experience in working with a range of *in vivo* models, including one not previously established in the lab, as well as broadening the understanding of the hCD20tg DBA strain used throughout this project.

Chapter 8: Summary

AC are able to modulate the immune system, dampening inflammation and eliciting anti-inflammatory responses by phagocytes as a consequence of interaction and uptake. RTX is an anti-CD20 monoclonal antibody used as a treatment in several autoimmune diseases, including RA. Treatment results in B cell depletion, with B cell apoptosis known to contribute to RTX-mediated B cell death. However the simple removal of pathogenic B cells from the system does not seem to account for all the beneficial effects of this biologic in the treatment of autoimmunity.

Multiple theories have been put forward to explain the beneficial effects of RTX treatment in autoimmunity, however a full understanding of all the processes involved has still not been reached. It is plausible that there will not be one single mechanism, but several, which, when combined, help to re-introduce a balance to the immune system. We have hypothesized that one of the potential mechanisms of action of RTX is the re-introduction of temporary tolerance to the immune system.

If apoptosis of B cells is caused as a result of RTX-mediated B cell depletion, these apoptotic B cells will be cleared by APC, with the binding and engulfment of apoptotic B cells inducing a range of anti-inflammatory responses in the APC. The phagocytosed B cell, and any antigens it has previously internalized, will be degraded, and presented by the APC in a local environment that is now anti-inflammatory, and therefore skewed toward tolerance. If the apoptotic B cell is an autoreactive cell which had previously taken up antigen, specifically auto-antigens the RA response is directed toward, presentation of this arthritogenic antigen in a non-inflammatory, tolerizing environment may result in the re-introduction of temporary tolerance in a dysregulated system, akin to the resolution stage of a non-chronic immune response.

In the preceding chapters steps were taken to begin to investigate the possibility of this hypothesis, with a focus on the role of apoptotic B cells and their immunomodulatory capacity.

Throughout this work, apoptotic B cells underwent similar levels of interaction with macrophages, and had comparable ability to alter macrophage phenotype and function, as the other apoptotic cells examined. Although the effects of AC are now known to be more complex than originally anticipated, this finding indicates that apoptotic B cells have the capacity to modulate the immune response, with the potential to exert anti-inflammatory effects on the system. Although far from conclusive, these preliminary results open up the possibility that in the setting of RTX-mediated B cell depletion, the generation of sufficient numbers of apoptotic B cells may be able to dampen down inflammation and help to halt the progression of autoimmunity.

The ability of RTX treatment to alter B cell interactions prior to depletion, and the possibility that these altered interactions could regulate responses by macrophages was also investigated. It has previously been shown that RTX stimulation alters the interaction of viable B cells with T cells, and can directly affect the subclass of immunoglobulin produced by B cells. In the current *in vitro* system, RTX pre-treated B cells underwent increased levels of interaction with macrophages, with enhanced phagocytosis of RTX-coated B cells also observed. However, this increased interaction did not affect the macrophage phenotype or function according to any of the parameters tested, indicating that RTX bound B cells do not modulate immune responses prior to their becoming apoptotic.

A key feature to understanding the hypothesis is the question of whether self-antigen taken up by autoreactive B cells could potentially be presented by other APCs after phagocytosis of the B cells. We found that successful secondary presentation of antigen was possible in this *in vitro* assay system, however the current results cannot answer the question of whether tolerance or activation would result from such antigen presentation *in vivo*. Nevertheless, they are a first step toward understanding this interaction, highlighting this as an interesting area for further investigation.

Importantly, one of the main findings throughout this thesis was the ability of viable cells to recapitulate the AC-driven modulation of macrophage phenotype and function. This finding was unexpected, and in comparison to the overwhelming AC data in the literature, would suggest that either the previous literature has not performed the correct controls or that this capacity of viable cells is specific to our experimental system. Regardless of the explanation, further work would be needed to fully explain this result.

In summation, to help enable a better understanding of the role B cells play in RA pathogenesis, we need to elucidate the mode of action of effective agents targeted at this cell population, such as RTX. The experiments presented in this thesis have begun to explore the immunomodulatory capacity of apoptotic B cells, and attempted to further the understanding of the mechanisms of action of RTX-mediated B cell depletion in autoimmunity and how they exert their beneficial effects. Additional work is needed before it can be concluded whether or not RTX-mediated B cell apoptosis and the re-introduction of tolerance plays a key role in the clinical efficacy of RTX treatment in autoimmunity. However, this is an interesting area of research, warranting further investigation.

Appendix

Media

Complete RPMI:

500ml incomplete RPMI (Gibco, Invitrogen)

50ml heat-inactivated foetal bovine serum

5ml penicillin-streptomycin (Sigma)

5ml L-Glutamine (Sigma)

5ml non-essential amino-acids (Invitrogen)

500µl beta-2-mercaptoethanol (Gibco, Invitrogen)

Peritoneal Wash Solution:

100mls 1x PBS

250mM EDTA

Buffers

General buffers

10x PBS:

10L dH_2O

800g NaCl

20g KCl

20g KH_2PO_4

290g $Na_2HPO_4.12H_20$

Genotyping buffers

Tris-acetate-EDTA (TAE) buffer:

242g Tris Base

57.1ml Glacial Acetic Acid

100ml 0.5M EDTA

make up to 1L with dH_20

Alkaline Lysis Buffer, pH 12:

25mM NaOH

0.2 mM EDTA

Neutralization buffer, pH 5:

40mM Tris HCl

FACS buffers

FACS Buffer:

1L 1x PBS

3% BSA

1mM EDTA

0.05% Sodium Azide

Sodium Phosphate Buffer, pH 8.0:

100mM sodium phosphate

ELISA buffers

Cytokine ELISA coating buffers:

a) **0.2M Sodium Phosphate, pH 6.5:**

1L dH_20

12.49g Na_2HPO_4

15.47g NaH_2PO_4

b) **0.1M Sodium Carbonate, pH 9.5:**

1L dH_20

7.13g NaHCO

1.59g NaCO

Cytokine ELISA Assay Diluent/Blocking Buffer:

1x PBS

10% FBS

Serum ELISA Blocking Buffer:

1x PBS

3% BSA

Serum ELISA Assay Diluent:

1x PBS

1% BSA

PBS-Tween (ELISA wash buffer):

1x PBS

0.5% Tween

References

[1] Janeway CA. Approaching the Asymptote? Evolution and Revolution in Immunology. Cold Spring Harbor Symposia on Quantitative Biology 1989;54:1–13.

[2] Heyworth PG, Cross AR, Curnutte JT. Chronic granulomatous disease. Curr Opin Immunol 2003;15:578–84.

[3] Figueroa JE, Densen P. Infectious diseases associated with complement deficiencies. Clinical Microbiology Reviews 1991;4:359–95.

[4] Shimazu R, Akashi S, Ogata H, Nagai Y, Fukudome K, Miyake K, et al. MD-2, a Molecule that Confers Lipopolysaccharide Responsiveness on Toll-like Receptor 4. J Exp Med 1999;189:1777–82.

[5] Heil F, Hemmi H, Hochrein H, Ampenberger F, Kirschning C, Akira S, et al. Species-Specific Recognition of Single-Stranded RNA via Toll-like Receptor 7 and 8. Science 2004;303:1526–9.

[6] Dunne DW, Resnick D, Greenberg J, Krieger M, Joiner KA. The type I macrophage scavenger receptor binds to gram-positive bacteria and recognizes lipoteichoic acid. Pnas 1994;91:1863–7.

[7] Shimaoka T, Kume N, Minami M, Hayashida K, Sawamura T, Kita T, et al. LOX-1 supports adhesion of Gram-positive and Gram-negative bacteria. The Journal of Immunology 2001;166:5108–14.

[8] Chen G, Shaw MH, Kim Y-G, Núñez G. NOD-Like Receptors: Role in Innate Immunity and Inflammatory Disease. Annu Rev Pathol Mech Dis 2009;4:365–98.

[9] Kato H, Takahasi K, Fujita T. RIG-I-like receptors: cytoplasmic sensors for non-self RNA. Immunological Reviews 2011;243:91–8.

[10] Holmskov U, Thiel S, Jensenius JC. Collectins and Ficolins: Humoral Lectins of the Innate Immune Defense. Annu Rev Immunol 2003;21:547–78.

[11] van Furth R, Cohn ZA, Hirsch JG, Humphrey JH, Spector WG, Langevoort HL. The mononuclear phagocyte system: a new classification of macrophages, monocytes, and their precursor cells. Bull World Health Organ 1972;46:845–52.

[12] Schulz C, Perdiguero EG, Chorro L, Szabo-Rodgers H, Cagnard N, Kierdorf K, et al. A Lineage of Myeloid Cells Independent of Myb and Hematopoietic Stem Cells. Science 2012;336:86–90.

[13] Hoeffel G, Wang Y, Greter M, See P, Teo P, Malleret B, et al. Adult Langerhans cells derive predominantly from embryonic fetal liver monocytes with a minor contribution of yolk sac-derived macrophages. J Exp Med 2012;209:1167–81.

[14] Ginhoux F, Geter M, Leboeuf M, Nandi S, See P, Gokhan S, et al. Fate Mapping Analysis Reveals That Adult Microglia Derive from Primitive Macrophages. Science 2010;330:841–5.

[15] Yona S, Kim K-W, Wolf Y, Mildner A, Varol D, Breker M, et al. Fate Mapping Reveals Origins and Dynamics of Monocytes and Tissue Macrophages under Homeostasis. Immunity 2013;38:79–91.

[16] Landsman L, Varol C, Jung S. Distinct Differentiation Potential of Blood Monocyte Subsets in the Lung. The Journal of Immunology 2007;178:2000-7

[17] Mosser DM, Edwards JP. Exploring the Full Spectrum of Macrophage Activation. Nature Reviews Immunology 2008;8:958–69.

[18] Stout RD, Jiang C, Matta B, Tietzel I, Watkins SK, Suttles J. Macrophages Sequentially Change Their Functional Phenotype in Response to Changes in Microenvironmental Influences. The Journal of Immunology 2005;175:342–9.

[19] Murray PJ, Wynn TA. Protective and pathogenic funcitons of macrophage subsets. Nature Reviews Immunology 2011;11:723–37.

[20] Galloway CJ, Dean GE, Marsh M, Rudnick G, Mellman I. Acidification of

macrophage and fibroblast endocytic vesicles in vitro. Pnas 1983;80:3334–8.
[21] Cohn ZA, Wiener E. The Particulate Hydrolases of Macrophages. J Exp Med 1963;118:1009–20.
[22] Biggar WD, Sturgess JM. Role of lysozyme in the microbicidal activity of rat alveolar macrophages. Infect Immun 1977;16:974–82.
[23] Babior BM. The respiratory burst of phagocytes. The Journal of Clinical Investigation 1984;73:599–601.
[24] Martinez FO, Helming L, Gordon S. Alternative Activation of Macrophages: An Immunologic Functional Perspective. Annu Rev Immunol 2009;27:451–83.
[25] Stein M, Keshav S, Harris N, Gordon S. Interleukin 4 potently enhances murine macrophage mannose receptor activity: a marker of alternative immunologic macrophage activation. J Exp Med 1992;176:287–92.
[26] Taylor PR, Martinez-Pomares L, Stacey M. Macrophage receptors and immune recognition. Annu Rev Immunol 2005;23:901–44.
[27] Hesse M, Modolell M, La Flamme AC, Schito M, Fuentes JM, Cheever AW, et al. Differential regulation of nitric oxide synthase-2 and arginase-1 by type 1/type 2 cytokines in vivo: granulomatous pathology is shaped by the pattern of L-arginine metabolism. The Journal of Immunology 2001;167:6533–44.
[28] Abramson SL, Gallin JI. IL-4 inhibits superoxide production by human mononuclear phagocytes. The Journal of Immunology 1990;144:625–30.
[29] Levings MK, Schrader JW. IL-4 inhibits the production of TNF-alpha and IL-12 by STAT6-dependent and -independent mechanisms. The Journal of Immunology 1999;162:5224–9.
[30] Ratnofsky SE, Peterson A, Greenstein JL, Burakoff SJ. Expression and function of CD8 in a murine T cell hybridoma. J Exp Med 1987;166:1747–57.
[31] Norment AM, Salter RD, Parham P, Engelhard V, Littman DR. Cell-cell adhesion mediated by CD8 and MHC class I molecules. Nature 1988;336:79–81.
[32] Doyle C, Strominger JL. Interaction between CD4 and class II MHC molecules mediates cell adhesion. Nature 1987;330:256–9.
[33] Mosmann TR, Coffman RL. TH1 and TH2 cells: different patterns of lymphokine secretion lead to different functional properties. Annu Rev Immunol 1989;7:145–73.
[34] Park H, Li Z, Yang X, Chang S, Nurieva R, Wang Y, et al. A distinct lineage of CD4 T cells regulates tissue inflammation by producing interleukin 17. Nat Immunol 2005;6:1133–41.
[35] Dieckmann D, Bruett CH, Ploettner H, Lutz MB, Schuler G. Human CD4+ CD25+ regulatory, contact-dependent T cells induce interleukin 10–producing, contact-independent type 1-like regulatory T cells. J Exp Med 2002;196:247–53.
[36] Caligaris-Cappio F, Gobbi M, Bofill M, Janossy G, Janossy G. Infrequent normal B lymphocytes express features of B-chronic lymphocytic leukemia. J Exp Med 1982;155:623–8.
[37] Stall AM, Adams S, Herzenberg LA, Kantor AB. Characteristics and Development of the Murine B-1b (Ly-1 B Sister) Cell Population. Annals of the New York Academy of Sciences 1992;651:33–43.
[38] Macpherson AJ, Gatto D, Sainsbury E, Harriman GR, Hengartner H, Zinkernagel RM, et al. A primitive T cell-independent mechanism of intestinal mucosal IgA responses to commensal bacteria. Science 2000;288:2222–6.
[39] Allman D, Pillai S. Peripheral B cell subsets. Curr Opin Immunol 2008;20:149–57.
[40] Namen AE, Lupton S, Hjerrild K, Wignall J, Mochizuki DY, Schmierer A, et al. Stimulation of B-cell progenitors by cloned murine interleukin-7. Nature 1988;333:571–3.
[41] Nishimoto N, Kubagawa H, Ohno T, Gartland GL, Stankovic AK, Cooper MD,

et al. Normal pre-B cells express a receptor complex of mu heavy chains and surrogate light-chain proteins. PNAS 1991;88:6284–8.
[42] Lassoued K. Expression of surrogate light chain receptors is restricted to a late stage in pre-B cell differentiation. Cell 1993;73:73–86.
[43] Reth M, Petrac E, Wiese P, Lobel L, Alt FW. Activation of V kappa gene rearrangement in pre-B cells follows the expression of membrane-bound immunoglobulin heavy chains. Embo J 1987;6:3299–305.
[44] Meffre E, Wardemann H. B-cell tolerance checkpoints in health and autoimmunity. Curr Opin Immunol 2008;20:632–8.
[45] Harless SM, Lentz VM, Sah AP, Hsu BL, Clise-Dwyer K, Hilbert DM, et al. Competition for BLyS-mediated signaling through Bcmd/BR3 regulates peripheral B lymphocyte numbers. Curr Biol 2001;11:1986–9.
[46] Lam KP, Kühn R, Rajewsky K. In vivo ablation of surface immunoglobulin on mature B cells by inducible gene targeting results in rapid cell death. Cell 1997;90:1073–83.
[47] Calame KL. Plasma cells: finding new light at the end of B cell development. Nature Immunology 2001;2:1103–8.
[48] Fairfax KA, Kallies A, Nutt SL, Tarlinton DM. Plasma cell development: From B-cell subsets to long-term survival niches. Seminars in Immunology 2008;20:49–58.
[49] Hargreaves DC, Hyman PL, Lu TT, Ngo VN, Bidgol A, Suzuki G, et al. A coordinated change in chemokine responsiveness guides plasma cell movements. J Exp Med 2001;194:45–56.
[50] Slifka MK, Antia R, Whitmire JK, Whitmire JK, Ahmed R. Humoral immunity due to long-lived plasma cells. Immunity 1998;8:363–72.
[51] Walport MJ. Complement. N Engl J Med 2001;344:1058–66.
[52] Liu Y, Wu Y, Ramarathinam L, Guo Y, Huszar D, Trounstine M, et al. Gene-targeted B-deficient mice reveal a critical role for B cells in the CD4 T cell response. International Immunology 1995;7:1353–62.
[53] Malynn BA, Romeo DT, Wortis HH. Antigen-specific B cells efficiently present low doses of antigen for induction of T cell proliferation. The Journal of Immunology 1985;135:980–8.
[54] O'Neill SK, Shlomchik MJ, Glant TT, Cao Y, Doodes PD, Finnegan A. Antigen-Specific B Cells Are Required as APCs and Autoantibody-Producing Cells for Induction of Severe Autoimmune Arthritis. The Journal of Immunology 2005;174:3781–8.
[55] Falcone M, Lee J, Patstone G, Yeung B, Sarvetnick N. B lymphocytes are crucial antigen-presenting cells in the pathogenic autoimmune response to GAD65 antigen in nonobese diabetic mice. The Journal of Immunology 1998;161:1163–8.
[56] Chan OTM, Hannum LG, Haberman AM, Madaio MP, Shlomchik MJ. A Novel Mouse with B Cells but Lacking Serum Antibody Reveals an Antibody-independent Role for B Cells in Murine Lupus. J Exp Med 1999;189:1639–48.
[57] Linton PJ, Harbertson J, Bradley LM. A critical role for B cells in the development of memory CD4 cells. The Journal of Immunology 2000;165:5558–65.
[58] Harris DP, Haynes L, Sayles PC, Duso DK, Eaton SM, Lepak NM, et al. Reciprocal regulation of polarized cytokine production by effector B and T cells. Nature Immunology 2000;1:475–82.
[59] Tian J, Zekzer D, Hanssen L, Lu Y, Olcott A, Kaufman DL. Lipopolysaccharide-Activated B Cells Down-Regulate Th1 Immunity and Prevent Autoimmune Diabetes in Nonobese Diabetic Mice. The Journal of Immunology 2001;167:1081–9.
[60] Duddy ME, Alter A, Bar-Or A. Distinct profiles of human B cell effector cytokines: a role in immune regulation? The Journal of Immunology 2004;172:3422–7.
[61] Fillatreau S, Sweenie CH, McGeachy MJ, Gray D, Anderton SM. B cells

regulate autoimmunity by provision of IL-10. Nature Immunology 2002;3:944–50.
[62] Mauri C, Gray D, Mushtaq N, Londei M. Prevention of arthritis by interleukin 10-producing B cells. J Exp Med 2003;197:489–501.
[63] Mizoguchi A, Mizoguchi E, Takedatsu H, Blumberg RS, Bhan AK. Chronic Intestinal Inflammatory Condition Generates IL-10-Producing Regulatory B Cell Subset Characterized by CD1d Upregulation. Immunity 2002;16:219–30.
[64] Yurasov S, Wardemann H, Hammersen J, Tsuiji M, Meffre E, Pascual V, et al. Defective B cell tolerance checkpoints in systemic lupus erythematosus. J Exp Med 2005;201:703–11.
[65] Samuels J, Ng Y-S, Coupillaud C, Paget D, Meffre E. Impaired early B cell tolerance in patients with rheumatoid arthritis. J Exp Med 2005;201:1659–67.
[66] Mamula MJ, Fatenejad S, Craft J. B cells process and present lupus autoantigens that initiate autoimmune T cell responses. The Journal of Immunology 1994;152:1453–61.
[67] Duddy M, Niino M, Adatia F, Hebert S, Freedman M, Atkins H, et al. Distinct Effector Cytokine Profiles of Memory and Naive Human B Cell Subsets and Implication in Multiple Sclerosis. The Journal of Immunology 2007;178:6092–9.
[68] Barr TA, Shen P, Brown S, Lampropoulou V, Lawrie S, Fan B, et al. B cell depletion therapy ameliorates autoimmune disease through ablation of IL-6-producing B cells. Journal of Experimental Medicine 2012;209:1001–10.
[69] De Vita S, Zaja F, Sacco S, Candia AD, Fanin R, Ferraccioli G. Efficacy of Selective B cell Blockade in the Treatment of Rheumatoid Arthritis: Evidence for a Pathogenetic Role of B cells. Arthritis & Rheumatology 2002;46:2029–33.
[70] Svensson L, Jirholt J, Holmdahl R, Jansson L. B cell-deficient mice do not develop type II collagen-induced arthritis (CIA). Clin Exp Immunol 1998;111:521–6.
[71] Hamel K, Doodes P, Cao Y, Wang Y, Martinson J, Dunn R, et al. Suppression of proteoglycan-induced arthritis by anti-CD20 B Cell depletion therapy is mediated by reduction in autoantibodies and CD4+ T cell reactivity. The Journal of Immunology 2008;180:4994–5003.
[72] Scott DL, Wolfe F, Huizinga TW. Rheumatoid arthritis. The Lancet 2010;376:1094–108.
[73] Tarkowski A, Czerkinsky C, Nilsson LA. Simultaneous induction of rheumatoid factor- and antigen-specific antibody-secreting cells during the secondary immune response in man. Clinical & Experimental Immunology 1985;61:379.
[74] Harris J, Vaughan JH. Transfusion studies in rheumatoid arthritis. Arthritis Rheum 1961:47–55.
[75] Klareskog L, Ronnelid J, Lundberg K, Padyukov L, Alfredsson L. Immunity to Citrullinated Proteins in Rheumatoid Arthritis. Annu Rev Immunol 2008;26:651–75.
[76] van der Woude D, Houwing-Duistermaat JJ, Toes REM, Huizinga TWJ, Thomson W, Worthington J, et al. Quantitative heritability of anti-citrullinated protein antibody-positive and anti-citrullinated protein antibody-negative rheumatoid arthritis. Arthritis & Rheumatism 2009;60:916–23.
[77] Litsiou E, Semitekolou M, Galani IE, Morianos I, Tsoutsa A, Kara P, et al. CXCL13 production in B cells via Toll-like receptor/lymphotoxin receptor signaling is involved in lymphoid neogenesis in chronic obstructive pulmonary disease. Am J Respir Crit Care Med 2013;187:1194–202.
[78] Rehman MQ, Beal D, Liang Y, Noronha A, Winter H, Farraye FA, et al. B cells secrete eotaxin-1 in human inflammatory bowel disease. Inflamm Bowel Dis 2013;19:922–33.

[79] Silverman GJ, Carson DA. Roles of B cells in Rheumatoid Arthritis. Arthritis Res Ther 2003;5:S1-5.
[80] Edwards JC, Cambridge G. Sustained improvement in rheumatoid arthritis following a protocol designed to deplete B lymphocytes. Rheumatology 2001;40:205–11.
[81] Edwards JCW, Szczepanski L, Szechinski J, Filipowicz-Sosnowska A, Emery P, Close DR, et al. Efficacy of B-Cell–Targeted Therapy with Rituximab in Patients with Rheumatoid Arthritis. N Engl J Med 2004;350:2572–81.
[82] Cohen SB, Emery P, Greenwald MW, Dougados M, Furie RA, Genovese MC, et al. Rituximab for rheumatoid arthritis refractory to anti–tumor necrosis factor therapy: Results of a multicenter, randomized, double-blind, placebo-controlled, phase III trial evaluating primary efficacy and safety at twenty-four weeks. Arthritis Rheum 2006;54:2793–806.
[83] Emery P, Fleischmann R, Filipowicz-Sosnowska A, Schechtman J, Szczepanski L, Kavanaugh A, et al. The efficacy and safety of rituximab in patients with active rheumatoid arthritis despite methotrexate treatment: Results of a phase IIB randomized, double-blind, placebo-controlled, dose-ranging trial. Arthritis Rheum 2006;54:1390–400.
[84] com R. FDA Approves First Rheumatoid Arthritis Indication for Rituxan (MabThera). Rochecom 2006.
[85] Teeling JL, Mackus WJM, Wiegman LJJM, van den Brakel JHN, Beers SA, French RR, et al. The biological activity of human CD20 monoclonal antibodies is linked to unique epitopes on CD20. The Journal of Immunology 2006;177:362–71.
[86] Jazirehi AR, Bonavida B. Cellular and molecular signal transduction pathways modulated by rituximab (rituxan, anti-CD20 mAb) in non-Hodgkin's lymphoma: implications in chemosensitization and therapeutic intervention. Oncogene 2005;24:2121–43.
[87] Srinivasan A, Mukherji SK. Tositumomab and Iodine I 131 Tositumomab (Bexaar). American Journal of Neuroradiology 2011;32:637–8.
[88] Uchida J, Hamaguchi Y, Oliver JA, Ravetch JV, Poe JC, Haas KM, et al. The Innate Mononuclear Phagocyte Network Depletes B Lymphocytes through Fc Receptor–dependent Mechanisms during Anti-CD20 Antibody Immunotherapy. J Exp Med 2004;199:1659–69.
[89] Di Gaetano N, Cittera E, Nota R, Vecchi A, Grieco V, Scanziani E, et al. Complement activation determines the therapeutic activity of Rituximab in vivo. The Journal of Immunology 2003;171:1581–7.
[90] Salama AD, Pusey CD. Drug Insight: rituximab in renal disease and transplantation. Nature Clin Prac 2006:1–10.
[91] Bello C, Sotomayor EM. Monoclonal Antibodies for B-Cell Lymphomas: Rituximab and Beyond. Hematology Am Soc Hematol Educ Program 2007;2007:233–42.
[92] Reff ME, Carner K, Chambers KS, Chinn PC, Leonard JE, Raab R, et al. Depletion of B Cells In Vivo by a Chimeric Mouse Human Monoclonal Antibody to CD20. Blood 1994;83:435–45.
[93] Harjunpää A, Junnikkala S, Meri S. Rituximab (Anti-CD20) Therapy of B-Cell Lymphomas: Direct Complement Killing Is Superior to Cellular Effector Mechanisms. Scandinavian Journal of Immunology 2000;51:634–41.
[94] Cartron G, Dacheux L, Salles G, Solal-Celigny P, Bardos P, Colombat P, et al. Therapeutic activity of humanized anti-CD20 monoclonal antibody and polymorphism in IgG Fc receptor Fc gamma RIIIa gene. Blood 2002:1–5.
[95] Treon SP, Mitsiades C, Mitsiades N, Young G, Doss D, Schlossman R, et al. Tumor Cell Expression of CD59 Is Associated With Resistance to CD20 Serotherapy in Patients With B-Cell Malignancies. Journal of Immunotherapy 2001:1–9.
[96] Weng W-K, Levy R. Expression of complement inhibitors CD46, CD55, and CD59 on tumor cells does not predict clinical outcome after rituximab

treatment in follicular non-Hodgkin lymphomat. Blood 2001:1–6.
[97] Beers SA, Chan CHT, James S, French RR, Attfield KE, Brennan CM, et al. Type II (Tositumomab) Anti-CD20 Monoclonal Antibody Out Performs Type I (Rituximab-Like) Reagents in B-Cell Depletion Regardless of Complement Activation. Blood 2008;112:4170–7.
[98] van Meerten T, van Rijn RS, Hol S, Hagenbeek A, Ebeling S. Complement-Induced Cell Death by Rituximab Depends on CD20 Expression Level and Acts Complementary to Antibody-Dependent Cellular Cytotoxicity. Clinical Cancer Research 2006;12:4027–35.
[99] Deans JP, Li H, Polyak MJ. CD20-Mediated Apoptosis: Signalling Through Lipid Rafts. Immunology 2002;107:176–82.
[100] Beers SA, French RR, Chan HTC, Lim SH, Jarrett TC, Vidal RM, et al. Antigenic Modulation Limits the Efficacy of Anti-CD20 Antibodies: Implications for Antibody Selection. Blood 2010;115:5191–201.
[101] Alas S, Emmanouilides C, Bonavida B. Inhibition of Interleukin 10 by Rituximab Results in Down-Regulation of Bcl-2 and Sensitization of B-cell Non-Hodgkin's Lymphoma to Apoptosis. Clinical Cancer Research 2001;7:709–23.
[102] Jazirehi AR. Inhibition of the Raf-MEK1/2-ERK1/2 Signaling Pathway, Bcl-xL Down-Regulation, and Chemosensitization of Non-Hodgkin's Lymphoma B Cells by Rituximab. Cancer Res 2004;64:7117–26.
[103] Odabaei G, Chatterjee D, Jazirehi AR, Goodglick L, Yeung K, Bonavida B. Raf-1 Kinase Inhibitor Protein: Structure, Function, Regulation of Cell Signaling, and Pivotal Role in Apoptosis. Advances in Cancer Research 2004:169–99.
[104] Byrd JC, Kitada S, Flinn IW, Aron JL, Pearson M, Lucas D, et al. The mechanism of tumor cell clearance by rituximab in vivo in patients with B-cell chronic lymphocytic leukemia: evidence of caspase activation and apoptosis induction. Blood 2002:1–6.
[105] Sfikakis PP, Sfikakis PP, Boletis JN, Boletis JN, Lionaki S, Lionaki S, et al. Remission of proliferative lupus nephritis following B cell depletion therapy is preceded by down-regulation of the T cell costimulatory molecule CD40 ligand: An open-label trial. Arthritis Rheum 2005;52:501–13.
[106] Taylor RP, Lindorfer MA. Drug Insight: the Mechanism of Action of Rituximab in Autoimmune Disease—the Immune Complex Decoy Hypothesis. Nature Clinical Practice: Rheumatology 2007;3:86–95.
[107] Silverman GJ, Boyle DL. Understanding the mechanistic basis in rheumatoid arthritis for clinical response to anti-CD20 therapy: the B-cell roadblock hypothesis. Immunological Reviews 2008;223:175–85.
[108] Kavanaugh A, Rosengren S, Lee S-J, Hammaker D, Firestein GS, Kalunian K, et al. Assessment of rituximab's immunomodulatory synovial effects (ARISE trial). 1: clinical and synovial biomarker results. Ann Rheum Dis 2007;67:402–8.
[109] Vos K, Thurlings RM, Wijbrandts CA, van Schaardenburg D, Gerlag DM, Tak PP. Early effects of rituximab on the synovial cell infiltrate in patients with rheumatoid arthritis. Arthritis Rheum 2007;56:772–8.
[110] Kroemer G, Galluzzi L, Vandenabeele P, Abrams J, Alnemri ES, Baehrecke EH, et al. Classification of cell death: recommendations of the Nomenclature Committee on Cell Death 2009. Cell Death and Differentiation 2008;16:3–11.
[111] Jäättelä M, Tschopp J. Caspase-independent cell death in T lymphocytes. Nature Immunology 2003;4:416–23.
[112] Krysko DV, Brouckaert G, Kalai M, Vandenabeele P, D'Herde K. Mechanisms of Internalization of Apoptotic and Necrotic L929 Cells by a Macrophage Cell Line Studied by Electron Microscopy. Journal of Morphology 2003;258:336–45.
[113] Saito K, Dai Y, Ohtsuka K. Enhanced expression of heat shock proteins in

gradually dying cells and their release from necrotically dead cells. Exp Cell Res 2005;310:229–36.
[114] Scaffidi P, Misteli T, Bianchi ME. Release of chromatin protein HMGB1 by necrotic cells triggers inflammation. Nature 2002;418:191–5.
[115] Miles K, Clarke DJ, Lu W, Sibinska Z, Beaumont PE, Davidson DJ, et al. Dying and Necrotic Neutrophils Are Anti-Inflammatory Secondary to the Release of Alpha-Defensins. The Journal of Immunology 2009;183:2122–32.
[116] Kerr JF, Wyllie AH, Currie AR. Apoptosis: a basic biological phenomenon with wide-ranging implications in tissue kinetics. Br J Cancer 1972;26:239–57.
[117] Klionsky DJ. Autophagy: from phenomenology to molecular understanding in less than a decade. Nat Rev Mol Cell Biol 2007;8:931–7.
[118] Bejarano E, Cuervo AM. Chaperone-Mediated Autophagy. Proceedings of the American Thoracic Society 2010;7:29–39.
[119] Yu L, Alva A, Su H, Dutt P, Freundt E, Welsh S, et al. Regulation of an ATG7-beclin 1 Program of Autophagic Cell Death by Caspase-8. Science 2004;304:1500–2.
[120] Pulendran B, Shimizu S, Tang H, Kanaseki T, Manicassamy S, Mizushima N, et al. Role of Bcl-2 family proteins in a non-apoptotic programmed cell death dependent on autophagy genes. Nature Cell Biology 2004;6:1221–8.
[121] Petrovski G, Zahuczky G, Katona K, Vereb G, Martinet W, Nemes Z, et al. Clearance of dying autophagic cells of different origin by professional and non-professional phagocytes. Cell Death and Differentiation 2007;14:1117–28.
[122] Boya P, González-Polo R-A, Casares N, Perfettini J-L, Dessen P, Larochette N, et al. Inhibition of Macroautophagy Triggers Apoptosis. Molecular and Cellular Biology 2005;25:1025–40.
[123] González-Polo R-A, Boya P, Pauleau A-L, Jalil A, Larochette N, Souquere S, et al. The apoptosis/autophagy paradox: autophagic vacuolization before apoptotic death. Journal of Cell Science 2005;118:3091–102.
[124] Nakanishi Y, Henson PM, Shiratsuchi A. Pattern Recognition in Phagocytic Clearance of Altered Self. Advances in Experimental Medicine and Biology, vol. 653, New York, NY: Springer New York; 2009, pp. 129–38.
[125] Fadok VA, Voelker DR, Campbell PA, Cohen JJ, Bratton DL, Henson PM. Exposure of phosphatidylserine on the surface of apoptotic lymphocytes triggers specific recognition and removal by macrophages. The Journal of Immunology 1992;148:2207–16.
[126] Fadok VA, Bratton DL, Rose DM, Pearson A, Ezekewitz RAB, Henson PM. A Receptor for Phosphatidylserine-Specific Clearance of Apoptotic Cells. Nature 2000;405:85–90.
[127] DeKruyff RH, Bu X, Ballesteros A, Santiago C, Chim YLE, Lee HH, et al. T Cell/Transmembrane, Ig, and Mucin-3 Allelic Variants Differentially Recognize Phosphatidylserine and Mediate Phagocytosis of Apoptotic Cells. The Journal of Immunology 2010;184:1918–30.
[128] Santiago C, Ballesteros A, Martínez-Muñoz L, Mellado M, Kaplan GG, Freeman GJ, et al. Structures of T Cell Immunoglobulin Mucin Protein 4 Show a Metal-Ion-Dependent Ligand Binding Site where Phosphatidylserine Binds. Immunity 2007;27:941–51.
[129] Nakayama M, Akiba H, Takeda K, Kojima Y, Hashiguchi M, Azuma M, et al. Tim-3 mediates phagocytosis of apoptotic cells and cross-presentation. Blood 2009;113:3821–30.
[130] Nakahashi-Oda C, Tahara-Hanaoka S, Honda S-I, Shibuya K, Shibuya A. Identification of phosphatidylserine as a ligand for the CD300a immunoreceptor. Biochem Biophys Res Commun 2012;417:646–50.
[131] He M, Kubo H, Morimoto K, Fujino N, Suzuki T, Takahasi T, et al. Receptor for advanced glycation end products binds to phosphatidylserine and assists in the clearance of apoptotic cells. EMBO Reports 2011;12:358–64.

[132] Park S-Y, Jung M-Y, Kim H-J, Lee S-J, Kim S-Y, Lee B-H, et al. Rapid cell corpse clearance by stabilin-2, a membrane phosphatidylserine receptor. Cell Death and Differentiation 2008;15:192–201.
[133] Park D, Tosello-Trampont A-C, Elliott MR, Lu M, Haney LB, Ma Z, et al. BAI1 is an engulfment receptor for apoptotic cells upstream of the ELMO/Dock180/Rac module. Nature 2007;450:430–4.
[134] Hanayama R, Tanaka M, Miwa K, Shinohara A, Iwamatsu A, Nagata S. Identification of a factor that links apoptotic cells to phagocytes. Nature 2002;417:182–7.
[135] Yamaguchi H, Takagi J, Miyamae T, Yokota S, Fujimoto T, Nakamura S, et al. Milk fat globule EGF factor 8 in the serum of human patients of systemic lupus erythematosus. J Leukoc Biol 2008;83:1300–7.
[136] Nakano T, Ishimoto Y, Kishino J, Umeda M, Inoue K, Nagata K, et al. Cell Adhesion to Phosphatidylserine Mediated by a Product of Growth Arrest-specific Gene 6. Journal of Biological Chemistry 1997;272:29411–4.
[137] Scott RS, McMahon EJ, Pop SM, Reap EA, Caricchio R, Cohen PL, et al. Phagocytosis and clearance of apoptotic cells is mediated by MER. Nature 2001;411:207–11.
[138] Balasubramanian K, Chandra J, Schroit AJ. Immune Clearance of Phosphatidylserine-Expressing Cells by Phagocytes. the Role of ß2-Glycoprotein I in Macrophage Recognition. The Journal of Biological Chemistry 1997;272:31113–7.
[139] Maiti SN, Balasubramanian K, Ramoth JA, Schroit AJ. ß-2-glycoprotein 1-dependent macrophage uptake of apoptotic cells: binding to lipoprotein receptor-related protein receptor family members. Journal of Biological Chemistry 2008;283:3761–6.
[140] Erwig L-P, Henson PM. Clearance of apoptotic cells by phagocytes. Cell Death and Differentiation 2008;15:243–50.
[141] Ogden CA, deCathelineau A, Hoffmann PR, Bratton D, Ghebrehiwet B, Fadok VA, et al. C1q and Mannose Binding Lectin Engagement of Cell Surface Calreticulin and Cd91 Initiates Macropinocytosis and Uptake of Apoptotic Cells. Journal of Experimental Medicine 2001;194:781–96.
[142] Gershov D, Kim S, Brot N, Elkon KB. C-Reactive protein binds to apoptotic cells, protects the cells from assembly of the terminal complement components, and sustains an anti-inflammatory innate immune response: implications for systemic autoimmunity. J Exp Med 2000;192:1353–64.
[143] Sambrano GR, Steinberg D. Recognition of oxidatively damaged and apoptotic cells by an oxidized low density lipoprotein receptor on mouse peritoneal macrophages: role of membrane phosphatidylserine. PNAS 1995;92:1396–400.
[144] Platt N, Suzuki H, Kurihara Y, Kodama T, Gordon S. Role for the class A macrophage scavenger receptor in the phagocytosis of apoptotic thymocytes in vitro. PNAS 1996;93:12456–60.
[145] Ramprasad MP, Fischer W, Witztum JL, Sambrano GR, Quehenberger O, Steinberg D. The 94- to 97-kDa mouse macrophage membrane protein that recognizes oxidized low density lipoprotein and phosphatidylserine-rich liposomes is identical to macrosialin, the mouse homologue of human CD68. PNAS 1995;92:9580–4.
[146] Oka K, Sawamura T, Kikuta K-I, Itokawa S, Kume N, Kita T, et al. Lectin-like oxidized low-density lipoprotein receptor 1 mediates phagocytosis of aged/apoptotic cells in endothelial cells. PNAS 1998;95:9535–40.
[147] Savill J, Hogg N, Ren Y, Haslett C. Thrombospondin cooperates with CD36 and the vitronectin receptor in macrophage recognition of neutrophils undergoing apoptosis. The Journal of Clinical Investigation 1992;90:1513–22.
[148] Simmons DL. The role of ICAM expression in immunity and disease. Cancer Surveys 1994;24:141–55.
[149] Moffatt OD, Devitt A, Bell ED, Simmons DL, Gregory CD. Macrophage

recognition of ICAM-3 on apoptotic leukocytes. The Journal of Immunology 1999;162:6800–10.
[150] Gregory CD, Devitt A, Moffatt O. Roles of ICAM-3 and CD14 in the recognition and phagocytosis of apoptotic cells by macrophages. Biochem Soc Trans 1998;26:644–9.
[151] Brown S, Heinisch I, Ross E, Shaw K, Buckley CD, Savill J. Apoptosis disables CD31-mediated cell detachment from phagocytes promoting binding and engulfment. Nature 2002;418:200–3.
[152] Brown E, Hooper L, Ho T, Gresham H. Integrin-Associated Protein: a 50-kD Plasma Membrane Antigen Physically and Functionally Associated with Integrins. J Cell Biol 1990;111:2785–94.
[153] Oldenborg PA, Zheleznyak A, Fang Y-F, Lagenaur CF, Gresham HD, Lindberg FP. Role of CD47 as a Marker of Self on Red Blood Cells. Science 2000;288:2051–4.
[154] Gardai SJ, McPhillips KA, Frasch SC, Janssen WJ, Starefeldt A, Murphy-Ullrich JE, et al. Cell-Surface Calreticulin Initiates Clearance of Viable or Apoptotic Cells through trans-Activation of LRP on the Phagocyte. Cell 2005;123:321–34.
[155] Elward K, Griffiths M, Mizuno M, Harris CL, Neal JW, Morgan BP, et al. CD46 Plays a Key Role in Tailoring Innate Immune Recognition of Apoptotic and Necrotic Cells. Journal of Biological Chemistry 2005;280:36342–54.
[156] Herrmann M, Voll RE, Zoller OM, Hagenhofer M, Ponner BB, Kalden JR. Impaired Phagocytosis of Apoptotic Cell Material by Monocyte-Derived Macrophages From Patients with Systemic Lupus Erythematosus. Arthritis Rheum 1998;41:1241–50.
[157] Fadok VA, Bratton DL, Konowal A, Freed PW, Westcott JY, Henson PM. Macrophages That Have Ingested Apoptotic Cells In Vitro Inhibit Proinflammatory Cytokine Production Through Autocrine/Paracrine Mechanisms Involving TGF-beta, PGE2, and PAF. The Journal of Clinical Investigation 1998;101:890–8.
[158] Voll RE, Herrmann M, Roth EA, Stach C, Kalden JR. Immunosuppressive effects of apoptotic cells. Nature 1997;390:350–1.
[159] Casares N, Pequignot MO, Tesniere A, Ghiringhelli F, Roux S, Chaput N, et al. Caspase-Dependent Immunogenicity of Doxorubicin-Induced Tumor Cell Death. Journal of Experimental Medicine 2005;202:1691–701.
[160] Obeid M, Tesniere A, Ghiringhelli F, Fimia GM, Apetoh L, Perfettini J-L, et al. Calreticulin Exposure Dictates the Immunogenicity of Cancer Cell Death. Nat Med 2007;13:54–61.
[161] Kepp O, Tesniere A, Schlemmer F, Michaud M, Senovilla L, Zitvogel L, et al. Immunogenic Cell Death Modalities and Their Impact on Cancer Treatment. Apoptosis 2009;14:364–75.
[162] Albert ML, Sauter B, Bhardwaj N. Dendritic Cells Acquire Antigen From Apoptotic Cells and Induce Class I-Restricted CTLs. Nature 1998;392:86–9.
[163] Kotera Y, Shimizu K, Mulé JJ. Comparative Analysis of Necrotic and Apoptotic Tumor Cells as a Source of Antigen(s) in Dendritic Cell-Based Immunization. Cancer Research 2001;61:8105–9.
[164] Obeid M, Panaretakis T, Joza N, Tufi R, Tesniere A, van Endert P, et al. Calreticulin Exposure Is Required for the Immunogenicity of Gamma-Irradiation and UVC Light-Induced Apoptosis. Cell Death and Differentiation 2007;14:1848–50.
[165] Ronchetti A, Rovere P, Iezzi G, Galati G, Heltai S, Protti MP, et al. Immunogenicity of apoptotic cells in vivo: role of antigen load, antigen-presenting cells, and cytokines. The Journal of Immunology 1999;163:130–6.
[166] Stuart LM, Lucas M, Simpson C, Lamb J, Savill J, Lacy-Hulbert A. Inhibitory Effects of Apoptotic Cell Ingestion Upon Endotoxin-Driven Myeloid Dendritic Cell Maturation. The Journal of Immunology 2002;168:1627–35.
[167] Chong WP, Zhou J, Law HKW, Tu W, Lau YL. Natural Killer Cells Become

Tolerogenic After Interaction with Apoptotic Cells. Eur J Immunol 2010;40:1718–27.
[168] Cvetanovic M, Ucker DS. Innate Immune Discrimination of Apoptotic Cells: Repression of Proinflammatory Macrophage Transcription Is Coupled Directly to Specific Recognition. The Journal of Immunology 2003;172:880–9.
[169] Freire-de-Lima CG, Xiao YQ, Gardai SJ, Bratton DL, Schiemann WP, Henson P. Apoptotic Cells, through Transforming Growth Factor-ß, Coordinately Induce Anti-inflammatory and Suppress Pro inflammatory Eicosanoid and NO Synthesis in Murine Macrophages. The Journal of Biological Chemistry 2006;281:38376–84.
[170] Marriott HM, Hellewell PG, Cross SS, Ince PG, Whyte MKB, Dockrell DH. Decreased Alveolar Macrophage Apoptosis Is Associated with Increased Pulmonary Inflammation in a Murine Model of Pneumococcal Pneumonia. The Journal of Immunology 2006;177:6480–8.
[171] Huynh M-LN, Fadok VA, Henson PM. Phosphatidylserine-Dependent Ingestion of Apoptotic Cells Promotes TGF-ß1 Secretion and the Resolution of Inflammation. Journal of Clinical Investigation 2002;109:41–50.
[172] Gray M, Miles K, Salter D, Gray D, Savill J. Apoptotic Cells Protect Mice From Autoimmune Inflammation by the Induction of Regulatory B Cells. PNAS 2007;104:14080–5.
[173] Johansson U, Walther-Jallow L, Smed-Sörensen A, Spetz A-L. Triggering of dendritic cell responses after exposure to activated, but not resting, apoptotic PBMCs. The Journal of Immunology 2007;179:1711–20.
[174] Albert ML, Pearce SF, Francisco LM, Sauter B, Roy P, Silverstein RL, et al. Immature Dendritic Cells Phagocytose Apoptotic Cells via Alphavbeta5 and CD36, and Cross-Present Antigens to Cytotoxic T Lymphocytes. J Exp Med 1998;188:1359–68.
[175] Lucas M, Stuart LM, Savill J, Lacy-Hulbert A. Apoptotic Cells and Innate Immune Stimuli Combine to Regulate Macrophage Cytokine Secretion. The Journal of Immunology 2003;171:2610–5.
[176] Chen W, Frank ME, Jin W, Wahl SM. TGF-beta Released by Apoptotic T Cells Contributes to an Immunosuppressive Milieu. Immunity 2001;14:715–25.
[177] Li AF, Hough J, Henderson D, Escher A. Co-Delivery of Pro-Apoptotic BAX with a DNA Vaccine Recruits Dendritic Cells and Promotes Efficacy of Autoimmune Diabetes Prevention in Mice. Vaccine 2004;22:1751–63.
[178] Li AF, Ojogho O, Franco E, Baron P, Iwaki Y, Escher A. Pro-Apoptotic DNA Vaccination Ameliorates New Onset of Autoimmune Diabetes in NOD Mice and Induces Foxp3+ Regulatory T Cells in Vitro. Vaccine 2006;24:5036–46.
[179] Weischenfeldt J, Porse B. Bone Marrow-Derived Macrophages (BMM): Isolation and Applications. Cold Spring Harbor Protocols 2008;2008:pdb.prot5080–0.
[180] Lim SH, Vaughan AT, Ashton-Key M, Williams EL, Dixon SV, Chan HTC, et al. Fc Gamma Receptor IIb on Target B Cells Promotes Rituximab Internalization and Reduces Clinical Efficacy. Blood 2011;118:2530–40.
[181] Bevaart L, Vervoordeldonk MJ, Tak PP. Collagen-Induced Arthritis in Mice. Methods in Molecular Biology 2009;602:182–92.
[182] Eagar TN, Karandikar NJ, Bluestone JA, Miller SD. The role of CTLA-4 in induction and maintenance of peripheral T cell tolerance. Eur J Immunol 2002;32:972–81.
[183] Strobel S, Mowat AM, Drummond HE, Pickering MG, Ferguson A. Immunological responses to fed protein antigens in mice. II. Oral tolerance for CMI is due to activation of cyclophosphamide-sensitive cells by gut-processed antigen. Immunology 1983;49:451–6.
[184] Martin SJ, Harrington LE, Reutelingsperger CP, Hatton RD, McGahon AJ, Mangan PR, et al. Early redistribution of plasma membrane phosphatidylserine is a general feature of apoptosis regardless of the initiating stimulus: inhibition by overexpression of Bcl-2 and Abl. J Exp Med

1995;182:1545–56.
[185] Golpon HA, Fadok VA, Taraseviciene-Stewart L, Scerbavicius R, Sauer C, Welte T, et al. Life After Corpse Engulfment: Phagocytosis of Apoptotic Cells Leads to VEGF Secretion and Cell Growth. Faseb J 2004;18:1716–8.
[186] Mevorach D, Mascarenhas JO, Gershov D, Elkon KB. Complement-dependent Clearance of Apoptotic Cells by Human Macrophages. J Exp Med 1998;188:2313–20.
[187] Chen Y, Park YB, Patel E, Silverman GJ. IgM Antibodies to Apoptosis-Associated Determinants Recruit C1q and Enhance Dendritic Cell Phagocytosis of Apoptotic Cells. J Immunol 2009;182:6031–43.
[188] Perruche S, Saas P, Chen W. Apoptotic cell-mediated suppression of streptococcal cell wall-induced arthritis is associated with alteration of macrophage function and local regulatory T-cell increase: a potential cell-based therapy? Arthritis Research & Therapy 2009;11:R104.
[189] Bonnefoy F, Perruche S, Couturier M, Sedrati A, Sun Y, Tiberghien P, et al. Plasmacytoid Dendritic Cells Play a Major Role in Apoptotic Leukocyte-Induced Immune Modulation. J Immunol 2011;186:5696–705.
[190] Uchimura E, Wantanabe N, Niwa O, Muto M, Kobayashi Y. Transient infiltration of neutrophils into the thymus in association with apoptosis induced by whole-body X-irradiation. J Leuk Bio 2000;67:780–4.
[191] Iyoda T, Nagata K, Akashi M, Kobayashi Y. Neutrophils Accelerate Macrophage-Mediated Digestion of Apoptotic Cells In Vivo as Well as In Vitro. The Journal of Immunology 2005;175:3475–83.
[192] Lowenthal JW, Harris AW. Activation of mouse lymphocytes inhibits induction of rapid cell death by x-irradiation. The Journal of Immunology 1985;135:1119–25.
[193] Chen Y, Khanna S, Goodyear CS, Park YB, Raz E, Thiel S, et al. Regulation of Dendritic Cells and Macrophages by an Anti-Apoptotic Cell Natural Antibody that Suppresses TLR Responses and Inhibits Inflammatory Arthritis. J Immunol 2009;183:1346–59.
[194] Filardy AA, Pires DR, Nunes MP, Takiya CM, Freire-de-Lima CG, Ribeiro-Gomes FL, et al. Proinflammatory Clearance of Apoptotic Neutrophils Induces an IL-12^{low}IL-10^{high} Regulatory Phenotype in Macrophages. The Journal of Immunology 2010;185:2044–50.
[195] Chaput N, De Botton S, Obeid M, Apetoh L, Ghiringhelli F, Panaretakis T, et al. Molecular determinants of immunogenic cell death: surface exposure of calreticulin makes the difference. J Mol Med 2007;85:1069–76.
[196] Karpinich NO, Tafani M, Rothman RJ, Russo MA, Farber JL. The Course of Etoposide-induced Apoptosis from Damage to DNA and p53 Activation to Mitochondrial Release of Cytochrome c. Journal of Biological Chemistry 2002;277:16547–52.
[197] Marzio R, Jirillo E, Ransijn A, Mauël J, Corradin SB. Expression and Function of the Early Activation Antigen CD69 in Murine Macrophages. J Leukoc Biol 1997;62:349–55.
[198] Bachwich PR, Chensue SW, Larrick JW, Kunkel SL. Tumor necrosis factor stimulates interleukin-1 and prostaglandin E_2 production in resting macrophages. Biochem Biophys Res Commun 1986;136:94–101.
[199] Eisengart CA, Mestre JR, Naama HA, Mackrell PJ, Rivadeneira DE, Murphy EM, et al. Prostaglandins Regulate Melanoma-Induced Cytokine Production in Macrophages. Cell Immunol 2000;204:143–9.
[200] Strassmann G, Patil-Koota V, Finkelman F, Fong M, Kambayashi T. Evidence for the Involvement of Interleukin 10 in the Differential Deactivation of Murine Peritoneal Macrophages by Prostaglandin E_2. Journal of Experimental Medicine 1994;180:2365–70.
[201] Zhong WW, Burke PA, Drotar ME, Chavali SR, Forse RA. Effects of prostaglandin E_2, cholera toxin and 8-bromo-cyclic AMP on lipopolysaccharide-induced gene expression of cytokines in human

macrophages. Immunology 1995;84:446–52.
[202] Fleetwood AJ, Lawrence T, Hamilton JA, Cook AD. Granulocyte-Macrophage Colony-Stimulating Factor (CSF) and Macrophage CSF-Dependent Macrophage Phenotypes Display Differences in Cytokine Profiles and Transcription Factor Activities: Implications for CSF Blockade in Inflammation. The Journal of Immunology 2007;178:5245–52.
[203] Joly E, Hudrisier D. What is trogocytosis and what is its purpose? Nature Immunology 2003;4:815–5.
[204] Hudrisier D, Riond J, Mazarguil H, Gairin JE, Joly E. Cutting edge: CTLs rapidly capture membrane fragments from target cells in a TCR signaling-dependent manner. The Journal of Immunology 2001;166:3645–9.
[205] Beum PV, Kennedy AD, Williams ME, Lindorfer MA, Taylor RP. The Shaving Reaction: Rituximab/CD20 Complexes Are Removed From Mantle Cell Lymphoma and Chronic Lymphocytic Leukemia Cells by THP-1 Monocytes. The Journal of Immunology 2006;176:2600–9.
[206] Beum PV, Mack DA, Pawluczkowycz AW, Lindorfer MA, Taylor RP. Binding of rituximab, trastuzumab, cetuximab, or mAb T101 to cancer cells promotes trogocytosis mediated by THP-1 cells and monocytes. The Journal of Immunology 2008;181:8120–32.
[207] Carlin LM, Eleme K, McCann FE, Davis DM. Intercellular transfer and supramolecular organization of human leukocyte antigen C at inhibitory natural killer cell immune synapses. J Exp Med 2001;194:1507–17.
[208] Batista FD, Iber D, Neuberger MS. B Cells Acquire Antigen From Target Cells After Synapse Formation. Nature 2001;411:489–94.
[209] Gerdes H-H, Carvalho RN. Intercellular transfer mediated by tunneling nanotubes. Current Opinion in Cell Biology 2008;20:470–5.
[210] Rustom A, Saffrich R, Markovic I, Walther P, Gerdes H-H. Nanotubular Highways for Intercellular Organelle Transport. Science 2004;303:1007–10.
[211] Watkins SC, Salter RD. Functional connectivity between immune cells mediated by tunneling nanotubules. Immunity 2005.
[212] Onfelt B, Nedvetzki S, Benninger RK, Purbhoo MA, Sowinski S, Hume AN, et al. Structurally distinct membrane nanotubes between human macrophages support long-distance vesicular traffic or surfing of bacteria. The Journal of Immunology 2006;177:8476–83.
[213] Onfelt B, Nedvetzki S, Yanagi K, Davis DM. Cutting Edge: Membrane Nanotubes Connect Immune Cells. The Journal of Immunology 2004;173:1511–3.
[214] Sowinski S, Jolly C, Berninghausen O, Purbhoo MA, Chauveau A, Köhler K, et al. Membrane Nanotubes Physically Connect T Cells Over Long Distances Presenting a Novel Route for HIV-1 Transmission. Nature Cell Biology 2008;10:211–9.
[215] Wurster AL, Rodgers VL, White MF, Rothstein TL, Grusby MJ. Interleukin-4-mediated Protection of Primary B Cells from Apoptosis through Stat6-dependent Up-regulation of Bcl-xL. Journal of Biological Chemistry 2002;277:27169–75.
[216] Green DR, Ferguson T, Zitvogel L, Kroemer G. Immunogenic and Tolerogenic Cell Death. Nature Publishing Group 2009;9:353–63.
[217] Fadok VA, Savill JS, Haslett C, Bratton DL, Doherty DE, Campbell PA, et al. Different Populations of Macrophages Use Either the Vitronectin Receptor or the Phosphatidylserine Receptor to Recognize and Remove Apoptotic Cells. The Journal of Immunology 1992;149:4029–35.
[218] McDonald PP, Fadok VA, Bratton D, Henson PM. Transcriptional and Translational Regulation of Inflammatory Mediator Production by Endogenous TGF-ß in Macrophages That Have Ingested Apoptotic Cells. The Journal of Immunology 1999;163:6164–72.
[219] Barker RN, Erwig L-P, Hill KSK, Devine A, Pearce WP, Rees AJ. Antigen Presentation by Macrophages Is Enhanced by the Uptake of Necrotic, but

Not Apoptotic, Cells. Clin Exp Immunol 2002;127:220–5.
[220] Inaba K, Inaba M, Romani N, Aya H, Deguchi M, Ikehara S, et al. Generation of large numbers of dendritic cells from mouse bone marrow cultures supplemented with granulocyte/macrophage colony-stimulating factor. J Exp Med 1992;176:1693–702.
[221] Lari R, Fleetwood AJ, Kitchener PD, Cook AD, Pavasovic D, Hertzog PJ, et al. Macrophage Lineage Phenotypes and Osteoclastogenesis—Complexity in the Control by GM-CSF and TGF-ß. Bone 2007;40:323–36.
[222] Boyle WJ, Simonet WS, Lacey DL. Osteoclast differentiation and activation. Nature 2003;423:337–42.
[223] Hume DA. Macrophages as APC and the dendritic cell myth. J Immunol 2008;181:5829–35.
[224] Geissmann F, Gordon S, Hume DA, Mowat AM, Randolph GJ. Unravelling mononuclear phagocyte heterogeneity. Nature Reviews Immunology 2010;10:453–60.
[225] Hashimoto D, Miller J, Merad M. Dendritic Cell and Macrophage Heterogeneity In Vivo. Immunity 2011;35:323–35.
[226] Fairweather D, Cihakova D. Alternatively activated macrophages in infection and autoimmunity. J Autoimmun 2009;33:222–30.
[227] Leidi M, Gotti E, Bologna L, Miranda E, Rimoldi M, Sica A, et al. M2 Macrophages Phagocytose Rituximab-Opsonized Leukemic Targets More Efficiently than M1 Cells In Vitro. The Journal of Immunology 2009;182:4415–22.
[228] Akagawa KS. Functional Heterogeneity of Colony-Stimulating Factor-Induced Human Monocyte-Derived Macrophages. International Journal of Hematology 2002;76:27–34.
[229] De Villiers WJ, Fraser IP, Hughes DA, Doyle AG, Gordon S. Macrophage-colony-stimulating factor selectively enhances macrophage scavenger receptor expression and function. J Exp Med 1994;180:705–9.
[230] Sun E, Zhang L, Zeng Y, Ge Q, Zhao M, Gao W. Apoptotic Cells Actively Inhibit the Expression of CD69 on Con A Activated T Lymphocytes. Scandinavian Journal of Immunology 2000;51:231–6.
[231] McGaha TL, Chen Y, Ravishankar B, van Rooijen N, Karlsson MCI. Marginal Zone Macrophages Suppress Innate and Adaptive Immunity to Apoptotic Cells in the Spleen. Blood 2011;117:5403–12.
[232] Fadok VA, Bratton DL, Guthrie L, Henson PM. Differential Effects of Apoptotic Versus Lysed Cells on Macrophage Production of Cytokines: Role of Proteases. The Journal of Immunology 2001;166:6847–54.
[233] Hamel KM, Cao Y, Olalekan SA, Finnegan A. B Cell-Specific Expression of Inducible Costimulator Ligand Is Necessary for the Induction of Arthritis in Mice. Arthritis & Rheumatology 2014;66:60–7.
[234] Liang Y, Tedder TF. Identification of a CD20-, FcεRIß-, and HTm4-Related Gene Family: Sixteen New MS4A Family Members Expressed in Human and Mouse. Genomics 2001;72:119–27.
[235] Shan D, Ledbetter JA, Press OW. Apoptosis of Malignant Human B Cells by Ligation of CD20 with Monoclonal Antibodies. Blood 1998;91:1644–52.
[236] Hofmeister JK, Cooney D, Coggeshall KM. Clustered CD20 Induced Apoptosis: Src-Family Kinase, the Proximal Regulator of Tyrosine Phosphorylation, Calcium Influx, and Caspase 3-Dependent Apoptosis. Blood Cells, Molecules, and Diseases 2000;26:133–43.
[237] Pedersen IM, Buhl AM, Geisler CH, Jurlander J. The Chimeric Anti-CD20 Antibody Rituximab Induces Apoptosis in B-Cell Chronic Lymphocytic Leukemia Cells Through a p38 Mitogen Activated Protein-Kinase-Dependent Mechanism. Blood 2002;99:1314–9.
[238] Glennie MJ, French RR, Cragg MS, Taylor RP. Mechanisms of Killing by Anti-CD20 Monoclonal Antibodies. Molecular Immunology 2007;44:3823–37.
[239] Golay J, Zaffaroni L, Vaccari T, Lazzari M, Borleri G-M, Bernasconi S, et al.

Biologic Response of B Lymphoma Cells to Anti-CD20 Monoclonal Antibody Rituximab in Vitro: CD55 and CD59 Regulate Complement-Mediated Cell Lysis. Blood 2000;95:3900–8.

[240] Cardarelli PM, Quinn M, Buckman D, Fang Y, Colcher D, King DJ, et al. Binding to CD20 by Anti-B1 Antibody or $F(ab')_2$ Is Sufficient for Induction of Apoptosis in B-Cell Lines. Cancer Immunol Immunother 2002;51:15–24.

[241] Schröder C, Azimzadeh AM, Wu G, Price JO, Atkinson JB, Pierson RN III. Anti-CD20 Treatment Depletes B-Cells in Blood and Lymphatic Tissue of Cynomolgus Monkeys. Transplant Immunology 2003;12:19–28.

[242] Gong Q, Ou Q, Ye S, Lee WP, Cornelius J, Diehl L, et al. Importance of Cellular Microenvironment and Circulatory Dynamics in B Cell Immunotherapy. The Journal of Immunology 2005;174:817–26.

[243] Genberg H, Hansson A, Wernerson A, Wennberg L, Tydén G. Pharmacodynamics of Rituximab in Kidney Allotransplantation. Am J Transplant 2006;6:2418–28.

[244] Kamburova EG, Koenen HJPM, Borgman KJE, Berge ten IJ, Joosten I, Hilbrands LB. A Single Dose of Rituximab Does Not Deplete B Cells in Secondary Lymphoid Organs but Alters Phenotype and Function. Am J Transplant 2013;13:1503–11.

[245] Kamburova EG, Koenen HJPM, Boon L, Hilbrands LB, Joosten I. In Vitro Effects of Rituximab on the Proliferation, Activation and Differentiation of Human B Cells. American Journal of Transplantation 2011;12:341–50.

[246] Sahlin S, Hed J, Rundquist I. Differentiation Between Attached and Ingested Immune Complexes by a Fluorescence Quenching Cytofluorometric Assay. Journal of Immunological Methods 1983;60:115–24.

[247] Loike JD, Silverstein SC. A Fluorescence Quenching Technique Using Trypan Blue to Differentiate Between Attached and Ingested Glutaraldehyde-Fixed Red Blood Cells in Phagocytosing Murine Macrophages. Journal of Immunological Methods 1983;57:373–9.

[248] Chung EY, Liu J, Homma Y, Zhang Y, Brendolan A, Saggese M, et al. Interleukin-10 Expression in Macrophages during Phagocytosis of Apoptotic Cells Is Mediated by Homeodomain Proteins Pbx1 and Prep-1. Immunity 2007;27:952–4.

[249] Mazanec MB, Kaetzel CS, Lamm ME, Fletcher D, Nedrud JG. Intracellular Neutralization of Virus by Immunoglobulin A Antibodies. PNAS 1992;89:6901–5.

[250] Carroll RC, Beattie EC, Xia H, Lüscher C, Altschuler Y, Nicoll RA, et al. Dynamin-Dependent Endocytosis of Ionotropic Glutamate Receptors. PNAS 1999;96:14112–7.

[251] Beers SA, Chan CHT, French RR, Cragg MS, Glennie MJ. CD20 as a Target for Therapeutic Type I and II Monoclonal Antibodies. Semin Hematol 2010;47:107–14.

[252] Beum PV, Peek EM, Lindorfer MA, Beurskens FJ, Engelberts PJ, Parren PWHI, et al. Loss of CD20 and Bound CD20 Antibody from Opsonized B Cells Occurs More Rapidly Because of Trogocytosis Mediated by Fc Receptor-Expressing Effector Cells Than Direct Internalization by the B Cells. J Immunol 2011;187:3438–47.

[253] Xu W, Roos A, Schlagwein N, Woltman AM, Daha MR, Kooten CV. IL-10-Producing Macrophages Preferentially Clear Early Apoptotic Cells. Blood 2006;107:4930–7.

[254] Brown JR, Goldblatt D, Buddle J, Morton L, Thrasher AJ. Diminished Production of Anti-Inflammatory Mediators During Neutrophil Apoptosis and Macrophage Phagocytosis in Chronic Granulomatous Disease (CGD). J Leukoc Biol 2003;73:591–9.

[255] Rejman J, Oberle V, Zuhorn IS, Hoekstra D. Size-dependent internalization of particles via the pathways of clathrin- and caveolae-mediated endocytosis. Biochem J 2004;377:159–69.

[256] Luckey CJ, Marto JA, Partridge M, Hall E, White FM, Lippolis JD, et al. Differences in the Expression of Human Class I MHC Alleles and Their Associated Peptides in the Presence of Proteasome Inhibitors. The Journal of Immunology 2001;167:1212–21.
[257] Mitchell H, Choudhury A, Pagano RE, Leof EB. Ligand-Dependent and -Independent Transforming Growth Factor- Receptor Recycling Regulated by Clathrin-Mediated Endocytosis and Rab11. Mol Biol Cell 2004;15:4166–78.
[258] Plasman N, Vray B. Mouse peritoneal macrophages: characterization of functional subsets following Percoll density gradients. Research in Immunology 1993;144:151–63.
[259] Liu G, Xia X-P, Gong S-L, Zhao Y. The macrophage heterogeneity: Difference between mouse peritoneal exudate and splenic F4/80+ macrophages. J Cell Physiol 2006;209:341–52.
[260] Uderhardt S, Herrmann M, Oskolkova OV, Aschermann S, Bicker W, Ipseiz N, et al.12/15-Lipoxygenase Orchestrates the Clearance of Apoptotic Cells and Maintains Immunologic Tolerance. Immunity 2012;36:834–46.
[261] Davies LC, Jenkins SJ, Allen JE, Taylor PR. Tissue-resident macrophages. Nature Immunology 2013;14:986–95.
[262] Cragg MS, Glennie MJ. Antibody Specificity Controls in Vivo Effector Mechanisms of Anti-CD20 Reagents. Blood 2004;103:2738–43.
[263] Rothlein R, Dustin ML, Marlin SD, Springer TA. A Human Intercellular Adhesion Molecule (ICAM-1) Distinct From LFA-1. The Journal of Immunology 1986;137:1270–4.
[264] Diamond MS, Staunton DE, de Fougerolles AR, Stacker SA, Garcia-Aguilar J, Hibbs ML, et al. ICAM-1 (CD54): a counter-receptor for Mac-1 (CD11b/CD18). J Cell Biol 1990;111:3129–39.
[265] Agarwal A, Vieira CA, Book BK, Sidner RA, Fineberg NS, Pescovitz MD. Rituximab, Anti-CD20, Induces In Vivo Cytokine Release But Does Not Impair Ex Vivo T-Cell Responses. American Journal of Transplantation 2004;4:1357–60.
[266] Díaz-Torné C, de Juana Ortiz MA, Geli C, Cantó E, Laiz A, Corominas H, et al. Rituximab-Induced IL-15 Reduction Associated with Clinical Improvement in Rheumatoid Arthritis. Immunology 2013;accepted article.
[267] Bouaziz J-D, Yanaba K, Venturi GM, Wang Y, Tisch RM, Poe JC, et al. Therapeutic B cell depletion impairs adaptive and autoreactive $CD4^+$ T cell activation in mice. Proceedings of the National Academy of Sciences 2007;104:20878–83.
[268] Smeekens SP, van den Hoogen MWF, Kamburova EG, van de Veerdonk FL, Joosten I, Koenen HJMP, et al. The Effects of in Vivo B-Cell Depleting Therapy on Ex-Vivo Cytokine Production. Transplant Immunology 2013;28:183–8.
[269] Bevan MJ. Cross-priming. Nature Immunology 2006;7:363–6.
[270] Crotzer VL, Blum JS. Autophagy and Its Role in MHC-Mediated Antigen Presentation. The Journal of Immunology 2009;182:3335–41.
[271] Berke G. The CTL's Kiss of Death. Cell 1995;81:9–12.
[272] Harrington LE, Hatton RD, Mangan PR, Turner H, Murphy TL, Murphy KM, et al. Interleukin 17-producing CD4+ effector T cells develop via a lineage distinct from the T helper type 1 and 2 lineages. Nat Immunol 2005;6:1123–32.
[273] Ren Y, Tang J, Mok MY, Chan AWK, Wu A, Lau CS. Increased Apoptotic Neutrophils and Macrophages and Impaired Macrophage Phagocytic Clearance of Apoptotic Neutrophils in Systemic Lupus Erythematosus. Arthritis Rheum 2003;48:2888–97.
[274] Baekkeskov S, Nielsen JH, Marner B, Bilde T, Ludvigsson J, Lernmark Å. Autoantibodies in Newly Diagnosed Diabetic Children Immunoprecipitate Human Pancreatic Islet Cell Proteins. Nature 1982;298:167–9.
[275] Notkins AL, Lernmark Å. Autoimmune type 1 diabetes: resolved and

unresolved issues. The Journal of Clinical Investigation 2001;108:1247–52.
[276] Robertson JM, Jensen PE, Evavold BD. DO11. 10 and OT-II T cells recognize a C-terminal ovalbumin 323–339 epitope. J Immunol 2000;164:4706–12.
[277] Andersson M, Cremer MA, Terato K, Burkhardt H, Holmdahl R. Analysis of Type II Collagen Reactive T Cells in the Mouse. Scandinavian Journal of Immunology 1991;33:505–10.
[278] Oppenheim JJ. IL-2: More Than a T Cell Growth Factor. The Journal of Immunology 2007;179:1413–4.
[279] Depper JM, Leonard WJ, Drogula C, Krönke M, Waldmann TA, Greene WC. Interleukin 2 (IL-2) Augments Transcription of the IL-2 Receptor Gene. PNAS 1985;82:4230–4.
[280] Malek TR, Ashwell JD. Interleukin 2 Upregulates Expression of Its Receptor on a T Cell Clone. J Exp Med 1985;161:1575–80.
[281] Mosmann TR, Cherwinski H, Bond MW, Giedlin MA, Coffman RL. Two types of murine helper T cell clone. I. Definition according to profiles of lymphokine activities and secreted proteins. J Immunol 1986;136:2348–57.
[282] Falk K, Rötzschke O, Stevanović S, Jung G, Rammensee HG. Allele-Specific Motifs Revealed by Sequencing of Self-Peptides Eluted From MHC Molecules. Nature 1991;351:290–6.
[283] Hosken NA, Bevan MJ, Carbone FR. Class I-restricted presentation occurs without internalization or processing of exogenous antigenic peptides. The Journal of Immunology 1989;142:1079–83.
[284] Vacchino JF, McConnell HM. Peptide binding to active class II MHC protein on the cell surface. The Journal of Immunology 2001;166:6680–5.
[285] Santambrogio L, Santambrogio L, Sato AK, Sato AK, Fischer FR, Fischer FR, et al. Abundant empty class II MHC molecules on the surface of immature dendritic cells. PNAS 1999;96:15050–5.
[286] Zhong G, Romagnoli P, Germain RN. Related Leucine-based Cytoplasmic Targeting Signals in Invariant Chain and Major Histocompatibility Complex Class II Molecules Control Endocytic Presentation of Distinct Determinants in a Single Protein. Journal of Experimental Medicine 1997;185:429–38.
[287] Fahnestock ML, Tamir I, Narhi L, Bjorkman PJ. Thermal Stability Comparison of Purified Empty and Peptide-Filled Forms of a Class I MHC Molecule. Science 1992;258:1658–62.
[288] Schumacher TN, Heemels MT, Neefjes JJ, Kast WM, Melief CJ, Ploegh HL. Direct Binding of Peptide to Empty MHC Class I Molecules on Intact Cells and in Vitro. Cell 1990;62:563–7.
[289] Ljunggren H-G, Stam NJ, Öhlén C, Neefjes JJ, Höglund P, Heemels M-T, et al. Empty MHC class I molecules come out in the cold. Nature 1990;346:476–80.
[290] Drake JR, Repasky EA, Bankert RB. Endocytosis of Antigen, Anti-Idiotype, and Anti-Immunoglobulin Antibodies and Receptor Re-Expression by Murine B Cells. The Journal of Immunology 1989;143:1768–76.
[291] Caruso A, Licenziati S, Corulli M, Canaris AD, De Francesco MA, Fiorentini S, et al. Flow Cytometric Analysis of Activation Markers on Stimulated T Cells and Their Correlation with Cell Proliferation. Cytometry 1997;27:71–6.
[292] Krieger JI, Grammer SF, Grey HM, Chesnut RW. Antigen presentation by splenic B cells: resting B cells are ineffective, whereas activated B cells are effective accessory cells for T cell responses. The Journal of Immunology 1985;135:2937–45.
[293] Chesnut RW, Colon SM, Grey HM. Antigen Presentation by Normal B Cells, B Cell Tumors, and Macrophages: Functional and Biochemical Comparison. The Journal of Immunology 1982;128:1764-8.
[294] Rock KL, Benacerraf B, Abbas AK. Antigen Presentation by Hapten-Specific B Lymphocytes. J Exp Med 1984;160:1102–13.
[295] Duclos S, Corsini R, Desjardins M. Remodeling of Endosomes During Lysosome Biogenesis Involves “Kiss and Run” Fusion Events Regulated by

Rab5. Journal of Cell Science 2003;116:907–18.
[296] Zerial M, McBride H. Rab Proteins as Membrane Organizers. Nat Rev Mol Cell Biol 2001;2:107–17.
[297] Grant BD, Grant BD, Donaldson JG, Donaldson JG. Pathways and mechanisms of endocytic recycling.Net Rev Mol Cell Biol 2009;10:597-608.
[298] Neefjes J. CIIV, MIIC and other compartments for MHC class II loading. Eur J Immunol 1999;29:1421–5.
[299] Alfaro C, Suarez N, Oñate C, Perez-Gracia JL, Martinez-Forero I, Hervas-Stubbs S, et al. Dendritic Cells Take up and Present Antigens from Viable and Apoptotic Polymorphonuclear Leukocytes. PLoS ONE 2011;6:e29300.
[300] Kambayashi T, Baranski JD, Baker RG, Zou T, Allenspach EJ, Shoag JE, et al. Indirect Involvement of Allergen-Captured Mast Cells in Antigen Presentation. Blood 2007;111:1489–96.
[301] Sancho D, Gómez M, Viedma F, Esplugues E, Gordón-Alonso M, Angeles García-López M, et al. CD69 downregulates autoimmune reactivity through active transforming growth factor-ß production in collagen-induced arthritis. The Journal of Clinical Investigation 2003;112:872–82.
[302] Sancho D, Gómez M, Sánchez-Madrid F. CD69 Is an Immunoregulatory Molecule Induced Following Activation. Trends Immunol 2005;26:136–40.
[303] Kawabe Y, Ochi A. Programmed cell death and extrathymic reduction of Vbeta8+ CD4+ T cells in mice tolerant to Staphylococcus aureus enterotoxin B. Nature 1991;349:245–8.
[304] Lenardo MJ. lnterleukin-2 programs mouse αß T lymphocytes for apoptosis. Nature 1991;353:858–61.
[305] Broere F, Apasov SG, Sitkovsky MV, Eden W. T cell subsets and T cell-mediated immunity. Principles of Immunopharmacology: 3rd revised and extended edition, Basel: Springer Basel; 2011, pp. 15–27.
[306] Muller G, Muller A, Tuting T, Steinbrink K, Saloga J, Szalma C, et al. Interleukin-10-Treated Dendritic Cells Modulate Immune Responses of Naive and Sensitized T Cells In Vivo. J Investig Dermatol 2002;119:836–41.
[307] Fiorentino DF, Zlotnik A, Mossmann TR, Howard M, O'Garra A. IL-10 Inhibits Cytokine Production by Activated Macrophages. The Journal of Immunology 1991;147:3851–3822.
[308] Goodyear CS, Silverman GJ. Death by a B Cell Superantigen: In Vivo VH-targeted Apoptotic Supraclonal B Cell Deletion by a Staphylococcal Toxin. Journal of Experimental Medicine 2003;197:1125–39.
[309] Tedder TF, Klejman G, Disteche CM, Adler DA, Schlossman SF, Saito H. Cloning of a complementary DNA encoding a new mouse B lymphocyte differentiation antigen, homologous to the human B1 (CD20) antigen, and localization of the gene to chromosome 19. The Journal of Immunology 1988;141:4288–94.
[310] McLaughlin P, Grillo-López AJ, Link BK, Levy R, Czuczman MS, Williams ME, et al. Rituximab Chimeric Anti-CD20 Monoclonal Antibody Therapy for Relapsed Indolent Lymphoma: Half of Patients Respond to a Four-Dose Treatment Program. Journal of Clinical Oncology 1998;16:2825–33.
[311] Looney RJ, Anolik JH, Campbell D, Felgar RE, Young F, Arend LJ, et al. B Cell Depletion as a Novel Treatment for Systemic Lupus Erythematosus. Arthritis Rheum 2004;50:2580–9.
[312] Hauser SL, Waubant E, Arnold DL, Vollmer T, Antel J, Fox RJ, et al. B-Cell Depletion with Rituximab in Relapsing–Remitting Multiple Sclerosis. N Engl J Med 2008;358:676–88.
[313] Naismith RT, Piccio L, Lyons JA, Lauber J, Tutlam NT, Parks BJ, et al. Rituximab add-on therapy for breakthrough relapsing multiple sclerosis A 52-week phase II trial. Neurology 2010;74:1860–7.
[314] Castillo-Trivino T, Braithwaite D, Bacchetti P, Waubant E. Rituximab in Relapsing and Progressive Forms of Multiple Sclerosis: A Systematic Review. PLoS ONE 2013;8:e66308.

[315] Tedder TF, Klejman G, Schlossman SF, Saito H. Structure of the Gene Encoding the Human B Lymphocyte Differentiation Antigen CD20 (B1). The Journal of Immunology 1989;142:2560–8.
[316] Hupp K, Siwarski D, Mock BA, Kinet JP. Gene mapping of the three subunits of the high affinity FcR for IgE to mouse chromosomes 1 and 19. The Journal of Immunology 1989;143:3787–91.
[317] Stashenko P, Nadler LM, Hardy R, Schlossman SF. Expression of Cell Surface Markers After Human B Lymphocyte Activation. PNAS 1981;78:3848–52.
[318] Tedder TF, Forsgren A, Boyd AW, Nadler LM, Schlossman SF. Antibodies Reactive with the B1 Molecule Inhibit Cell Cycle Progression but Not Activation of Human B Lymphocytes. Eur J Immunol 1986;16:881–7.
[319] Kuijpers TW, Bende RJ, Baars PA, Grummels A, Derks IAM, Dolman KM, et al. CD20 Deficiency in Humans Results in Impaired T Cell–Independent Antibody Responses. The Journal of Clinical Investigation 2010;120:214–22.
[320] Bubien JK, Zhou LJ, Bell PD, Frizzell RA, Tedder TF. Transfection of the CD20 Cell Surface Molecule Into Ectopic Cell Types Generates a Ca^{2+} Conductance Found Constitutively in B Lymphocytes. J Cell Biol 1993;121:1121–32.
[321] O'Keefe TL, Williams GT, Davies SL, Neuberger MS. Mice Carrying a CD20 Gene Disruption. Immunogenetics 1998;48:125–32.
[322] Yang XW, Model P, Heintz N. Homologous recombination based modification in Esherichia coli and germline transmission in transgenic mice of a bacterial artificial chromsome. Nat Biotechnol 1997;15:859–65.
[323] Giraldo P, Montoliu L. Size matters: use of YACs, BACs and PACs in transgenic animals. Transgenic Research 2001;10:83–103.
[324] Ahuja A, Dunn R, Kehry MR, Shlomchik MJ. Depletion of B Cells in Murine Lupus: Efficacy and Resistance. The Journal of Immunology 2007;179:3351–61.
[325] Hu C-Y, Rodriguez-Pinto D, Du W, Ahuja A, Henegariu O, Wong FS, et al. Treatment with CD20-specific antibody prevents and reverses autoimmune diabetes in mice. The Journal of Clinical Investigation 2007;117:3857–67.
[326] Mei HE, Frölich D, Giesecke C, Loddenkemper C, Reiter K, Schmidt S, et al. Steady-State Generation of Mucosal IgA^+ Plasmablasts Is Not Abrogated by B-Cell Depletion Therapy with Rituximab. Immunobiology 2010;116:5181–90.
[327] Michel RB, Mattes MJ. Intracellular Accumulation of the Anti-CD20 Antibody 1F5 in B-Lymphoma Cells. Clinical Cancer Research 2002;8:2701–13.
[328] Tedder TF, Schlossman SF. Phosphorylation of the B1 (CD20) Molecule by Normal and Malignant Human B Lymphocytes. The Journal of Biological Chemistry 1988;263:10009–15.
[329] Tedder TF, McIntyre G, Schlossman SF. Heterogeneity in the B1 (CD20) cell surface molecule expressed by human B-lymphocytes. Molecular Immunology 1988;25:1321–30.
[330] Du J, Wang H, Zhong C, Peng B, Zhang M, Li B, et al. Crystal structure of chimeric antibody C2H7 Fab in complex with a CD20 peptide. Molecular Immunology 2008;45:2861–8.
[331] Press OW, Appelbaum F, Ledbetter JA, Martin PJ, Zarling J, Kidd P, et al. Monoclonal antibody 1F5 (anti-CD20) serotherapy of human B cell lymphomas. Blood 1987;69:584–91.
[332] Maloney DG, Liles TM, Czerwinski DK, Waldichuk C, Rosenberg J, Grillo-Lopez A, et al. Phase I clinical trial using escalating single-dose infusion of chimeric anti-CD20 monoclonal antibody (IDEC-C2B8) in patients with recurrent B-cell lymphoma. Blood 1994;84:2457–66.
[333] Leandro MJ, Cooper N, Cambridge G, Ehrenstein MR, Edwards JCW. Bone Marrow B-Lineage Cells in Patients with Rheumatoid Arthritis Following Rituximab Therapy. Rheumatology 2007;46:29–36.
[334] Ditzel HJ. The K/BxN mouse: a model of human inflammatory arthritis. Trends in Molecular Medicine 2004;10:40–5.

[335] Brand DD, Latham KA, Rosloniec EF. Collagen-induced arthritis. Nature Protocols 2007;2:1269–75.
[336] Glant TT, Cs-Szabó G, Nagase H, Jacobs JJ, Mikecz K. Progressive Polyarthritis Induced in BALB/c Mice by Aggrecan From Normal and Osteoarthritic Human Cartilage. Arthritis Rheum 1998;41:1007–18.
[337] Schubert D, Maier B, Morawietz L, Krenn V, Kamradt T. Immunization with Glucose-6-Phosphate Isomerase Induces T Cell-Dependent Peripheral Polyarthritis in Genetically Unaltered Mice. The Journal of Immunology 2004;172:4503–9.
[338] Khachigian LM. Collagen Antibody-Induced Arthritis. Nature Protocols 2006;1:2512–6.
[339] Trentham DE, Townes AS, Kang AH. Autoimmunity to type II collagen an experimental model of arthritis. J Exp Med 1977;146:857–68.
[340] Wooley PH, Luthra HS, Stuart JM, David CS. Type II collagen-induced arthritis in mice. I. Major histocompatibility complex (I region) linkage and antibody correlates. J Exp Med 1981;154:688–700.
[341] Mauri C, Williams RO, Walmsley M, Feldmann M. Relationship Between Th1/Th2 Cytokine Patterns and the Arthritogenic Response in Collagen-Induced Arthritis. Eur J Immunol 1996;26:1511–8.
[342] Ranges GE, Sriram S, Cooper S. Prevention of Type II Collagen-Induced Arthritis by in Vivo Treatment with Anti-L3T4. Journal of Experimental Medicine 1985;162:1105–10.
[343] Chiocchia G, Boissier M-C, Fournier C. Therapy against murine collagen-induced arthritis with T cell receptor Vß-specific antibodies. Eur J Immunol 1991;21:2899–905.
[344] Wooley PH, Luthra HS, Lafuse WP, Huse A, Stuart JM, David CS. Type II Collagen-Induced Arthritis in Mice. III. Suppression of Arthritis by Using Monoclonal and Polyclonal Anti-Ia Antisera. The Journal of Immunology 1985;134:2366–74.
[345] Marinova-Mutafchieva L, Williams RO, Mason LJ, Mauri C, Feldmann M, Maini RN. Dynamics of Proinflammatory Cytokine Expression in the Joints of Mice with Collagen-Induced Arthritis (CIA). Clinical & Experimental Immunology 1997;107:507–12.
[346] Stasiuk LM, Abehsira-Amar O, Fournier C. Collagen-Induced Arthritis in DBA/1 Mice: Cytokine Gene Activation Following Immunization with Type II Collagen. Cell Immunol 1996;173:269–75.
[347] Sasai M, Saeki Y, Ohshima S, Nishioka K, Mima T, Tanaka T, et al. Delayed onset and reduced severity of collagen-induced arthritis in interleukin-6-deficient mice. Arthritis Rheum 1999;42:1635–43.
[348] Watson WC, Watson WC, Townes AS, Townes AS. Genetic Susceptibility to Murine Collagen II Autoimmune Arthritis Proposed Relationship to the IgG2 Autoantibody Subclass Response, Complement C5, Major Histocompatibility Complex (MHC) and Non-MHC Loci. J Exp Med 1985;162:1878–91.
[349] Wang Y, Kristan J, Hao L, Lenkoski CS, Shen Y, Matis LA. A Role for Complement in Antibody-Mediated Inflammation: C5-Deficient DBA/1 Mice Are Resistant to Collagen-Induced Arthritis. The Journal of Immunology 2000;164:4340–7.
[350] Courtenay JS, Dallman MJ, Dayan AD, Martin A, Mosedale B. Immunisation Against Heterologous Type II Collagen Induces Arthritis in Mice. Nature 1980;283:666–8.
[351] Terato K, Hasty KA, Reife RA, Cremer MA, Kang AH, Stuart JM. Induction of Arthritis with Monoclonal Antibodies to Collagen. The Journal of Immunology 1992;148:2103–8.
[352] Webb LMC, Walmsley MJ, Feldmann M. Prevention and amelioration of collagen-induced arthritis by blockade of the CD28 co-stimulatory pathway: requirement for both B7-1 and B7-2. Eur J Immunol 1996;26:2320–8.
[353] Wang Q-T, Wu Y-J, Huang B, Ma Y-K, Song S-S, Zhang L-L, et al. Etanercept

Attenuates Collagen-Induced Arthritis by Modulating the Association Between BAFFR Expression and the Production of Splenic Memory B Cells. Pharmacological Research 2013;68:38–45.
[354] Thompson HS, Staines NA. Gastric Administration of Type II Collagen Delays the Onset and Severity of Collagen-Induced Arthritis in Rats. Clinical & Experimental Immunology 1986;64:581–6.
[355] Millington OR, Mowat AM, Garside P. Induction of Bystander Suppression by Feeding Antigen Occurs despite Normal Clonal Expansion of the Bystander T Cell Population. The Journal of Immunology 2004;173:6059–64.
[356] Leishman AJ, Garside P, Mowat AM. Induction of Oral Tolerance in the Primed Immune System: Influence of Antigen Persistence and Adjuvant Form. Cell Immunol 2000;202:71–8.
[357] Smith KM, Garside P, Davidson JM. T-cell activation occurs simultaneously in local and peripheral lymphoid tissue following oral administration of a range of doses of immunogenic or tolerogenic antigen although tolerized T cells display a defect in cell division. Immunology 2002;106:144–58.
[358] Monson NL, Cravens P, Hussain R, Harp CT, Cummings M, De Pilar Martin M, et al. Rituximab Therapy Reduces Organ-Specific T Cell Responses and Ameliorates Experimental Autoimmune Encephalomyelitis. PLoS ONE 2011;6:e17103.
[359] Kennedy MK, Clatch RJ, Dal Canto MC, Trotter JL, Miller SD. Monoclonal antibody-induced inhibition of relapsing EAE in SJL/J mice correlates with inhibition of neuroantigen-specific cell-mediated immune responses. J Neuroimmunol 1987;16:345–64.
[360] Huber B, Devinsky O, Gershon RK, Cantor H. Cell-mediated immunity: delayed-type hypersensitivity and cytotoxic responses are mediated by different T-cell subclasses. J Exp Med 1976;143:1534–9.
[361] Tedder TF, Baras A, Xiu Y. Fcγ receptor-dependent effector mechanisms regulate CD19 and CD20 antibody immunotherapies for B lymphocyte malignancies and autoimmunity. Springer Semin Immun 2006;28:351–64.
[362] Yanaba K, Hamaguchi Y, Venturi GM, Steeber DA, St Clair EW, Tedder TF. B Cell Depletion Delays Collagen-Induced Arthritis in Mice: Arthritis Induction Requires Synergy Between Humoral and Cell-Mediated Immunity. The Journal of Immunology 2007;179:1369–80.
[363] Li J, Kuzin I, Moshkani S, Proulx ST, Xing L, Skrombolas D, et al. Expanded CD23+/CD21hi B Cells in Inflamed Lymph Nodes Are Associated with the Onset of Inflammatory-Erosive Arthritis in TNF-Transgenic Mice and Are Targets of Anti-CD20 Therapy. J Immunol 2010;184:6142–50.
[364] Huang H, Benoist C, Mathis D. Rituximab Specifically Depletes Short-Lived Autoreactive Plasma Cells in a Mouse Model of Inflammatory Arthritis. Proceedings of the National Academy of Sciences 2010;107:4658–63.
[365] Inglis JJ, Simelyte E, McCann FE, Criado G, Williams RO. Protocol for the induction of arthritis in C57BL/6 mice. Nature Protocols 2008;3:612–8.
[366] Klareskog L, Holmdahl R, Larsson E, Wigzell H. Role of T Lymphocytes in Collagen II Induced Arthritis in Rats. Clinical & Experimental Immunology 1983;51:117–25.
[367] Seki N, Sudo Y. Induction and Perpetuation of Arthritis Require Synergy between Humoral and Cell-Mediated Immunity. The Journal of Immunology 1988;140:1477–84.
[368] Kjellen P, Brunsberg U, Broddefalk J, Hansen B, Vestberg M, Ivarsson I, et al. The structural basis of MHC control of collagen- induced arthritis; binding of the immunodominant type II collagen 256–270 glycopeptide to H-2Aq and H-2Ap molecules. Eur J Immunol 1998;28:755–67.
[369] van Lent PL, Licht R, Dijkman H, Holthuysen AE, Berden JH, van den Berg WB. Uptake of Apoptotic Leukocytes by Synovial Lining Macrophages Inhibits Immune Complex-Mediated Arthritis. J Leukoc Biol 2001;70:708–14.
[370] Notley CA, Brown MA, Wright GP, Ehrenstein MR. Natural IgM Is Required for

Suppression of Inflammatory Arthritis by Apoptotic Cells. J Immunol 2011;186:4967–72.
[371] Parnaik R, Raff MC, Scholes J. Differences between the clearance of apoptotic cells by professional and non-professional phagocytes. Current Biology 2000;10:857–60.
[372] Williams PJ, Jones R, Rademacher TW. Correlation Between IgG Anti-Type II Collagen Levels and Arthritic Severity in Murine Arthritis. Autoimmunity 1998;27:201–7.
[373] Kerwar SS, Englert ME, McReynolds RA, Landes MJ, Lloyd JM, Oronsky AL, et al. Type II Collagen-Induced Arthritis: Studies with Purified Anticollagen Immunoglobulin. Arthritis Rheum 1983;26:1120–31.
[374] Vieira P, Rajewsky K. The half-lives of serum immunoglobulins in adult mice. Eur J Immunol 1988;18:313–6.
[375] Morell A, Terry WD, Waldmann TA. Metabolic Properties of IgG Subclasses in Man. Journal of Clinical Investigation 1970;49:673–80.
[376] Brambell FW, Hemmings WA, Morris IG. A Theoretical Model of Gamma-Globulin Catabolism. Nature 1964;203:1352–5.
[377] Junghans RP, Anderson CL. The Protection Receptor for IgG Catabolism Is the Beta2-Microglobulin-Containing Neonatal Intestinal Transport Receptor. PNAS 1996;93:5512–6.
[378] Fahey JL, Robinson AG. Factors Controlling Serum Gamma-Globulin Concentration. Journal of Experimental Medicine 1963;118:845–68.
[379] Hamel KM, Cao Y, Ashaye S, Wang Y, Dunn R, Kehry MR, et al. B Cell Depletion Enhances T Regulatory Cell Activity Essential in the Suppression of Arthritis. J Immunol 2011;187:4900–6.
[380] Dunussi-Joannopoulos K, Hancock GE, Kunz A, Hegen M, Zhou XX, Sheppard BJ, et al. B-cell depletion inhibits arthritis in a collagen-induced arthritis (CIA) model, but does not adversely affect humoral responses in a respiratory syncytial virus (RSV) vaccination model. Blood 2005;106:2235–43.
[381] Elliott DE, Weinstock JV. Helminth-host immunological interactions: prevention and control of immune-mediated diseases. Annals of the New York Academy of Sciences 2012;1247:83–96.
[382] Kremer JM, Westhovens R, Leon M, Di Giorgio E, Alten R, Steinfeld S, et al. Treatment of Rheumatoid Arthritis by Selective Inhibition of T-Cell Activation with Fusion Protein CTLA4Ig. N Engl J Med 2003;349:1907–15.